

# **The Influence of Lewis Bases in $\text{MgCl}_2$ Supported Ziegler-Natta Catalysis: A DFT Study**

**Thesis Submitted to AcSIR for the Award of  
the Degree of  
DOCTOR OF PHILOSOPHY  
In Chemical Sciences**



**By**

**Mr. Jugal Kishore Kumawat**

**Registration Number: 10CC11J26090**

**Under the guidance of**

**Dr. Kumar Vanka**

**Physical and Materials Chemistry Division**

**CSIR-National Chemical Laboratory**

**Pune – 411008, India**

**May 2016**



# सीएसआयआर-राष्ट्रीय रासायनिक प्रयोगशाला

(वैज्ञानिक तथा औद्योगिक अनुसंधान परिषद)

डॉ. होमी भाभा मार्ग, पुणे - 411 008. भारत



## CSIR-NATIONAL CHEMICAL LABORATORY

(Council of Scientific & Industrial Research)

Dr. Homi Bhabha Road, Pune - 411008. India

### Certificate

This is to certify that the work incorporated in this Ph.D. thesis entitled "*The Influence of Lewis Bases in MgCl<sub>2</sub> Supported Ziegler-Natta Catalysis: A DFT Study*" submitted by **Mr. Jugal Kishore Kumawat** to Academy of Scientific and Innovative Research (AcSIR) in fulfillment of the requirements for the award of the Degree of **Doctor of Philosophy In Chemical Sciences**, embodies original research work under my supervision. I further certify that this work has not been submitted to any other University or Institution in part or full for the award of any degree or diploma. Research material obtained from other sources has been duly acknowledged in the thesis. Any text, illustration, table etc., used in the thesis from other sources, have been duly cited and acknowledged.

*Jugal K2*

Mr. Jugal Kishore Kumawat  
(Student)

*Kumar Vanka*

Dr. Kumar Vanka  
(Supervisor)

Date: 30/05/2016

Place: Pune



FAX

WEBSITE

Communications Channels  
NCL Level DID : 2590  
NCL Board No. : +91-20-25902000  
Four PRI Lines : +91-20-25902000

Director's Office : +91-20-25902601  
COA's Office : +91-20-25902660  
SPO's Office : +91 20 25902664


[www.ncl-india.org](http://www.ncl-india.org)

## DECLARATION BY RESEARCH SCHOLAR

I hereby declare that the work incorporated in this thesis entitled "*The Influence of Lewis Bases in MgCl<sub>2</sub> Supported Ziegler-Natta Catalysis: A DFT Study*" submitted for the degree of *Doctor of Philosophy in Chemical Sciences* to the Academy of Scientific & Innovative Research (AcSIR), has been carried out by me at the Physical and Materials Chemistry Division of CSIR-National Chemical Laboratory, Pune under the guidance of *Dr. Kumar Vanka*. Such material as has been obtained by other sources has been duly acknowledged in this thesis. The work is original and has not been submitted in part or full by me for any other degree or diploma to any other Institution or University.

Date: 30/05/2016

CSIR- National Chemical Laboratory  
Pune-411008

Research student  
  
Mr. Jugal Kishore Kumawat

*Dedicated*  
*to*  
*My Family*

## Acknowledgment

It gives me great pleasure to thank all the people who helped me throughout my Ph.D. life in CSIR-National Chemical Laboratory.

I would like to express my gratitude to my research supervisor Dr. Kumar Vanka, for his patient guidance, enthusiastic encouragement and useful analysis of my research work. I would also like to thank our collaborator Dr. Virendra Kumar Gupta, Reliance Industries Limited - Mumbai, for his advice and assistance in keeping my research work easy and interesting.

I would also like to extend my thanks to my DAC chairperson Dr. RamRup Sarkar and DAC members Dr. Neelanjana Sengupta and Nayana Vaval for their valuable time and constructive guidance. I would also like to take this opportunity to thank Dr. Sourav Pal for his regular quantum classes despite his busy schedule as a Director of the CSIR-NCL.

I also thank all my labmates Shantanu Kadam, Manoj Mane, Tamal Das, Subrashis Banerjee, Vipin Raj, Shailaja Jain for their kind support throughout my Ph.D. I would like to express my very great appreciation to Mrityunjay Tiwari and Yuvraj Dangat for the healthy discussion as well as motivated critics punches that helped me to improve my research carrier. I also thank to all my friends outside our group in NCL Deepak kumar, Shahbaz, Sakeel, Arun, Yashpal, Deepak Chand, Pinka, Manoj, Amit, Sandeep, Vijay, Kundan and Rakesh (DRDO, Pune).

My sincere and heartfelt thanks to my roommates Dr. Bhan Prakash, Puneet Khandelwal and Rajendra Prasad for providing a home like environment and togetherness while cooking food in the SA-58. I also thank to our special guests Parul, Amie, Sandhya, Deepika, Vikas, Yachita, Kavita, Anita, Suman, Asheesh and Omkar for making weekends more enjoyable.

I am thankful to CSIR, New Delhi, for the financial support and to Academy of Scientific & Innovative Research (AcSIR) for giving me an opportunity for pursuing a

doctoral degree. I would also like to thank SAO, CSIR-NCL for their support in official work.

Finally, I wish to thank my family members for their support and encouragement throughout my Ph.D life. Specially, my father without him it would have been impossible to reach this level. At the end I would like express appreciation to my beloved niece Garima (Gudiya) and nephew Ramesh (Babu) for their cute smiles that make me always happy.

Jugal Kumawat

# Contents

Abstract	iv
Abbreviations	viii
List of Publications	x
<b>1. Introduction</b>	<b>1</b>
1.1 Introduction	1
1.2 Development in ZN catalysis	1
1.3 Catalyst Support and Active Sites for TiCl <sub>4</sub>	2
1.4 Lewis Bases “Donor” and its Role in ZN system	4
1.5 Activation of TiCl <sub>4</sub> and Donor Displacement	6
1.6 Cossee-Arlman mechanism	8
1.7 Chain Termination and Chain Transfer Steps	9
1.8 Conclusion Remarks	11
1.9 References	11
<b>2. Theoretical Background of Electronic Structure</b>	<b>18</b>
2.1 The Many-Body Schrodinger Equation	19
2.1.1 Born-Oppenheimer approximation	19
2.2 Density Functional Theory	21
2.2.1 Thomas-Fermi Model	21
2.2.2 Hohenberg-Kohn (HK) Theorems	22
2.2.3 Kohn-Sham Method	24
2.2.4 Exchange-Correlation Functionals	25
2.2.5 Local Density Approximation (LDA)	26
2.2.6 Generalized Gradient Approximation (GGA)	26
2.2.7 Hybrid Functionals	27
2.3. References	28

<b>3. The Nature of the Active Site in Ziegler-Natta Olefin Polymerization Catalyst Systems: A Computational Investigation</b>	<b>30</b>
3.1 Introduction	31
3.2 Computational Details	34
3.3 Results and Discussion	35
3.3.1. Validation of the MgCl <sub>2</sub> Model Employed in the Current Calculations	35
3.3.2. Insertion and Termination Studies with the MgCl <sub>2</sub> Model	38
3.3.3. OC <sub>2</sub> H <sub>5</sub> as a Ligand at the Titanium Center	49
3.3.4. The Overall Picture for Insertion and Termination for the Ethylene Monomer	53
3.3.5. H <sub>2</sub> Response in the ZN systems	56
3.3.6. Insertion and Termination for the Propylene Monomer Case	58
3.3.7. The Overall Picture of Multi-Site Catalysis in Ziegler-Natta Systems	60
3.4 Conclusions	66
3.5 References	67
<b>4. Donor Decomposition by Lewis Acids in Ziegler-Natta Catalyst Systems: A Computational Investigation</b>	<b>72</b>
4.1 Introduction	73
4.2 Computational Details	79
4.3 Results and Discussion	81
4.3.1 The Interaction of different ester donors with Al <sub>2</sub> Et <sub>6</sub>	82
4.3.2 The Interaction of the donors with TiCl <sub>2</sub> Et on the MgCl <sub>2</sub> supported layer	91
4.4 Conclusions	105
4.5 References	105



<b>5. The Effect of Donors on the Activation Mechanism in Ziegler-Natta Catalysis: A Computational Study</b>	<b>111</b>
5.1 Introduction	112
5.2 Computational Details	117
5.3 Results and Discussion	119
5.3.1 Validation of the chosen $\text{MgCl}_2$ model system.	119
5.3.2 Activation Study	123
5.4 Conclusions	140
5.5 References	142
<b>6. Ethylene Polymerization on the (110) and (104) lateral cuts of the <math>\text{MgCl}_2</math> Surface with Ethoxy Ligand Containing Titanium Complexes in Ziegler-Natta Catalysis: A Computational Study</b>	<b>147</b>
6.1 Introduction	148
6.2 Computational Details	150
6.3 Results and Discussions	151
6.3.1 Validation of $\text{MgCl}_2$ Model	151
6.3.2 The binding of different $\text{Ti}-(\text{Cl})_{4-n}(\text{OEt})_n$ ( $n= 1-4$ ) catalysts to the (110) and (104) $\text{MgCl}_2$ surfaces	153
6.3.3 The Comparative Study of All the Titanium Catalysts (Cat-A-E)	155
6.3.4 $\text{TiCl}_3(\text{OC}_4\text{H}_8\text{Cl})$ catalyst	158
6.4 Conclusions	160
6.5 Reference	161
<b>7. Summary of the Thesis</b>	<b>165</b>

## Abstract

MgCl<sub>2</sub> supported Ziegler-Natta (ZN) olefin polymerization catalysis is one of the most important chemical processes in industry today. It is responsible for the production of a wide variety of plastics, including elastomers and fibers. In the sixty years since their discovery, it would be no exaggeration to say the ZN catalysts have transformed the polymer industry, performing at near enzymatic rates and annually producing hundreds of millions of tons of polymers such as polyethylene and isotactic polypropylene.

However, despite their enormous importance and impact, ZN catalyst systems have not been completely understood to date. The multi-site, heterogeneous nature of the ZN catalysis process is responsible in part for this, but what has also contributed is the complexity of the system, which includes the MgCl<sub>2</sub> support, the active titanium species, usually in the (III) or (II) oxidation state, AlR<sub>3</sub> (where R = alkyl group such as ethyl): the trialkylaluminium, alkylating agent, the substrate olefin monomer, and also oxygen containing Lewis bases which act as donors: “internal” (donors such as diether, alkoxy silane, diisobutyl phthalate and succinate) if added during MgCl<sub>2</sub> surface preparation, “external” (donors such as alkoxy silan) if added later into the system with AlR<sub>3</sub> or the monomer.

The main motivation of this thesis is to use density functional theory (DFT) based computational approaches to evaluate the effect of oxygen containing donors on the different ZN catalyst steps, such as the activation step, the insertion, and the termination processes.

This thesis, entitled “*The Influence of Lewis Bases in MgCl<sub>2</sub> Supported Ziegler-Natta Catalysis: A DFT Study*” contains six chapters.

## Chapter 1

Chapter 1 begins with a brief introduction to Ziegler-Natta (ZN) catalysts that have been used for olefin polymerization, followed by the developments in ZN systems in the last sixty years. In this chapter, we have also discussed the main components of ZN systems

and their roles. The main components in ZN system are (i) the  $\text{MgCl}_2$  support, (ii) the active titanium species, (iii)  $\text{AlR}_3$  (where R = alkyl group such as ethyl), the trialkylaluminium, alkylating agent and (iv) the oxygen containing Lewis base “donors”. Then, we have discussed the different active sites of the titanium binding on the  $\text{MgCl}_2$  surface in ZN systems followed by the activation mechanism where we have shown how the inactive titanium catalyst converts into the active catalyst. In the next section, the Cossee-Arlman mechanism has been discussed in which we have shown how the olefin monomer converts into polymer.

## **Chapter 2**

In this chapter, we have discussed different theoretical methods that help to solve the Schrodinger equation. The chapter begins with a brief introduction of the many-body problem in which we have discussed the Börn-Oppenheimer approximation followed by density functional theory (DFT) as another means of solving the many particle Schrodinger equation. In DFT, a number of methods have been considered by different groups. These include the Thomas-Fermi model, Hohenberg-Kohn (HK) Theorems and the Kohn-Sham method. Furthermore, we have also discussed the different functionals, such as the local density approximation (LDA), generalized gradient approximation (GGA) and the hybrid functional, in order to improve the DFT results.

## **Chapter 3**

In this chapter, we have attempted to show that the principal role of donors in Ziegler-Natta (ZN) olefin polymerization catalysts is to coordinate to the metal center in the active sites on the  $\text{MgCl}_2$  surface and hence modulate the behavior of the catalyst to favor insertion over termination. For this study four different types of donor have been considered. The calculations indicate that active sites featuring anionic chloride ligands at the titanium center would lead to lower molecular weight polymers. It is shown that in the place of a chloride, if an  $\text{OC}_2\text{H}_5$  group were to be present instead, it would lead to an active site that would be much more effective at producing long chain polymers.

## Chapter 4

Discussed in this chapter are the unwanted side reactions, specifically, donor decomposition possibilities, in ZN systems. The decomposition of donors has been shown with two different Lewis acidic species (i) the triethylaluminium ( $\text{AlEt}_3$ ) and (ii) the titanium complex on the  $\text{MgCl}_2$  surface. The donor decomposition mechanism has been investigated through two different pathways: (i) ketone – in this pathway, the transfer of an ethide group occurs from triethylaluminium to the carbonyl carbon of the ester donor and (ii) aldehyde – transfer of hydride from the ethyl group of triethylaluminium to the carbonyl carbon of the ester donor (if the Lewis acidic species is  $\text{Al}_2\text{Et}_6$ ). To make the donor more robust and to reduce the possibility of donor decomposition, a modification in the silyl ester donor has been taken where the alkyl group ( $-\text{R}$ ) is replaced by more bulky alkyl groups.

## Chapter 5

In this chapter, we have shown the effect of donors on the activation mechanism in Ziegler-Natta (ZN) catalysis. In the activation mechanism, the inactive titanium catalyst converts into the active catalyst with the help of triethylaluminium ( $\text{AlEt}_3$ ), which is already present in the ZN system. The activation mechanism has been studied as a process occurring through two consecutive steps (i) Ti-Cl bond cleavage, and (ii) transalkylation, where the transfer of the ethide group from triethylaluminum to the titanium center has been considered. Furthermore, a donor displacement study has also been investigated, which would lead to the donor displacement product, the  $\text{AlEt}_3$ -donor. This  $\text{AlEt}_3$ -donor complex has also been studied for the activation mechanism as a separate donor.

## Chapter 6

In this chapter, we have shown an ethylene polymerization study with five different titanium catalysts on the (104) lateral cuts of the  $\text{MgCl}_2$  surface. The five catalysts are different due to the nature of the ethoxy (OEt) groups attached to the titanium center. The titanium based catalysts are:  $\text{Ti(III)Et(OR)(OR')}$  (where  $\text{R} = -\text{CH}_3, -\text{Et}, -\text{t-butyl}$ ,  $\text{R}' = -\text{CH}_3, -\text{Et}, -\text{t-butyl}$ ). Furthermore, for some catalyst cases, the olefin polymerization study have been done on the (110) as well as the (104)  $\text{MgCl}_2$  surface, in order to compare the surface effect on the olefin polymerization process. It was observed that the (104) surface was as important as the (110)  $\text{MgCl}_2$  surface for olefin polymerization, for the case of ethoxy containing ZN catalysts.

## Abbreviations

AIMD	Ab initio molecular dynamics
BOMD	Börn-Oppenheimer Molecular Dynamics
BP	Becke and Perdew
CC	Coupled cluster
CI	Configuration interaction
COSMO	conductor-like screening model
CPMD	Car-Parrinello molecular dynamics
DFT	Density functional theory
E	Electronic energy
<i>eb</i>	ethylbenzoate
ECP	Effective core potential
Et	Ethyl group
fcc	Face centered cubic
G	Gibbs free energy
GC-MS	Gas Chromatography Mass Spectrometry
GGA	Gradient corrected approximation
HOMO	Highest occupied molecular orbital
kcal	kilocalorie
LDA	Local density approximation
LUMO	Lowest occupied molecular orbital
marij	Multipole accelerated resolution of identity
MD	Molecular Dynamics
Me	Methyl group
MP	Møller-Plesset
NBO	Natural Bond Orbital
PBE	Perdew, Becke, and Ernzerhof
PW	Perdew and Wang
<i>peeb</i>	<i>p</i> -ethoxyethylbenzoate
PES	Photoelectron spectroscopy

pipeb	<i>p</i> -isopropoxyethylbenzoate
R	alkyl group
RI	Resolution of Identity
SOMO	Singly occupied molecular orbital
THF	Tetrahydrofurane
TZVP	Triple Zeta Valance Polarization
<i>teal</i>	Triethylaluminium
<i>t</i> -butyl	Tertiarybutyl
ZN	Ziegler Natta
ZNC	Ziegler Natta catalyst

## List of Publications

1. **Jugal Kumawat**, Virendra Kumar Gupta, and Kumar Vanka. The Nature of the Active Site in Ziegler–Natta Olefin Polymerization Catalysis Systems – A Computational Investigation. *Eur. J. Inorg. Chem.* **2014**, 5063–5076.
2. **Jugal Kumawat**, Virendra Kumar Gupta, and Kumar Vanka. Donor Decomposition by Lewis Acids in Ziegler–Natta Catalyst Systems: A Computational Investigation. *Organometallics* **2014**, 33, 4357–4367.
3. **Jugal Kumawat**, Virendra Kumar Gupta, and Kumar Vanka. Effect of Donors on the Activation Mechanism in Ziegler–Natta Catalysis: A Computational Study. *ChemCatChem* **2016**, 8, 1809–1818.
4. **Jugal Kumawat**, Virendra Kumar Gupta and Kumar Vanka. Ethylene Polymerization on the (110) and (104) lateral cuts of the MgCl<sub>2</sub> Surface with Ethoxy Ligand Containing Titanium Complexes in Ziegler-Natta Catalysis: A Computational Study. (*Manuscript Communicated*).



# **Chapter 1**

## **Introduction**

## 1.1 Introduction

Polymers are materials that are essential for our day-to-day existence. There are a number of catalyst systems that produce polymers in the form of plastics, rubbers and elastomers. Among them, the Ziegler-Natta (ZN) catalyst is one of the most important industrial catalysts for the commercial production of polyolefins. In 1953, the discovery of ZN catalysis was a major breakthrough for the polymer industry. Since then, several experimental<sup>1-46</sup> and theoretical<sup>4,47-73</sup> studies have been done in order to understand and improve ZN catalysis. But, despite their huge importance and impact, ZN catalyst systems have not been fully understood till today. The multi-site, heterogeneous ZN catalysis process is responsible, in part, for this, but what has also contributed is the complexity of the system, which contains the  $MgCl_2$  support, the active titanium species, usually present in the (III)<sup>49,51</sup> or (II)<sup>74</sup> oxidation state,  $AlR_3$  (where R = alkyl group such as ethyl): the trialkylaluminium, alkylating agent, the substrate olefin monomer, and also oxygen containing Lewis bases that act as donors: “internal” (donors such as ethylbenzoate (*eb*)<sup>75</sup>, diether<sup>3,14,18,19,49,76-78</sup>, alkoxy silane<sup>79</sup>, diisobutylphthalate<sup>2,22</sup> and succinate<sup>79</sup>) if added during the catalyst preparation, or “external” (donors such as alkoxy silane<sup>2,80</sup> and *p*-ethoxyethylbenzoate (*peeb*)<sup>18</sup>) if added after the catalyst preparation or with  $AlR_3$ . The addition of such donors has led to the improvement in the activity and selectivity of ZN systems.

## 1.2 Development in ZN catalysis

The evolution of ZN catalysis since the eighties has involved the active participation of donors.<sup>81</sup> In particular, the fourth and the fifth generations where electron donors had been introduced in the system led to considerable improvement in ZN catalysis. In the third generation, the catalyst contained the ethyl benzoate (*eb*) as an internal donor with a different aromatic ester donor behaving as the external donor,<sup>82</sup> but after that, the catalyst widely used for polypropylene production contained diisobutylphthalates or other phthalates as the internal donor and the silylethers as the external donor (the fourth generation). Since then, numerous studies have been carried out where different electron donors were considered. These include phthalate, succinate, 1,3 diether, glutaric acid, cycloalkyl ester and 1,4-diol. Presently, catalysts

using 1,3 diether and succinate have been commercialized. In the fifth generation, the catalysts contain a diether (typically a 2,2-disubstituted-1,3-dimethoxypropane) and have high stereospecificity even in the absence of an external donor.<sup>83</sup> Subsequently, a new catalyst was reported having a phthalate as an internal donor and 1,3 diether as an external donor. This catalyst provided the same activity and hydrogen response in comparison to earlier catalysts where diether had been employed as the internal donor. The performance of the catalysts has improved significantly in each generation in the ZN catalyst system. The polypropylene yield obtained in particular polymerization conditions (liquid monomer, in the presence of hydrogen, 70°C, 1–2 h), increased from 15 – 30 kg/g cat. (third generation) to 30 – 80 kg/g cat. (fourth generation) to 80 – 160 kg/g cat. (fifth generation).

### 1.3 Catalyst Support and Active Sites for $\text{TiCl}_4$

Since it is a heterogeneous system, ZN systems require a support for the catalyst. In 1953, when ZN catalyst had just been just discovered, the titanium surface ( $\alpha\text{TiCl}_3$ ) was the one employed for the catalyst support for the olefin polymerization. In the early 1970s, a major breakthrough was achieved when the  $\text{MgCl}_2$  support was found to be an effective replacement of  $\alpha\text{TiCl}_3$  in the ZN systems, and helped in improving the catalyst activity and selectivity for propylene polymerization. Till date, several  $\text{MgCl}_2$  model systems have been employed by different groups<sup>49,52,84,85</sup> in order to understand the role of each lateral cut (mainly, 110 and 104) of the  $\text{MgCl}_2$  surface and to develop better sites for the titanium binding. The most commonly observed lateral cuts on the  $\text{MgCl}_2$  surface are four and five-coordinate. The four-coordinated magnesium atom belongs to (110) and the five coordinated magnesium atom belongs to the (104) and the (100) surfaces. It is to be noted that experimental studies<sup>44</sup> suggest that the majority of the  $\text{MgCl}_2$  surface has five coordinated (104) lateral cuts, with the four coordinated (110)  $\text{MgCl}_2$  lateral cuts found to make up a minor portion of the available  $\text{MgCl}_2$  surface. The absorption of  $\text{TiCl}_4$  on the (110)  $\text{MgCl}_2$  surface is energetically more favorable in comparison to the (100) and the (104)  $\text{MgCl}_2$  surface<sup>65,71,86</sup>. The binding of  $\text{TiCl}_4$  to the  $\text{MgCl}_2$  surface through Ti-Cl and Cl-Mg bonds decides the possible active site in ZN catalysis. The active sites that are present in the ZN are (i) the Corradini site, (ii) the edge site and (iii) the slope site. The

Corradini site involves the four coordinate magnesium atom (110), where the titanium atom is bound to the  $\text{MgCl}_2$  surface through two bridging and two surface chlorine atoms. In the edge site, titanium is bound to the (110) surface through two bridging chlorine atoms to a single magnesium atom and a surface chlorine atom. In the Corradini site, the titanium has two bridging and two surface chlorine atoms, making it five coordinate. It has only one vacancy for the monomer and donor coordination. The binding of an electron donor to the titanium center (Corradini site) would lead to the poisoning of the catalyst active site. The poisoning of this Corradini site with the phthalate donor has been reported by Boero and coworkers<sup>59</sup>. However, in case of the edge and slope sites (as shown in Figure 1), both have four coordinate species, where two vacancies are available for the monomer and donor. In the slope site, the titanium atom is bound to the five coordinate (100) or (104) magnesium surface through two bridging chlorine atoms and a surface chlorine atom. Although the titanium is added to the  $\text{MgCl}_2$  surface in the form of  $\text{TiCl}_4$ , there are several experimental studies<sup>74,87-89</sup> indicating that after the reaction with trialkylaluminum, the titanium may be present in the +4, +3, and in the +2 oxidation states. In Figure 1, the titanium is present in the +3 oxidation state for all three sites.

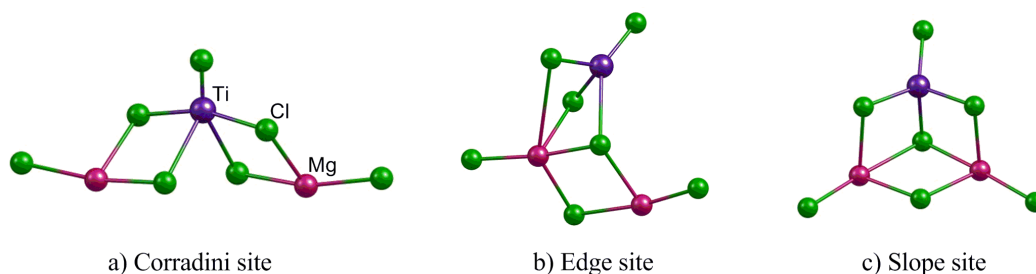


Figure 1. Different active sites present in the ZN catalyst, a) Corradini, b) edge and c) slope.

The titanium tetrachloride complex may form the dimer on the  $\text{MgCl}_2$  surfaces<sup>86,90-94</sup>. There are also computational studies that have shown that the dimerization of the titanium tetrachloride complex on the  $\text{MgCl}_2$  surface is more favorable in comparison to the mononuclear complex<sup>90</sup>. However, there is another group that has shown the opposite result - that mononuclear binding is more favorable<sup>95</sup>. The formation of a mononuclear species from the binuclear during binding to the surface has been shown by Martinsky and workers<sup>96</sup>.

## 1.4 Lewis Bases “Donor” and its Role in ZN system

In the 1980s, the oxygen containing Lewis base “donor” became one of the most important components in the ZN systems. Figure 2 shows the different classes of oxygen containing donors that have been employed since then. It has been postulated that the role of internal and external donors is to sit beside the titanium center on the  $\text{MgCl}_2$  surface and thereby influence the ZN catalysis. The role of internal and the external donors are as follows:

Internal donors:

- prevent the coagulation of  $\text{MgCl}_2$  molecules during the milling process, therefore, increase the effective surface.
- help to increase the isospecific sites.
- prevent the formation of non-isospecific sites on the  $\text{MgCl}_2$  surface by absorbing on it whereas the  $\text{TiCl}_4$  is supposed to form non-isospecific sites.
- help in the formation of more isospecific sites by replacing the external donor.

External donors

- change a non-stereospecific site into a highly isospecific site
- change an isospecific site into a more highly isospecific site
- poison a non-stereospecific site
- replace the internal donor to form a more isospecific site

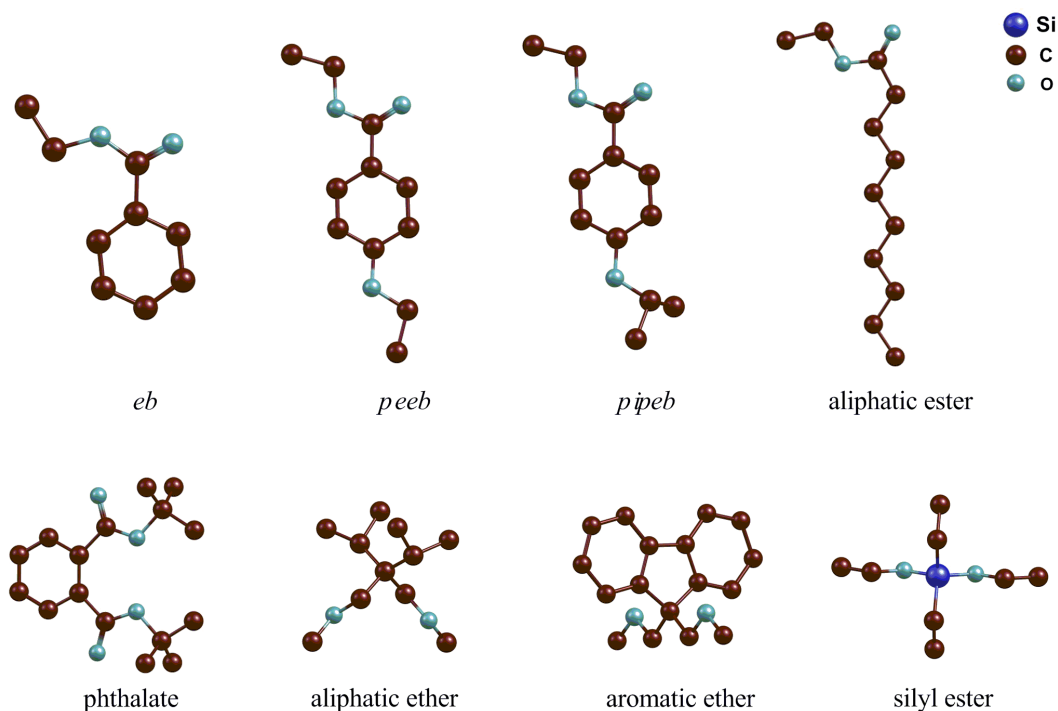


Figure 2. Different classes of donors that have been used in  $\text{MgCl}_2$  supported Ziegler-Natta catalysis.

The binding of donors on the  $\text{MgCl}_2$  support is very important in terms of stability of the surface and stereoregularity of the polymer. There are four types of coordination that are possible between donors and the  $\text{MgCl}_2$  support (here, as seen in Figure 3, we are taking the example of diisobutyl phthalate donor binding to the  $\text{MgCl}_2$  surface to show all the binding possibilities.): a) mono coordination: one oxygen atom of the donor molecule coordinated to one magnesium atom, b) chelate coordination: two oxygen atoms of the donor coordinated to one magnesium atom. c) bridge coordination: two oxygen atoms of the donor molecule coordinated to two magnesium atoms on the same layer, and d) zip coordination: two oxygen atoms of the donor molecule coordinated to two magnesium atoms in adjacent layers. Figure 3 shows the four different binding modes.

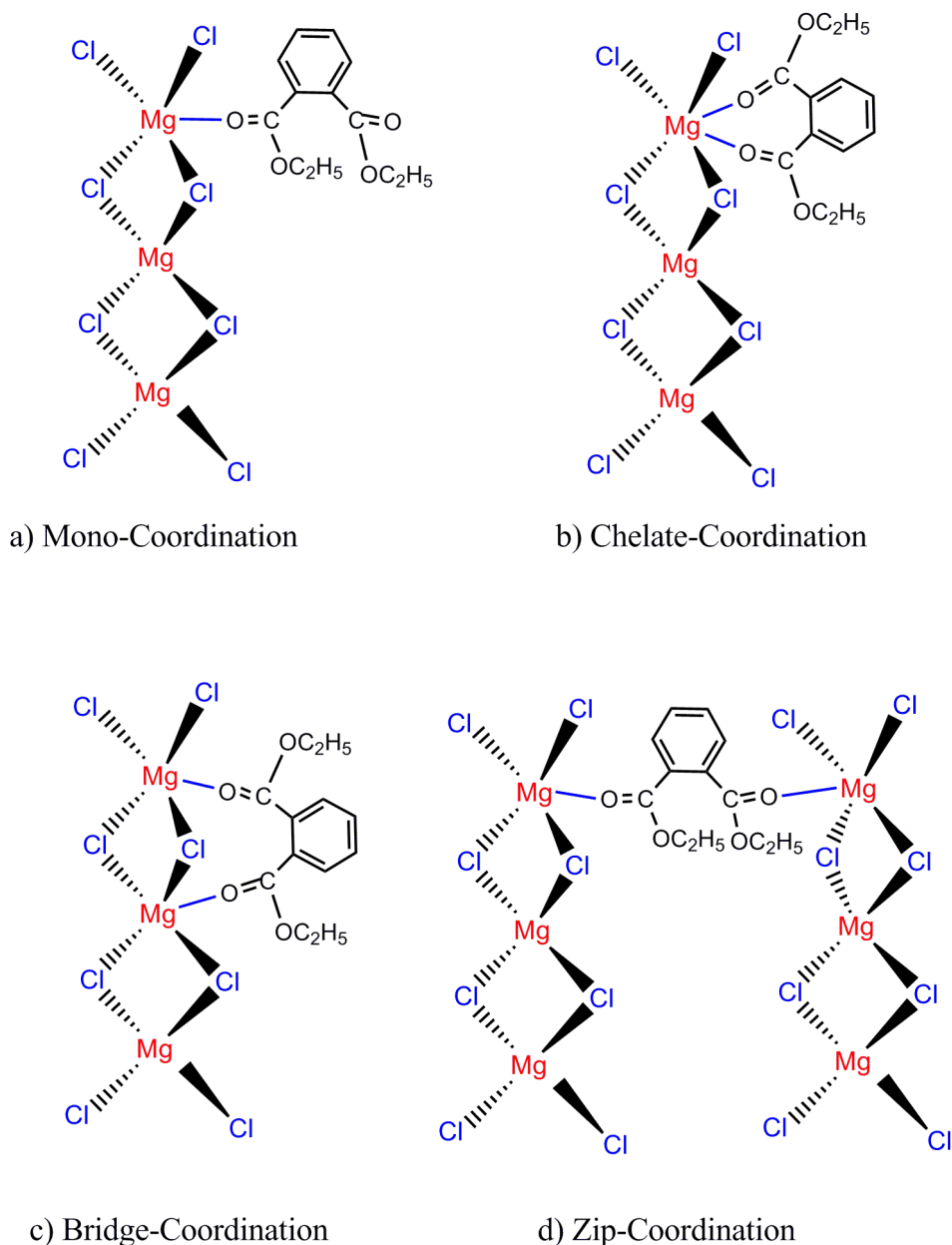


Figure 3. The four different binding modes of the phthalate donor to the  $\text{MgCl}_2$  surface.

### 1.5 Activation of $\text{TiCl}_4$ and Donor Displacement

The absorption of the catalyst precursor,  $\text{Ti}^{(\text{IV})}\text{Cl}_4$ , on the  $\text{MgCl}_2$  surface leads to the active catalyst,  $\text{Ti}^{(\text{III})}\text{Cl}_2\text{R}$ , and this active catalyst may further undergo reduction to form the  $\text{Ti}^{(\text{II})}$  species. The  $\text{AlR}_3$  (R = alkyl group) species is important for both these conversions. For the ethylene monomer case, titanium in (III)<sup>49,51,84,85</sup> and (II)<sup>74</sup>

oxidation states are seen to be active catalysts for polymerization but for propylene polymerization, only the titanium in the (III) oxidation states is the active catalyst. However, there is still a significant lack of understanding of the nature of the activation mechanism in the Z-N systems: of how the catalyst precursor - the  $\text{Ti}^{(\text{IV})}\text{Cl}_4$ , is converted into the  $\text{Ti}^{(\text{III})}\text{Cl}_2\text{R}$  species. This activation mechanism has been investigated in computational studies done by the groups of Zakharov<sup>97</sup> and Cavallo<sup>50</sup> (in the activation mechanism, the inactive catalyst,  $\text{Ti}^{(\text{IV})}\text{Cl}_4$ , converts into the active catalyst,  $\text{Ti}^{(\text{III})}\text{Cl}_2\text{R}$ , with the help of the  $\text{AlR}_3$  moiety which is already present in the system). Zakharov and coworkers<sup>97</sup> have studied the four membered transition states, involving the titanium complex and tri-ethyl aluminium,  $\text{AlEt}_3$ , where an alkyl group is transferred from the aluminium to the titanium center, leading to the formation of the Ti-C bond through the trans-alkylation mechanism. The transition states have been approximated in their studies through the linear scan of the potential energy surface. In 2011, Cavallo *et al.*<sup>50</sup> have reported the systematic study of the possible activation mechanism by considering two consecutive steps: (i) the Ti-Cl bond cleavage and (ii) the transalkylation step, where the transfer of one ethyl group from the aluminium to the titanium center has been considered (see Figure 4).

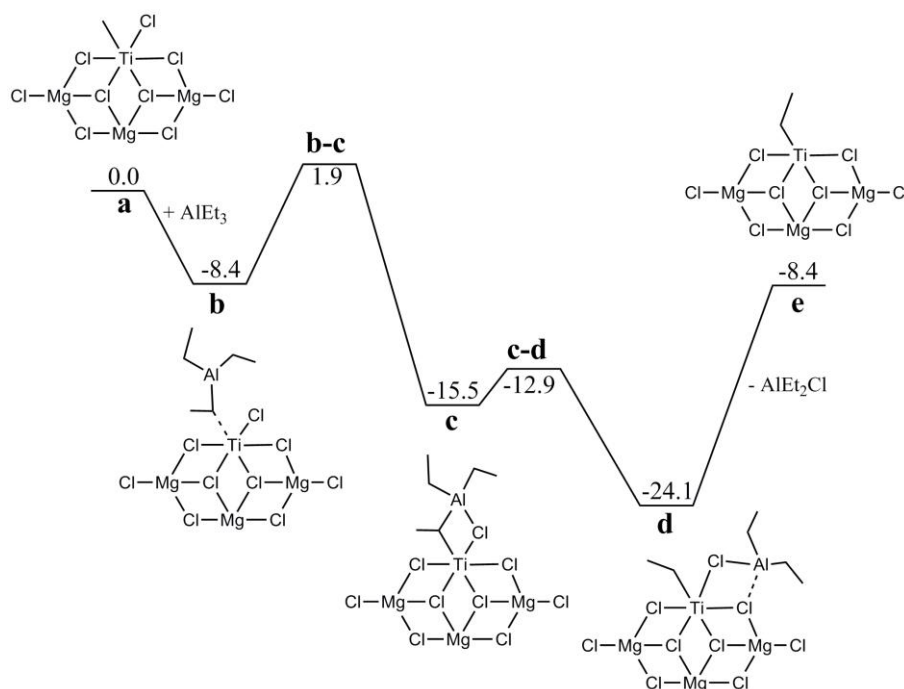


Figure 4. The energy profile ( $\Delta E$  in kcal/mol) of the direct transalkylation reaction on the (110)  $\text{MgCl}_2$  layer.



The effect of the donors on the olefin polymerization reaction has been studied by several groups and it has been seen that the donor significantly improves the catalyst activity and the selectivity of the polypropylene. In this study, Cavallo and coworkers did not take into account the effect of the donors in the activation mechanism.

Later on, Vanka and coworkers reported the effect of different classes of oxygen containing donors on the activation mechanism. Furthermore, the same group has also studied donor displacement from the (110)  $\text{MgCl}_2$  surface upon contact with the triethylaluminium cocatalyst, which leads to the  $\text{AlEt}_3$ -donor complex as a product. This complex,  $\text{AlEt}_3$ -donor, was also studied for the activation mechanism as a separate donor.

It has been reported<sup>99</sup> that the 1,3 diethers have the greatest stereoregulating effect because diethers have strong binding on the (110) rather than the (100) lateral cuts of the  $\text{MgCl}_2$  surface. Systems where the internal donor is diether show high isospecificity even in the absence of the external donor, due to the fact that the diether donors are not displaced from the  $\text{MgCl}_2$  surface on contact with the trialkylaluminium cocatalyst. In the case of catalysts in which the internal donor is ethylbenzoate (eb) or diisobutyl phthalate, a large number of donors are displaced during the reaction with the trialkylaluminium cocatalyst.

## 1.6 The Cossee-Arlman mechanism

In ZN systems, an important question is how the monomer forms the polymer with the help of the titanium catalyst and triethylaluminium. In 1964, Cossee and Arlman solved this mystery and came up with a mechanism that explains the reaction pathway of olefin polymerization. Henceforth, this mechanism will be known as the Cossee-Arlman mechanism<sup>12,13</sup>. Among of all the mechanisms (Cossee-Arlman, Green-Rooney and Rooney-Brookhart), Cossee-Arlman is the most commonly accepted mechanism in ZN systems (see Figure 5). It is assumed that the chloride ligands in titanium are replaced by the ethyl group through the mediation of the activator (triethylaluminium) and leads to the active catalyst consisting of a Ti-C bond and one vacancy. As mentioned above, several groups<sup>50,97,98</sup> have also later explained this conversion in a similar fashion. The  $\alpha$ -olefin monomer binds on the vacant site and

forms the  $\pi$ -complex on the titanium center followed by chain migratory insertion into Ti–C bond, which leads to an increase in the carbon atoms in the polymer chain (see Figure 5) and the same isomerization happens again and again, which leads to an increase in the carbon chain length. For the chain migratory insertion step, a four membered transition state is formed. It has also been observed that the stability of the reactant and the product of the olefin polymerization reaction also depends upon the  $\alpha$  and  $\beta$  agostic interactions (hydrogen of the  $\alpha$  or  $\beta$  carbon in the chain to the titanium center).

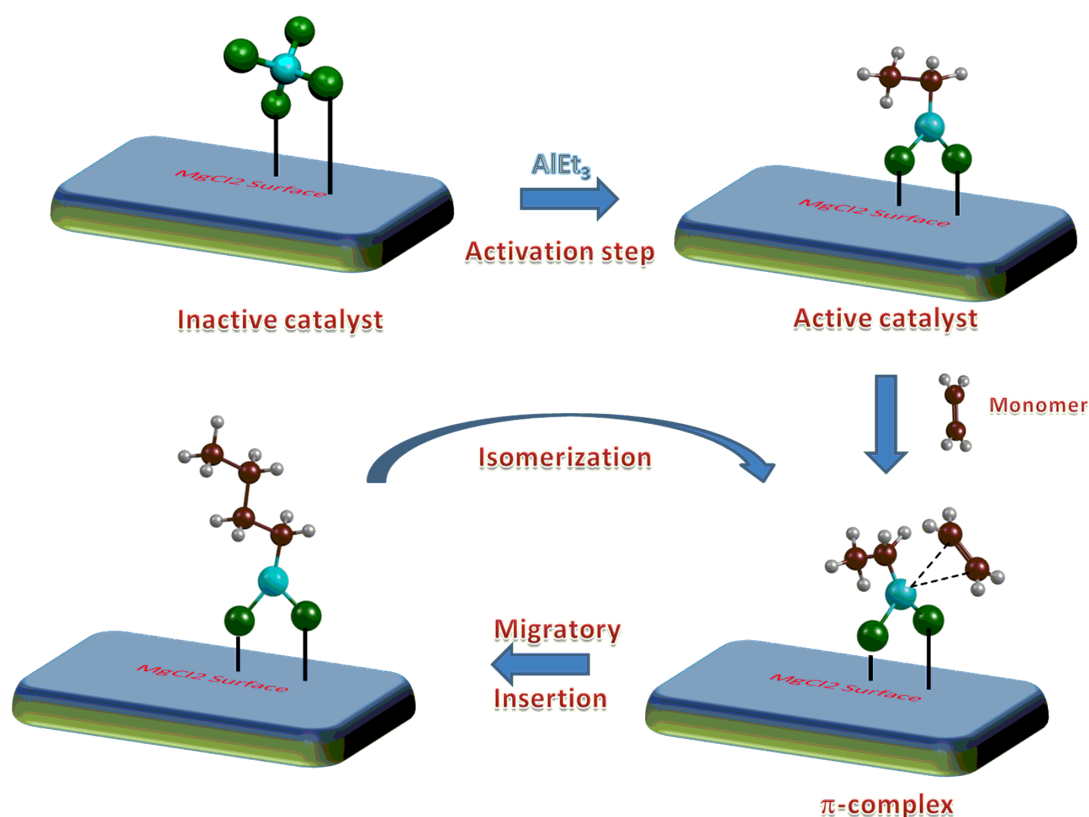


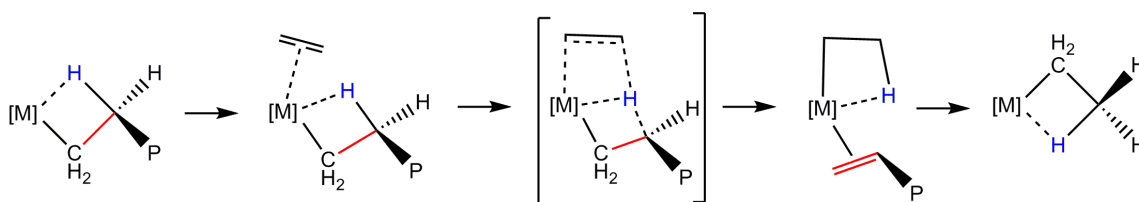
Figure 5. The Cossee-Arlman mechanism<sup>12,13</sup> for olefin polymerization in ZN catalysis.

## 1.7 Chain Termination and Chain Transfer Steps

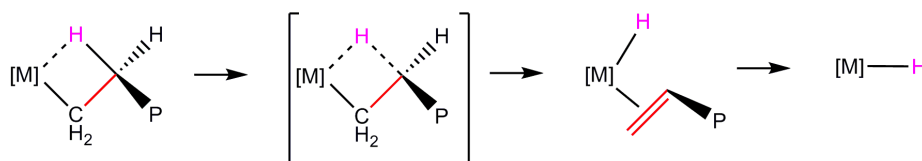
Termination is a process by which the carbon chain gets terminated from the titanium catalyst. In the ZN system, four different types of termination processes are possible. These are as follows – a)  $\beta$ -H transfer to monomer, b)  $\beta$ -H elimination, c) chain

transfer to aluminium, and d) hydrogen response (see Figure 6). For a), b) and c), chain termination processes are possible without any external influence but for d) – the hydrogen response case,  $H_2$  is added externally. This is the reason why hydrogen response is the best method to get the desired molecular weight of the polymer. Among all of the termination steps, the one competitive with the insertion step are a)  $\beta$ -H transfer to monomer, b)  $\beta$ -H elimination, c) chain transfer to aluminium.

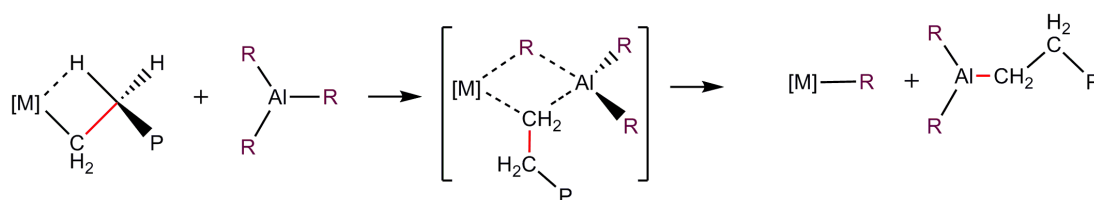
a)  $\beta$  Hydrogen Transfer to Monomer



b)  $\beta$  Hydrogen Transfer to Metal



c) Chain Transfer to Aluminium



d) Hydrogen Response

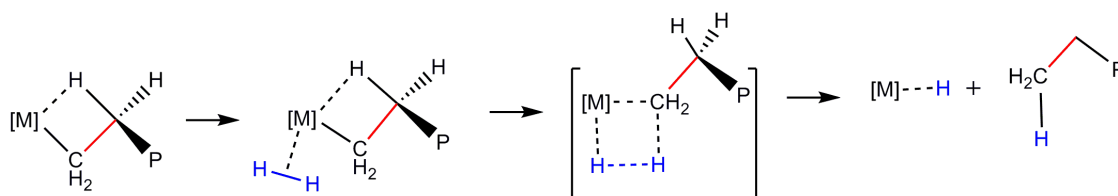


Figure 6. Different chain termination processes possible during the ZN olefin polymerization.

The molecular weight of the polymer depends upon the difference between the insertion and termination barriers ( $\Delta X$ ): if the  $\Delta X$  is large, then high molecular polymer will be formed and vice-versa. It has mentioned that the presence of the donor in the ZN catalyst systems increases the molecular weight of the polymer. It is assumed that donors increase the energy gap ( $\Delta X$ ), as agreed upon later by different groups.<sup>63,65,85</sup>

## 1.8 Conclusion Remarks

After numerous studies during the past six decades, the current status of ZN catalysis says that there still many unresolved questions that remain in this field which need to be clarified to understand the ZN catalysts fully. Although, as mentioned in the “Development in ZN Catalysis section”, enormous progress has been seen in ZN catalysis over the years. Owing to the multi-component nature of the system, it is very difficult to understand the workings of the ZN catalyst systems completely. Furthermore, a major issue in this field is not how much polymer is produced by this catalyst but how this produced polymer will be degraded, because every year tons of non-degradable (or difficult to degrade) products are being produced by ZN catalysts in the form of plastics, rubbers and elastomers. As is well accepted today, polymers are environmentally unfriendly because they are not easy to digest by living organisms and it therefore takes years and years to totally degrade. The next goal of the researcher would be to make such polymers that are environmentally friendly and easily degradable. However, seeing the progress in current ZN catalysis research, it might take years to even think about the catalyst that would produce the bio-degradable polymer.

## 1.9 References:

- (1) Grau, E.; Lesage, A.; Norsic, S. b.; Coperet, C.; Monteil, V.; Sautet, P. *ACS Catalysis* **2012**, *3*, 52-56.
- (2) Chadwick, J. C.; Van der Burgt, F. P. T. J.; Rastogi, S.; Busico, V.; Cipullo, R.; Talarico, G.; Heere, J. J. R. *Macromolecules* **2004**, *37*, 9722-9727.

- (3) Morini, G.; Albizzati, E.; Balbontin, G.; Mingozzi, I.; Sacchi, M. C.; Forlini, F.; Tritto, I. *Macromolecules* **1996**, *29*, 5770-5776.
- (4) Sacchi, M. C.; Forlini, F.; Tritto, I.; Locatelli, P.; Morini, G.; Noristi, L.; Albizzati, E. *Macromolecules* **1996**, *29*, 3341-3345.
- (5) Potapov, A. G.; Bukatov, G. D.; Zakharov, V. A. *Journal of Molecular Catalysis A: Chemical* **2010**, *316*, 95-99.
- (6) Wen, X.; Ji, M.; Yi, Q.; Niu, H.; Dong, J.-Y. *Journal of Applied Polymer Science* **2010**, *118*, 1853-1858.
- (7) Andoni, A.; Chadwick, J. C.; Niemantsverdriet, H. J. W.; Thuene, P. *C. J. Catal.* **2008**, *257*, 81-86.
- (8) Zhong, C.; Gao, M.; Mao, B. *Macromolecular Chemistry and Physics* **2005**, *206*, 404-409.
- (9) Shen, X.-r.; Fu, Z.-s.; Hu, J.; Wang, Q.; Fan, Z.-q. *The Journal of Physical Chemistry C* **2013**, *117*, 15174-15182.
- (10) Thushara, K. S.; Gnanakumar, E. S.; Mathew, R.; Jha, R. K.; Ajithkumar, T. G.; Rajamohanam, P. R.; Sarma, K.; Padmanabhan, S.; Bhaduri, S.; Gopinath, C. S. *The Journal of Physical Chemistry C* **2011**, *115*, 1952-1960.
- (11) Gnanakumar, E. S.; Thushara, K. S.; Bhange, D. S.; Mathew, R.; Ajithkumar, T. G.; Rajamohanam, P. R.; Bhaduri, S.; Gopinath, C. S. *Dalton Transactions* **2011**, *40*, 10936-10944.
- (12) Arlman, E. J.; Cossee, P. *Journal of Catalysis* **1964**, *3*, 99-104.
- (13) Cossee, P. *J. Catal.* **1964**, *3*, 80-8.
- (14) Coutinho, F. B.; Costa, M. S.; Santa Maria, L. *Polymer Bulletin* **1992**, *28*, 55-59.
- (15) Baba, Y. *Bulletin of the Chemical Society of Japan* **1968**, *41*, 1022-1023.
- (16) Baba, Y. *Bulletin of the Chemical Society of Japan* **1968**, *41*, 1020-1021.
- (17) Xu, S.; Feng, Z.-F.; Huang, J.-L. *Journal of Molecular Catalysis A: Chemical* **2006**, *250*, 35-39.
- (18) Chadwick, J. C. *Macromol. Symp.* **2001**, *173*, 21-35.
- (19) Cui, N.; Ke, Y.; Li, H.; Zhang, Z.; Guo, C.; Lv, Z.; Hu, Y. *Journal of Applied Polymer Science* **2006**, *99*, 1399-1404.

- (20) Xu, D.; Liu, Z.; Zhao, J.; Han, S.; Hu, Y. *Macromolecular Rapid Communications* **2000**, *21*, 1046-1049.
- (21) Kissin, Y. V.; Rishina, L. A.; Vizen, E. I. *J. Polym. Sci., Part A: Polym. Chem.* **2002**, *40*, 1899-1911.
- (22) Kissin, Y. V.; Rishina, L. A. *J. Polym. Sci., Part A: Polym. Chem.* **2002**, *40*, 1353-1365.
- (23) Kissin, Y. V.; Mink, R. I.; Nowlin, T. E.; Brandolini, A. J. *Top. Catal.* **1999**, *7*, 69-88.
- (24) Kissin, Y. V.; Mink, R. I.; Nowlin, T. E.; Brandolini, A. J. *J. Polym. Sci., Part A: Polym. Chem.* **1999**, *37*, 4281-4294.
- (25) Kissin, Y. V. *Journal of Catalysis* **2012**, *292*, 188-200.
- (26) Panchenko, V. N.; Goryachev, A. N.; Vorontsova, L. V.; Paukshtis, E. A.; Zakharov, V. A. *The Journal of Physical Chemistry C* **2014**, *118*, 28572-28579.
- (27) Chirinos, J.; Fernandez, J.; Perez, D.; Rajmankina, T.; Parada, A. *Journal of Molecular Catalysis A: Chemical* **2005**, *231*, 123-127.
- (28) Chadwick, J. C.; Morini, G.; Balbontin, G.; Camurati, I.; Heere, J. J. R.; Mingozzi, I.; Testoni, F. *Macromolecular Chemistry and Physics* **2001**, *202*, 1995-2002.
- (29) Soga, K.; Shiono, T.; Doi, Y. *Die Makromolekulare Chemie* **1988**, *189*, 1531-1541.
- (30) Vähäsarja, E.; Pakkanen, T. T.; Pakkanen, T. A.; Iiskola, E.; Sormunen, P. *Journal of Polymer Science Part A: Polymer Chemistry* **1987**, *25*, 3241-3253.
- (31) Koo, K.; Marks, T. J. *Journal of the American Chemical Society* **1999**, *121*, 8791-8802.
- (32) Chien, J. C. W.; Wu, J.-C. *Journal of Polymer Science: Polymer Chemistry Edition* **1982**, *20*, 2461-2476.
- (33) Chien, J. C. W.; Wu, J.-C. *Journal of Polymer Science: Polymer Chemistry Edition* **1982**, *20*, 2445-2460.
- (34) Corradini, P.; Guerra, G.; Cavallo, L. *Acc. Chem. Res.* **2004**, *37*, 231-241.
- (35) Sergeev, S. A.; Bukatov, G. D.; Zakharov, V. A. *Die Makromolekulare Chemie* **1984**, *185*, 2377-2385.

- (36) Huang, Y.; Qin, Y.; Zhou, Y.; Niu, H.; Yu, Z.-Z.; Dong, J.-Y. *Chemistry of Materials* **2010**, *22*, 4096-4102.
- (37) Kvashina, E. F.; Efimov, O. N.; Chapysheva, N. V.; Roshchupkina, O. *S. Russian Chemical Bulletin* **2007**, *56*, 2115-2117.
- (38) Kvashina, E. F.; Dzhabieva, Z. M.; Efimov, O. N.; Kaplunov, M. G. *Russian Chemical Bulletin* **2009**, *58*, 1669-1671.
- (39) Pakkanen, T. T.; Vahasarja, E.; Pakkanen, T. A.; Iiskola, E.; Sormunen, P. *Journal of Catalysis* **1990**, *121*, 248-261.
- (40) Corradini, P.; Guerra, G.; Pucciariello, R. *Macromolecules* **1985**, *18*, 2030-2034.
- (41) Singh, G.; Kaur, S.; Makwana, U.; Patankar, R. B.; Gupta, V. K. *Macromolecular Chemistry and Physics* **2009**, *210*, 69-76.
- (42) Stukalov, D. V.; Zakharov, V. A.; Potapov, A. G.; Bukatov, G. D. *J. Catal.* **2009**, *266*, 39-49.
- (43) Ribour, D.; Monteil, V.; Spitz, R. *J. Polym. Sci., Part A Polym. Chem.* **2008**, *46*, 5461-5470.
- (44) Busico, V.; Causa, M.; Cipullo, R.; Credendino, R.; Cutillo, F.; Friederichs, N.; Lamanna, R.; Segre, A.; Van Axel Castelli, V. *The Journal of Physical Chemistry C* **2008**, *112*, 1081-1089.
- (45) Brambilla, L.; Zerbi, G.; Piemontesi, F.; Nascetti, S.; Morini, G. *J. Mol. Catal. A Chem.* **2007**, *263*, 103-111.
- (46) Brambilla, L.; Zerbi, G.; Piemontesi, F.; Nascetti, S.; Morini, G. *The Journal of Physical Chemistry C* **2010**, *114*, 11475-11484.
- (47) Cavallo, L.; Del Piero, S.; Ducere, J.-M.; Fedele, R.; Melchior, A.; Morini, G.; Piemontesi, F.; Tolazzi, M. *The Journal of Physical Chemistry C* **2007**, *111*, 4412-4419.
- (48) Cavallo, L.; Guerra, G.; Corradini, P. *J. Am. Chem. Soc.* **1998**, *120*, 2428-2436.
- (49) Correa, A.; Credendino, R.; Pater, J. T. M.; Morini, G.; Cavallo, L. *Macromolecules* **2012**, *45*, 3695-3701.
- (50) Bahri-Laleh, N.; Correa, A.; Mehdipour-Ataei, S.; Arabi, H.; Haghghi, M. N.; Zohuri, G.; Cavallo, L. *Macromolecules* **2011**, *44*, 778-783.
- (51) Correa, A.; Piemontesi, F.; Morini, G.; Cavallo, L. *Macromolecules (Washington, DC, U. S.)* **2007**, *40*, 9181-9189.

- (52) Credendino, R.; Liguori, D.; Fan, Z.; Morini, G.; Cavallo, L. *ACS Catalysis* **2015**, *5*, 5431-5435.
- (53) Credendino, R.; Liguori, D.; Morini, G.; Cavallo, L. *The Journal of Physical Chemistry C* **2014**, *118*, 8050-8058.
- (54) Credendino, R.; Pater, J. T. M.; Liguori, D.; Morini, G.; Cavallo, L. *The Journal of Physical Chemistry C* **2012**, *116*, 22980-22986.
- (55) Stukalov, D. V.; Zakharov, V. A.; Zilberberg, I. L. *The Journal of Physical Chemistry C* **2010**, *114*, 429-435.
- (56) Ghorbani, N.; Mahdizadeh Ghohe, N.; Torabi, S.; Yates, B. F.; Ariafard, A. *Organometallics* **2013**, *32*, 1687-1693.
- (57) Flisak, Z.; Spaleniak, G. P.; Bremmek, M. *Organometallics* **2013**, *32*, 3870-3876.
- (58) Barino, L.; Scordamaglia, R. *Macromolecular Symposia* **1995**, *89*, 101-111.
- (59) Boero, M.; Parrinello, M.; Weiss, H.; Häfner, S. *The Journal of Physical Chemistry A* **2001**, *105*, 5096-5105.
- (60) Correa, A.; Bahri-Laleh, N.; Cavallo, L. *Macromolecular Chemistry and Physics* **2013**, *214*, 1980-1989.
- (61) Ferreira, M. I. a. L. n.; Damiani, D. E. *Journal of Molecular Catalysis A: Chemical* **1999**, *150*, 53-69.
- (62) Wondimagegn, T.; Ziegler, T. *The Journal of Physical Chemistry C* **2012**, *116*, 1027-1033.
- (63) Seth, M.; Ziegler, T. *Macromolecules* **2003**, *36*, 6613-6623.
- (64) Seth, M.; Ziegler, T. *Macromolecules* **2004**, *37*, 9191-9200.
- (65) Seth, M.; Margl, P. M.; Ziegler, T. *Macromolecules* **2002**, *35*, 7815-7829.
- (66) Taniike, T.; Terano, M. *Macromol. Chem. Phys.* **2009**, *210*, 2188-2193.
- (67) Flisak, Z. *Macromolecules (Washington, DC, U. S.)* **2008**, *41*, 6920-6924.
- (68) Trubitsyn, D. A.; Zakharov, V. A.; Zakharov, I. I. *J. Mol. Catal. A Chem.* **2007**, *270*, 164-170.
- (69) Taniike, T.; Terano, M. *Macromol. Symp.* **2007**, *260*, 98-106.



- (70) Mukhopadhyay, S.; Kulkarni, S. A.; Bhaduri, S. *Journal of Organometallic Chemistry* **2005**, *690*, 1356-1365.
- (71) Boero, M.; Parrinello, M.; Weiss, H.; Hueffer, S. *J. Phys. Chem. A* **2001**, *105*, 5096-5105.
- (72) Boero, M.; Parrinello, M.; Hueffer, S.; Weiss, H. *J. Am. Chem. Soc.* **2000**, *122*, 501-509.
- (73) Toto, M.; Morini, G.; Guerra, G.; Corradini, P.; Cavallo, L. *Macromolecules* **2000**, *33*, 1134-1140.
- (74) Kashiwa, N.; Yoshitake, J. *Die Makromolekulare Chemie* **1984**, *185*, 1133-1138.
- (75) Potapov, A. G.; Bukatov, G. D.; Zakharov, V. A. *J. Mol. Catal. A Chem.* **2006**, *246*, 248-254.
- (76) Vittadello, M.; Stallworth, P. E.; Alamgir, F. M.; Suarez, S.; Abbrent, S.; Drain, C. M.; Di Noto, V.; Greenbaum, S. G. *Inorg. Chim. Acta* **2006**, *359*, 2513-2518.
- (77) Andoni, A.; Chadwick, J. C.; Niemantsverdriet, H.; Thuene, P. C. *Macromol. Symp.* **2007**, *260*, 140-146.
- (78) Sacchi, M. C.; Forlini, F.; Tritto, I.; Locatelli, P. *Macromolecular Symposia* **1995**, *89*, 91-100.
- (79) Correa, A.; Credendino, R.; Pater, J. T. M.; Morini, G.; Cavallo, L. *Macromolecules*, *45*, 3695-3701.
- (80) Kissin, Y. V. *Macromolecular Symposia* **1995**, *89*, 113-123.
- (81) Albizzati, E.; Giannini, G.; Noristi, C. L.; Resconi, L. *In polypropylene Handbook*, Pihlipsis, R. A., Wolkowicz, M. D., Moore, E.P, Eds. Hanser: New York **1996**, Chapter 2, 12 - 13.
- (82) Barbe, P. C.; Cecchin, G.; Noristi, L. *adv. polym. sci* **1987**, *81*, 1.
- (83) Albizzati, E.; Giannini, U.; Morini, G.; Galimberti, M.; Barino, L.; Scordamaglia, R. *Macromolecular Symposia* **1995**, *89*, 73-89.
- (84) Kumawat, J.; Gupta, V. K.; Vanka, K. *Organometallics* **2014**, *33*, 4357-4367.
- (85) Kumawat, J.; Kumar Gupta, V.; Vanka, K. *European Journal of Inorganic Chemistry* **2014**, *2014*, 5063-5076.
- (86) Monaco, G.; Toto, M.; Guerra, G.; Corradini, P.; Cavallo, L. *Macromolecules* **2000**, *33*, 8953-8962.

- (87) Zakharov, V. A.; Makhtarulin, S. I.; Poluboyarov, V. A.; Anufrienko, V. F. *Die Makromolekulare Chemie* **1984**, *185*, 1781-1793.
- (88) Brant, P.; Speca, A. N. *Macromolecules* **1987**, *20*, 2740-2744.
- (89) Magni, E.; Somorjai, G. A. *Catalysis Letters* **1995**, *35*, 205-214.
- (90) Stukalov, D. V.; Zilberberg, I. L.; Zakharov, V. A. *Macromolecules* **2009**, *42*, 8165-8171.
- (91) Taniike, T.; Terano, M. *Macromol. Rapid Commun.* **2008**, *29*, 1472-1476.
- (92) Lee, J. W.; Jo, W. H. *J. Organomet. Chem.* **2009**, *694*, 3076-3083.
- (93) Brambilla, L.; Zerbi, G.; Piemontesi, F.; Nascetti, S.; Morini, G. *Journal of Molecular Catalysis A: Chemical* **2007**, *263*, 103-111.
- (94) Martinsky, C.; Minot, C. *Surface Science* **2000**, *467*, 152-168.
- (95) Boero, M.; Parrinello, M.; Terakura, K.; Weiss, H. *Molecular Physics* **2002**, *100*, 2935-2940.
- (96) Martinsky, C.; Minot, C.; Ricart, J. M. *Surface Science* **2001**, *490*, 237-250.
- (97) Stukalov, D. V.; Zakharov, V. A. *The Journal of Physical Chemistry C* **2009**, *113*, 21376-21382.
- (98) Kumawat, J.; Gupta, V. K.; Vanka, K. *ChemCatChem* **2016**, *8*, 1809-1818.
- (99) Barino, L.; Scordamaglia, R. *Macromol. Theory Simul.* **1998**, *7*, 407-419.

# Chapter 2

## Abstract

Over the years, many methods have been developed in order to determine the energy of a many-body system. This is because the many-body Schrodinger equation cannot be solved exactly, without any approximations. Therefore, several approaches have been developed in order to overcome this problem. In Section **2.1.1**, the Börn-Oppenheimer approximation has been discussed. Then, in Section **2.1.2**, density functional theory (DFT) is touched upon. Here, the equation is rewritten in the form of electron density [ $\rho(r)$ ] instead of the wavefunction. A number of different aspects of DFT are touched upon, which include the Thomas-Fermi model, Hohenberg-Kohn (HK) Theorems and the Kohn-Sham method. In order to improve the DFT calculations, different types of functionals have been discussed in the Sections **2.2.5**, **2.2.6** and **2.2.7**. These include the local density approximation (LDA), generalized gradient approximation (GGA) and the hybrid functionals.

## 2.1 The Many-Body Schrodinger Equation

For the approximate solution of the many-body Schrodinger equation<sup>1</sup>, different types of approaches in quantum mechanics are involved. The many-body Schrodinger equation for a system with  $n$  electrons and  $m$  nuclei is given by

$$\hat{H}\Psi(x_1, x_2, x_3, \dots, x_n, r_1, r_2, r_3, \dots, r_m) = E\Psi(x_1, x_2, x_3, \dots, x_n, r_1, r_2, r_3, \dots, r_m) \quad 2.1$$

where  $\hat{H}(x_n, r_m)$  represents the molecular Hamiltonian and  $\Psi(x_n, r_m)$  represents the wave function for the system and is a function of the  $3n$  space coordinates and  $n$  spin coordinates.  $E$  is the total energy of the system. For the multi-electron system, the Hamiltonian  $\hat{H}$  is given by

$$\hat{H} = -\frac{\hbar}{2} \sum_{a=1}^m \frac{1}{m_a} \nabla_a^2 - \frac{\hbar}{2m_e} \sum_{i=1}^n \nabla_i^2 + \sum_a \sum_{a>b} \frac{Z_a Z_b e^2}{r_{ab}} - \sum_a \sum_i \frac{Z_a e^2}{r_{ia}} + \sum_j \sum_{i>j} \frac{e^2}{r_{ij}} \quad 2.2$$

where  $\hbar = h/2\pi$  and  $h$  is the Planck's constant,  $m_a$  and  $m_e$  are the masses of the nuclei and electrons,  $Z_a$  and  $Z_b$  are the charges on the  $a$  and  $b$  nuclei,  $r_{ab}$  is the distance between the  $a$  and  $b$  nuclei,  $r_{ia}$  is the distance between the  $i$ 'th electron and the  $a$ 'th nuclei and  $r_{ij}$  is the distance between the  $i$ 'th and  $j$ 'th electron. The first two terms in the Hamiltonian represent the kinetic energy of the nuclei and electrons respectively. The rest of the three terms are the nuclear-nuclear repulsion, nuclear-electron attraction and electron-electron repulsion terms respectively. The exact solution of the Schrodinger equation for the multi-electron systems is not possible and therefore different approximations have been made over the years to address this problem.

### 2.1.1 The Born-Oppenheimer approximation

Born and Oppenheimer<sup>2</sup> approximation is one by which we can simplify the Schrodinger equation. This is based on the fact that the mass of the nuclei is larger in comparison to the mass of the electrons and thus the

nuclei move slower in comparison to the electrons. The realistic effect of this is that the nuclear and electronic motions can be separated and as a result the electrons can be considered to be moving in the field of fixed nuclei. Hence, the first term of fixed nuclei in Equation 2.2 becomes zero and the third term is just a constant. Therefore, Equation 2.2 will reduce to the electronic Hamiltonian only and, as a result, Equation 2.1 reduces to

$$\hat{H}_{el} \Psi_{el} = E_{el} \Psi_{el} \quad 2.3$$

where  $\hat{H}_{el}$  represents the electronic Hamiltonian,  $\Psi_{el}$  represents the electronic wave function and  $E_{el}$  is the electronic energy of the system.

The  $\hat{H}_{el}$  electronic Hamiltonian is represented by

$$\hat{H}_{el} = -\frac{\hbar}{2m_e} \sum_{i=1}^n \nabla_i^2 - \sum_a \sum_i \frac{Z_a e^2}{r_{ia}} + \sum_j \sum_{i>j} \frac{e^2}{r_{ij}} \quad 2.4$$

The total energy of the system  $E_{el}$  is given by

$$E_{tot} = E_{el} + E_{nn} \quad 2.5$$

where  $E_{nn}$  is the nuclear-nuclear repulsion term given by

$$E_{nn} = \sum_a \sum_{a>b} \frac{Z_a Z_b e^2}{r_{ab}} \quad 2.6$$

Although the Born-Oppenheimer approximation reduces the molecular Schrodinger equation to the electronic Schrodinger equation, there are still a significant number of terms in the Schrodinger equation. Thus, over the years, a number of approximate methods have been developed in order to solve the electronic Schrodinger equation. These include the Hartree-Fock Approximation and methods beyond the Hartree-Fock Approximation. These include perturbative methods such as Møller-Plesset (MP) perturbation theory<sup>5</sup> and the multi-determinantal wave function based methods such as configuration interaction (CI)<sup>6</sup> and coupled cluster (CC)<sup>7</sup>. Along with these methods, density functional theory (DFT) has also become one of the effective methods for solving the Schrodinger equation.

## 2.2 Density Functional Theory

Density functional theory (DFT) is a powerful computational technique and has influenced computational chemistry to a great extent.<sup>3</sup> As the name indicates, DFT evaluates energy on the basis of the much simpler electron density  $\rho(r)$  instead of the complicated  $n$  electron wave function (a function of  $3n$  spatial and  $n$  spin coordinates). However, an important question with regard to DFT is whether the complicated  $n$  electron wave function can be replaced by a simpler quantity such as electron density  $\rho(r)$  which is a function of only three spatial variables. There are certain methods in DFT to solve the Schrodinger equation using electron density as the basic variable.

### 2.2.1 The Thomas-Fermi Model

This model is based on a quantum statistical approach which had been originally proposed by Thomas<sup>4</sup> and Fermi<sup>5</sup> in 1927. The model takes into account only the kinetic energy, where the nuclear-electron and nuclear-nuclear interactions have been considered classically. It is a fictitious model of a homogeneous electron gas with constant electron density. The kinetic energy expression derived by Thomas and Fermi is as follows:

$$T_{TF}[\rho(r)] = \frac{3}{10}(3\pi^2)^{2/3} \int \rho^{5/3}(r) dr \quad 2.7$$

The combination of classical expressions of the nuclear-electron attractive and electron-electron repulsive potentials in Equation 2.7 gives rise to a full Thomas-Fermi expression of energy of an atom.

$$E_{TF}[\rho(r)] = \frac{3}{10}(3\pi^2)^{2/3} \int \rho^{5/3}(r) dr - Z \int \frac{\rho(r)}{r} dr + \frac{1}{2} \iint \frac{\rho(r_1)\rho(r_2)}{r_{12}} dr_1 dr_2 \quad 2.8$$

As Equation 2.22 indicates, the Thomas-Fermi model totally neglects the exchange and the correlation part. Only the kinetic energy is represented to

some degree of completion. The relevance of this model lies in the fact that the final energy is completely given in terms of the electron density.

### 2.2.2 Hohenberg-Kohn (HK) Theorems

This is the modern density functional theory proposed by Pierre Hohenberg and Walter Kohn<sup>6</sup> in 1964, which is fundamentally based on two theorems. The first Hohenberg-Kohn theorem states that *‘for a non-degenerate ground state, the external potential  $V_{ext}(r)$  within a trivial additive constant, is a unique functional of the electron density  $\rho(r)$ ’*. The electronic ground state wave function and all other Hamiltonian terms such as kinetic energy  $T[\rho]$ , potential energy  $V[\rho]$  and total energy  $E[\rho]$  are uniquely determined by the electron density  $\rho(r)$ .

We consider two external potentials  $V_{ext}$  and  $V'_{ext}$ , which differ by no more than an additive constant, both of which give rise to the same ground state electron density  $\rho(r)$ . Let the two  $n$ -electron Hamiltonians  $\hat{H}_{ext}$  and  $\hat{H}'_{ext}$  correspond to the external potentials  $V_{ext}$  and  $V'_{ext}$ , belonging to the two different ground state wave functions  $\Psi_0$  and  $\Psi'_0$ , which lead to the same electron density  $\rho(r)$ . Let  $E_0$  and  $E'_0$  be the energies for the Hamiltonians  $\hat{H}_{ext}$  and  $\hat{H}'_{ext}$ . Using  $\Psi'_0$  as a trivial function for the Hamiltonian  $\hat{H}_{ext}$ , we have

$$E_0 < \langle \Psi'_0 | \hat{H}_{ext} | \Psi'_0 \rangle = \langle \Psi'_0 | \hat{H}'_{ext} | \Psi'_0 \rangle + \langle \Psi'_0 | \hat{H}_{ext} - \hat{H}'_{ext} | \Psi'_0 \rangle \quad 2.9$$

Since  $\hat{H}_{ext}$  and  $\hat{H}'_{ext}$  differ only in the external potential, we can write

$$E_0 < E'_0 + \langle \Psi'_0 | \hat{T} + \hat{V}_{ee} + \hat{V}_{ext} - \hat{T} - \hat{V}_{ee} - \hat{V}'_{ext} | \Psi'_0 \rangle \quad 2.10$$

which gives

$$E_0 < E'_0 + \int \rho(r) \{V_{ext} - V'_{ext}\} dr \quad 2.11$$

Repeating the above step by interchanging the prime and unprimed quantities gives the equation

$$E'_0 < E_0 - \int \rho(r) \{V_{ext} - V'_{ext}\} dr \quad 2.12$$

After adding Equations 2.11 and 2.12, we have

$$E_0 + E'_0 < E'_0 + E_0 \quad 2.13$$

So there cannot be two different  $V_{ext}$  that give the same ground state electron density.

Since the total ground state energy is a unique functional of the ground state electron density, so must be its individual components.

$$E_v[\rho_0] = T[\rho_0] + V_{ne}[\rho_0] + V_{ee}[\rho_0] \quad 2.14$$

The expression can be further separated into those parts that depend on the actual system, i.e., the nuclear-electron attraction and those that are independent of the external potential and the number of electrons.

$$E_v[\rho_0] = \int \rho_0(r)v(r) dr + F_{HK}[\rho_0] \quad 2.15$$

where,

$$F_{HK}[\rho_0] = T[\rho_0] + V_{ee}[\rho_0] \quad 2.16$$

$F_{HK}[\rho_0]$  is considered as the Holy Grail of density functional theory and contains the functional for the electronic kinetic energy and that of the electron-electron interaction  $V_{ee}[\rho_0]$ .  $F_{HK}$  is a Hohenberg-Kohn universal functional and it is only dependent on  $\rho$  and independent of any external potential  $v(r)$ .

The second HK theorem states that *the true ground-state density minimizes the energy functional  $E_v[\rho_{tr}]$* . Thus, for a trial density  $\rho_{tr}$  which



is non-zero and integrates to the number of electrons in the system i.e  $\int \rho_{tr} dr = n$ , the energy functional is always greater than or equal to the exact ground state energy,  $E_0$ ,

$$E_0 \leq E_v[\rho_{tr}] \quad 2.17$$

Hohenberg and Kohn explained their theorems for the non-degenerate ground state. The Hohenberg and Kohn theorems tell us that it is possible in principle to calculate energy and other molecular properties from the ground state electron density. However, the theorems do not provide a practical means of calculating the energy from the ground state electron density.

### 2.2.3 Kohn-Sham Method

Kohn and Sham<sup>7</sup> in 1965 developed a practical procedure for finding  $\rho_0$  and for finding  $E_0$  from  $\rho_0$ . Kohn and Sham substituted the interacting many electron system by a fictitious system of non-interacting electrons with the same electron density. Kohn and Sham rewrote the Hohenberg-Kohn equation 2.15 by defining the following terms

$$\Delta T[\rho_0] = T[\rho_0] - T_s[\rho_0] \quad 2.18$$

where  $\Delta T[\rho_0]$  represents the difference in the average ground-state electronic kinetic energy between the actual system and the non-interacting reference system

$$\Delta V_{ee}[\rho_0] = V_{ee}[\rho_0] - \frac{1}{2} \iint \frac{\rho(r_1)\rho(r_2)}{r_{12}} dr_1 dr_2 \quad 2.19$$

where  $V_{ee}[\rho_0]$  is the electron-electron interaction in the actual system and the quantity  $\frac{1}{2} \iint \frac{\rho(r_1)\rho(r_2)}{r_{12}} dr_1 dr_2$  represents the classical electrostatic

repulsion energy. Introducing Equations 2.18 and 2.19 in Equation 2.15, we have

$$E_v[\rho_0] = \int \rho_0(r)v(r)dr + T_s[\rho_0] + \frac{1}{2} \iint \frac{\rho(r_1)\rho(r_2)}{r_{12}} dr_1 dr_2 + \Delta T[\rho_0] + \Delta V_{ee}[\rho_0] \quad 2.20$$

In the above equations, the functionals  $\Delta T[\rho_0]$  and  $\Delta V_{ee}[\rho_0]$  are unknown and are defined jointly as the exchange-correlation functional,  $E_{xc}[\rho_0]$ ,

$$\text{Hence, } E_{xc}[\rho_0] = \Delta T[\rho_0] + \Delta V_{ee}[\rho_0] \quad 2.21$$

Thus,

$$E_v[\rho_0] = \int \rho_0(r)v(r)dr + T_s[\rho_0] + \frac{1}{2} \iint \frac{\rho(r_1)\rho(r_2)}{r_{12}} dr_1 dr_2 + E_{xc}[\rho_0] \quad 2.22$$

Equation 2.22 represents the major contribution to the total ground-state energy and can be calculated from  $\rho_0$ .

#### 2.2.4 Exchange-Correlation Functionals

The Kohn-Sham formalism contains the exchange-correlation functional ( $E_{xc}[\rho_0]$ ). The exchange-correlation functional includes the non-classical part of the electron-electron interaction and the kinetic energy of the real system, which is not covered by the fictitious system of non-interacting electrons. The accuracy of the Kohn-Sham DFT calculations decides the exchange-correlation term in the energy expression. The exchange-correlation term depends upon the functional for determining its accuracy. However, finding the accurate functional in DFT is a difficult task. The most common types of exchange-correlation functionals are a) functionals from the local-density approximation (LDA), and b) the generalized-gradient approximation (GGA), and c) the hybrid functional.

### 2.2.5 Local Density Approximation (LDA)

Kohn and Sham proposed the simplest approximation for the exchange and correlation energy, which is the local density approximation (LDA). The LDA exchange-correlation energy functional can be written as

$$E_{xc}^{LDA}[\rho_0] = \int \rho_0(r) \varepsilon_{xc}[\rho_0(r)] dr \quad 2.23$$

where  $\varepsilon_{xc}$  represents the exchange-correlation energy for every electron of the interacting uniform electron gas with electron density  $\rho_0(r)$ . The exactly expression for the exchange part is written as

$$E_x^{LDA}[\rho_0] = -\frac{3}{4} \left( \frac{3}{\pi} \right)^{\frac{1}{3}} \int \rho_0(r) dr \quad 2.24$$

The correlation part is more complex and can be acquired from perturbation theory. The commonly used LDA functionals are Vosko-Wilk-Nusair (VWN),<sup>8</sup> Perdew-Zunger (PZ)<sup>9</sup> and Perdew-Wang (PW)<sup>10</sup> which are similar and differ in the correlation part.

While, LDA is well known to work for cases with slowly varying electron densities, the approximation has not been found very well to work for atoms, molecules and metals. The LDA based functionals overestimate the cohesive energy by ~15-20% for metals and insulators and the errors become worse for weakly bonded systems where Van der Waal's forces are prominent, as well as for hydrogen bonded systems. In a molecular system, the electron density is far from uniformly distributed spatially. Hence, it is believed that the LDA approach has limitations. To overcome this problem, the generalized gradient approximation (GGA) has become more popular.

### 2.2.6 The Generalized Gradient Approximation (GGA)

The general form of the GGA functional is

$$E_x^{GGA}[\rho_0] = \int f^{GGA}(s)(\rho_0(r), \nabla\rho_0(r))dr \quad 2.25$$

In this term, the gradient corrected functional has been used.  $f^{GGA}$  in Equation 2.25 contains some function of the spin density and its gradient.  $s$  is dimensionless and has the functional form

$$s = \frac{\nabla\rho_0(r)}{2(3\pi^2)^{1/3}\rho_0(r)^{4/3}} \quad 2.26$$

All the GGA functionals are defined by the  $f^{GGA}$ . The form of  $f_x^{GGA}$  for the Perdew-Becke-Ernzerhof (PBE)<sup>11</sup> and Becke88 (B88)<sup>12</sup> functionals is written as

$$f_x^{PBE}(s) = 1 + \kappa - \frac{\kappa}{\left(1 + \frac{\mu s^2}{\kappa}\right)} \quad 2.27$$

$$f_x^{B88}(s) = 1 + \frac{\beta x(s)^2}{C[1 + 6\beta x(s)\sinh^{-1}(x(s))]} \quad x(s) = 2(6\pi^2)^{1/3}s \quad 2.28$$

In Equation 2.27, parameters  $\kappa$  and  $\mu$  are acquired non-empirically, whereas in Equation 2.28, the parameters  $\beta$  and  $C$  are obtained empirically. The functional form of the gradient corrected correlation energy can also be expressed as a functional form of  $s$ . Some of the commonly used GGA functionals are PBE,<sup>12</sup> PW91<sup>13</sup> and Lee-Yang-Parr (LYP).<sup>13</sup>

The GGA functionals can be further improved by adding a second derivate of  $\rho_0$ . The examples of second derivative containing functionals are TPSS,<sup>14</sup> and RevTPSS,<sup>15</sup> which are meta-GGA functionals.

### 2.2.7 Hybrid Functionals

Hybrid functionals involve combination of the Hartree-Fock “exact exchange” and the DFT exchange-correlation function. The most typically

used hybrid functional in quantum chemistry is B3LYP,<sup>16,17</sup> the functional form of which is

$$E_{xc} = E_{xc}^{LDA} + a_1 (E_x^{HF} - E_x^{LDA}) + a_2 \Delta E_x^{GGA} + a_3 \Delta E_c^{GGA} \quad 2.29$$

Some other examples of hybrid functionals are PBE1PBE,<sup>18</sup> and MO6.<sup>19</sup>

## 2.3 References

- (1). Schrödinger, E. *Ann. Phys.* **1926**, 79, 361.
- (2). Börn, M.; Oppenheimer, J. R. *Ann. Phys.* **1927**, 84, 457.
- (3). Parr, R. G.; Yang, W. *Density functional theory of atoms and molecules*, Clarendon Press, New York **1989**.
- (4). Thomas, L. H. *Proc. Cambr. Phil. Soc.* **1927**, 23, 542.
- (5). Fermi, E. *Z. Phys.* **1828**, 48, 73.
- (6). Hohenberg, P.; Kohn, W. *Phys. Rev.* **1964**, 136, 864.
- (7). Kohn, W.; Sham, L. J. *Phys. Rev.* **1995**, 140, 1133.
- (8). Vosko, S. H.; Wilk, L.; Nusair, M. *Can. J. Phys.* **1980**, 58, 1200-1211.
- (9). Perdew, J. P.; Zunger, A. *Phys. Rev. B* **1981**, 23, 5048.
- (10). Perdew, J. P.; Wang, Y. *Phys. Rev. B* **1992**, 45, 13244-13249.
- (11). Becke, A. D. *Phys. Rev. A* **1988**, 38, 3098.
- (12a). Perdew, J. P.; Burke, S.; Ernzerhof, M. *Phys. Rev. Lett.* **1996**, 77, 3865.
- (12b). Perdew, J. P.; Wang, Y.; *Phys. Rev. B* **1992**, 45, 13244.
- (13). Lee, C.; Yang, W.; Parr, R. G. *Phys. Rev. B* **1988**, 37, 785.

- (14). Tao, J.; Perdew, J. P.; Staroverov, V. N.; Scuseria, G. E. *Phys. Rev. Lett.* **2003**, *91*, 146401.
- (15). Perdew, J. P.; Ruzisinszky, A.; Csonka, G. I.; Constantin, L. A.; Sun, J. *Phys. Rev. Lett.* **2009**, *103*, 026403.
- (16). Becke, A. D. *J. Chem. Phys.* **1993**, *98*, 5648-5652.
- (17). Stephens, S. H.; Devlin, F. J.; Chabalowski, C. F.; Frisch, M. J. *J. Phys. Chem.* **1998**, *98*, 11623-11627.
- (18). Adamo, C.; Barone, V. *J. Chem. Phys.* **1999**, *110*, 6158.
- (19). Zhao, Y.; Truhlar, D. G. *Theor. Chem. Acc.* **2008**, *120*, 215.

## Chapter 3

### Abstract

Full quantum chemical calculations with density functional theory (DFT) show that a principal role of donors in Ziegler-Natta (ZN) olefin polymerization catalysts is to coordinate to the metal center in the active sites on the  $\text{MgCl}_2$  surface and thereby modulate the behavior of the catalyst to favor insertion over termination, thus leading to polymerization. This is shown to be true for a range of different donors considered. The calculations indicate that active sites featuring anionic chloride ligands at the titanium center (the conventional model for the active site), would lead to lower molecular weight polymers. It is shown that in the place of a chloride, if an  $\text{OC}_2\text{H}_5$  group were present instead, it would lead to an active site that would be much more effective at producing long chain polymers. The current work therefore provides important new insights about the nature of the ZN polymerization catalysis process.

### 3.1 Introduction

MgCl<sub>2</sub> supported Ziegler-Natta (ZN) olefin polymerization catalysis is one of the most important chemical processes in Industry today. It is responsible for the production of a wide variety of plastics, including elastomers and fibers. In the sixty years since their discovery, it would be no exaggeration to say the ZN catalysts have revolutionized the polymer industry, performing at near enzymatic rates and annually producing hundreds of millions of tons of polymers such as polyethylene and isotactic polypropylene. Despite advances such as the advent of metallocenes<sup>1-5</sup> and supported catalysts<sup>6-11</sup>, it is still the ZN catalyst systems that are responsible for the production of a significant majority of polymer products today.

However, despite their enormous importance and impact, ZN catalyst systems have not been completely understood to date. The multi-site, heterogeneous nature of the ZN catalysis process is responsible in part for this, but what has also contributed is the complexity of the system, which comprises of the MgCl<sub>2</sub> support, the active titanium species, usually in the (III)<sup>8, 12</sup> or (II)<sup>13</sup> oxidation state, AlR<sub>3</sub> (where R = alkyl group such as ethyl): the trialkylaluminium, alkylating agent, the substrate olefin monomer, and also oxygen containing Lewis bases which act as donors: “internal” (donors such as diether<sup>8, 14-17</sup>, alkoxysilane<sup>8</sup>, diisobutylphthalate<sup>18</sup> and succinate<sup>8</sup>) if added during MgCl<sub>2</sub> surface preparation, “external” (donors such as alkoxysilane<sup>18</sup>) if added later into the system with AlR<sub>3</sub> or the monomer.

It is likely that in such a multi-component system there are several factors that influence the nature and efficiency of the catalysis process, but nevertheless, it is also likely that some factors are more prominent than others. Perhaps the most important factor in determining the efficiency and selectivity of the ZN systems is the nature of the active catalytic species. In a multi-site catalyst system, there are likely to be different type of active sites, but the active site that has been most considered in ZN catalysis – the conventional model of the active site – has the titanium bound to the MgCl<sub>2</sub> support, with chlorides as coordinating anionic ligands and the growing chain as the other ligand<sup>8, 10, 19</sup>. However, since the internal donors are added during the active site preparation, it is possible that these Lewis bases can coordinate to the acidic titanium center and thereby “tune” the activity of the active site. While a few computational studies have focused on this possibility<sup>8, 10, 20</sup>, to date there has been no



systematic study of how different donor molecules could be affecting the ZN catalysis process by changing the barriers to insertion and termination through their electronic and steric influence at the metal center. This is one of the objectives of the current computational investigation, where ethylene polymerization has been considered at a Ti(III) center, with the coordination of ethyl benzoate (eb), para-ethoxyethylbenzoate (peeb), para-isopropoxyethylbenzoate (pipeb) and ethyldecanoate (aliphatic ester) considered at the titanium. The structures of the four donor molecules are shown in Figure 1 below.

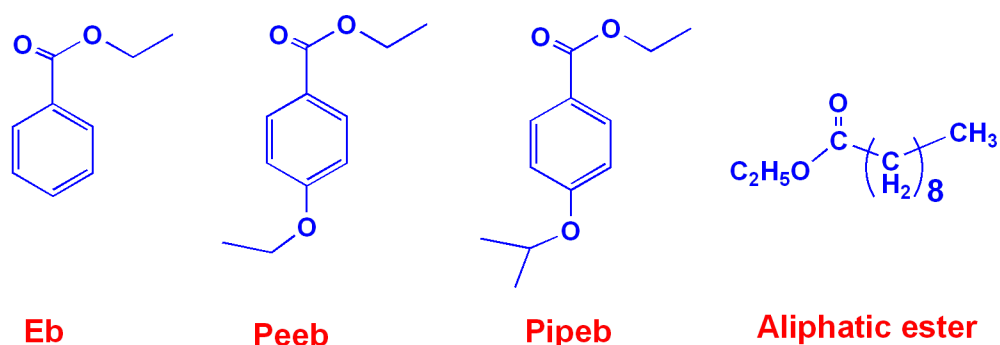


Figure. 1 The four donors that have been considered in this study.

In this context, it is relevant to note that the other role of the donor that has been envisaged in ZN systems is that the donors bind on the MgCl<sub>2</sub> surface to the side of the active catalyst and thereby serve to tune the activity and selectivity of the catalysts<sup>8-10, 12, 21-24</sup>. Moreover, since the free exposed surface area of MgCl<sub>2</sub> is significantly greater than the area containing the titanium species, it could be argued that the donor would prefer binding to the surface significantly more than binding directly to the titanium. The arguments against this are as follows: (i) recent work suggests that the donor could “walk” on the MgCl<sub>2</sub> surface towards the titanium catalyst species<sup>25</sup>, which indicates that even if the donor does bind to the free MgCl<sub>2</sub> surface, there is a distinct possibility that it would end up in the proximity of the titanium catalyst, and (ii) recent experimental work<sup>9</sup> indicates that the donor bound to the vicinity of the titanium can, through a series of steps, eventually be bound directly to the titanium center. Hence, the possibility of the effect of the donor binding to the titanium deserves to be seriously investigated.

It is also important to note that in order to provide reliable information about such ligand modulated active sites, it is necessary to have a good model for the  $\text{MgCl}_2$  support, based on an understanding of its nature during ZN catalysis. While models for the support have been proposed in the past<sup>7, 26-28</sup>, a new model proposed by Cavallo and co-workers<sup>8</sup> holds special promise. This is because their model is based on a careful understanding of the conclusions of experimental and computational investigations reported in the literature. The conclusions are as follows: (i) the  $\text{MgCl}_2$  support consists of a few layers of  $\text{MgCl}_2$  sandwiches<sup>29</sup>, with the surface primarily consisting of (104) and (110) lateral cuts, (ii) the (104) lateral cuts are significantly greater in number than the (110)<sup>30</sup>, though (iii) the  $\text{TiCl}_4$  is seen to prefer the more acidic, four coordinated magnesium atoms on the (110) lateral cuts over the less acidic five coordinated magnesium atoms on the (104) lateral cuts<sup>31</sup>. These experimental and computational findings have recently led Cavallo and co-workers<sup>8</sup> to propose an interesting new model for the  $\text{MgCl}_2$  support that convincingly accounts for the seemingly contradictory findings listed from (i) to (iii) above. Their model is described in the first sub-section of the Results and Discussion section. We have employed this promising new  $\text{MgCl}_2$  model, with some modifications that have been validated, as detailed in the Results and Discussion section, for all the computational investigations that are discussed in the manuscript. Our modifications have allowed, for the first time in  $\text{MgCl}_2$  supported ZN systems, the determination of exact transition states, and the evaluation of free energies, for all the cases considered. With this modified model, we have systematically investigated the “ligand influence” of several different donors at the titanium active site, leading to the interesting observation that the presence of the donor at the titanium center increases the difference between insertion and termination barriers substantially, thus leading to the formation of higher molecular weight polymers. Moreover, the fact that olefin polymerization occurred in  $\text{MgCl}_2$  supported ZN catalyst systems before donors were introduced in the 1980s has led us to propose, and demonstrate computationally, that an  $\text{OC}_2\text{H}_5$  group would be a better anionic ligand at the titanium active site rather than a chloride. This is shown to be true not only for ethylene, but also for the case of the propylene monomer, thus showing the result to be generally true for olefin monomers. These results provide important new insights into the nature of the active species in ZN catalysis.

## 3.2 Computational Details

All the calculations have been carried out using density functional theory (DFT), employing the Turbomole 6.0 suite of program<sup>32-34</sup>. Geometry optimizations have been performed using the Perdew, Burke, and Ernzerhof (PBE) functional<sup>35, 36</sup>. The electronic configuration of the atoms have been described by a triple- $\xi$  basis set augmented by a polarization function (TURBOMOLE basis set TZVP)<sup>32</sup>. Subsequent single point calculations were done with the optimized structures, employing the TZVPP<sup>37</sup> basis set for all the atoms. It is to be noted that for the validation calculations that were done to compare the  $\Delta E$  values calculated with our  $\text{MgCl}_2$  model to published  $\Delta E$  values by Cavallo *et al.*<sup>8</sup> with their proposed  $\text{MgCl}_2$  model, the BP86 functional<sup>38-40</sup> was employed for the geometry optimizations, since this was the functional that Cavallo's group had used in their calculations. The TZVP basis set was employed for these specific calculations, followed by single point calculations with the TZVPP basis set. The resolution of identity (RI)<sup>41</sup>, along with the multipole accelerated resolution of identity (marij)<sup>42</sup> approximations were employed for an accurate and efficient treatment of the electronic Coulomb term in the density functional calculations. The values reported are  $\Delta G$  values, with zero point energy, internal energy and entropic contributions included through frequency calculations on the optimized minima and transition state structures, with the temperature taken to be 298.15 K. Care has been taken to ensure that all the reported transition state structures contained only one negative frequency corresponding to the correct normal mode.

It is to be noted that the entropic term is likely to be mis-represented when the reactants are considered separately in a reaction pathway: it is well known that the translational entropy is artificially increased in such case<sup>43</sup>. In order to avoid this problem, all the reaction pathways have been determined starting with the reactants (the  $\text{MgCl}_2$  supported active titanium species and the olefin monomer), in the vicinity of each other, instead of beginning from the completely separated reactant species, a procedure that has also been followed by other groups<sup>44-52</sup>. In this study we have considered the starting reactant together (in *vicinity* to each other) and product is separate species. Such an approach is particularly correct for the current systems, where the substrate, the ethylene or the propylene monomer, is a relatively small entity in comparison to the significantly larger  $\text{MgCl}_2$  supported titanium active

species. A further point is that for every geometry considered with the donor attached, there can be different conformations for the optimized structures: the alkyl chain can be in different orientations, the groups in the donor can be switched and so on. We have considered such conformational possibilities for the case of the Eb donor binding to the titanium center, and our finding is that the conformations are of comparable energy, lying within 0.5 kcal/mol of each other. Hence, for the rest of the donor cases, a single conformation has been considered.

### 3.3 Results and Discussion

#### 3.3.1 Validation of the $\text{MgCl}_2$ Model Employed in the Current Calculations.

The  $\text{MgCl}_2$  model that has been proposed by Cavallo and coworkers<sup>8</sup> is shown in the Figure 2a and Figure 2b below. In their model, they assumed the  $\text{MgCl}_2$  bulk to be in the  $\alpha$  crystalline phase, with the surface comprising of (104) lateral cuts. The surface was characterized by an overall angle of  $120^\circ$  between the two (104) lateral cuts (see Figure 2a). The (104) lateral cut has five coordinated magnesium centers, and is therefore equivalent to the (100) lateral cuts because the five-fold magnesium exists in an identical defective octahedral coordination that characterizes both the (100) and (104) surfaces<sup>53</sup>. The removal of one  $\text{MgCl}_2$  unit from this structure would lead to the exposure of a new surface, which would be (110), a surface that can coordinate the titanium species (see Figure 2b). Such a surface explains how (104) lateral cuts would be able to predominate in the  $\text{MgCl}_2$  support while providing room through surface defects for the exposure of the necessary (110) lateral cuts, as found from computational<sup>8, 20, 54-56</sup> and experimental studies. There are two new modifications that we have made to the  $\text{MgCl}_2$  model:

(i) Since the computational investigation encompasses a large number of different insertion and termination calculations involving several donor cases, we have decided to reduce the size of the  $\text{MgCl}_2$  support, for the purpose of computational expediency. As shown in Figure 2c, we have kept the (104) and (110) lateral cuts intact. But we have reduced the number of layers from six to four.

(ii) All the layers of the  $\text{MgCl}_2$  were allowed to relax, with none of the lower layers kept fixed. This was done so that exact transition states for the insertion and termination processes could be calculated. Moreover, doing this has allowed the calculation of free energy values ( $\Delta G$ ) for the different processes.

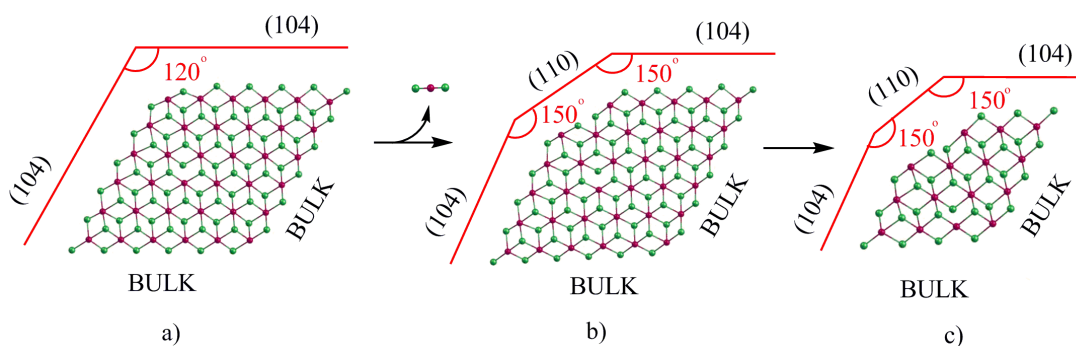


Figure 2. The model for the  $\text{MgCl}_2$  layers developed by Cavallo *et al.*<sup>8</sup> are shown in Figure 2a and Figure 2b; Figure 2c shows the modified  $\text{MgCl}_2$  model, with four layers instead of six, that we have employed in the current computational investigations.

That our modified  $\text{MgCl}_2$  model provides reliable results has been verified by validation calculations that we have done comparing the published ( $\Delta E$ ) results obtained with the Cavallo Model with our model. As shown in Table 1, Cavallo *et al.*<sup>8</sup> have calculated the  $\Delta E$  values for the binding of different donors to the (104) lateral cut of the  $\text{MgCl}_2$  surface. We have calculated the binding to the (104) lateral cut of three of the donor cases that Cavallo's group had considered, 1,3-diether, succinate and alkoxy silane, with our model. As mentioned in the Computational Details section, we have employed a BP86/TZVP/TZVPP approach, as opposed to the BP86/TZVPP approach that Cavallo *et al.* had employed<sup>8</sup>. As Table 1 indicates, the  $\Delta E$  values obtained from our model compare favorably with the corresponding values obtained with the Cavallo model: the binding of the 1,3 diether and alkoxy silane is predicted to be of similar magnitude by both the models, while the succinate is predicted to bind more strongly in both cases. Further validation has been provided by the comparison of the insertion barriers for the 1,3 propylene monomer that has been reported by Cavallo's group<sup>8</sup>, for the case with no donor bound to the  $\text{MgCl}_2$  support. As Table 2 indicates, our modified model provides the same results as obtained by the Cavallo Model. It is also to be noted that the final geometry optimized structure of the  $\text{MgCl}_2$  layers in our model did not drift away to form an unconnected set of molecules, even

though all the atoms had been kept unfixed in the calculations. Figure 3 shows the front view and the side view of the optimized structure of the  $\text{MgCl}_2$  model obtained: it is seen that the layered nature of the  $\text{MgCl}_2$  structure is maintained in the unfixed structure. This provides further proof of the robustness of the model employed in the insertion and termination calculations that are discussed in the subsequent subsections of the manuscript.

Table 1  $\Delta E$  values (in kcal/mol) for different donor coordination to the magnesium atom in  $\text{MgCl}_2$  layers; comparison between the Cavallo Model and our modified  $\text{MgCl}_2$  model.

Donors	$\Delta E$ (kcal/mol)	
	Cavallo Model	Our Model
1,3-diether	-29.8	-29.5
succinate	-42.2	-39.3
alkoxysilane	-30.5	-32.9

Table 2  $\Delta E$  values (in kcal/mol) for the insertion barriers of propylene with no donor attached to the metal centre; comparison between the Cavallo Model and our modified  $\text{MgCl}_2$  model.

Results	Insertion barriers(in kcal/mol)			
	Cavallo Model		Our Model	
Pathway	1,2-re	1,2-si	1,2-re	1,2-si
Without donor	0.0	-0.2	0.0	-0.1

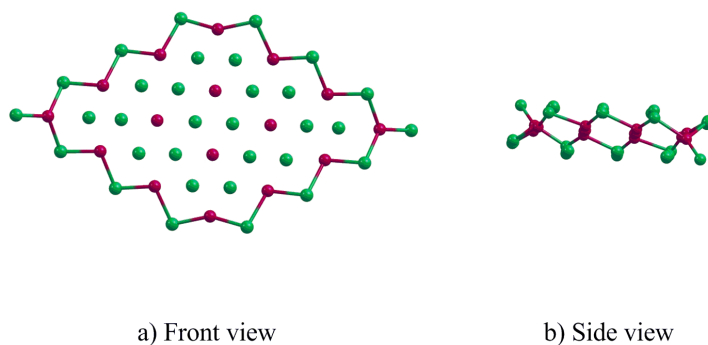


Figure 3. The front view and the side view of the DFT optimized structure of the  $\text{MgCl}_2$  model that we have employed in our calculations: it is seen that the  $\text{MgCl}_2$  model retains its layered structure even though all the atoms had been kept unfixed in the calculations.

### 3.3.2 Insertion and Termination Studies with the $\text{MgCl}_2$ Model.

As mentioned in the Introduction, we have done computational investigations for ethylene polymerization in the ZN system. Specifically, insertion and termination processes have been considered with the donor coordinated to the titanium center. The four donor cases considered have been shown in Figure 1 earlier. Shown in Figure 4 is the energy profile that would be obtained for the insertion process with the ethyl chain attached to the metal center (the “primary insertion case”), with the donor molecule, “OD”, behaving as a ligand by being coordinated to the titanium. It is to be noted that the four donors that have been considered can coordinate to the titanium center through a single C=O bond. There are other donors<sup>8, 10-12, 57</sup> that have two oxygen sites, each of which can donate electron density to the titanium center. These donors have not been considered in the current study because of the added computational complexity that is entailed for such donors, because of their ability to coordinate not only to the titanium, but also to the  $\text{MgCl}_2$  support in different conformations through the oxygen atoms. Studies with such “bidentate” donor cases will be taken up and reported in the near future.

As in previous experimental<sup>58, 59</sup> and computational studies<sup>8, 19, 56, 60</sup>, titanium is assumed to be in the (III) oxidation state. Before donor coordination, the titanium is attached through two chlorine atoms of the (110)  $\text{MgCl}_2$  surface (shown as the two lower chlorine atoms of the surface in the representative Figure 4 below). The

structure of the tethered titanium complex is octahedral but five coordinate, with a vacant site. Upon addition of the donor, the structure becomes six coordinate, gaining a stabilization that is denoted as  $\Delta G_a$  in the Figure. It should also be noted that, in the presence of excess donor concentrations, two donors might attack the titanium center instead of one. Calculations have been done for the case of ethyl benzoate in order to check this possibility. The calculations indicate that the total displacement of the titanium complex due to the coordination of two donor molecules is a process that is endergonic by 22.3 kcal/mol. On the other hand, calculations indicate that an alternate possibility exists, that of the titanium not being displaced from the  $MgCl_2$  surface despite the addition of two donor molecules: the titanium remains bound to the  $MgCl_2$  surface by means of the two chloride groups. The optimized structure of this complex has been shown in Figure 5. The process for the making of this complex is seen to be exergonic by 10.3 kcal/mol. This result suggests that the titanium complex would be unlikely to be displaced from the  $MgCl_2$  surface even in the presence of excess donor. It is likely that such a titanium complex, modified by two donors, would also be able to function as an active catalyst. However, the current investigation focuses on the effect of having one donor coordinated to the titanium center. This is partly for the purpose of reducing computational complexity and partly because such dual donor coordinated donor complexes would be likely to be formed only in the presence of excess donor.

The catalyst, now modified with the coordination of the Lewis base, can then be approached by the ethylene monomer. Our studies of the approach and complexation of ethylene to the octahedral titanium complex show that, in all the donor cases, the titanium prefers to lose the coordination to one of the chlorine atoms of the  $MgCl_2$  support, and thus remains six coordinate and octahedral, but still tethered to the  $MgCl_2$  surface through the lone chlorine atom. There is an energy cost to this, denoted as  $\Delta G_b$ . This cost is not only due to the loss of coordination to the chlorine, but also because of the entropic cost of adding an extra ligand to the titanium center. After the formation of the alkene  $\pi$  complex, the next step is the formation of the four-centered transition state, having a barrier shown as  $\Delta G_c$ , following the well-established Cossee-Arlman mechanism<sup>61, 62</sup>. Finally, the energy of the system moves downhill, leading to the formation of the inserted product: the butyl chain,  $\Delta G_d$  lower in energy than the transition state. The DFT optimized structures for the donor (Eb)



coordinated titanium complex before and after  $\pi$  complexation are shown in Figure 6 below.

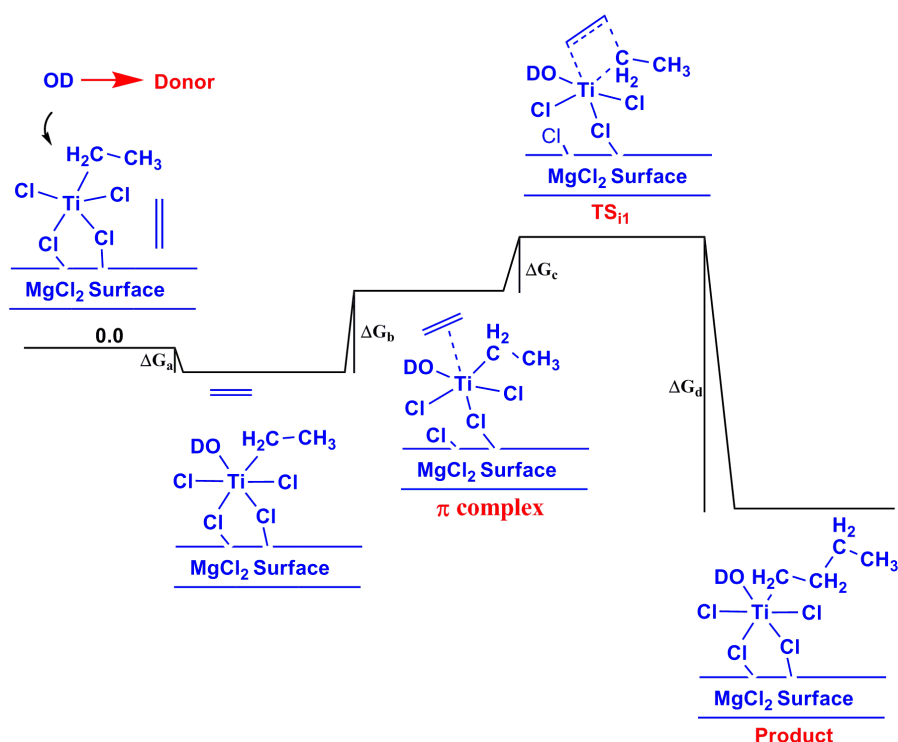


Figure 4. The free energy profile for the insertion of ethylene into the Ti-C<sub>2</sub>H<sub>5</sub> bond, with the donor (“OD”) coordinated to the titanium center.

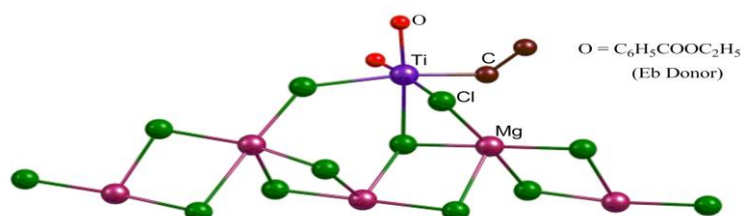


Figure 5. The optimized structure obtained by the addition of two donors to the titanium center; the titanium complex is still bound to the MgCl<sub>2</sub> surface through the chloride groups on the titanium; only the oxygen atoms of the ethyl benzoate donor binding to the titanium are shown; the hydrogens on the ethyl chain on the titanium are not shown and only a few layers of the MgCl<sub>2</sub> surface have been shown, for the purpose of clarity.

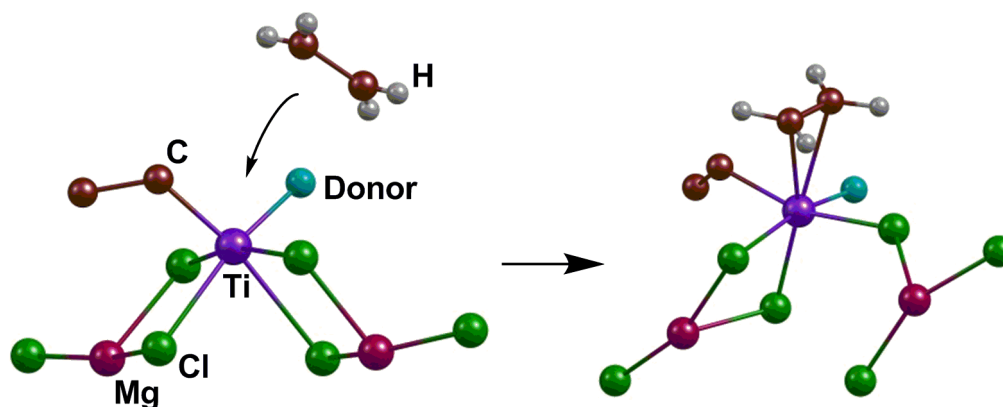


Figure 6. The optimized structures for the tethered titanium complex having the donor ligand (the donor in this being ethyl benzoate) before  $\pi$  complexation (5a), during the  $\pi$  complexation (5b); the hydrogens on the ethyl chain on the titanium are not shown and only a few atoms of the  $\text{MgCl}_2$  surface are shown, for the purpose of clarity.

The other competing possibility, after the formation of the  $\pi$ -complex, is the transfer of the  $\beta$  hydrogen of the ethyl chain to the complexed ethylene, leading to chain transfer and the termination of the chain. The corresponding energy changes in this process are denoted as  $\Delta G_e$  and  $\Delta G_f$  in Figure 7 below. For the polymerization process to be successful, the insertion barrier, which is calculated as the sum total of the complexation and insertion processes, should be lower than the termination barrier, calculated as the sum total of the complexation and termination processes. The greater the difference between the termination and insertion barriers the more successful would be the polymerization, and the higher the molecular weights of the polyethylene product that would be formed.

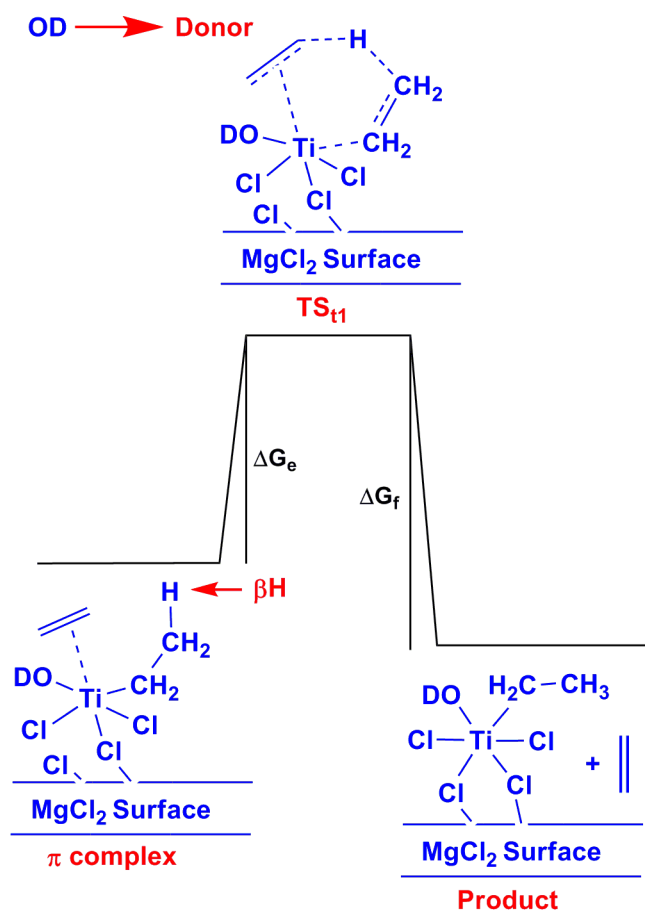


Figure 7. The free energy profile for termination: chain transfer to complexed ethylene, with the donor (“OD”) coordinated to the titanium center.

The values of  $\Delta G_a$ ,  $\Delta G_b$ ,  $\Delta G_c$ ,  $\Delta G_d$ ,  $\Delta G_e$ , and  $\Delta G_f$  that have been obtained for the four different donor cases studied are collected together in Table 3. Also shown in Table 3 are the values obtained for the insertion and termination barriers for the case when no donor is attached to the titanium center.

Table 3 The free energy ( $\Delta G$ ) values, in kcal/mol, for the insertion and termination steps for the primary insertion of ethylene into the  $\text{Ti-C}_2\text{H}_5$  bond in donor modified ZN catalyst systems; the final column shows the difference in the free energy between the competing insertion and termination steps.

Donors Wd= Without donor	Energy in (kcal/mol)								
	Primary Insertion					Primary Termination			Diff.( $\Delta X$ )
	$\Delta G_a$	$\Delta G_b$	$\Delta G_c$	Barrier	$\Delta G_d$	$\Delta G_e$	Barrier	$\Delta G_f$	$\Delta G_e - \Delta G_c$
Wd (Cl coordinated to Ti)	----	-2.6	8.7	8.7	-22.3	9.9	9.9	-12.5	1.2
EB	-1.0	13.0	8.9	21.9	-40.2	21.7	34.7	-44.8	12.8
PEEB	-3.8	12.5	9.7	22.2	-40.8	22.4	34.9	-42.0	12.7
PIPEB	-2.5	12.8	7.8	20.6	-39.0	19.9	32.7	-39.1	12.1
Aliphatic Ester	-7.3	13.5	9.8	23.3	-39.5	23.4	36.9	-44.2	13.6

A perusal of the numbers in Table 3 leads to the following observations:

(i) For the case where no donor is attached to the titanium center, the insertion barrier calculated from the stable  $\pi$  complex species) is only 1.2 kcal/mol lower than the competing termination barrier ( $\Delta G_b + \Delta G_e$ ). This suggests that in the absence of the donor, there is no significant preference for insertion over termination.

(ii) Four donor cases have been studied where the donor coordinates to the metal center (see Figure 1). For each of these cases, the coordination of the donor to the metal center is an exothermic process, with the binding of the aliphatic ester donor being the most favorable (see Table 3). This suggests that when the donors are “internal”, i.e., when they are added during the formation of the  $MgCl_2$  supported active catalyst, then the formation of donor coordinated titanium sites on the  $MgCl_2$  surface is a likely possibility. At these donor coordinated titanium active sites, there is a drastic change in the energy landscape. It is to be noted that here, unlike in the no-donor case discussed in (i) above, the barrier is considered from the active species without the olefin complexed to the metal center. This is because, unlike in the no-donor case, there is an energy cost to forming the  $\pi$  complex at the titanium center. Thus, it is seen that the barriers to insertion are increased: without the donor, the insertion barrier is 8.7 kcal/mol, while with the donor coordinated to the titanium, the insertion barrier is increased to about 22.0 kcal/mol in all the cases considered. Thus,

at these sites, the insertion would occur at a slower rate in comparison to the no-donor case. However, a barrier height of 22.0 kcal/mol is not formidable, especially since the ZN catalysis is usually carried out at temperatures greater than 60°C<sup>63, 64</sup>. (It is well established that reactions having barriers of 20.0 – 25.0 kcal/mol occur readily at room temperature<sup>65-67</sup>). What is more pertinent is the result that the insertion process becomes significantly more preferred in comparison to termination, by more than 12.0 kcal/mol, for every donor case that has been considered. The reason for this marked preference can be understood by a comparison of the insertion and termination transition states. Shown in Figure 8 are the optimized transition state structures for insertion and termination for the case where the donor is coordinated to the titanium center. The transition state for the termination by chain transfer is five membered, with the  $\beta$  hydride of the alkyl chain gaining some stabilization by coordination to the metal center. The insertion transition state is, in contrast, a less crowded four-member transition state, with an  $\alpha$  agostic interaction with the titanium center helping to provide stability for the transition state in this case (see Figure 8). The increased steric crowding in the case of the termination transition state accounts for the greater difference in the barriers between the two transition states, for all the donor cases considered.

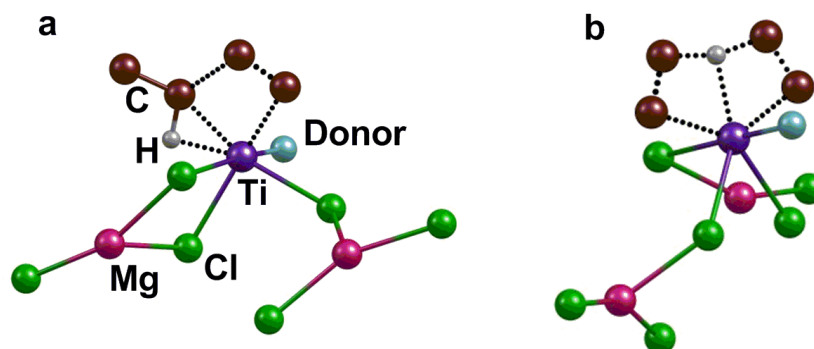


Figure 8. The optimized structures for the (a) insertion and (b) termination transition states for the “donor” coordinated active titanium species; there is higher steric crowding in the case of “b” the  $\beta$  hydride transfer termination transition state; only a lone hydrogen and a few atoms of the  $\text{MgCl}_2$  support are shown, for the purpose of clarity.

While the calculations discussed above have focused on the termination pathway involving chain transfer to monomer, there also exists the possibility of chain termination by the transfer of a  $\beta$  hydrogen from the chain to the titanium center (see Figure 9). This has also been considered for different donor coordinated cases, as well as for the case with no donor coordinated to the titanium center. The barriers, collected in Table 4, show that this termination pathway would actually be the preferred route, over the alternate termination route involving chain transfer to monomer (discussed and shown earlier in Table 3 above) for all the donor coordinated cases. The reason for this is that this process is unimolecular, and is therefore more entropically favored, over the bimolecular chain transfer process. Hence a proper comparison of the difference between insertion and termination would be to compare the  $\beta$ -hydride elimination to the insertion. This difference in barrier height (shown as  $\Delta X$  in Figure 10 below) would therefore provide the proper picture of the preference for insertion over termination. As shown in Table 4, even though the termination barriers are lower, there is still a distinct difference between the insertion and termination barriers for all the donor coordinated cases. This interesting result indicates that donor coordination to the titanium leads to a significant improvement in the preference for insertion over termination, which would lead to higher molecular weight polymers.

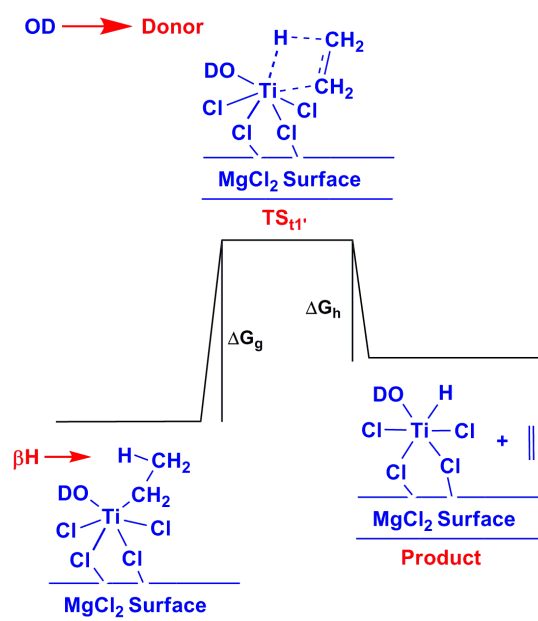


Figure 9. The free energy profile for termination:  $\beta$  hydride elimination from the chain to the titanium center with the donor (“OD”) coordinated to the titanium center.

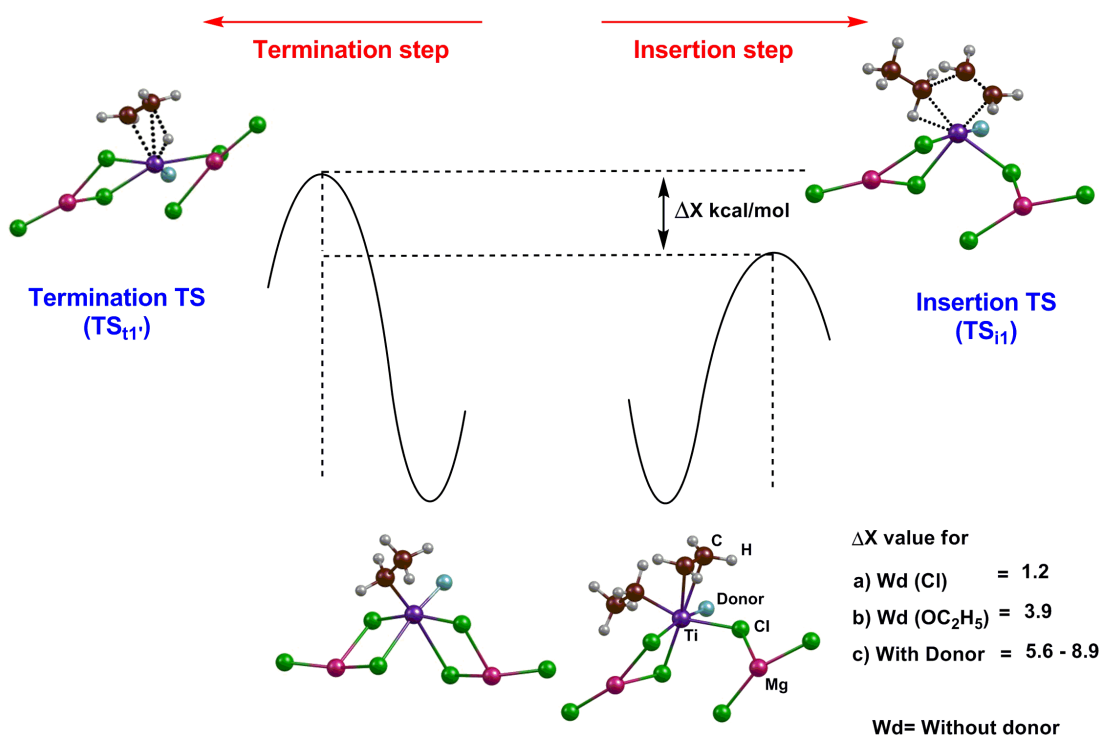


Figure 10. The optimized structures for the tethered titanium complex having the donor ligand with two possible pathways, one for insertion and one for termination by  $\beta$ -hydride elimination; the complete donor structure is not shown and only the top layer of the MgCl<sub>2</sub> surface is shown, for the purpose of clarity.

Table 4. The free energy ( $\Delta G$ ) values, in kcal/mol, for the termination process of  $\beta$  hydride elimination from the chain to the titanium center.

Donors	Energy in kcal/mol	
	$\beta$ Hydride transfer to titanium (Ti-C <sub>2</sub> H <sub>5</sub> carbon chain termination)	
	$\Delta G_g$	$\Delta G_h$
Wd = Without donor		
Wd (Cl coordinated to Ti)	21.4	-6.9
Eb	30.8	-12.2
Peeb	27.7	-8.1
Pipeb	26.2	-7.1
Aliphatic Ester	29.7	-8.7

In order to confirm that the results that have been obtained with the donor coordinated systems is not just true for the primary insertion case, the corresponding calculations have also been done with the butyl chain,  $C_4H_9$ , attached to the titanium center: the “secondary insertion” case. Figure 11 and Figure 12 show the representative energy profiles for insertion and termination (chain transfer to monomer), and Table 5 shows the values obtained for the insertion and termination barriers for all the different cases considered. A perusal of the results indicates that the conclusions regarding the polymerization process remain unchanged when considering the secondary insertion and termination cases.

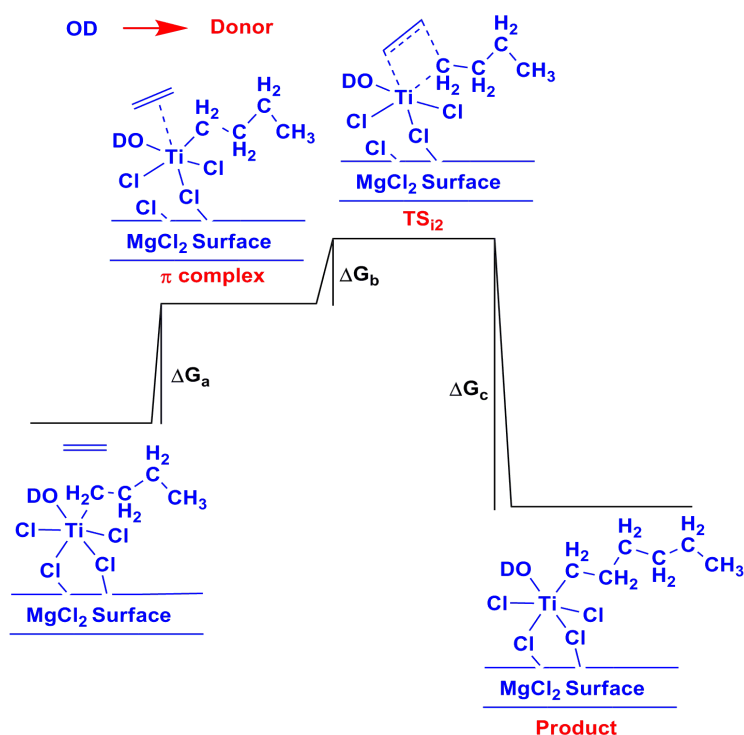


Figure 11. The energy profile for the insertion of ethylene into the Ti-C<sub>4</sub>H<sub>9</sub> bond, with the donor (“OD”) coordinated to the titanium center.



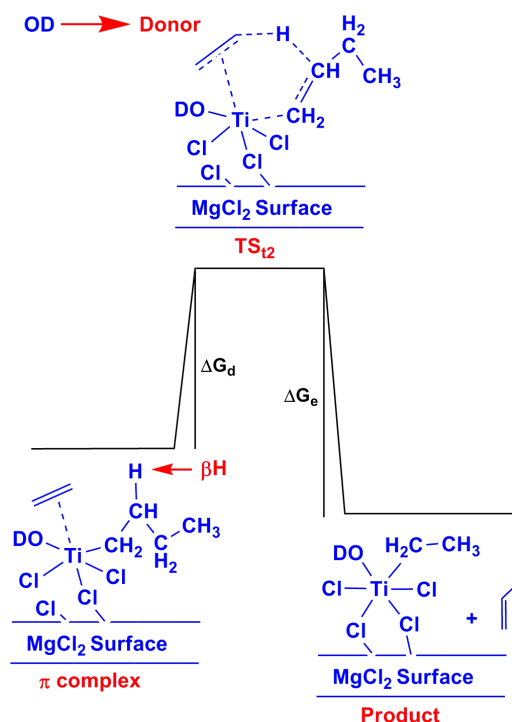


Figure 12. The energy profile for termination: chain transfer to complexed ethylene, with the donor (“OD”) coordinated to the titanium center.

Table 5. The free energy ( $\Delta G$ ) values, in kcal/mol, for the insertion and termination steps for the secondary insertion of ethylene into the Ti-C<sub>4</sub>H<sub>9</sub> bond in donor modified ZN catalyst systems; the final column shows the difference in the free energy between the competing insertion and termination steps.

Donors	Energy in (kcal/mol)							
	Secondary Insertion				Secondary Termination (Chain transfer to monomer)			Diff. ( $\Delta X$ )
	$\Delta G_a$	$\Delta G_b$	Barrier	$\Delta G_c$	$\Delta G_d$	Barrier	$\Delta G_e$	$\Delta G_d - \Delta G_b$
Wd (Cl coordinated to Ti)	-1.3	8.6	8.6	-21.9	8.0	8.0	-14.2	-0.6
EB	13.9	8.8	22.7	-40.8	18.9	32.8	-45.7	10.1
PEEB	10.8	11.2	22.0	-39.4	22.4	33.2	-44.3	11.2
PIPEB	11.3	10.4	21.7	-39.6	22.2	33.5	-42.4	11.8
Aliphatic Ester	8.7	9.7	18.4	-37.1	20.5	29.2	-45.0	10.8

Therefore, the free energy calculations, which includes the determination of exact transition states in all the cases, gives rise to the interesting result that the donor can influence the olefin polymerization catalysis significantly by directly binding to the titanium as a ligand. Indeed, the calculations suggest that this may be the primary role of the donor, as without it, the molecular weight of the polymer formed would be likely to be reduced.

It is also important to note that the current calculations suggest that the active species in the absence of donors cannot be the Ti(III) species coordinated to only the chloride ligands, the growing polymer chain and the chlorines of the  $\text{MgCl}_2$  surface: the “Without Donor case” in Tables 3 and 4 above. This species has been generally considered<sup>8, 10, 19, 20</sup> to be the active species in ZN catalysis, but the current calculations indicate that such an active site would show a lower preference for insertion over termination, as there would be a smaller difference between the insertion and termination barriers. This leads to the conclusion that the active catalyst sites, even when donors are not present, *are likely to have other species coordinating to the titanium center as ligands*, since high molecular weight polyethylene has been obtained in ZN systems when donors had not been added<sup>68-70</sup>. This possibility has been explored in the next sub-section, by considering the  $\text{OC}_2\text{H}_5$  group as a possible ligand at the active catalyst center.

### 3.3.3 $\text{OC}_2\text{H}_5$ as a Ligand at the Titanium Center.

The coordination of an  $\text{OC}_2\text{H}_5$  group at the titanium center, is very much a possibility in ZN systems, since the active species is formed, in most ZN systems, by the reaction of  $\text{TiCl}_4$  and  $\text{Mg}(\text{OC}_2\text{H}_5)_2$ <sup>63</sup>. Our calculations indicate that this is a favorable reaction, being exergonic by 21.9 kcal/mol ( $\Delta G$  value). What has been explored, and shown in the Figure 13, Figure 14 and Figure 15 below, is the possibility of the  $\text{OC}_2\text{H}_5$  group coordinating as a replacement to the anionic chloride ligand at the metal center. The results due to the presence of the  $\text{OC}_2\text{H}_5$  group at the metal center are shown to be significant: as Figure 13, Figure 14 and Figure 15 show, this leads to the preference of 3.9 kcal/mol for insertion over termination.

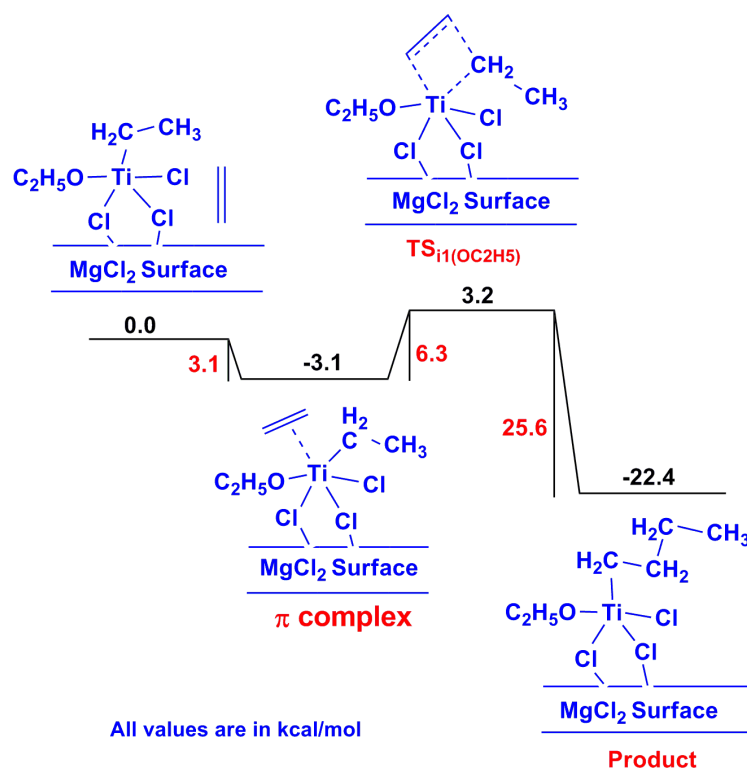


Figure 13. The free energy profile for the insertion of ethylene into the Ti-CH<sub>2</sub>CH<sub>3</sub> chain, with an OC<sub>2</sub>H<sub>5</sub> group coordinated to Ti metal centre.

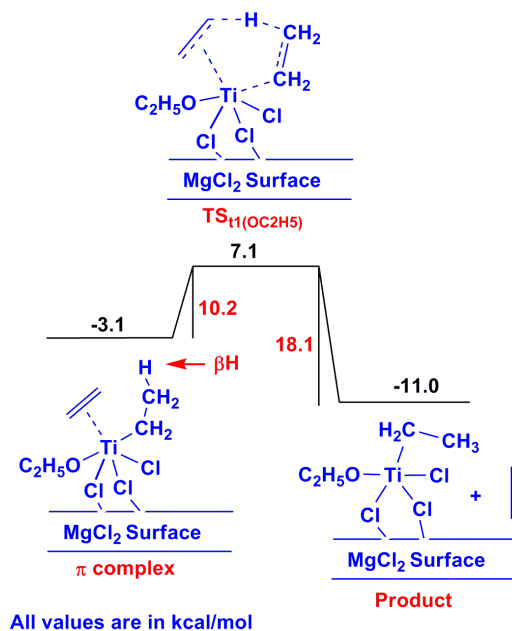


Figure 14. The free energy profile for the termination of the chain through chain transfer to the monomer; with an OC<sub>2</sub>H<sub>5</sub> group coordinated to Ti metal centre.

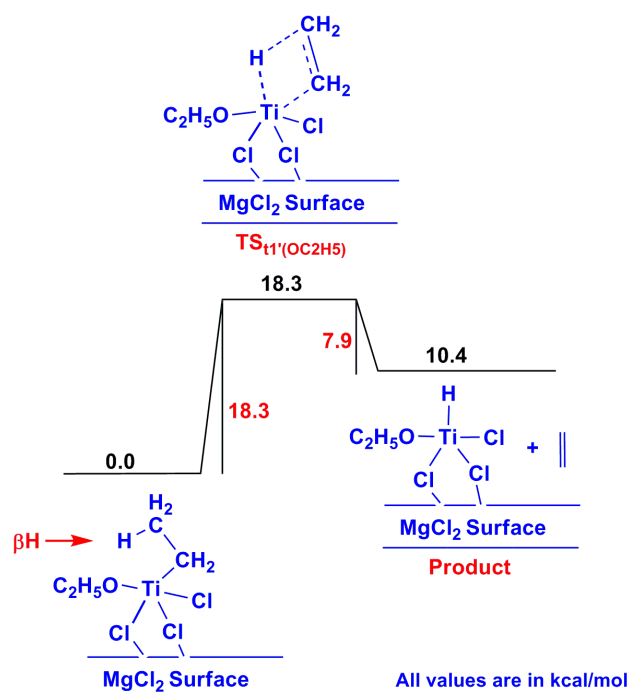


Figure 15. The free energy profile for the termination of the chain through  $\beta$  hydride transfer to the titanium from the chain; with an  $\text{OC}_2\text{H}_5$  group coordinated to Ti metal centre.

A similar result is obtained when the secondary insertion of ethylene has been considered for this case (as shown in Figure 16, Figure 17 and Figure 18). The increase in the molecular weight of polyethylene when the  $\text{OC}_2\text{H}_5$  group is present at the titanium center has been noted experimentally<sup>71</sup> but what the current studies indicate is that a titanium complex with one (or more)  $\text{OC}_2\text{H}_5$  group (s) coordinated to the metal center is likely to be a major active catalytic species, and not the chloride coordinated complexes that have been considered in the literature to date. This is an interesting result that provides new insights into the nature of the active species during the polymerization process in ZN catalysis.

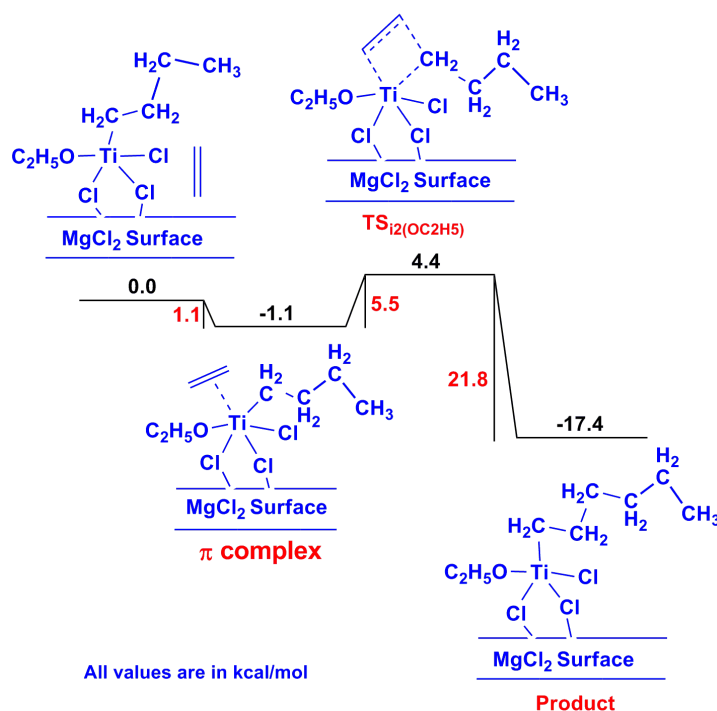


Figure 16. The free energy profile for the insertion of ethylene into the Ti-C<sub>4</sub>H<sub>9</sub> chain, with an OC<sub>2</sub>H<sub>5</sub> group coordinated to Ti metal centre.

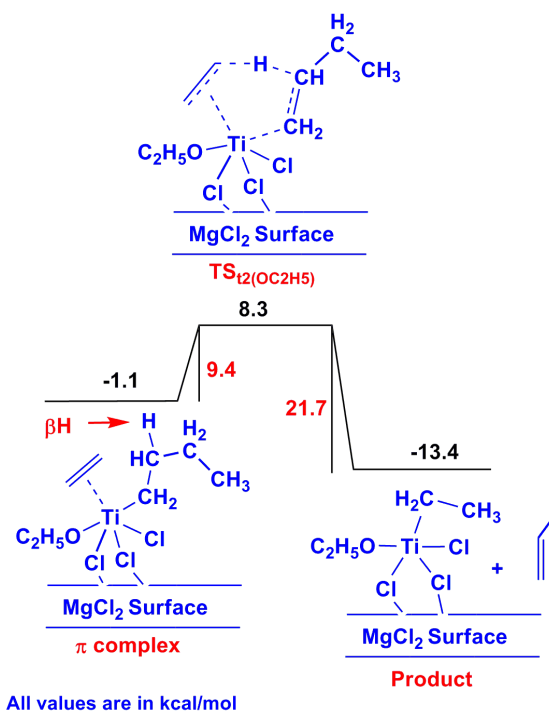


Figure 17. The free energy profile for the termination of the chain through chain transfer to the monomer; with an OC<sub>2</sub>H<sub>5</sub> group coordinated to Ti metal centre.

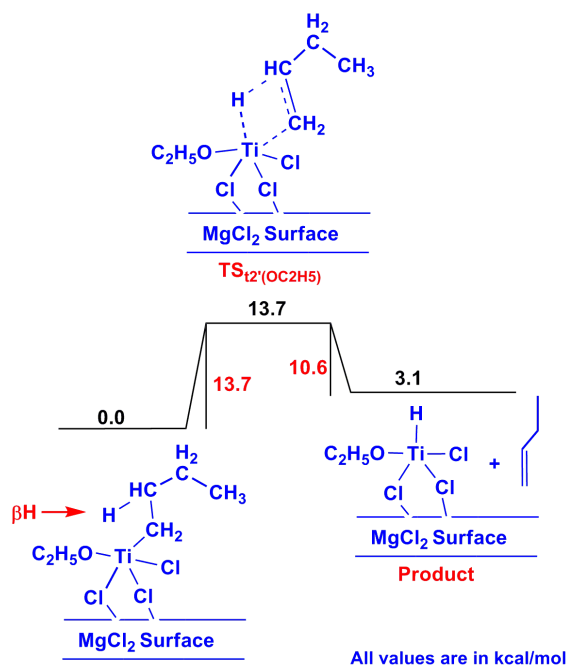


Figure 18. The free energy profile for the termination of the chain through  $\beta$  hydride transfer to the titanium from the chain; with an  $\text{OC}_2\text{H}_5$  group coordinated to Ti metal centre.

### 3.3.4 The Overall Picture for Insertion and Termination for the Ethylene Monomer.

Compiled in Table 6, and illustrated in Figure 19, are the values that have been obtained for all the different cases considered in this study, for insertion, termination through chain transfer to monomer, and  $\beta$  hydride elimination. The corresponding table and Figure for the secondary insertion case are shown in the Table 7 and Figure 20. The results indicate clearly that the species that has conventionally been considered the active species during ZN catalysis, with chlorides and the growing chain as the ligands {the case “Wd (Cl coordinated to Ti)” in Table 6}, is the one that is least likely to form long chain polymers, due to the small difference between the insertion and termination barriers. Indeed, the calculations suggest that it is likely that  $\text{OC}_2\text{H}_5$  coordinated to the metal center might be the most important active species when donors are not present in the system. It is also worth noting that the principal termination route in the absence of donor coordination (for the chloride and  $\text{OC}_2\text{H}_5$  coordinated cases), is the chain transfer to monomer pathway, while it is the  $\beta$  hydride

elimination pathway for the donor coordinated cases. The compiled results also indicate that the presence of the donor at the metal center leads to a significant improvement in the difference between the insertion and termination barriers, thus suggesting that an important role of the donor may be to increase the molecular weight of the polymer chains by coordinating to the metal center.

Table 6 The comparative study of primary insertion of ethylene and the termination barriers: the free energy ( $\Delta G$ ) values, in kcal/mol, has been considered.

Donors	Energy in kcal/mol			
	Primary			
	Insertion Barrier	Termination Barrier		Diff.( $\Delta X$ )
Chain transfer to monomer		$\beta$ H transfer to metal	Lower termi. barrier - Insertion barrier	
Wd= Without donor				
Wd (Cl coordinated to Ti)	8.7	9.9	21.4	1.2
Wd (OC <sub>2</sub> H <sub>5</sub> coordinated to Ti)	6.3	10.2	18.3	3.9
Eb	21.9	34.7	30.8	8.9
Peeb	22.2	34.9	27.7	5.5
Pipeb	20.6	32.7	26.2	5.6
Aliphatic Ester	23.3	36.9	29.7	6.4

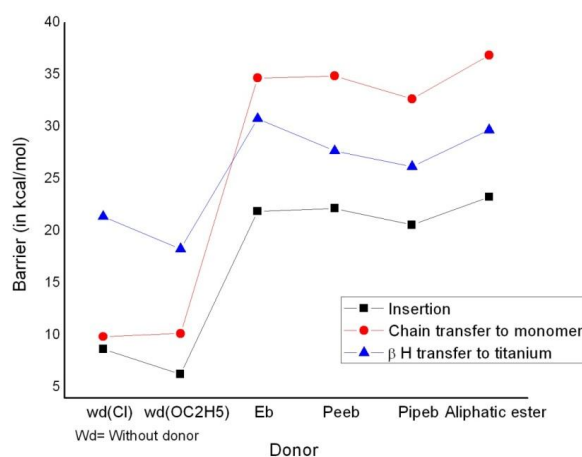


Figure 19. The free energy graph for comparative study of insertion and termination barrier with different donor cases.

Table 7. The free energy ( $\Delta G$ ) values, in kcal/mol, the comparative study of insertion and termination barriers, in termination case  $\beta$  hydride transfer to monomer and  $\beta$  hydride transfer to metal have been considered, the final column shows the difference in the free energy between the competing insertion barrier and lower termination barrier.

Donors  Wd= without donor	Energy in kcal/mol			
	Secondary			
	Insertion Barrier	Termination Barrier		Diff. ( $\Delta X$ )
$\beta$ H transfer to monomer		$\beta$ H transfer to metal	Lower termi. barrier - Insertion barrier	
Wd (Cl coordinated to Ti)	8.6	8.0	20.4	-0.6
Wd (OC <sub>2</sub> H <sub>5</sub> coordinated to Ti)	5.5	9.4	13.7	3.9
Eb	22.7	32.8	25.2	2.5
Peeb	22.0	33.2	26.6	4.6
Pipeb	21.7	33.5	25.2	4.5
Aliphatic Ester	18.4	29.2	27.4	9.0



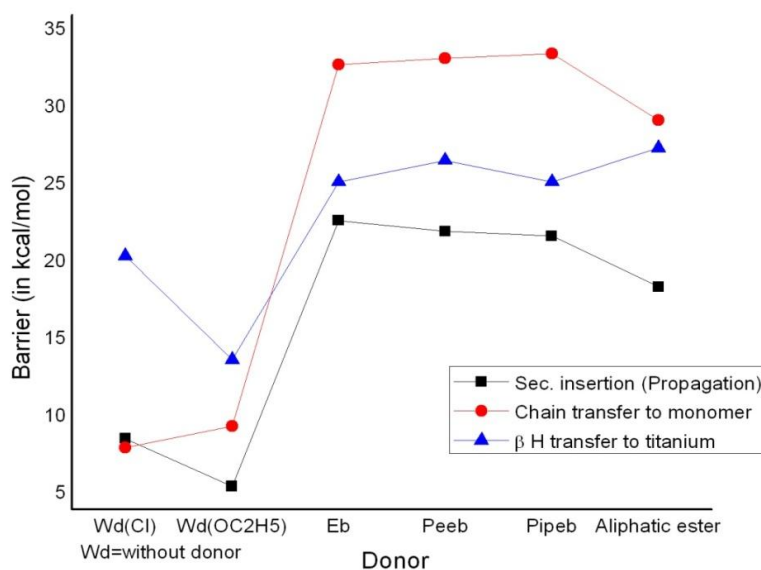


Figure 20. The free energy graph for comparative study of insertion and termination barrier with different donor cases.

### 3.3.5 H<sub>2</sub> Response in the ZN systems.

For the purpose of completion, this sub-section looks at the way the ligand modified active sites in ZN systems would react to the introduction of H<sub>2</sub> into the system. The introduction of H<sub>2</sub> in ZN systems is usually done in order to terminate the chain<sup>72</sup>. As shown in Figure 21 below, the addition of dihydrogen can effect the termination of the chain by the transfer of a hydrogen to the  $\alpha$  carbon of the chain. As the collected  $\Delta G$  values in Table 8 indicate, the termination of the chain *via* hydrogen response would almost be the same for all the donor cases considered. The values of the barrier heights also show that this termination route would be feasible at temperatures at which ZN catalysis is done. This indicates that the donor coordination as a ligand to the titanium center would also not get in the way of termination of the chain, when required, though hydrogen response. The other point that is clear from the values collected in Table 8 is that the formation of the products subsequent to the termination barrier would be significantly more favored for the donor coordinated cases, in comparison to the donor-absent case. This result again highlights the significance of donor coordination to the titanium center. For the OC<sub>2</sub>H<sub>5</sub> case, the barrier to

termination is quite comparable to the conventionally considered no-donor case where a chloride is attached to the metal center, and here, too, the product of the termination is seen to be stable. The secondary termination values for the H<sub>2</sub> response case have been collected in Table 9.

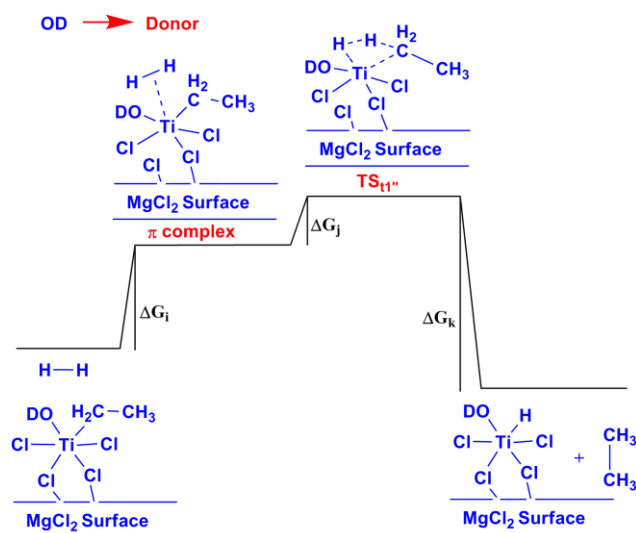


Figure 21. The free energy profile for the termination of the chain by addition of H<sub>2</sub> at the titanium center.

Table 8 The energy values for the termination process through hydrogen response for the different donor modified ZN catalyst systems.

Donors	Energy in kcal/mol			
	Hydrogen response (Ti-C <sub>2</sub> H <sub>5</sub> carbon chain termination)			
Wd=Without donor	$\Delta G_i$	$\Delta G_j$	$\Delta G_i + \Delta G_j$	$\Delta G_k$
Wd (Cl coordinated to Ti)	2.8	5.3	8.1	-11.9
Wd (OC <sub>2</sub> H <sub>5</sub> coordinated to Ti)	4.4	5.8	10.2	-17.4
Eb	13.4	3.5	16.9	-31.7
Peeb	12.7	3.6	16.3	-27.9
Pipeb	15.1	2.1	17.2	-26.8
Aliphatic Ester	14.2	2.9	17.1	-30.0

Table 9. The energy values for the termination process through hydrogen response for the different donor modified ZN catalyst systems.

Donors  Wd= without donor	Energy in kcal/mol			
	Hydrogen response (Ti-C <sub>4</sub> H <sub>9</sub> carbon chain termination)			
	$\Delta G_h$	$\Delta G_i$	$\Delta G_h + \Delta G_i$	$\Delta G_j$
Wd (Cl coordinated to Ti)	1.0	5.6	6.6	-11.5
Wd (OC <sub>2</sub> H <sub>5</sub> coordinated toTi)	6.3	7.9	14.2	-19.3
MgCl <sub>2</sub>	10.3	4.7	15.0	-33.8
Eb	14.1	3.5	17.6	-31.7
Peeb	13.3	3.2	16.5	-27.5
Pipeb	15.4	4.3	19.7	-27.7
Aliphatic Ester	13.5	6.8	20.3	-31.5

### 3.3.6 Insertion and Termination for the Propylene Monomer Case.

Studies similar to ethylene insertion and termination can also be done for substituted olefin monomers such as propylene. However, here the presence of the methyl group in place of hydrogen leads to several possibilities of insertion and termination, essentially quadrupling the number of calculations required, and thus making the investigations more computationally expensive. However, given the importance of propylene as a monomer in ZN catalysis, we decided to investigate whether the presence of the OC<sub>2</sub>H<sub>5</sub> group at the titanium center has a marked effect over other active sites having chlorides at the titanium center: the conventional model for the active site.

As shown in Figure 22 below, different possibilities exist for the propylene monomer: there can be 1,2 or 2,1 insertion (with the corresponding termination cases through chain transfer to monomer), and there can be the “*re*” and “*si*” face insertions possible in each case. Since it is known that isotactic polypropylene is produced when titanium based ZN catalyst systems are employed, it is likely that the titanium catalyst

would exercise enantiomorphic site control by being in a given configuration ( $\Lambda$  or  $\Delta$ ) throughout the polymerization process<sup>73</sup>. For the current calculations, the titanium complex has been considered to be in the  $\Lambda$  configuration. It is also to be noted that since the growing chain has been considered to be  $C_2H_5$ , the termination cases by  $\beta$  hydride elimination will be the same as considered for the ethylene monomer case. As discussed earlier, these values had been found to be higher (see Tables 3, 4 and 6) than the barriers to insertion and chain termination by transfer to monomer for the no-donor active site cases. Hence, for the purpose of comparison of the insertion and termination possibilities (shown in Table 10 below), only the insertion and the chain termination by transfer to monomer barriers have been considered.

As Table 10 indicates, the most favorable route for the propylene monomer would be through 1,2 *si* insertion for both the cases considered. However, what is again to be noted is how the presence of the  $OC_2H_5$  group at the titanium leads to a marked preference for the insertion over the termination for the 1,2 *si* case: the difference between insertion and termination is 5.4 kcal/mol as compared to the difference of only 1.9 kcal/mol for the case where the chloride is the ligand. This again shows that sites with  $OC_2H_5$  instead of chloride are likely to not only be more active, but also likely to lead to the formation of high molecular weight polymer chains, with almost the same stereoselectivity as present at active sites with chloride as the ligand.

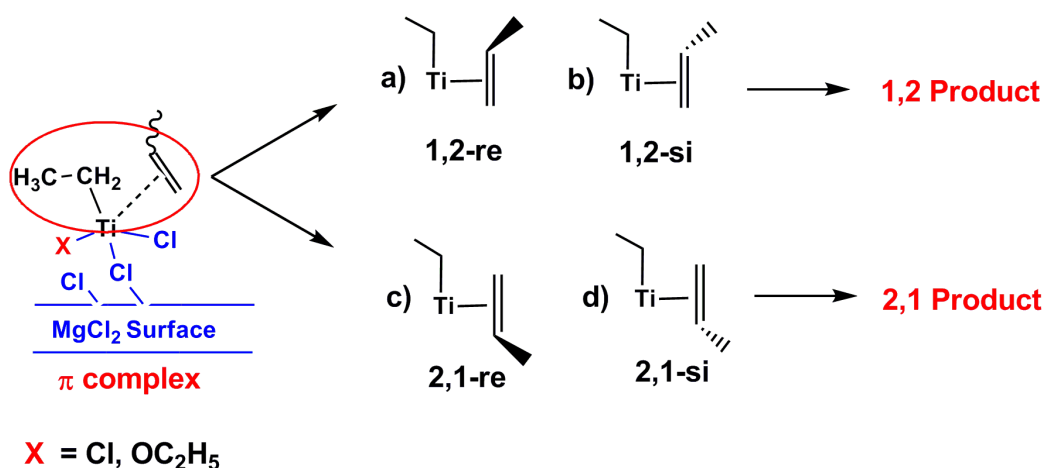


Figure 22. Four different possibilities for the insertion of propylene into the  $Ti-C_2H_5$  bond, with different ( $X=Cl, OC_2H_5$ ) group coordinated to the titanium metal center.

Table 10 The free energy ( $\Delta G$ ) values, in kcal/mol, for the insertion and termination steps for the primary insertion of propylene into the Ti-C<sub>2</sub>H<sub>5</sub> bond with different (X=Cl, OC<sub>2</sub>H<sub>5</sub>) group attached on titanium in ZN catalyst systems; the final row shows the difference in the free energy between the competing insertion and termination steps.

Without Donor (Wd)	Energy Barriers (kcal/mol)							
	Wd (Cl coordinated to Ti)				Wd (OC <sub>2</sub> H <sub>5</sub> coordinated to Ti)			
	1,2-re	1,2-si	2,1-re	2,1-si	1,2-re	1,2-si	2,1-re	2,1-si
Insertion (X <sub>1</sub> )	12.1	9.2	11.6	11.6	10.0	7.8	11.2	10.6
Termination (X <sub>2</sub> )	11.3	11.6	12.7	11.8	13.6	13.2	14.1	14.6
Diff. ( $\Delta X$ ) = (X <sub>2</sub> ) - (X <sub>1</sub> )	-0.8	1.9	1.1	0.2	3.6	5.4	2.9	4.0

### 3.3.7 The Overall Picture of Multi-Site Catalysis in Ziegler-Natta Systems.

Figure 23. below encapsulates the findings from the calculations discussed in this manuscript. The results reveal an important fact about olefin polymerization: the conventional model for the active site of ZN catalysts, having chloride as the ligand at the titanium center, would be likely to lead to lower molecular weight polymers. The results also show that sites having OC<sub>2</sub>H<sub>5</sub> group(s) as ligands at the titanium center that can yield higher molecular weight polymers, by increasing the gap between the insertion and termination barriers.

The calculations also make it clear that the coordination of internal donors to the titanium center is a feasible prospect, with the binding found to be exothermic in all the cases considered. Such active sites, having the donor coordinated at the titanium, would allow olefin insertion, but at higher barriers in comparison to non-donor active sites. Since the barrier heights are in the region of 20.0 kcal/mol for these cases, the insertion process would be quite likely at the temperatures at which ZN catalysis is done (above 60 °C<sup>63, 64</sup>). It is well known that barrier heights in the region of 20.0-25.0 kcal/mol are easily surmountable at room temperature<sup>65-67</sup>. What is interesting is the finding that such sites would further favor insertion over termination, with the

difference between insertion and termination increased, thus leading to higher molecular weight polymer chains.

Now, as illustrated in Figure 24 below, this means that the overall productivity of the polymerization catalysis will improve with the addition of donors to the system. This is because of the fact that donor addition to the titanium center will convert sites that were “bad”: the chloride coordinated titanium sites that would have led to lower molecular weight polymer, to “good” sites that will yield high molecular weight polymer chains, because of the increased gap between insertion and termination. Hence the number of “good” active sites on the titanium surface will increase because of the addition of the donor molecules. The increase in the number of “good” sites would lead to an increased polymer output in a given interval of time. Indeed, these results suggest that one of the primary functions of internal donors in ZN catalysis might be to coordinate to the titanium center to boost polymer productivity.

It should, however, be noted that the addition of excess amounts of donors might have the effect of reducing the activity, since the excess donor molecules might also convert some of the sites that were already “good”– sites that have  $\text{OC}_2\text{H}_5$  (or analogous) groups on the titanium and that produce the polymer at low barriers and high rates – to less effective sites that would produce polymer at higher barriers. This provides an explanation of the experimental observation, in some ZN systems, of the addition of excess donor leading to the poisoning of the catalyst<sup>16, 74, 75</sup>.

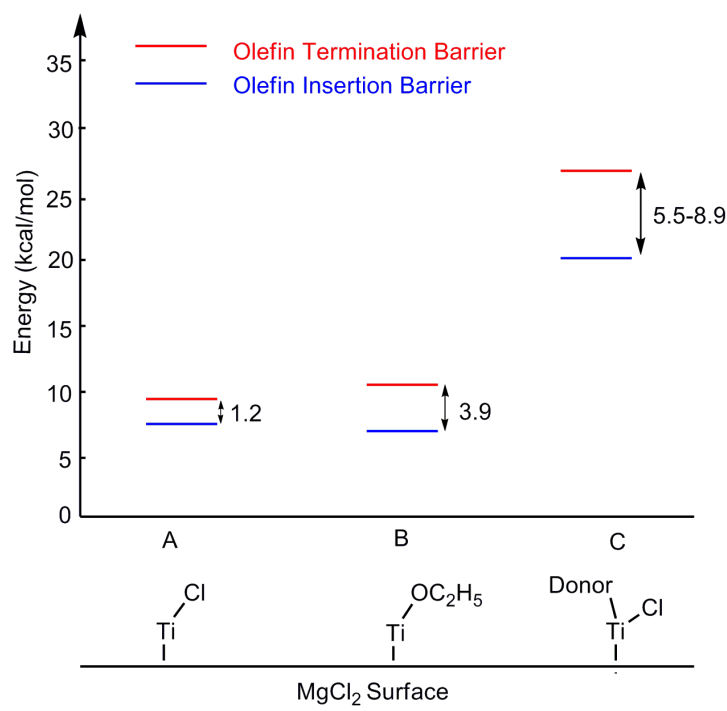


Figure 23. The overall picture of the nature of the polymerization process happening at the different titanium sites in Ziegler-Natta olefin polymerization.

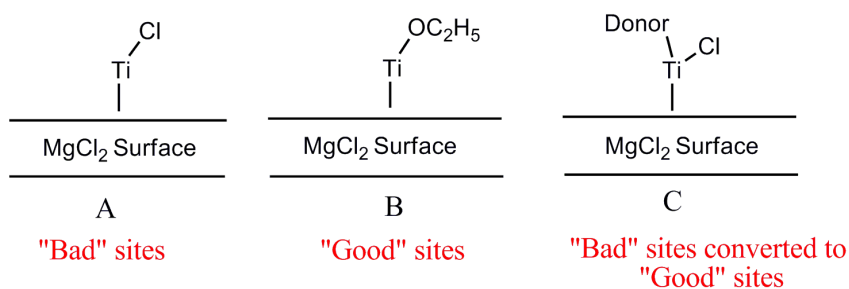


Figure 24. The role of the donor in increasing the activity of Ziegler Natta catalyst systems.

An added conclusion that can be drawn from the results is that other species that are present in the system can also act as “donors” by coordinating to the titanium and thus converting “bad” sites to “good” sites. For instance, species such as AlClR<sub>2</sub> (where R is an alkyl group) are likely to be present in ZN systems as a consequence of the exchange of an alkyl group with a chloride of the titanium. It is likely that such species can coordinate to the titanium center *via* the chloride and thus act to increase

the gap between insertion and termination as a donor would do, thereby leading to the formation of polymers. Previous computational studies have investigated the chelation of the aluminium complex to the titanium center<sup>76-79</sup>. The current DFT calculations that we have done indicate that the binding of the AlClR<sub>2</sub> group as a donor at the titanium center is exergonic by 8.2 kcal/mol. As shown in the Figure 25 and Figure 26 below, the AlClEt<sub>2</sub> bound titanium complex would prefer insertion to termination by 3.0 kcal/mol, for the case of the ethylene monomer. This explains how ZN systems in the past were successful at producing polymers, even when OC<sub>2</sub>H<sub>5</sub> groups or donor molecules could not have been present: for example, for traditional ZN systems where MgCl<sub>2</sub> and TiCl<sub>4</sub> were co-ground and no donors were employed<sup>68-70</sup>.

Since the current calculations indicate that the aluminium complexes present in the system can bind to the titanium metal center, it is also important to consider the possibility of chain termination by transfer of the chain to the aluminium. Our calculations indicate that this would be an unfavorable process, with the product of the chain transferred to the aluminium being endergonic by 12.7 kcal/mol. This indicates that the transition state for the chain transfer to aluminium would also be high. In comparison, the competing termination process of the chain transfer to monomer, in the presence of the aluminium complex, leads to a product that is exergonic by 13.0 kcal/mol, and has a barrier of 18.8 kcal/mol (see Figure 26 below). The energy barrier for the  $\beta$  H elimination for this case is 21.4 kcal/mol, which is higher than the chain transfer to the monomer. This indicates that the primary route to chain termination in the presence of aluminium would be chain transfer to monomer and not chain transfer to aluminium or  $\beta$  H elimination.

It is to be noted that the hydrogen response for the AlClEt<sub>2</sub> bound titanium complex is quite poor: 21.5 kcal/mol (see Figure 27). Since the compiled results in Table 8 indicated that the unmodified titanium complex would show excellent hydrogen response, which would decrease with the addition of the donors, the experimental observation that the addition of Lewis bases as donors improves the hydrogen response in ZN systems<sup>80-82</sup> further suggests the likelihood of the active species not being the unmodified titanium complex bound to the surface, but titanium modified by the binding of AlClEt<sub>2</sub>, or analogous complexes of aluminium, playing the role of donors for the Ziegler-Natta systems.



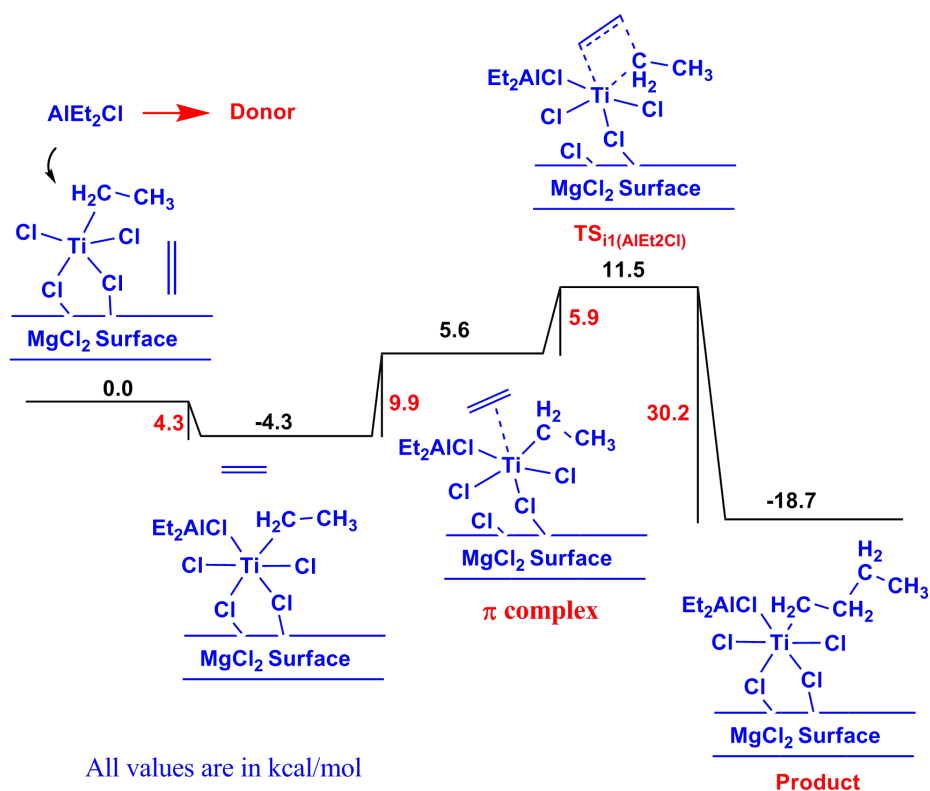


Figure 25. The free energy profile for the insertion of ethylene into the Ti-CH<sub>2</sub>CH<sub>3</sub> chain, with an AlClEt<sub>2</sub> group coordinated to Ti metal centre.

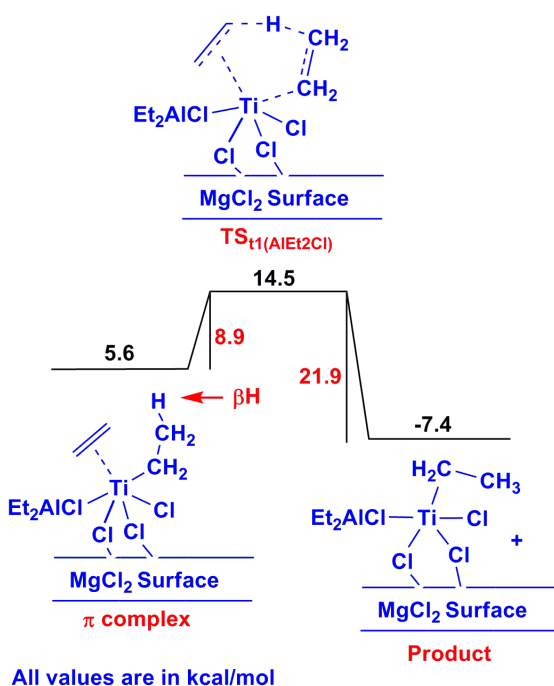


Figure 26. The free energy profile for the termination of the chain through chain transfer to the monomer; with an  $\text{AlClEt}_2$  group coordinated to Ti metal centre.

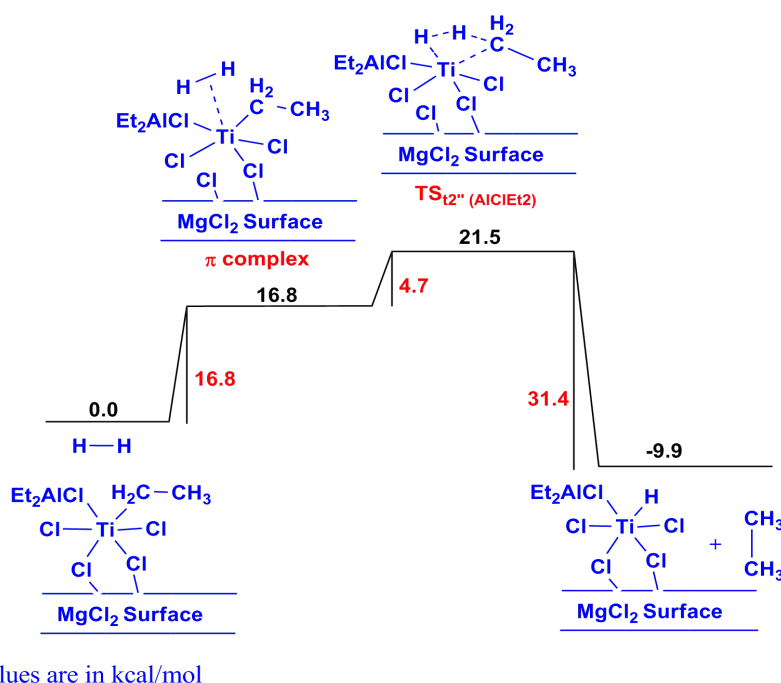


Figure 27. The energy profile for the termination of the chain by addition of  $\text{H}_2$  at the titanium center: with an  $\text{AlClEt}_2$  group coordinated to Ti metal centre.

### 3.4 Conclusions

Ziegler-Natta (ZN) catalyst systems are extremely important – a significant majority of polyolefins today are produced through ZN catalysis. However, their multi-component, multi-site nature has made them difficult to understand and study. The current full quantum chemical (QM) calculations, employing density functional theory (DFT) discuss insertion and termination processes at different active sites for supported ZN systems. The calculations have been done by employing a validated model for the  $\text{MgCl}_2$  support, and a variety of different active sites including (i) the conventional active site, featuring a chloride as the anionic ligand on the titanium, (ii) a  $\text{OC}_2\text{H}_5$  group as the anionic ligand on the titanium, and (iii) four different donors that can act as neutral ligands to the titanium. An important outcome of the current extensive investigations is the realization that the true titanium active sites on the  $\text{MgCl}_2$  surface are likely to possess at least one  $\text{OC}_2\text{H}_5$  group instead of chloride (s) at the titanium center, indicating that the conventional representation of the active site in ZN catalysts may not be correct. What is further shown is that one of the principal roles of internal donors in ZN catalysis is likely to be to increase the effectiveness of the active sites towards producing long chain polymers. Finally, also discussed is the response of the donor modified systems to the addition of dihydrogen to the system, the results again indicating that the thermodynamic favorability of the process would be enhanced by donor coordination to the metal center. The results from the current work have also led to new insights about the nature of the active species in ZN systems in the absence of donors: it is likely that in such systems, aluminium complexes, that are always present in ZN systems and assumed to date to be acting only as alkylating agents, can also play the role of donors to enhance the molecular weight of the polymer.

The current investigations therefore shed new light on these challenging, yet extremely important systems. It is expected that the understanding gained will aid further experimental and computational work in this field.

### 3.5 References

1. W. Kaminsky, *J. Polym. Sci., Part A: Polym. Chem.* **2004**, 42, 3911-3921.
2. W. Kaminsky, *Macromol. Chem. Phys.* **1996**, 197, 3907-3945.
3. W. Apisuk, N. Suzuki, H. J. Kim, D. H. Kim, B. Kitiyanan and K. Nomura, *J. Polym. Sci., Part A: Polym. Chem.* **2013**, 51, 2565-2574.
4. K. Liu, Q. Wu, W. Gao, Y. Mu and L. Ye, *Eur. J. Inorg. Chem.* **2011**, 1901-1909.
5. W. Kaminsky, O. Sperber and R. Werner, *Coord. Chem. Rev.* **2006**, 250, 110-117.
6. P. Sautet and F. o. Delbecq, *Chem. Rev.* **2009**, 110, 1788-1806.
7. M. Boero, M. Parrinello, S. Hueffer and H. Weiss, *J. Am. Chem. Soc.* **2000**, 122, 501-509.
8. A. Correa, R. Credendino, J. T. M. Pater, G. Morini and L. Cavallo, *Macromolecules* **2012**, 45, 3695-3701.
9. E. Grau, A. Lesage, S. b. Norsic, C. CopÃ©ret, V. Monteil and P. Sautet, *ACS Catal.* **2012**, 3, 52-56.
10. T. Wondimagegn and T. Ziegler, *J. Phys. Chem. C* **2012**, 116, 1027-1033.
11. D. V. Stukalov, V. A. Zakharov and I. L. Zilberberg, *J. Phys. Chem. C* **2010**, 114, 429-435.
12. A. Correa, F. Piemontesi, G. Morini and L. Cavallo, *Macromolecules* **2007**, 40, 9181-9189.
13. N. Kashiwa and J. Yoshitake, *Die Makromolekulare Chemie* **1984**, 185, 1133-1138.
14. N. Cui, Y. Ke, H. Li, Z. Zhang, C. Guo, Z. Lv and Y. Hu, *J. Appl. Polym. Sci.* **2006**, 99, 1399-1404.
15. J. C. Chadwick, *Macromol. Symp.* **2001**, 173, 21-35.
16. F. B. Coutinho, M. S. Costa and L. Santa Maria, *Polym. Bull.* **1992**, 28, 55-59.
17. G. Morini, E. Albizzati, G. Balbontin, I. Mingozzi, M. C. Sacchi, F. Forlini and I. Tritto, *Macromolecules* **1996**, 29, 5770-5776.
18. J. C. Chadwick, F. P. T. J. Van der Burgt, S. Rastogi, V. Busico, R. Cipullo, G. Talarico and J. J. R. Heere, *Macromolecules* **2004**, 37, 9722-9727.
19. N. Bahri-Laleh, M. Nekoomanesh-Haghighi and S. A. Mirmohammadi, *J. Organomet. Chem.* **2012**, 719, 74-79.

20. M. Seth and T. Ziegler, *Macromolecules* **2003**, 36, 6613-6623.
21. P. Margl, L. Deng and T. Ziegler, *J. Am. Chem. Soc.* **1998**, 121, 154-162.
22. G. Talarico, V. Busico and L. Cavallo, *Organometallics* **2004**, 23, 5989-5993.
23. M. Terano, T. Kataoka and T. Keii, *Die Makromolekulare Chemie* **1987**, 188, 1477-1487.
24. M. Terano, T. Kataoka, M. Hosaka and T. Keii, *Transition Metals and Organometallics as Catalysts for Olefin Polymerization; ed.; Kaminsky, W. and Sinn, H., Ed.* **1988**.
25. R. Credendino, D. Liguori, G. Morini and L. Cavallo, *J. Phy. Chem. C* **2014** **118**, 8050-8058.
26. A. Shiga, *Macromol. Res.* **2010**, 18, 956-959.
27. T. Taniike and M. Terano, *J. Catal.* **2012**, 293, 39-50.
28. S. H. Kim and G. A. Somorjai, *Proc. Natl. Acad. Sci.* **2006**, 103, 15289-15294.
29. H. Mori, M. Sawada, T. Higuchi, K. Hasebe, N. Otsuka and M. Terano, *Macromol. Rapid Commun.* **1999**, 20, 245-250.
30. D. V. Stukalov, V. A. Zakharov, A. G. Potapov and G. D. Bukatov, *J. Catal.* **2009**, 266, 39-49.
31. R. Credendino, J. T. M. Pater, A. Correa, G. Morini and L. Cavallo, *J. Phy. Chem. C* **2011**, 115, 13322-13328.
32. A. Schaefer, H. Horn and R. Ahlrichs, *J. Chem. Phys.* **1992**, 97, 2571-2577.
33. A. Schaefer, C. Huber and R. Ahlrichs, *J. Chem. Phys.* **1994**, 100, 5829-5835.
34. D. Andrae, U. Haeussermann, M. Dolg, H. Stoll and H. Preuss, *Theoretica Chimica Acta* **1990**, 77, 123-141.
35. J. P. Perdew, K. Burke and M. Ernzerhof, *Phys. Rev. Lett.* **1996**, 77, 3865-3868.
36. J. P. Perdew and Y. Wang, *Phys. Rev. B* **1992**, 45, 13244-13249.
37. S. Ansgar, H. Christian and A. Reinhart, *J. Chem. Phys.* **1994**, 100, 5829-5835.
38. A. D. Becke, *Phys. Rev. A* **1988**, 38, 3098-3100.
39. J. P. Perdew, *Phys. Rev. B* **1986**, 33, 8822-8824.
40. J. P. Perdew, *Phys. Rev. B* **1986**, 34, 7406-7406.
41. K. Eichkorn, O. Treutler, H. Oehm, M. Haeser and R. Ahlrichs, *Chem. Phys. Lett.* **1995**, 240, 283-290.

42. M. Sierka, A. Hoge Kamp and R. Ahlrichs, *J. Chem. Phys.* **2003**, 118, 9136-9148.
43. M. Mammen, E. I. Shakhnovich and G. M. Whitesides, *J. Org. Chem.* **1998**, 63, 3168-3175.
44. E. Kelly, M. Seth and T. Ziegler, *J. Phys. Chem. A* **2004**, 108, 2167-2180.
45. H. Yin, D. Wang and M. Valiev, *J. Phys. Chem. A* **2011**, 115, 12047-12052.
46. V. M. Williams, J. R. Kong, B. J. Ko, Y. Mantri, J. S. Brodbelt, M.-H. Baik and M. J. Krische, *J. Am. Chem. Soc.* **2009**, 131, 16054-16062.
47. W. Janse van Rensburg, C. Grove, J. P. Steynberg, K. B. Stark, J. J. Huyser and P. J. Steynberg, *Organometallics* **2004**, 23, 1207-1222.
48. Y. Qi, Q. Dong, L. Zhong, Z. Liu, P. Qiu, R. Cheng, X. He, J. Vanderbilt and B. Liu, *Organometallics* **2010**, 29, 1588-1602.
49. A. Bagno, W. Kantlehner, R. Kress, G. Saielli and E. Stoyanov, *J. Org. Chem.* **2006**, 71, 9331-9340.
50. J.-N. Li, M. Pu, C.-C. Ma, Y. Tian, J. He and D. G. Evans, *J. Mol. Catal. A: Chem.* **2012**, 359, 14-20.
51. I. Nikiforidis, A. Görling and W. Hieringer, *J. Mol. Catal. A: Chem.* **2011**, 341, 63-70.
52. X. Cao, R. Cheng, Z. Liu, L. Wang, Q. Dong, X. He and B. Liu, *J. Mol. Catal. A: Chem.* **2010**, 321, 50-60.
53. M. Boero, M. Parrinello, H. Weiss and S. Hueffer, *J. Phys. Chem. A* **2001**, 105, 5096-5105.
54. M. Boero, M. Parrinello and K. Terakura, *J. Am. Chem. Soc.* **1998**, 120, 2746-2752.
55. M. Seth, P. M. Margl and T. Ziegler, *Macromolecules* **2002**, 35, 7815-7829.
56. G. Monaco, M. Toto, G. Guerra, P. Corradini and L. Cavallo, *Macromolecules* **2000**, 33, 8953-8962.
57. J. W. Lee and W. H. Jo, *J. Organomet. Chem.* **2009**, 694, 3076-3083.
58. P. Brant and A. N. Speca, *Macromolecules* **1987**, 20, 2740-2744.
59. J. C. W. Chien and Y. Hu, *J. Mol. Catal. A: Chem.* **1989**, 27, 897-913.
60. N. Bahri-Laleh, A. Correa, S. Mehdipour-Ataei, H. Arabi, M. N. Haghighi, G. Zohuri and L. Cavallo, *Macromolecules* **2011**, 44, 778-783.
61. P. Cossee, *J. Catal.* **1964**, 3, 80-88.
62. E. J. Arlman and P. Cossee, *J. Catal.* **1964**, 3, 99-104.

63. G. H. Zohuri, A. B. Kasaeian, M. Torabi Angagi, R. Jamjah, M. A. Mousavian, M. Emami and S. Ahmadjo, *Polym. Int.* **2005**, 54, 882-885.
64. X. Wen, M. Ji, Q. Yi, H. Niu and J.-Y. Dong, *J. Appl. Polym. Sci.* **2010**, 118, 1853-1858.
65. A. V. Protchenko, K. H. Birjkumar, D. Dange, A. D. Schwarz, D. Vidovic, C. Jones, N. Kaltsoyannis, P. Mountford and S. Aldridge, *J. Am. Chem. Soc.* **2012**, 134, 6500-6503.
66. A. Paul and C. B. Musgrave, *Angew. Chem., Int. Ed.* **2007**, 46, 8153-8156.
67. P. M. Zimmerman, A. Paul, Z. Zhang and C. B. Musgrave, *Angew. Chem., Int. Ed.* **2009**, 48, 2201-2205.
68. S. Sivaram, *Product R&D*, **1977**, 16, 121-128.
69. Y. Doi, R. Ohnishi and K. Soga, *Die Makromolekulare Chemie, Rapid Communications* **1983**, 4, 169-174.
70. K. Soga, J. R. Park, H. Uchino, T. Uozumi and T. Shiono, *Macromolecules* **1989**, 22, 3824-3826.
71. M. X. Zhao, Yi, *Shiyong Huagong* **1987**, 16, 206-212.
72. Y. V. Kissin, L. A. Rishina and E. I. Vizen, *J. Polym. Sci., Part A: Polym. Chem.* **2002**, 40, 1899-1911.
73. P. Corradini, G. Guerra and L. Cavallo, *Acc. Chem. Res.* **2004**, 37, 231-241.
74. N. Kashiwa, *MMI Press. Symp. Ser.* **1983**, 4, 379.
75. A. Alshaiban and J. B. P. Soares, *Macromolecular Reaction Engineering* **2011**, 5, 96-116.
76. R. Robinson, D. S. McGuinness and B. F. Yates, *ACS Catal.* **2011**, 3, 3006-3015.
77. O. Novaro, S. Chow and P. Magnouat, *J. Catal.* **1976**, 42, 131-134.
78. O. Novaro, S. Chow and P. Magnouat, *J. Catal.* **1976**, 41, 91-100.
79. O. Novaro, S. Chow and P. Magnouat, *J. Polym. Sci.: Polym. Lett. Ed.* **1975**, 13, 761-765.
80. J. C. Chadwick, G. M. M. Van Kessel and O. Sudmeijer, *Macromol. Chem. Phys.* **1995**, 196, 1431-1437.
81. J. C. Chadwick, G. Morini, G. Balbontin, I. Camurati, J. J. R. Heere, I. Mingozi and F. Testoni, *Macromol. Chem. Phys.* **2001**, 202, 1995-2002.

82. J. C. Chadwick, G. Morini, E. Albizzati, G. Balbontin, I. Mingozi, A. Cristofori, O. Sudmeijer and G. M. M. Van Kessel, *Macromol. Chem. Phys.* **1996**, 197, 2501-2510.



## Chapter 4

### Abstract

The development of new donors (Lewis bases, usually containing oxygen atoms) is one of the chief areas of research in Ziegler Natta (ZN) olefin polymerization systems. The addition of such donors has led to the improvement in the activity and selectivity of ZN systems. However, in order for the donor to be effective, it has to be chemically stable and resistant to decomposition by Lewis acidic species such as  $\text{AlEt}_3$ . Discussed in the current work is the chemical stability of different ester donors, including aromatic benzoate donors and the silyl ester— a promising new donor class in ZN systems. Full quantum chemical calculations with density functional theory (DFT) indicate that esters can undergo decomposition through different pathways upon interaction with species such as the  $\text{AlEt}_3$  dimer:  $\text{Al}_2\text{Et}_6$ . Moreover, the studies show that the active, supported titanium catalyst species can cause donor decomposition and, in fact, is likely to be the bigger threat to donor decomposition than  $\text{Al}_2\text{Et}_6$ . This explains why the addition of excess donors can lead to the poisoning of the active site in ZN systems. We have also computationally investigated means of improving the silyl ester donors in order to make them more robust and resilient to donor decomposition by  $\text{Al}_2\text{Et}_6$  and the supported active titanium species.

## 4.1 Introduction

The development of Ziegler Natta (ZN) catalysis represents one of the most significant achievements in organometallic and inorganic chemistry in the past century. ZN catalysis is responsible for the production of over a hundred million tons of plastics per year in the form of a wide range of elastomers and fibers. In addition to developing the polymer industry enormously, ZN catalysis has also had a significant impact on how macromolecular chemistry is viewed in scientific and academic circles today.

There are several important chemical species that constitute the Ziegler-Natta (ZN) catalyst system. These include (a)  $\text{TiCl}_4$ : the precursor to the active catalyst, (b) the alkylating agent for  $\text{TiCl}_4$ , the most prominent example of which is the Lewis acidic tri-ethyl aluminium (*teal*), as well as (c) the catalyst support, the most common of which is  $\text{MgCl}_2$ . In addition to these species, over the last three decades, oxygen containing Lewis base “donor” molecules have also become an important component in ZN systems. The primary function of the donor species appears to be to influence the stereo and regio-selectivity of polymer formation by binding in the vicinity of the active catalyst<sup>1-6</sup>. Other possible functions attributed to the donor include influencing the polymerization kinetics by coordinating to the titanium center<sup>1,2</sup>, and making the (104)  $\text{MgCl}_2$  surface more accessible by coordinating more to the more acidic (110)  $\text{MgCl}_2$  surface<sup>3</sup>, according to the former Corradini model whose revisitation is still ongoing. It is, however, also known that the Lewis base donors can take part in undesired side reactions with Lewis acidic species present in the system, such as *teal*, a reaction that can lead to the decomposition of the donors<sup>4-10</sup>. The best donors are therefore the ones that are good at the primary function of influencing ZN catalysis, while showing a reduced tendency to take part in unwanted side reactions. Over the years, many donors<sup>1-3,11-26</sup> have been tested, and currently, silyl ether<sup>1,12</sup>, along with diethers<sup>12,22,23</sup>, are considered to be the most effective classes of donors for ZN catalysis. However, despite this progress in donor development, the most important subject of research in ZN systems today is the study and introduction of new donors that can significantly improve the activity and the selectivity of the catalyst systems.

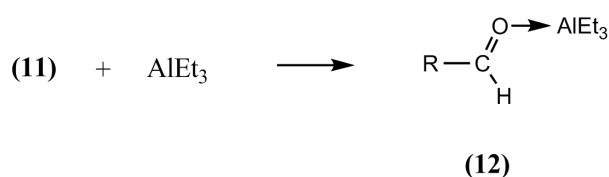
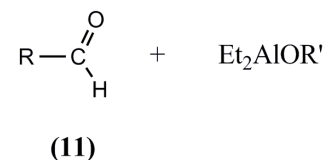
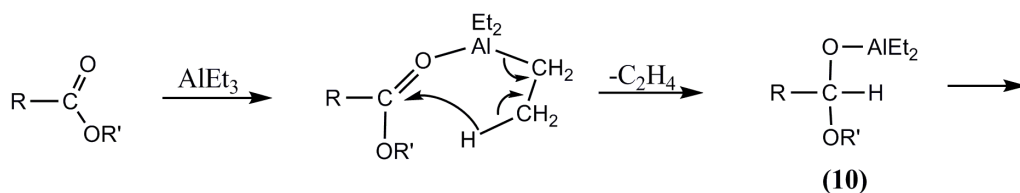
An important new donor class in this regard is that of the silyl ester:  $(\text{R})_2\text{Si}(\text{CH}_2\text{COOC}_2\text{H}_5)_2$ , ( $\text{R}=\text{C}_2\text{H}_5$ , isopropyl, cyclohexyl and phenyl). Studies have

emerged recently that indicate that this new class of molecules can be an alternative to the existing donors. However, in order for silyl esters to be effective, it is important they not show facile behavior with respect to unwanted side reactions during ZN catalysis. Pathways have been proposed in the literature by which esters present in ZN systems can be decomposed by the Lewis acidic *teal* moiety<sup>6</sup>. In the past, Chien *et al.*<sup>6</sup> had obtained the products **(9)**, **(11)** and **(14)** (characterized by GC-MS) leading to the proposal of the following pathways for ester decomposition by *teal*: a) the ketone pathway and b) the aldehyde pathway (see Figure 1).

While the ester studied by Chien and coworkers was ethyl benzoate (*eb*), the same decomposition pathways will be functional for any other donor having an ester group. Therefore, it is important to study these reaction pathways in ZN systems for the newly proposed silyl ester donors. This is the focus of the current computational investigation. The interaction of the silyl ester donor  $(\text{CH}_3)_2\text{Si}(\text{CH}_2\text{COOCH}_3)_2$  with *teal* has been investigated with full quantum chemical calculations with density functional theory (DFT). The dimeric form of *teal*,  $\text{Al}_2\text{Et}_6$ , has been considered in the calculations, keeping in mind experimental evidence that indicates that this is the most stable form of *teal*<sup>27-29</sup>. The aldehyde and ketone decomposition pathways have also been considered for ethylbenzoate (*eb*), *para*-ethoxyethylbenzoate (*peeb*), and *para*-isopropoxyethylbenzoate (*pipeb*). These donors have been considered because aromatic esters such as *eb* and *peeb* have been employed as donors in ZN systems<sup>14,15,23,30,31</sup>. Moreover, in addition to these aromatic ester moieties, ethyldecanoate, an aliphatic ester, has also been considered for the purpose of comparison. These five donors are shown in Figure 2 below. The reason for considering five different ester donors was to evaluate how the silyl ester fared in comparison to the other four ester donor in terms of the favorability/unfavorability of the decomposition pathways upon interaction with  $\text{Al}_2\text{Et}_6$ .



(4) Reduction to form aldehyde



(5) Alkylation of the aldehyde

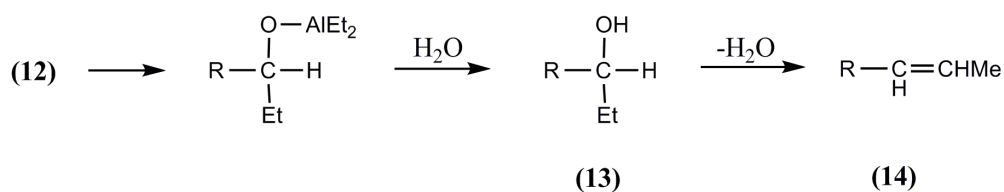


Figure 1. The mechanism of decomposition of donor with *teal*, reported by Chien and coworkers.

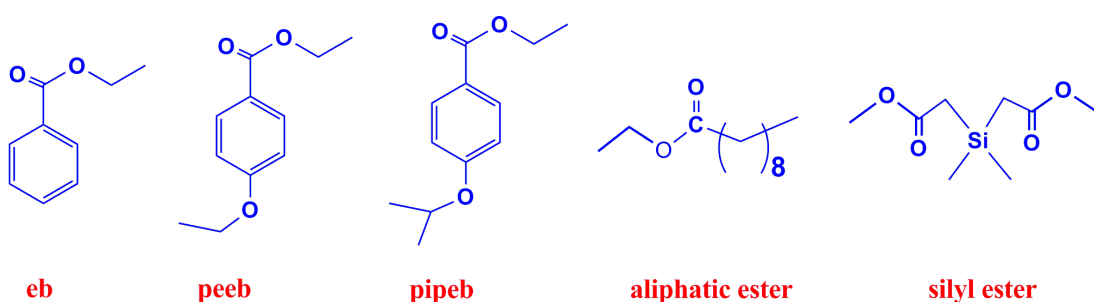


Figure 2. The five ester donors that have been considered in this study.

It is interesting to note that *teal* is not the only Lewis acidic species present in ZN systems. An important question that has been addressed in the current work is: why

cannot the titanium species in the ZN systems also interact with the donor and serve to decompose it? Like aluminium, titanium is also electron deficient, and therefore can function as an effective Lewis acidic center for the Lewis basic donor molecules. Indeed, donor interaction with titanium has been proposed in the literature<sup>1,2</sup>. This interaction can lead to decomposition of the donors. This interesting possibility of donor decomposition by the titanium complex has been considered for all the five ester cases. While the decomposition of donor (THF) by the titanium center has recently been studied by Sautet *et al.*<sup>3</sup>, the current work represents the first instance of systematic computational studies on donor decomposition by the titanium center.

The modeling of the  $\text{TiCl}_2\text{Et}$  species on the  $\text{MgCl}_2$  support has been done using a cluster model that is a modification of the  $\text{MgCl}_2$  model proposed by Cavallo's group<sup>12</sup>. The structure of the cluster model of  $\text{TiCl}_2\text{Et}$  species on the  $\text{MgCl}_2$  support is shown in Figure 3 below. The  $\text{MgCl}_2$  support is created by removing one molecule of  $\text{MgCl}_2$  from connecting (104) surfaces at an angle of  $120^\circ$ . This creates a small (110) surface between the (104) surfaces. This short (110) lateral cut has  $150^\circ$  bond angles with the (104) cuts, and serves as the site for the binding of the titanium species. The site for the binding of the titanium at the (110) lateral cut is the Corradini site, originally proposed by Corradini and coworkers<sup>32,33</sup>. It is to be noted that there are several other models that have been employed to mimic the  $\text{MgCl}_2$  surface<sup>34-39</sup>. The currently adopted Cavallo model is similar to these models in that it also involves the binding of the titanium center to the (110) surface, though there is a significant difference in that the current work focuses on the binding of the donor to the titanium metal centre whereas previous studies have considered donor coordination to the (110) lateral cuts on  $\text{MgCl}_2$  support<sup>35,38,39</sup>. Furthermore, this model also has the advantage of having features that compare favorably to experimentally observed  $\text{MgCl}_2$  surfaces, as discussed in the work of Cavallo and coworkers<sup>12</sup>.

In using the Cavallo model, we have made some modifications. As shown in Figure 4, we have reduced the number of  $\text{MgCl}_2$  layers from six to four. Furthermore, all the atoms in the cluster model were kept completely relaxed. In order to show that this does not create structures that are very different from the original fixed model employed, we have also done some calculations where we relaxed three conjugative  $\text{MgCl}_2$  moieties near the titanium centre, while the remaining  $\text{MgCl}_2$  surface atoms

were kept fixed. Specifically, the calculations pertained to the migration of the ethyl group from the titanium center to the *eb* donor. The barrier obtained from the fixed geometry  $\text{MgCl}_2$  model case is exactly the same (24.7 kcal/mol) as the barrier for the fully relaxed  $\text{MgCl}_2$  model case, thereby confirming the robustness of the applied model. Details of the employed model, as well as the validation done in comparison to the Cavallo model, are provided in the Figures 4 and Tables 1 and 2.

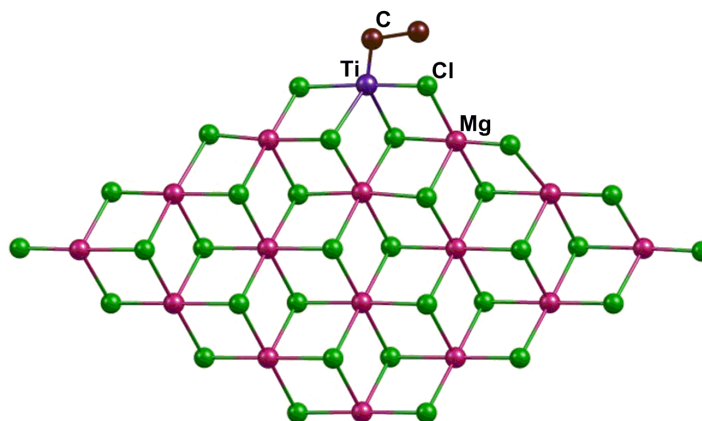


Figure 3. The model employed for representing  $\text{TiCl}_2\text{Et}$  on the (110)  $\text{MgCl}_2$  lateral cuts; the hydrogens of ethyl group are not shown for the purpose of clarity.

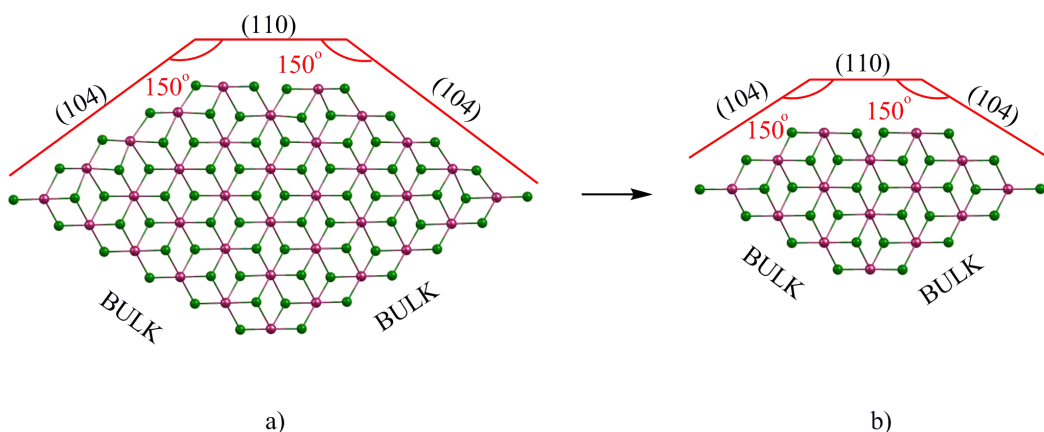


Figure 4. The previously proposed model for the  $\text{MgCl}_2$  layers developed by Cavallo *et al.* are shown in Figure 4a ; Figure 4b shows the current model, with four layers instead of six, that we have employed in the current computational investigations.

Table 1.  $\Delta E$  values (in kcal/mol) for different donor coordination to the magnesium atom in  $MgCl_2$  layers; comparison between the previously proposed model and our current model.

Donors	$\Delta E$ (kcal/mol)	
	Previously Proposed Model	The Current Model Employed in the Calculations
1,3-diether	-29.8	-29.5
succinate	-42.2	-39.3
alkoxysilane	-30.5	-32.9

Table 2.  $\Delta E$  values (in kcal/mol) for the insertion barriers of propylene with no donor attached to the metal centre; comparison between the previously proposed model and our current model.

Results	Insertion barriers (in kcal/mol)			
	Previously Proposed Model		The Current Model Employed in the Calculations	
Pathway	1,2-re	1,2-si	1,2-re	1,2-si
Without donor	0.0	-0.2	0.0	-0.1

Finally, from the insights gained of the propensity of the unwanted side reactions of the silyl esters with  $Al_2Et_6$  and  $TiCl_2Et$  on the  $MgCl_2$  support, we have proposed modifications for the silyl ester donors that would make them more robust against decomposition by the Lewis acidic species present in ZN systems.

## 4.2 Computational Details

All the calculations have done with density functional theory (DFT), employing the Turbomole 6.0 suite of programs<sup>40-42</sup>. Geometry optimizations have been performed





Closed shell calculations were done for the  $\text{Al}_2\text{Et}_6$  on  $\text{MgCl}_2$  layer model system cases, while open shell calculations have been considered for the  $\text{TiCl}_2\text{Et}$  on  $\text{MgCl}_2$  layer model system cases. No spin contamination was observed in any of the open shell calculations.

The values reported are  $\Delta G$  values, with zero point energy, internal energy and entropic contributions (including translational, rotational and vibrational entropy contributions) included through frequency calculations on the optimized minima and transition state structures, with the temperature taken to be 298.15 K. Care has been taken to ensure that all the reported transition state structures contained only one imaginary frequency corresponding to the correct normal mode. The Turbomole package employs the quasi-Newton-Josephson method for finding the transition state. It is based on the restricted second-order method, which employs Hessian shift parameters. IRC<sup>58</sup> calculations have been considered for the confirmation of the transition states. In every case, the IRC calculations have yielded the correct reactant and product structures. It is to be noted that in order to do the IRC calculations, Turbomole 6.4 has been employed.

In order to avoid the problem of mis-representation of the entropic term when the reactants are considered separately in a reaction pathway<sup>59</sup>, all the reaction pathways have been determined starting with the reactants in the vicinity of each other, instead of beginning from the separated reactant species, a procedure that has also been followed in several previous computational studies<sup>60-68</sup>.

### 4.3 Results and Discussion

As mentioned in the Introduction, the pathways for the decomposition of five ester donors: the aromatic esters (*eb*, *peeb*, *pipeb*), the aliphatic ester and the silyl ester with different Lewis acidic moieties ( $\text{Al}_2\text{Et}_6$  and  $\text{TiCl}_2\text{Et}$  on  $\text{MgCl}_2$  support) have been investigated. For the decomposition studies, we have considered two particular pathways: the ketone and the aldehyde pathways, based on the experimental observations of Chien and coworkers<sup>6</sup>, as discussed in the Introduction. Both the pathways differ based on the nature of the migratory group: the ethyl group in the ketone pathway and the hydride in the aldehyde pathway. The energy profiles for the

decomposition pathways are shown in the Figures 5 and 6 below, for the case of the *eb* donor (R = Ph in the figures).

#### 4.3.1 The Interaction of different ester donors with Al<sub>2</sub>Et<sub>6</sub>:

The interaction between the ester and Al<sub>2</sub>Et<sub>6</sub> is favorable, leading to an stable adduct complex (see Table 4 below). Discussed below are the ketone and aldehyde pathways for ester decomposition with Al<sub>2</sub>Et<sub>6</sub>. The decomposition pathways are considered first for the *eb* donor, followed by a section where the results for the decomposition of all the donors are compared.

Table 4.  $\Delta G$  values (in kcal/mol) for the donor co-ordination to the Al<sub>2</sub>Et<sub>6</sub> species.

Donors	$\Delta G$ (in kcal/mol)
<i>eb</i>	-12.4
<i>peeb</i>	-11.7
<i>pipeb</i>	-14.3
aliphatic ester	-12.7
silyl ester	-18.7

**4.3.1.1 The Ketone Pathway:** After the formation of the adduct complex, the transfer of an ethyl group from Al<sub>2</sub>Et<sub>6</sub> to the donor carbon would initiate the ketone pathway (KP). This route is shown in black in Figure 5 below, for the case of the *eb* donor. It is this first step: that is the slowest, having a barrier of 31.4 kcal/mol (see Figure 5). This reaction also leads to the dissociation of the Al-C bond, so that the complex **1a'** that is formed has an AlEt<sub>3</sub> species lying in the vicinity of (OC<sub>2</sub>H<sub>5</sub>)(Et)(R)C-O-AlEt<sub>2</sub> (see Figure 5 below). This species can rearrange to give to a new complex, **1c**, that lies 9.8 kcal/mol lower in energy than **1a'** on the free energy landscape. This change occurs with a small barrier of 3.3 kcal/mol. In **1c**, the free AlEt<sub>3</sub> has shifted to the oxygen of the OC<sub>2</sub>H<sub>5</sub> group (see Figure 5).

Subsequent to this, from **1c**, the reaction proceeds in a facile manner with very low barriers leading to a C=O---Al adduct that can dissociate to yield the ketone. The reaction is also thermodynamically favorable, being exergonic by 19.9 kcal/mol. The reason for the reactions being so favorable after the first step is due to the cooperation between the two aluminium groups in Al<sub>2</sub>Et<sub>6</sub>. The transfer of the ether group from the carbonyl carbon of the donor to the aluminium occurs through a favorable six membered transition state **TS<sub>1c,1c'</sub>**, involving the two AlEt<sub>3</sub> molecules. Overall, the reaction is exergonic by 22.6 kcal/mol.

**4.3.1.2 The Aldehyde Pathway:** Beginning from the adduct complex **1a**, the alternate route to the ketone pathway is the aldehyde pathway (AP). This is shown in red in Figure 5. Here, the first step involves the transfer of a hydrogen from an ethyl group of Al<sub>2</sub>Et<sub>6</sub> to the carbonyl carbon of the donor, leading to the formation of **1a''** along with the release of CH<sub>2</sub>CH<sub>2</sub> (see Figure 5). As in the case of KP, the first step is seen to be the slowest step. **1a''** can be converted to the more stable complex **1b** through a process having a small barrier of 1.1 kcal/mol, by the rearrangement of the free AlEt<sub>3</sub> group. Subsequent to this, the cooperation between the two AlEt<sub>3</sub> groups leads to a favorable six membered transition state **TS<sub>1b,1b'</sub>**, just as in KP, having a barrier of only 7.1 kcal/mol. The subsequent steps are analogous to KP, leading finally to the aldehyde product. The reaction is thermodynamically favorable by 4.0 kcal/mol (see Figure 5).

A perusal of the two pathways: KP and AP, indicates that both are competitive: the slowest step in the AP decomposition pathway has a barrier of 31.1 kcal/mol, which is only 0.3 kcal/mol lower than the barrier for the slowest step in KP (31.4 kcal/mol). This indicates that both the aldehyde (**1d**) and the ketone (**1e**) can be formed in the reaction vessel due to the decomposition of the *eb* donor by Al<sub>2</sub>Et<sub>6</sub>.

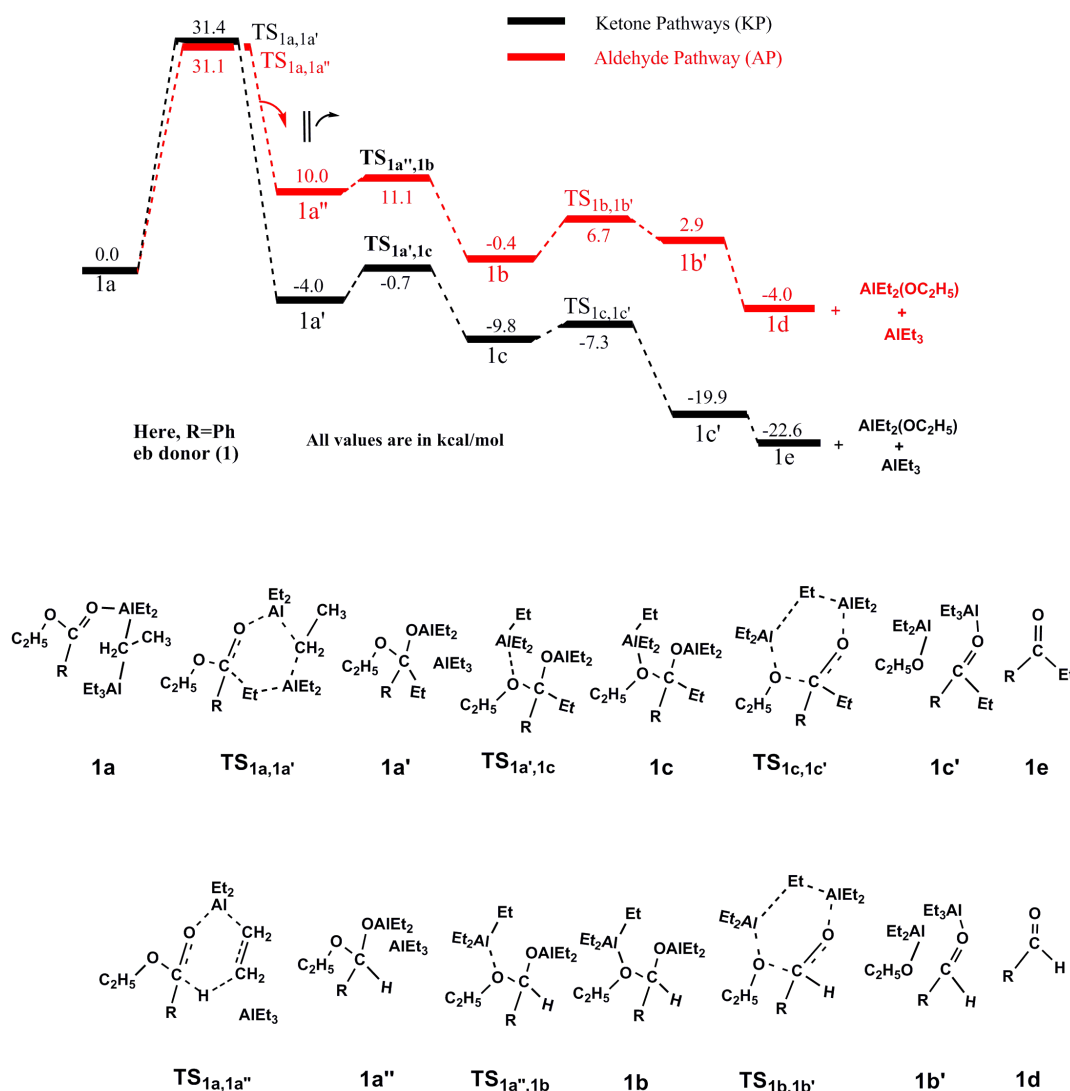


Figure 5. The free energy profile for the decomposition of the aromatic ester (*eb*) donor (R= Ph) by  $\text{Al}_2\text{Et}_6$  through the ketone and aldehyde pathways (KP and AP).

**4.3.1.3 Extension of the Ketone and aldehyde Pathway:** In KP, the product of the interaction between the ester donor and  $\text{Al}_2\text{Et}_6$  is a ketone. For the case of the *eb* donor, this is the species  $\text{PhCOEt}$  (**1e**). In the presence of  $\text{Al}_2\text{Et}_6$ , it is possible that the formed ketone can take part in further reactions. Moreover, since the KP and the AP would also lead to the formation of an  $\text{AlR}_x(\text{OEt})$  species, there is the possibility that the ketone formed can interact not only with  $\text{Al}_2\text{Et}_6$ , but also with species such as  $\text{Al}_2\text{Et}_5\text{OEt}$  and  $\text{Al}_2\text{Et}_4(\text{OEt})_2$ . However, the calculations indicate that adduct complex formation is the most favorable for  $\text{Al}_2\text{Et}_6$ , the resulting adduct, **C**, being stable by 25.5 kcal/mol (see Figure 6 below). Hence, **C** is the species that is most likely to be

formed. Moreover, since  $\text{Al}_2\text{Et}_5\text{OEt}$  or  $\text{Al}_2\text{Et}_4(\text{OEt})_2$  would be formed only as a result of the decomposition interactions between the donor and  $\text{Al}_2\text{Et}_6$ , they are likely to exist in much lower concentrations than  $\text{Al}_2\text{Et}_6$ , which further suggests that the ketone- $\text{Al}_2\text{Et}_6$  adduct is the most likely species that would be formed for the subsequent reactions of the ketone in the ZN catalyst system.

As shown in Figure 6, **C** can undergo reactions similar to the KP and the AP discussed earlier: it can follow a pathway where an ethyl group is transferred to the carbonyl carbon. Due to the cooperation between the two  $\text{AlEt}_3$  groups, this reaction also goes through a six-membered transition state ( $\text{TS}_{\mathbf{1f},\mathbf{1k}}$ ), having a barrier of 24.7 kcal/mol. The product of this reaction is the complex having a C-O-Al bond: the complex **1k** (see Figure 6). Analogous to this pathway is the route where a hydrogen is transferred from the ethyl group on the aluminium to the carbonyl carbon in the adduct complex **1f**, a route that is similar to AP discussed earlier. The slowest step in this pathway has a barrier of 19.9 kcal/mol, which indicates that it would be the kinetically preferred pathway.

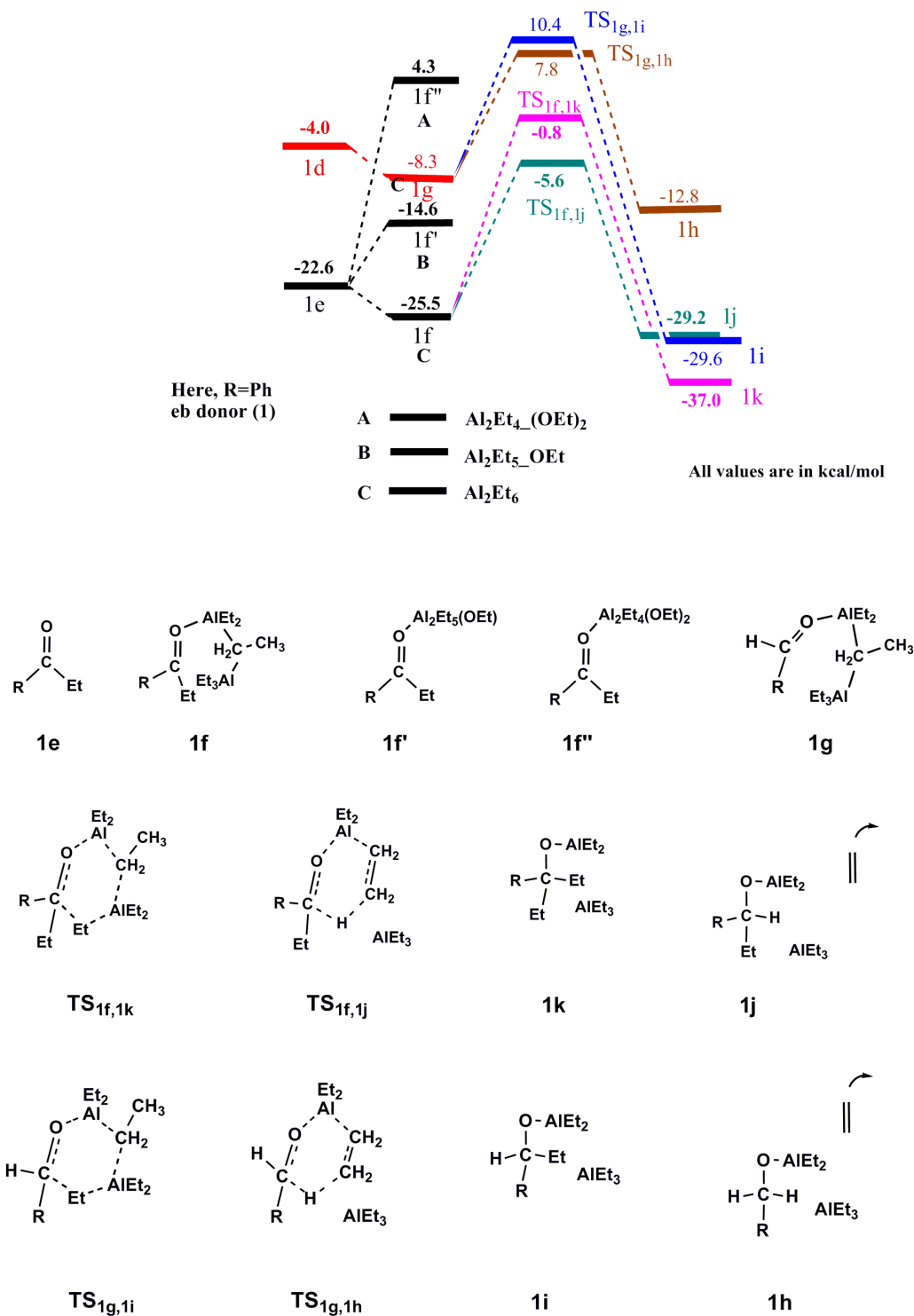


Figure 6. The free energy profile for the subsequent decomposition of the ketone and aldehyde pathways formed by decomposition of the aromatic ester (*eb*) donor by  $\text{Al}_2\text{Et}_6$ .

Just as the ketone product **1e** of the KP route can take part in further decomposition reactions with  $\text{Al}_2\text{Et}_6$ , so can the aldehyde product **1d**, formed as a result of the AP route. Figure 6 shows that, just as in the case of **1e**, **1d** also prefers to bind to  $\text{Al}_2\text{Et}_6$  over aluminium species having OEt groups ( $\text{Al}_2\text{Et}_5\text{OEt}$  and  $\text{Al}_2\text{Et}_4(\text{OEt})_2$ ). Furthermore, the adduct complex formed, **1g**, can interact with  $\text{Al}_2\text{Et}_6$  in the same manner as the adduct complex **1f** discussed in the previous section. As before, there are two pathways involving ethyl transfer and hydrogen transfer respectively to the carbonyl carbon of the aldehyde. The slowest step of these routes is, as before, the first step, having barriers of 18.7 kcal/mol and 16.1 kcal/mol respectively.

**4.3.1.4 Comparison of Different Donor Cases:** The previous sections discussed the possibilities of donor decomposition through the interaction of the *eb* donor with  $\text{Al}_2\text{Et}_6$ . This particular donor has been considered in the previous sections in order to compare with the decomposition experiments between  $\text{Al}_2\text{Et}_6$  and *eb* by Chien *et al.*<sup>6</sup>. As shown in the previous sections, the current computational results match well with the experimental findings, indicating the feasibility and validity of the considered mechanistic routes.

The same pathways as discussed in the sections **i(a)-i(c)** above have also been investigated for the other four donor cases considered: *peeb*, *pipeb*, aliphatic ester and the silyl ester. The free energies corresponding to the barrier heights and the intermediates relative to the reactant species have been gathered together in the Tables 5, 6, 7, and 8 (the nomenclature employed in the tables is analogous to the *eb* case, with **2**, **3**, **4**, and **5** used for *peeb*, *pipeb*, aliphatic and silyl ester respectively). The calculations indicate that all the donor cases have similar energy profiles. Shown in Figure 7 are the barrier heights for the slowest step during the KP and AP routes for the five donor cases. What becomes clear from the results is that the silyl ester compares quite favorably with the other donors with regard to AP. However, it is also clear that the silyl ester donor is more susceptible to donor decomposition by the KP route: it has a lower barrier to decomposition for the slowest step in comparison to all the other donors. Since the slowest step in KP involves a six-membered transition state in close proximity to the R groups of the ester donor (see Figure 5 above), the means to increasing the barrier for this step would be to increase the steric bulk of the



R groups in the silyl ester. This has been done and the results are discussed in the next section.

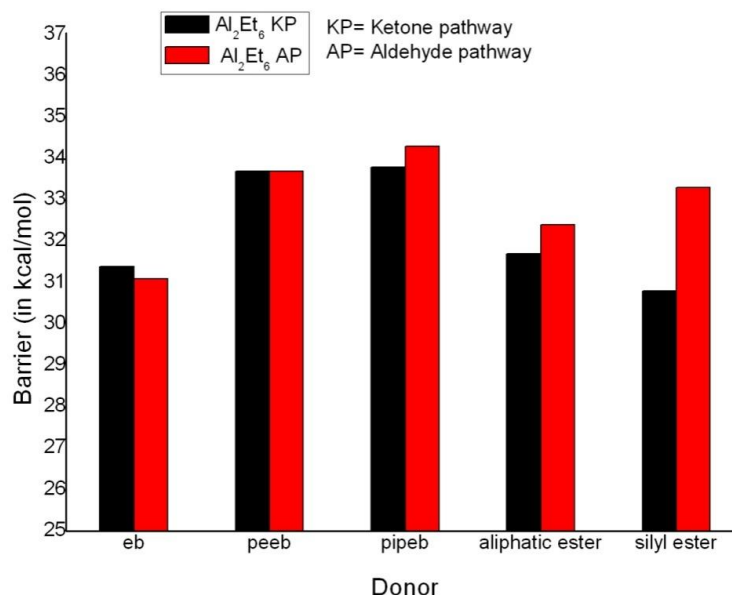


Figure 7. Relative barriers for the slowest step for the decomposition of different donors through their interaction with Al<sub>2</sub>Et<sub>6</sub> through the ketone and aldehyde pathways.

Table 5.  $\Delta G$  values (in kcal/mol) for decomposition of the *peeb* donor with Al<sub>2</sub>Et<sub>6</sub> species through the ketone and aldehyde pathways (KP and AP); the highest barrier, corresponding to the slowest step in each pathway, is highlighted in bold.

<i>peeb</i> donor  (2)	K P	2a	TS <sub>2a,2c</sub>	2a'	TS <sub>2a',2c</sub>	2c	TS <sub>2c,2c'</sub>	2c'	2e	2f	TS <sub>2f,2k</sub>	2k
		0.0	<b>33.7</b>	-0.6	2.4	-8.4	-5.8	-20.9	-20.9	-26.0	1.0	-33.8
	A P	2a	TS <sub>2a,2b</sub>	2a''	TS <sub>2a'',2b</sub>	2b	TS <sub>2b,2b'</sub>	2b'	2d	2g	TS <sub>2f,2j</sub>	2j
		0.0	<b>33.7</b>	13.2	14.9	2.3	7.3	-3.8	-2.6	-6.4	-1.7	-22.1
										TS <sub>2g,2i</sub>	2i	
											12.8	-25.5
										TS <sub>2g,2h</sub>	2h	
											11.0	-8.9

Table 6.  $\Delta G$  values (in kcal/mol) for decomposition of the *pipeb* donor with  $Al_2Et_6$  species through the ketone and aldehyde pathways (KP and AP); the highest barrier, corresponding to the slowest step in each pathway, is highlighted in bold.

<i>pipeb</i> donor  (3)	K P	3a	TS <sub>3a,3c</sub>	3a'	TS <sub>3a',3c</sub>	3c	TS <sub>3c,3c'</sub>	3c'	3e	3f	TS <sub>3f,3k</sub>	3k
		0.0	<b>33.8</b>	-1.7	1.7	-	-7.1	-22.6	-16.5	-27.3	TS <sub>3f,3j</sub>	3j
						8.7					-3.8	-26.4
	A P	3a	TS <sub>3a,3b</sub>	3a''	TS <sub>3a'',3b</sub>	3b	TS <sub>3b,3b'</sub>	3b'	3d	3g	TS <sub>3g,3i</sub>	3i
		0.0	<b>34.3</b>	13.5	15.3	2.6	7.0	-3.7	1.6	-6.8	12.3	-25.4
											TS <sub>3g,3h</sub>	3h
										10.9	-9.1	

Table 7.  $\Delta G$  values (in kcal/mol) for decomposition of the aliphatic ester donor with  $Al_2Et_6$  species through the ketone and aldehyde pathways (KP and AP); the highest barrier, corresponding to the slowest step in each pathway, is highlighted in bold.

Aliphatic ester donor  (4)	K P	4a	TS <sub>4a,4c</sub>	4a'	TS <sub>4a',4c</sub>	4c	TS <sub>4c,4c'</sub>	4c'	4e	4f	TS <sub>4f,4k</sub>	4k
		0.0	<b>31.7</b>	0.5	5.3	-9.0	-6.8	-20.7	-23.0	-24.7	TS <sub>4f,4j</sub>	4j
											-4.9	-23.7
	A P	4a	TS <sub>4a,4b</sub>	4a''	TS <sub>4a'',4b</sub>	4b	TS <sub>4b,4b'</sub>	4b'	4d	4g	TS <sub>4g,4i</sub>	4i
		0.0	<b>32.4</b>	9.6	11.1	-1.5		0.3	-2.3	-2.2	17.0	-27.5
							5.0				TS <sub>4g,4h</sub>	4h
										11.7	-12.3	

Table 8.  $\Delta G$  values (in kcal/mol) for decomposition of the silyl ester donor with  $Al_2Et_6$  species through the ketone and aldehyde pathways (KP and AP); the highest barrier, corresponding to the slowest step in each pathway, is highlighted in bold.

silyl ester donor	K P	5a	TS <sub>5a,5c</sub>	5a'	TS <sub>5a',5c</sub>	5c	TS <sub>5c,5c'</sub>	5c'	5e	5f	TS <sub>5f,5k</sub>	5k	
		0.0	<b>30.8</b>	1.4	4.2	-5.6	-4.5	-19.1	-19.9	-23.5	9.7	-29.3	
	(5)	A P	5a	TS <sub>5a,5b</sub>	5a''	TS <sub>5a'',5b</sub>	5b	TS <sub>5b,5b'</sub>	5b'	5d	5g	TS <sub>5g,5i</sub>	5i
			0.0	<b>33.3</b>	11.5	13.6	-2.4	2.5	-3.3	-2.2	-4.4	17.9	-23.3
											TS <sub>5g,5h</sub>	5h	
											13.6	-10.9	

#### 4.3.1.5 Modifications to the silyl ester donor and impact on decomposition barrier:

Since the silyl ester donor is susceptible to decomposition by the KP route, we have investigated the effect of modifying the R groups in the silyl ester on the barrier for the slowest step in the KP. As Table 9 shows below, different R groups have been considered for the silyl ester case, including  $-C_2H_5$ ,  $-iPr$ ,  $-Ph$  and cyclohexyl in different combinations, in comparison to the two  $-CH_3$  groups coordinated silyl ester that had been considered in the previous section. The slowest step of the KP route was considered for each of the six cases. The results indicate that increasing the steric bulk on the ester indeed does have a salutary effect of raising the barrier height and making it comparable to the other donor cases (see Table 9). The most effective donor for resisting decomposition by  $Al_2Et_6$  is seen to be the  $(C_2H_5COOCH_2)_2SiC_2H_5(Ph)$  (**5D**) donor, where the two  $-CH_3$  groups in **5A** have been replaced by a  $C_2H_5$  and a phenyl group. As shown in Table 9, the difference between the barriers for the **5A** and **5D** cases is 2.3 kcal/mol. While this suggests that replacing smaller groups with more bulky groups leads to a small change in the barrier height, especially keeping the accuracy of DFT in mind, this also indicates that there could be a significant change in the rates of the reactions when one considers the Eyring equation. The barrier to

decomposition for the **5D** donor case (33.1 kcal/mol) is higher than when two phenyl groups are coordinated to the silicon center, which suggests that increasing steric bulk has to be balanced with the increased electron donation of the R group to the silicon. Hence, a silyl ester donor with moderate steric bulk but with reduced electron density at the metal center is likely to be the most robust donor for ZN systems with regard to decomposition by  $\text{Al}_2\text{Et}_6$ .

Table 9.  $\Delta G$  values (in kcal/mol) for the barrier for the slowest step in the decomposition of different silyl ester donor cases with  $\text{Al}_2\text{Et}_6$ , through the ketone pathway.

Serial no.	Silyl ester donor	Free Energy barriers (in kcal/mol)
		$\text{Al}_2\text{Et}_6$ (ketone pathway)
5A	$(\text{CH}_3\text{COOCH}_2)_2\text{Si}(\text{CH}_3)_2$	30.8
5B	$(\text{C}_2\text{H}_5\text{COOCH}_2)_2\text{Si}(\text{C}_2\text{H}_5)_2$	31.1
5C	$(\text{C}_2\text{H}_5\text{COOCH}_2)_2\text{Si}(i\text{Pr})_2$	32.1
5D	$(\text{C}_2\text{H}_5\text{COOCH}_2)_2\text{SiC}_2\text{H}_5(\text{Ph})$	33.1
5E	$(\text{C}_2\text{H}_5\text{COOCH}_2)_2\text{Si}(\text{Ph})_2$	32.3
5F	$(\text{C}_2\text{H}_5\text{COOCH}_2)_2\text{SiC}_2\text{H}_5(\text{cyclohexyl})$	32.3
5G	$(\text{C}_2\text{H}_5\text{COOCH}_2)_2\text{Si}(\text{cyclohexyl})_2$	32.8

#### 4.3.2 The Interaction of the donors with $\text{TiCl}_2\text{Et}$ on the $\text{MgCl}_2$ supported layer:

The previous sections have considered the interaction of  $\text{Al}_2\text{Et}_6$  with different ester donors, leading to their decomposition through the ketone and the aldehyde pathways (KP and AP respectively). However, as mentioned in the Introduction, the donors can also interact with the titanium complex present on the  $\text{MgCl}_2$  surface. This is because the titanium complex can also behave as a Lewis acidic site to the donor molecules. However, as shown in Table 10 below, the coordination of the different ester donors to the titanium center of  $\text{TiCl}_2\text{Et}$  on the  $\text{MgCl}_2$  surface is a favorable, exergonic process in all the cases considered. This indicates that there exists the distinct possibility that the donor can indeed bind to the titanium center, which further

suggests that donor decomposition by titanium bound on the  $\text{MgCl}_2$  surface is a feasible proposition. What is also of interest is the fact that the binding of the silyl ester on to the titanium is the most favorable, among all the donors considered: its binding is seen to be exergonic by 30.0 kcal/mol (see Table 10). This is because the silyl ester can not only bind to the titanium, but can also employ its other oxygen to simultaneously bind to an adjoining magnesium atom of the (110) lateral cut. The optimized structure of the silyl ester bound to the  $\text{MgCl}_2$  layer has been shown in Figure 8 (please note that the figure has only one  $\text{MgCl}_2$  layer in the structure, for the purpose of clarity). This possibility does not exist for the other case of the donors because the steric nature of the dual binding makes it impossible for the two oxygens of the donors to bind to the titanium and magnesium centers simultaneously for all the other donor cases.

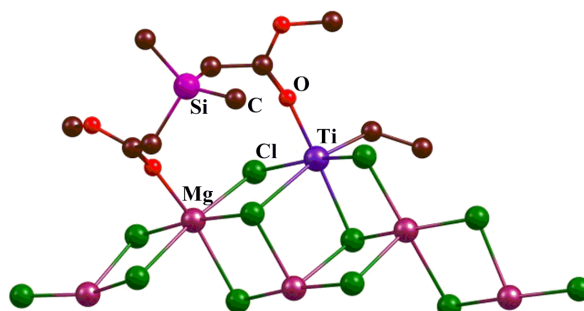


Figure 8. The optimized structure of the silyl ester donor coordinating to the titanium and magnesium centers through two of its oxygens; hydrogen atoms are not shown, and only one  $\text{MgCl}_2$  layer is shown, for the purpose of clarity.

Table 10.  $\Delta G$  values (in kcal/mol) for the coordination of the ester donors to  $\text{TiCl}_2\text{Et}$  supported on  $\text{MgCl}_2$ .

Donors	$\Delta G$ (in kcal/mol)
<i>eb</i>	-4.9
<i>peeb</i>	-7.0
<i>pipeb</i>	-6.2
aliphatic ester	-12.6
silyl ester	-30.0

**4.3.2.1 The Ketone Pathway:** Like in the case of the interaction of the ester donors with  $\text{Al}_2\text{Et}_6$ , the interaction of the five ester donors with  $\text{TiCl}_2\text{Et}$  supported on  $\text{MgCl}_2$  would also lead to the decomposition through two pathways. Considered first is the ketone pathway (KP). As shown in Figure 9 below, for the case of the *eb* donor, the first step is the transfer of the  $\text{C}_2\text{H}_5$  group from titanium to the donor carbon, which is the slowest of the reaction pathway, having a barrier of 24.7 kcal/mol. This leads to the formation of the complex **Ia'**. Subsequent to this, the  $\text{OC}_2\text{H}_5$  species is seen to transfer in a barrierless fashion to the titanium center from the donor carbon. The barrierless nature of this second step has been confirmed by a linear transit calculation, which showed that the transfer of the  $\text{OC}_2\text{H}_5$  group from the donor carbon to the titanium occurs with a lowering of energy without any barrier. The reason for this is the electron deficient nature of the titanium in the complex **Ia'**, due to its having lost the coordination to the  $\text{C}_2\text{H}_5$  group. This makes its conversion to the complex **Ic** a very facile process.

It is to be noted that the transition state  $\text{TS}_{\text{Ia,Ia}'}$  for the  $\text{C}_2\text{H}_5$  transfer is a four membered ring, which is in contrast to the corresponding transition state for the interaction of the donors with  $\text{Al}_2\text{Et}_6$ , where the transition state was six-membered. This was due to the cooperation between the two aluminium centers in the previous case, which is not present for the case of the titanium complex. The optimized structure of the transition state is shown in Figure 10. However, interestingly, the barrier is lower for the transfer step: here it is 24.7 kcal/mol, as shown in Figure 9, as compared to 31.4 kcal/mol for the  $\text{Al}_2\text{Et}_6$  case (the *eb* donor considered for both cases). The reason for the higher barrier in case of  $\text{Al}_2\text{Et}_6$  is the more acidic nature (more positive charge) of the aluminium center compared to titanium. The positive charge on titanium in the transition state for the slowest (first) step is stabilized by an  $\alpha$  agostic interaction with a hydrogen of the ethyl group. The charges on the aluminium and titanium centers in the first transition state have been calculated by NBO analysis<sup>69</sup>, for both the KP and the AP routes, and shown in Table 11. In case of  $\text{Al}_2\text{Et}_6$ , the charge at the aluminium center, lies in the range 1.88-1.89 and 1.95-1.98 for the transition states in the KP and the AP routes respectively, for the different donor cases, while the charge on titanium on  $\text{MgCl}_2$  support is in the range 1.35-1.43 in the KP route and 1.48-1.63 in the AP route. The values indicate that the charge on titanium with  $\text{MgCl}_2$  support is less positive compared to the charge on aluminium.

This is the reason that the loss of the ethyl or hydride from the aluminum comes at a greater energetic cost than for titanium.

Table 11. The charge obtained for the aluminium and titanium metal center for the transition state structure for the slowest, first step of the KP and the AP decomposition pathways upon interaction with  $\text{Al}_2\text{Et}_6$  and  $\text{TiCl}_2\text{Et}$  on  $\text{MgCl}_2$  support respectively.

Donor	Charge on the aluminium center		Charge on the titanium center	
	$\text{Al}_2\text{Et}_6$		$\text{TiCl}_2\text{Et}$ on $\text{MgCl}_2$ support	
	For KP	For AP	For KP	For AP
<i>eb</i>	1.89	1.98	1.41	1.49
<i>peeb</i>	1.89	1.98	1.43	1.50
<i>pipeb</i>	1.89	1.98	1.43	1.50
aliphatic ester	1.89	1.96	1.37	1.63
silyl ester	1.88	1.95	1.35	1.48

This result indicates that the possibility of the donor being decomposed by the titanium center is higher than it being decomposed by the aluminum center, since it comes at a lower energetic cost. This is a significant result, and also serves to provide an explanation for why the addition of excess donors leads to the poisoning of the active site in ZN catalysts<sup>13,70,71</sup>. Subsequent to the formation of **Ic**, as in the  $\text{Al}_2\text{Et}_6$  case, the reaction proceeds in a facile manner to result in the formation of the ketone.

**4.3.2.2 The Aldehyde Pathway:** As shown in Figure 9, the AP yields the same products as in the previously considered  $\text{Al}_2\text{Et}_6$  interaction with the donors. As for the KP with  $\text{TiCl}_2\text{Et}$  supported on  $\text{MgCl}_2$ , the slowest step is the first step. In this step, as discussed for the AP with  $\text{Al}_2\text{Et}_6$ , a hydrogen atom is transferred, with the elimination of  $\text{C}_2\text{H}_4$ , to the donor carbon center. Also, like in  $\text{Al}_2\text{Et}_6$ , the transition state for this conversion is six-membered (the optimized structure for the transition state is shown in Figure 10). The barrier for this conversion is 30.0 kcal/mol, which suggests that this pathway is a lot less likely than the KP (though the barrier is still lower than the

corresponding barrier for the  $\text{Al}_2\text{Et}_6$  case), when the donor *eb* interacts with the titanium center.

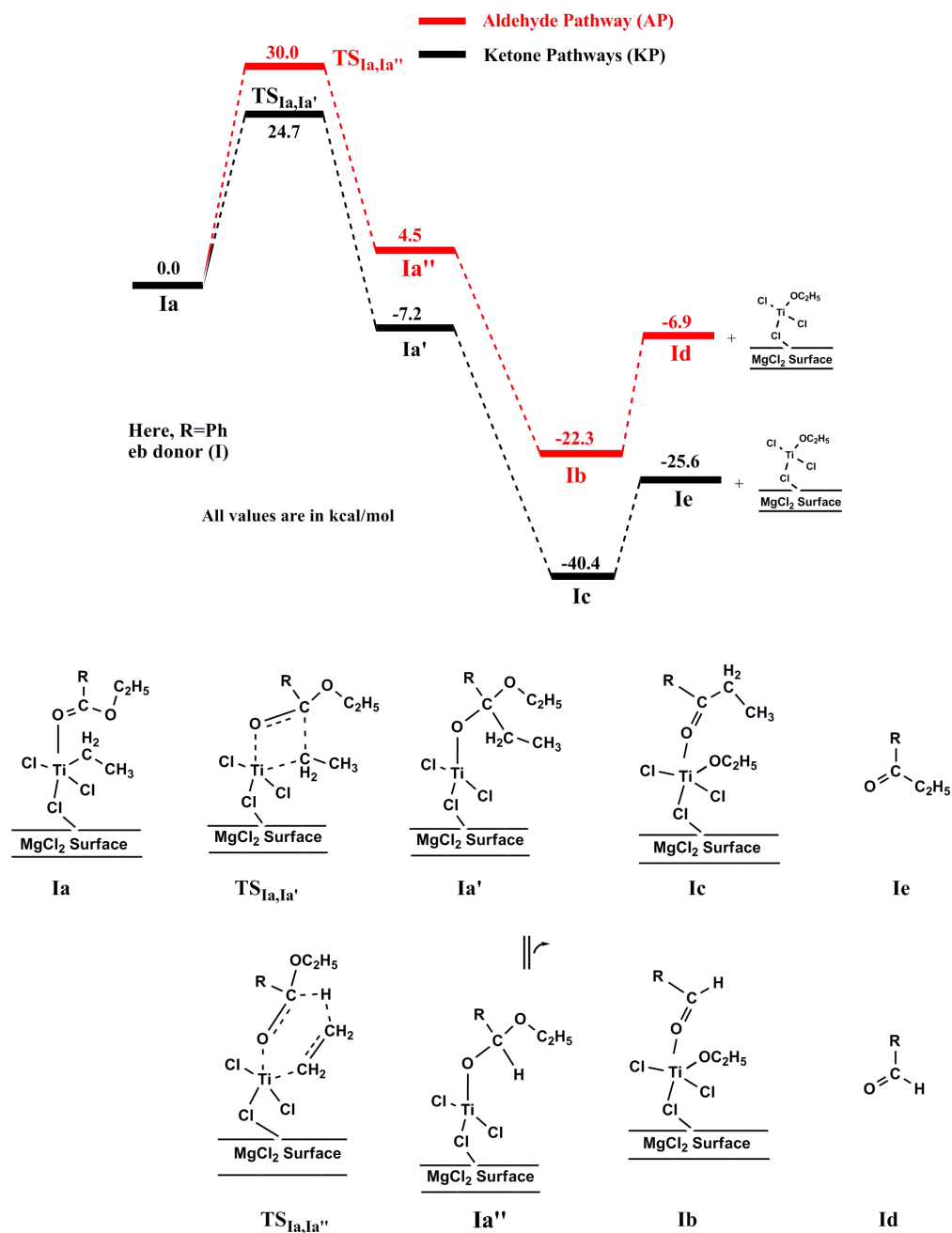


Figure 9. The energy profile for the decomposition of aromatic ester (*eb*) donor by  $\text{TiCl}_2\text{Et}$  supported on  $\text{MgCl}_2$  via the ketone and aldehyde pathways.



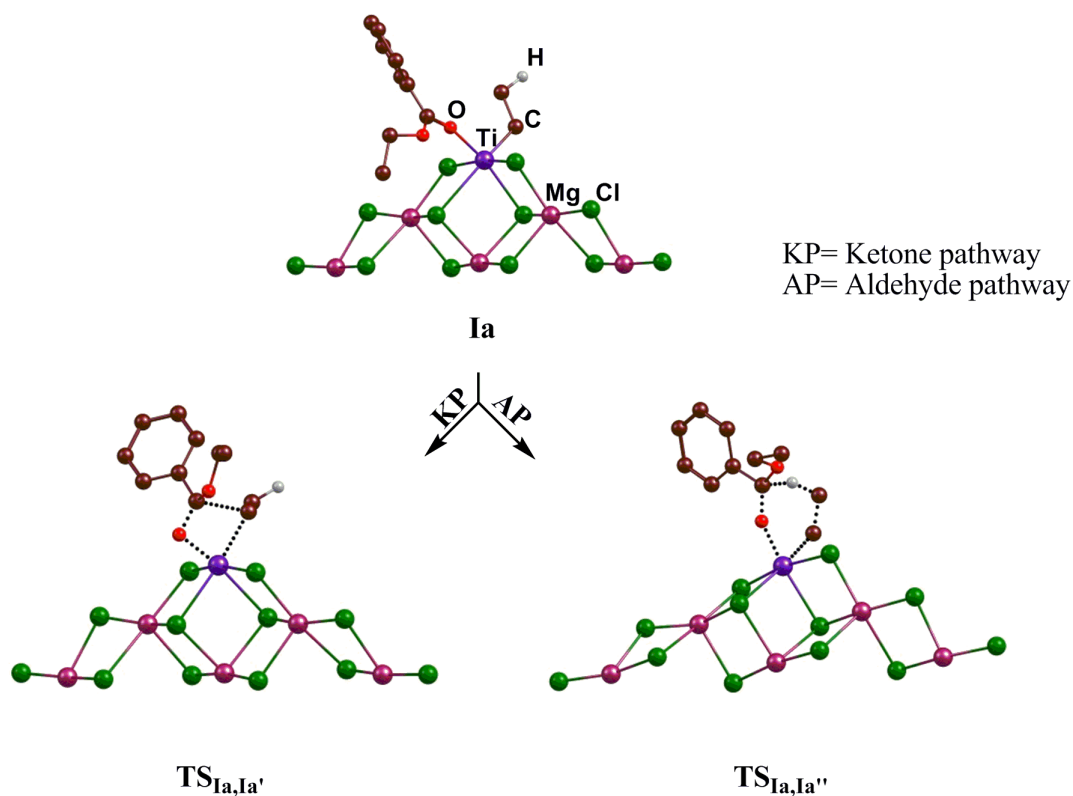


Figure 10. The optimized structures of the transition state for the first step of the ketone and the aldehyde pathways for donor interaction with  $\text{TiCl}_2\text{Et}$  supported on the  $\text{MgCl}_2$  layer; all the  $\text{MgCl}_2$  layers are not shown, and only the transferring hydrogen in the aldehyde pathway is shown for the purpose of clarity.

**4.3.2.3 Extension of the Ketone and Aldehyde Pathways:** Like in the  $\text{Al}_2\text{Et}_6$  case, we have considered the subsequent reactions of the ketone and the aldehyde formed from the KP and AP routes. The aldehyde **1d** can form a stable adduct **1g** with the titanium center on the  $\text{MgCl}_2$  surface, subsequent to which the system can undergo ethylene elimination or an ethyl group transfer, just like earlier, to yield the products **1h** and **1i** respectively (see Figure 11). The calculations indicate that the ethyl group transfer process is the more facile one, from both a thermodynamic and a kinetic point of view (see Figure 11). The same two pathways are also possible for the ketone product **1e**, and here again, the ethyl transfer pathways is found to be the more facile.

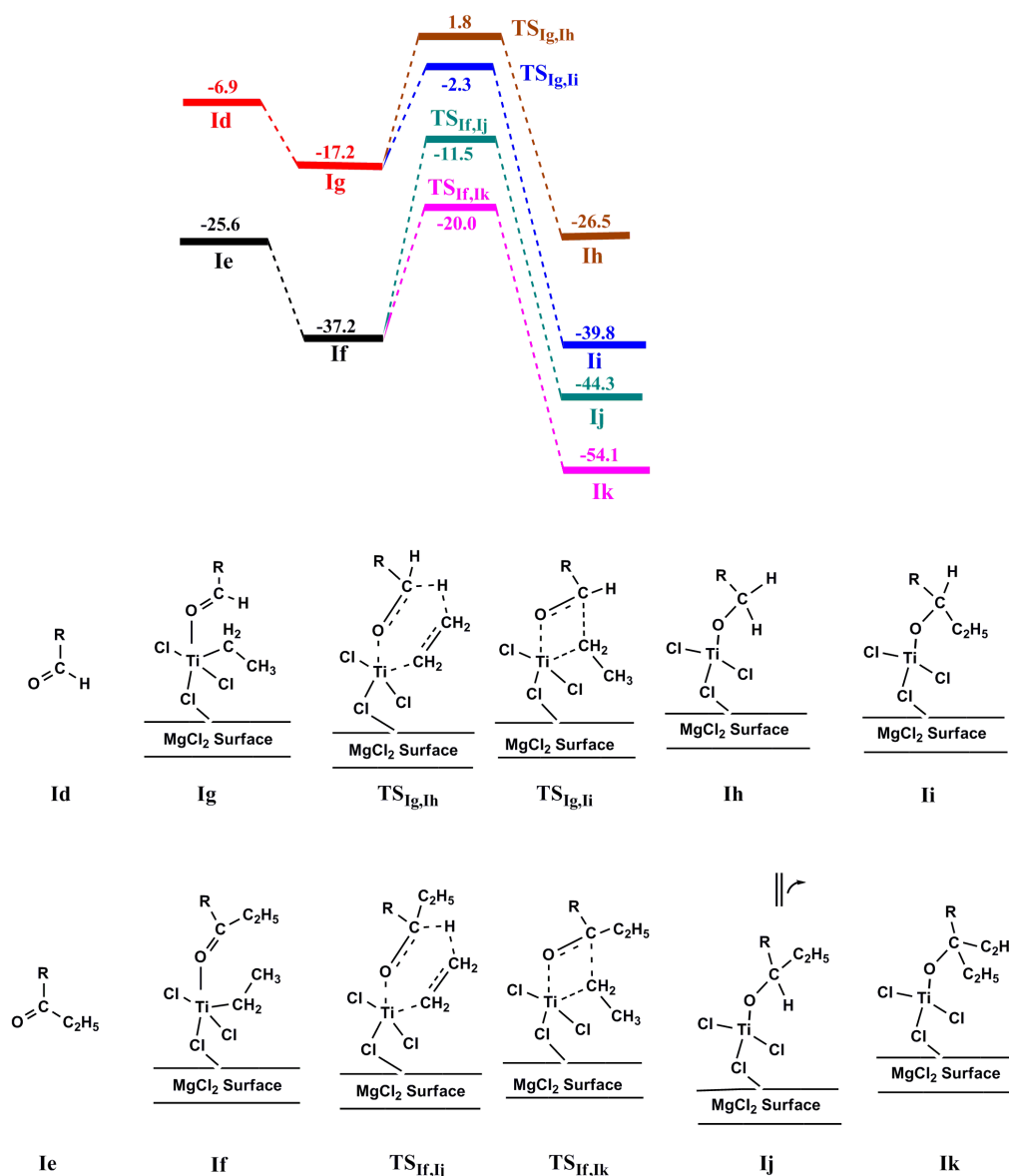


Figure 11. The energy profile for the subsequent reactions of the ketone and aldehyde (formed by *eb* decomposition) with  $\text{TiCl}_2\text{Et}$  supported on  $\text{MgCl}_2$ .

**4.3.2.4 Comparison of Different Donor Cases:** The previous sections have provided information on only the *eb* donor case interacting with  $\text{TiCl}_2\text{Et}$  supported on  $\text{MgCl}_2$ , but all the corresponding calculations have been done for all the five donor cases: *eb*, *peeb*, *pipeb*, aliphatic ester and the silyl ester. The results have been compiled in the Tables 12, 13, 14 and 15. What is shown in the bar graphs in Figure 12 below are the barrier height values for the slowest step of the KP and AP routes for the five donor cases considered. It is seen that the silyl ester donor shows the highest barrier for the AP route among all the donors, which effectively eliminates the AP route for the

interaction of the silyl ester with  $\text{TiCl}_2\text{Et}$  supported on  $\text{MgCl}_2$ . This, coupled with the results for the  $\text{Al}_2\text{Et}_6$  interaction with the donors, again shows that the silyl ester donor would show resilience against decomposition in ZN systems, and thus is a promising donor for ZN catalysis. However, it should also be noted that, for the KP route, the silyl ester is susceptible, having a barrier of 24.2 in the slowest step. This is lower than the corresponding barriers for the *eb*, *peeb* and the *pipeb* donor cases for the KP route. The reason for this is the stability of the transition state by the  $\alpha$  agostic interaction in the KP route (Figure 13, shows the optimized structure for the *eb* donor case, indicating the  $\alpha$  agostic interaction between  $\alpha$  hydrogen of ethyl group and the titanium center). As shown in Figure 13, the bond distance between the titanium and  $\alpha$  hydrogen is 2.064 Å in the KP route and 2.328 Å in the AP route, which shows that in the AP route,  $\alpha$  agostic interaction is not that much effective in comparison to the KP route. In order to investigate this further, we have also done the NBO charge analysis for all the ester donor cases for the transition state for the slowest (first) step for both the KP and AP routes. The results indicate that the charge on the titanium is less positive in case of KP in the transition state (see Table 16) for all the cases considered, which corroborates the structural observation of greater agostic interaction in the case of the KP route. Interestingly the difference in the positive charge is greater for the aliphatic ester and the silyl ester donor cases, which provides the explanation for the greater difference in the barrier heights between the KP and the AP routes for these two cases.

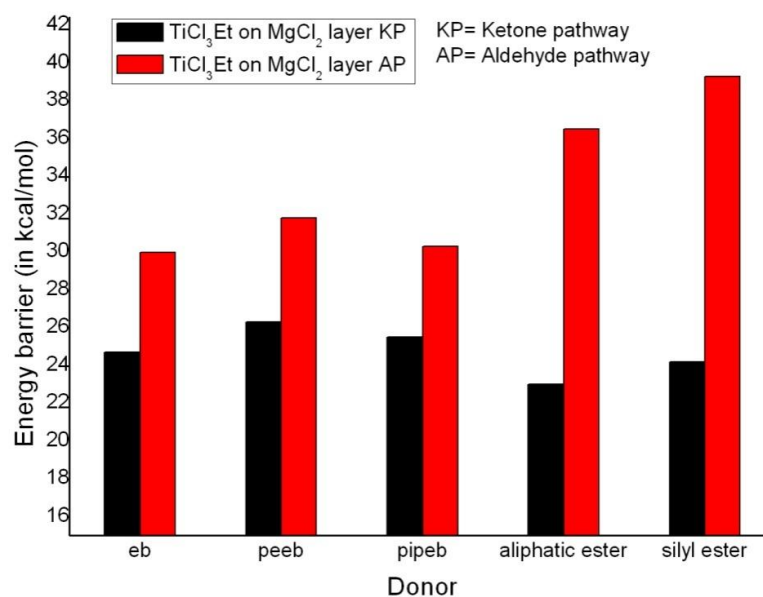


Figure 12. The relative barriers for the slowest step for the decomposition of different donors through their interaction with  $\text{TiCl}_2\text{Et}$  supported on  $\text{MgCl}_2$  through the ketone and aldehyde pathways.

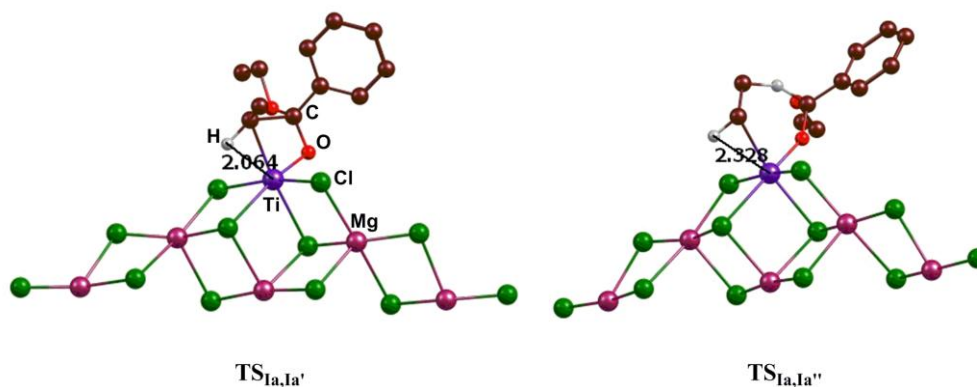


Figure 13. The optimized structures of the transition states for the slowest step in the KP and AP routes involving  $\text{TiCl}_2\text{Et}$  on  $\text{MgCl}_2$ ; the  $\alpha$  agostic interaction is seen to be greater for the transition state involving the KP route; all the  $\text{MgCl}_2$  layers are not shown, and only the relevant hydrogen atoms are shown for the purpose of clarity.

Table 12.  $\Delta G$  values (in kcal/mol) for decomposition of the *peeb* donor with  $\text{TiCl}_2\text{Et}$  supported on  $\text{MgCl}_2$  through the ketone and aldehyde pathways (KP and AP); the highest barrier, corresponding to the slowest step in each pathway, is highlighted in bold.

II <i>peeb</i> donor	KP	IIa	$\text{TS}_{\text{IIa,IIa}'}$	IIa'	IIc	IIe	IIf	$\text{TS}_{\text{IIf,IIk}}$	IIk
		0.0	<b>26.3</b>	-3.5	-41.4	-23.4	-37.4	-20.0	-49.7
	AP	IIa	$\text{TS}_{\text{IIa,IIa}''}$	IIa''	IIb	IId	IIg	$\text{TS}_{\text{IIg,IIi}}$	IIi
		0.0	<b>31.8</b>	4.2	-23.8	-5.3	-20.7	-5.6	-38.7
							$\text{TS}_{\text{IIg,IIh}}$	IIh	
							3.4	-25.5	

Table 13.  $\Delta G$  values (in kcal/mol) for decomposition of the *pipeb* donor with  $\text{TiCl}_2\text{Et}$  supported on  $\text{MgCl}_2$  through the ketone and aldehyde pathways (KP and AP); the highest barrier, corresponding to the slowest step in each pathway, is highlighted in bold.

III <i>pipeb</i> donor	KP	IIIa	$\text{TS}_{\text{IIIa,IIIa}'}$	IIIa'	IIIc	IIIe	IIIf	$\text{TS}_{\text{IIIf,IIIk}}$	IIIk
		0.0	<b>25.5</b>	-3.7	-43.3	-18.6	-38.9	-20.5	-50.3
	AP	IIIa	$\text{TS}_{\text{IIIa,IIIa}''}$	IIIa''	IIIb	III d	IIIg	$\text{TS}_{\text{IIIg,IIIi}}$	IIIi
		0.0	<b>30.3</b>	6.9	-21.5	-1.9	-20.0	-7.1	-39.5
							$\text{TS}_{\text{IIIg,IIIh}}$	IIIh	
							3.8	-28.0	

Table 14.  $\Delta G$  values (in kcal/mol) for decomposition of the aliphatic ester donor with  $\text{TiCl}_2\text{Et}$  supported on  $\text{MgCl}_2$  through the ketone and aldehyde pathways (KP and AP); the highest barrier, corresponding to the slowest step in each pathway, is highlighted in bold.

IV Aliphatic donor	KP	IVa	$\text{TS}_{\text{IVa,IVa}'}$	IVa'	IVc	IVe	IVf	$\text{TS}_{\text{IVf,IVk}}$	IVk
		0.0	<b>23.0</b>	-4.8	-34.2	-19.7	-25.1	-15.1	-47.5
	AP	IVa	$\text{TS}_{\text{IVa,IVa}''}$	IVa''	IVb	IVd	IVg	$\text{TS}_{\text{IVf,IVj}}$	IVj
		0.0	<b>36.5</b>	6.9	-9.0	1.0	-8.8	-5.4	-38.7
							$\text{TS}_{\text{IVg,IVi}}$	IVi	
								6.8	-37.3
								$\text{TS}_{\text{IVg,IVh}}$	IVh
								9.8	-19.4

Table 15.  $\Delta G$  values (in kcal/mol) for decomposition of the silyl ester donor with  $\text{TiCl}_2\text{Et}$  supported on  $\text{MgCl}_2$  through the ketone and aldehyde pathways (KP and AP); the highest barrier, corresponding to the slowest step in each pathway, is highlighted in bold and red.

V Silyl ester donor	KP	Va	$\text{TS}_{\text{Va,Va}'}$	Va'	Vc	Ve	Vf	$\text{TS}_{\text{Vf,Vk}}$	Vk
		0.0	<b>24.2</b>	-2.2	-33.8	-0.1	-20.8	-15.8	-47.9
	AP	Va	$\text{TS}_{\text{Va,Va}''}$	Va''	Vb	Vd	Vg	$\text{TS}_{\text{Vf,Vj}}$	Vj
		0.0	<b>39.3</b>	4.3	-12.0	20.3	2.9	-1.0	-30.7
							$\text{TS}_{\text{Vg,Vi}}$	Vi	
								4.1	-35.3
								$\text{TS}_{\text{Vg,Vh}}$	Vh
								17.5	-15.7

Table 16. The charge obtained for the titanium metal center for the transition state structure for the slowest, first step of the KP and the AP decomposition pathways upon interaction with TiCl<sub>2</sub>Et on MgCl<sub>2</sub> support.

Donor	Charge on the titanium center	
	For KP	For AP
<i>eb</i>	1.41	1.49
<i>peeb</i>	1.43	1.50
<i>pipeb</i>	1.43	1.50
aliphatic ester	1.37	1.63
silyl ester	1.35	1.48

#### 4.3.2.5 Modification of Silyl Ester donors.

The previous sections have discussed four different decomposition routes for ester donors: (I) the ketone pathway (KP) with Al<sub>2</sub>Et<sub>6</sub>, (II) the aldehyde pathway (AP) with Al<sub>2</sub>Et<sub>6</sub>, (III) KP with TiCl<sub>2</sub>Et on MgCl<sub>2</sub> support and (IV) AP with TiCl<sub>2</sub>Et on MgCl<sub>2</sub> support. Since five ester donors have been considered, this adds up to twenty different decomposition routes (170 intermediates and 92 transition states) that have been computationally investigated, including additional reactions for the products formed for the decomposition reactions. The overall picture that emerges from these comprehensive calculations is summarized in Figure 14. Figure 14 shows the barrier for the slowest step for each of the decomposition routes (I)-(IV) for each of the five donor cases. A perusal of the figure shows that the silyl ester compares favorably with the other donors, with respect to the AP with TiCl<sub>2</sub>Et on MgCl<sub>2</sub> support (IV). For the KP on Al<sub>2</sub>Et<sub>6</sub> route (I), we have computationally shown, in the preceding section (e), how increasing the steric bulk on the silyl ester donor can lead to the increase of the barriers and make the silyl ester donors more robust. With regard to the AP on Al<sub>2</sub>Et<sub>6</sub> route (II), the barrier for the slowest step for the silyl ester (33.3 kcal/mol), while not the highest barrier obtained for (II) among all the donors studied, is within a kcal/mol to the barriers obtained with *peeb* (33.7 kcal/mol) and with *pipeb* (34.3 kcal/mol). Moreover, since the value of the barriers are above 30.0 kcal/mol, and since this corresponds to the first step for the overall decomposition process for (II), it can be concluded that the silyl ester donor is quite robust with regard to the AP on Al<sub>2</sub>Et<sub>6</sub>

decomposition route as well. However, the remaining decomposition pathway III is where the silyl ester donor could be susceptible. The barrier for the slowest step for this decomposition pathway is 24.2 kcal/mol for the silyl ester donor case. This is 1.3 kcal/mol lower than for the *pipeb* case, and more than 2.0 kcal/mol lower than the barrier for the slowest step with *peeb*. Hence, any alteration of the silyl ester donor that would lead to it becoming more resistant to decomposition by this route would make it a better donor for ZN catalysis. Some possible modifications to the silyl ester donor are discussed here. Specifically, the ketone pathway for the interaction of the silyl ester donor with  $\text{TiCl}_2\text{Et}$  on  $\text{MgCl}_2$  support (pathway III) has been considered, and the transition step for the first step has been determined for modified silyl ester donor cases. Six new silyl ester donor cases have been considered. The results are tabulated in Table 17 below, and indicate that the increase of steric bulk in the alkyl groups attached to the silicon center leads to an increase in the barrier height. This suggests that undesirable steric interactions between the donor and the  $\text{TiCl}_2\text{Et}$  on  $\text{MgCl}_2$  can offer a solution to the possibility of decomposition of the silyl ester donors by the titanium active species. It is, however, also interesting to note that increasing steric bulk to a greater extent leads to a reduction of the decomposition barrier. For instance, for the  $(\text{C}_2\text{H}_5\text{COOCH}_2)_2\text{SiC}_2\text{H}_5(\text{Ph})$  donor, the barrier is 25.9 kcal/mol, but for the more bulky  $(\text{C}_2\text{H}_5\text{COOCH}_2)_2\text{Si}(\text{Ph})_2$  donor, the barrier is reduced to 24.2 kcal/mol (see Table 17). The reason for this is that the additional phenyl group can also have a salutary electronic effect in stabilizing the silicon center in the transition state during the  $-\text{C}_2\text{H}_5$  group transfer process. This lowering of the barrier is also observed for the  $(\text{C}_2\text{H}_5\text{COOCH}_2)_2\text{SiC}_2\text{H}_5(\text{cyclohexyl})$  and the  $(\text{C}_2\text{H}_5\text{COOCH}_2)_2\text{Si}(\text{cyclohexyl})_2$  cases. This result indicates that the silyl ester donors that would be most resistant to decomposition will be those that can balance steric and electronic factors in favor of higher decomposition barriers. Since this has also been observed in the preceding section (e) for the decomposition of the silyl ester donors with different bulky R groups by  $\text{Al}_2\text{Et}_6$ , the results suggest overall that the best silyl ester donors, the ones that would be the most robust in ZN systems, would be the ones that have some, but not excessive, degree of steric bulk in their R groups.



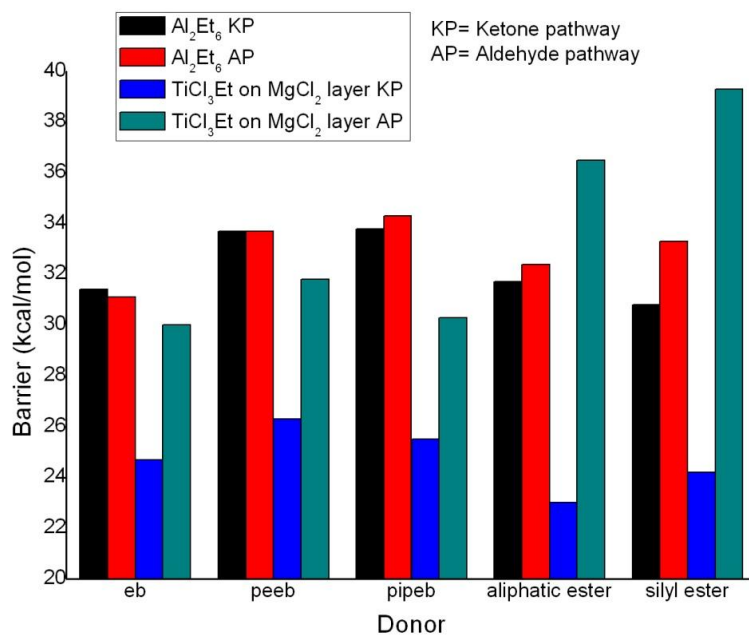


Figure 14. A comparison of the highest barriers for the ketone and aldehyde decomposition pathways, for the case of different donors, with two different Lewis acidic species ( $\text{Al}_2\text{Et}_6$ , and  $\text{TiCl}_2\text{Et}$  on  $\text{MgCl}_2$  support).

Table 17.  $\Delta G$  values (in kcal/mol) for the barrier for the slowest step in the decomposition of different silyl ester donor cases with  $\text{TiCl}_2\text{Et}$  on  $\text{MgCl}_2$  support, through the ketone pathway.

Serial no.	Silyl ester donor	Free Energy barriers (in kcal/mol)
		$\text{TiCl}_2\text{Et}$ on $\text{MgCl}_2$ supported layer (ketone pathway)
VA	$(\text{CH}_3\text{COOCH}_2)_2\text{Si}(\text{CH}_3)_2$	24.2
VB	$(\text{C}_2\text{H}_5\text{COOCH}_2)_2\text{Si}(\text{C}_2\text{H}_5)_2$	23.7
VC	$(\text{C}_2\text{H}_5\text{COOCH}_2)_2\text{Si}(i\text{Pr})_2$	24.1
VD	$(\text{C}_2\text{H}_5\text{COOCH}_2)_2\text{SiC}_2\text{H}_5(\text{Ph})$	25.9
VE	$(\text{C}_2\text{H}_5\text{COOCH}_2)_2\text{Si}(\text{Ph})_2$	24.2
VF	$(\text{C}_2\text{H}_5\text{COOCH}_2)_2\text{SiC}_2\text{H}_5(\text{cyclohexyl})$	26.0
VG	$(\text{C}_2\text{H}_5\text{COOCH}_2)_2\text{Si}(\text{cyclohexyl})_2$	25.4

## 4.4. Conclusions

Lewis bases (donors) play a key role in ZN olefin polymerization, aiding in increasing polymerization activity and selectivity<sup>1,3,11,14,15,72</sup>. However, due to the possibility of interaction of the donor with Lewis acidic species present in ZN systems, a number of undesired side reactions are possible. Full quantum chemical investigations, employing density functional theory (DFT) have been done in order to study different decomposition pathways of a variety of ester donors with different Lewis acidic species present in Ziegler Natta (ZN) catalysis systems. While tri-ethyl aluminium (*teal*) (usually present as its dimer  $\text{Al}_2\text{Et}_6$ ) has been considered in the past<sup>6,10,16</sup> as the species present in ZN systems that can decompose donors and vice versa, the current calculations systematically show, for the first time, how the acidic titanium center in the active catalytic species:  $\text{TiCl}_2\text{Et}$  on  $\text{MgCl}_2$  support, can participate in undesired, decomposing, side reactions with donors. Indeed, the current calculations reveal that the threat of decomposition of the donor is significantly greater with the titanium complex than with the aluminium complex – a result that sheds new light on the nature of the interactions between the different component species present in ZN systems. This also provides an explanation for why adding excess donors can poison the active site<sup>73</sup> in ZN systems.

Since the family of silyl ester donors shows promise as potential donors in future ZN catalysis systems<sup>74-76</sup>, the current calculations provide a means of comparing their robustness against decomposition in ZN systems in comparison to other ester donors. The calculations show that the silyl esters are likely to be quite resilient to decomposition by both  $\text{Al}_2\text{Et}_6$  and  $\text{TiCl}_2\text{Et}$  on the  $\text{MgCl}_2$  surface, provided sterically bulky alkyl groups are employed on the silyl ester. The current work can thus serve as a guide for the development of important new classes of donors such as silyl esters for the ZN catalyst systems.

## 4.5 References

- (1) Wondimagegn, T.; Ziegler, T. *The Journal of Physical Chemistry C* **2012**, *116*, 1027-1033.
- (2) Seth, M.; Ziegler, T. *Macromolecules* **2003**, *36*, 6613-6623.

- (3) Grau, E.; Lesage, A.; Norsic, S. b.; CopÃ©ret, C.; Monteil, V.; Sautet, P. *ACS Catalysis* **2013**, *3*, 52-56.
- (4) Baba, Y. *Bulletin of the Chemical Society of Japan* **1968**, *41*, 1022-1023.
- (5) Baba, Y. *Bulletin of the Chemical Society of Japan* **1968**, *41*, 1020-1021.
- (6) Chien, J. C. W.; Wu, J.-C. *Journal of Polymer Science: Polymer Chemistry Edition* **1982**, *20*, 2445-2460.
- (7) Vähäsarja, E.; Pakkanen, T. T.; Pakkanen, T. A.; Iiskola, E.; Sormunen, P. *Journal of Polymer Science Part A: Polymer Chemistry* **1987**, *25*, 3241-3253.
- (8) Flisak, Z.; Spaleniak, G. P.; Bremmek, M. *Organometallics*, *32*, 3870-3876.
- (9) Starowieyski, K. B.; Pasynkiewicz, S.; Sporzynski, A.; Wisniewska, K. *Journal of Organometallic Chemistry* **1976**, *117*, C1-C3.
- (10) Sergeev, S. A.; Bukatov, G. D.; Zakharov, V. A. *Die Makromolekulare Chemie* **1984**, *185*, 2377-2385.
- (11) Correa, A.; Piemontesi, F.; Morini, G.; Cavallo, L. *Macromolecules (Washington, DC, U. S.)* **2007**, *40*, 9181-9189.
- (12) Correa, A.; Credendino, R.; Pater, J. T. M.; Morini, G.; Cavallo, L. *Macromolecules* **2012**, *45*, 3695-3701.
- (13) Coutinho, F. B.; Costa, M. S.; Santa Maria, L. *Polymer Bulletin* **1992**, *28*, 55-59.
- (14) Chadwick, J. C.; Van der Burgt, F. P. T. J.; Rastogi, S.; Busico, V.; Cipullo, R.; Talarico, G.; Heere, J. J. R. *Macromolecules* **2004**, *37*, 9722-9727.
- (15) Stukalov, D. V.; Zakharov, V. A.; Zilberberg, I. L. *The Journal of Physical Chemistry C* **2010**, *114*, 429-435.
- (16) Zhong, C.; Gao, M.; Mao, B. *Macromolecular Chemistry and Physics* **2005**, *206*, 404-409.
- (17) Chadwick, J. C.; Morini, G.; Balbontin, G.; Camurati, I.; Heere, J. J. R.; Mingozi, I.; Testoni, F. *Macromol. Chem. Phys.* **2001**, *202*, 1995-2002.
- (18) Morini, G.; Albizzati, E.; Balbontin, G.; Mingozi, I.; Sacchi, M. C.; Forlini, F.; Tritto, I. *Macromolecules* **1996**, *29*, 5770-5776.

- (19) Chirinos, J.; Fernandez, J.; Perez, D.; Rajmankina, T.; Parada, A. *Journal of Molecular Catalysis A: Chemical* **2005**, *231*, 123-127.
- (20) Shen, X.-r.; Fu, Z.-s.; Hu, J.; Wang, Q.; Fan, Z.-q. *The Journal of Physical Chemistry C* **2013**, *117*, 15174-15182.
- (21) Zohuri, G. H.; Kasaeian, A. B.; Torabi Angagi, M.; Jamjah, R.; Mousavian, M. A.; Emami, M.; Ahmadjo, S. *Polymer International* **2005**, *54*, 882-885.
- (22) Cui, N.; Ke, Y.; Li, H.; Zhang, Z.; Guo, C.; Lv, Z.; Hu, Y. *Journal of Applied Polymer Science* **2006**, *99*, 1399-1404.
- (23) Chadwick, J. C. *Macromol. Symp.* **2001**, *173*, 21-35.
- (24) Vanka, K.; Singh, G.; Iyer, D.; Gupta, V. K. *Journal of Physical Chemistry C* **2010**, *114*, 15771-15781.
- (25) Andoni, A.; Chadwick, J. C.; Niemantsverdriet, H. J. W.; Thuene, P. *C. J. Catal.* **2008**, *257*, 81-86.
- (26) Mukhopadhyay, S.; Kulkarni, S. A.; Bhaduri, S. *Journal of Organometallic Chemistry* **2005**, *690*, 1356-1365.
- (27) Cerny, Z.; Hermanek, S.; Fusek, J.; Kriz, O.; Casensky, B. *Journal of Organometallic Chemistry* **1988**, *345*, 1-9.
- (28) Smith, M. B. *Journal of Organometallic Chemistry* **1972**, *46*, 31-49.
- (29) Smith, M. B. *Journal of Organometallic Chemistry* **1972**, *46*, 211-217.
- (30) Ferreira, M. Ì. a. L. n.; Damiani, D. E. *Journal of Molecular Catalysis A: Chemical* **1999**, *150*, 53-69.
- (31) Makwana, U. C.; Singala, K. J.; Patankar, R. B.; Singh, S. C.; Gupta, V. K. *Journal of Applied Polymer Science*, *125*, 896-901.
- (32) Busico, V.; Cipullo, R.; Corradini, P.; De Biasio, R. *Macromolecular Chemistry and Physics* **1995**, *196*, 491-498.
- (33) Corradini, P.; Busico, V.; Guerra, G. *Comprehensive Polymer Science*, Pergamon Press, Oxford **1988**, *4*, 29-50.
- (34) Kim, S. H.; Somorjai, G. A. *Proceedings of the National Academy of Sciences* **2006**, *103*, 15289-15294.
- (35) Taniike, T.; Terano, M. *Journal of Catalysis*, *293*, 39-50.
- (36) Boero, M.; Parrinello, M.; Hueffer, S.; Weiss, H. *J. Am. Chem. Soc.* **2000**, *122*, 501-509.
- (37) Shiga, A. *Macromolecular Research*, *18*, 956-959.

- (38) Capone, F.; Rongo, L.; D' Amore, M.; Budzelaar, P. H. M.; Busico, V. *The Journal of Physical Chemistry C*, **117**, 24345-24353.
- (39) Boero, M.; Parrinello, M.; Weiss, H.; Hueffer, S. *J. Phys. Chem. A* **2001**, *105*, 5096-5105.
- (40) Schaefer, A.; Horn, H.; Ahlrichs, R. *J. Chem. Phys.* **1992**, *97*, 2571-7.
- (41) Schaefer, A.; Huber, C.; Ahlrichs, R. *J. Chem. Phys.* **1994**, *100*, 5829-35.
- (42) Andrae, D.; Haeussermann, U.; Dolg, M.; Stoll, H.; Preuss, H. *Theor. Chim. Acta* **1990**, *77*, 123-41.
- (43) Perdew, J. P.; Burke, K.; Ernzerhof, M. *Phys. Rev. Lett.* **1996**, *77*, 3865-3868.
- (44) Perdew, J. P.; Wang, Y. *Physical Review B* **1992**, *45*, 13244-13249.
- (45) Eichkorn, K.; Treutler, O.; Oehm, H.; Haeser, M.; Ahlrichs, R. *Chem. Phys. Lett.* **1995**, *240*, 283-90.
- (46) Sierka, M.; Hogeckamp, A.; Ahlrichs, R. *J. Chem. Phys.* **2003**, *118*, 9136-9148.
- (47) Adamo, C.; Barone, V. *The Journal of Chemical Physics* **1999**, *110*, 6158-6170.
- (48) Perdew, J. P.; Burke, K.; Ernzerhof, M. *Physical Review Letters* **1996**, *77*, 3865.
- (49) Johnson, B. G.; Gill, P. M. W.; Pople, J. A. *J. Chem. Phys.* **1993**, *98*, 5612.
- (50) Credendino, R.; Liguori, D.; Morini, G.; Cavallo, L. *The Journal of Physical Chemistry C*, **118**, 8050-8058.
- (51) Zhang, Y.; Yang, W. *Physical Review Letters* **1998**, *80*, 890-890.
- (52) Lousada, C. M.; Johansson, A. J.; Brinck, T.; Jonsson, M. *Physical Chemistry Chemical Physics* **2013**, *15*, 5539-5552.
- (53) Li, Z.; Pan, Y. *Physical Review B* **2011**, *84*, 115112.
- (54) List, N. H.; Curutchet, C.; Knecht, S.; Mennucci, B.; Kongsted, J. *Journal of Chemical Theory and Computation* **2013**, *9*, 4928-4938.
- (55) Blancafort, L.; Williams, F. *The Journal of Physical Chemistry A* **2012**, *116*, 10607-10614.
- (56) Svozil, D.; Jungwirth, P. *The Journal of Physical Chemistry A* **2006**, *110*, 9194-9199.

- (57) Adamo, C.; Scuseria, G. E.; Barone, V. *The Journal of Chemical Physics* **1999**, *111*, 2889-2899.
- (58) Fukui, K. *Acc. Chem. Res.* **1981**, *14*, 363-368.
- (59) Mammen, M.; Shakhnovich, E. I.; Whitesides, G. M. *The Journal of Organic Chemistry* **1998**, *63*, 3168-3175.
- (60) Kelly, E.; Seth, M.; Ziegler, T. *The Journal of Physical Chemistry A* **2004**, *108*, 2167-2180.
- (61) Yin, H.; Wang, D.; Valiev, M. *The Journal of Physical Chemistry A*, *115*, 12047-12052.
- (62) Williams, V. M.; Kong, J. R.; Ko, B. J.; Mantri, Y.; Brodbelt, J. S.; Baik, M.-H.; Krische, M. J. *Journal of the American Chemical Society* **2009**, *131*, 16054-16062.
- (63) Janse van Rensburg, W.; Grove, C.; Steynberg, J. P.; Stark, K. B.; Huyser, J. J.; Steynberg, P. J. *Organometallics* **2004**, *23*, 1207-1222.
- (64) Qi, Y.; Dong, Q.; Zhong, L.; Liu, Z.; Qiu, P.; Cheng, R.; He, X.; Vanderbilt, J.; Liu, B. *Organometallics*, *29*, 1588-1602.
- (65) Bagno, A.; Kantlehner, W.; Kress, R.; Saielli, G.; Stoyanov, E. *The Journal of Organic Chemistry* **2006**, *71*, 9331-9340.
- (66) Li, J.-N.; Pu, M.; Ma, C.-C.; Tian, Y.; He, J.; Evans, D. G. *Journal of Molecular Catalysis A: Chemical*, *359*, 14-20.
- (67) Nikiforidis, I.; Görling, A.; Hieringer, W. *Journal of Molecular Catalysis A: Chemical*, *341*, 63-70.
- (68) Cao, X.; Cheng, R.; Liu, Z.; Wang, L.; Dong, Q.; He, X.; Liu, B. *Journal of Molecular Catalysis A: Chemical*, *321*, 50-60.
- (69) Ghiasi, R.; Mokaram, E. E. *Journal of Applied Chemical Research* **2012**, *20*, *1*, 7-13.
- (70) Toto, M.; Morini, G.; Guerra, G.; Corradini, P.; Cavallo, L. *Macromolecules* **2000**, *33*, 1134-1140.
- (71) Busico, V.; Corradini, P.; De Martino, L.; Proto, A.; Savino, V.; Albizzati, E. *Die Makromolekulare Chemie* **1985**, *186*, 1279-1288.
- (72) Flisak, Z.; Ziegler, T. *Macromolecules* **2005**, *38*, 9865-9872.
- (73) Kashiwa, N. *MMI Press. Symp. Ser.*, **1983**, *4*, 379.
- (74) Chen, L. *U.S. Pat. Appl. Publ.* **2010**, US 20100130710 A1.

(75) Chen, L.; Leung, T. W.; Tao, T. *U.S. Pat. Appl. Publ.* **2010**, US 20100130709 A1.

(76) Gonzalez, K.; Tao, T.; Leung, W. *U.S. Pat. Appl. Publ.* **2010**, US 20100267911 A1.

## Chapter 5

### Abstract

Full quantum chemical calculations, using density functional theory (DFT), have been done in order to explain the effect of donors on the “activation mechanism” in the Ziegler-Natta (Z-N) catalyst system. In the activation mechanism, the inactive Ti(IV)Cl<sub>4</sub> catalyst converts into the active Ti(III)Cl<sub>2</sub>Et catalyst with the help of the AlEt<sub>3</sub> present in the system. The donors that have been considered in this study are: ethyl benzoate (*eb*), two representative diether cases, a phthalate donor and a silyl ester donor. The results indicate that *eb* and the diether donor cases donor have a negative effect on the barriers for the activation mechanism. However, the *eb* donor can be displaced from the MgCl<sub>2</sub> surface by AlEt<sub>3</sub>, which matches experimental observations. For the phthalate, silyl ester and TiCl<sub>3</sub>-OC<sub>4</sub>H<sub>8</sub>Cl cases, the results indicate that a significant induction period would be present in Z-N systems employing such donors or having such a catalytic center, before catalysis could commence.



## 5.1 Introduction

In 1953, the discovery of the process now known as Ziegler-Natta (Z-N) olefin polymerization catalysis was a huge breakthrough for the polymer industry. Given the significance of this process for the production of plastics, elastomers and fibres<sup>1-23</sup>, considerable effort has been expended over sixty years towards the development of Z-N systems, so as to improve catalyst activity as well as the selectivity of the polymer formed. The current generation of Z-N systems is multi-component in nature, consisting of  $\text{TiCl}_4$ , the catalyst precursor,  $\text{AlR}_3$ , the alkylating agent (R- alkyl group) and the  $\text{MgCl}_2$  support. An important new additional component to these systems was introduced in the 1980s: the “donor”, which led to significant improvement in catalyst activity and selectivity. Donors are Lewis bases that contain at least one oxygen atom that can coordinate either to the  $\text{MgCl}_2$  support, or the titanium catalyst during the polymerization process. The most commonly used donors are as follows: (i) internal donors (added during the catalyst preparation) – ethyl benzoate, *eb*,<sup>12,24-28</sup> diethers,<sup>29,30</sup> phthalates,<sup>5,22,31,32</sup> tetrahydrofuran (THF)<sup>33</sup> and succinates<sup>1,29</sup> and (ii) external donors (added along or after the reaction of  $\text{AlR}_3$ ), such as alkoxysilanes.<sup>5,7</sup>

Many computational investigations including static density functional theory (DFT)<sup>5,29,34-36</sup> and periodic DFT<sup>37,38</sup> calculations, as well as molecular simulations<sup>39-41</sup> have been reported in the field of chemistry in order to see the chemical changes during the reaction proceeding. In recent times *ab initio* molecular dynamics simulations on large scale systems have also become feasible<sup>39-42</sup>. The current work, however, focuses on static density functional theory calculations.

In the ZN system, several studies have shed light on the nature of the interactions between the different components, and on their influence on the behavior of the active catalyst. However, there is still a significant lack of understanding of the nature of the activation process in the Z-N systems: on how the catalyst precursor - the Ti(IV) species, is converted into the Ti(III) species, and eventually into the catalytically active Ti(III) compound containing the Ti-C bond. The role of the  $\text{AlR}_3$  group is important in this transformation, and this has been investigated in the computational studies done by the groups of Zakharov<sup>36</sup> and Cavallo<sup>43</sup>. Zakharov and coworkers<sup>36</sup> looked at four membered transition states, involving the titanium complex and triethyl aluminium,  $\text{AlEt}_3$ , where an alkyl group is transferred from the aluminium to the

titanium center, leading to the formation of the Ti-C bond – the trans-alkylation mechanism. The transition states were approximated in their studies by being considered through the linear scan of the potential energy surface. Cavallo *et al.*<sup>43</sup> have reported the systematic study of the possible activation mechanism by considering two consecutive steps: (i) the cleavage of the Ti-Cl bond and (ii) the alkylation of titanium with the help of AlEt<sub>3</sub> (see Figure 1). However, while these studies have increased the understanding of the activation mechanism, an important question that remains is: is there any role of the donor on the activation process? Previous investigations<sup>5,29</sup> have focused on the influence of the donor on the behavior of the active catalyst species—in determining chain growth and selectivity, but, to date, no studies have been reported investigating the possibility of donor influence on the activation process. Since the “internal donors” are present in the Z-N system during the time of the activation, it is quite possible that their influence on activation could be significant. Therefore, a systematic investigation of the donor effect on the activation process can provide valuable new insights into their role in Z-N catalysis.

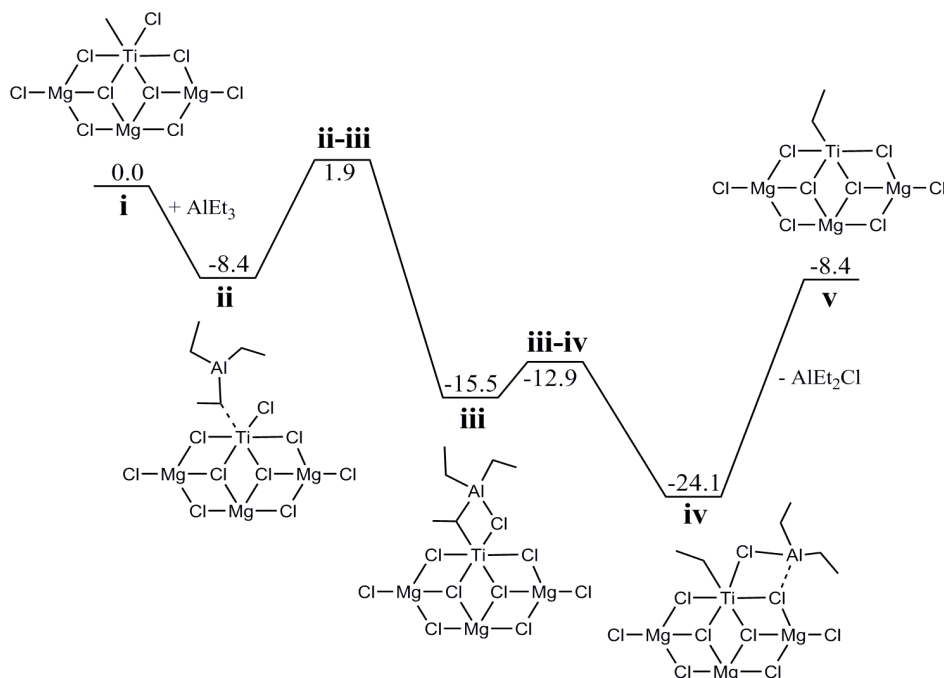


Figure 1. The energy profile ( $\Delta E$  in kcal/mol) of the direct transalkylation reaction with no donor attached to the (110) MgCl<sub>2</sub> layers.

This is the principal objective of the current computational investigation – to investigate the role of donors on the activation process. To this end, five different internal donors have been considered: *eb*,  $(\text{CH}_3\text{OCH}_2)_2\text{C}(\text{iPr})_2$  (“diether1”),  $(\text{CH}_3\text{O})_2\text{C}(\text{C}_6\text{H}_4)_2$  (“diether2”), a silyl ester and a phthalate. The structures of the donors are shown in Figure 2 below. While benzoates, diethers and phthalates represent the most common families of internal donors employed and studied<sup>5,27-31</sup>, the silyl ester internal donor has been chosen to represent promising donors that might be employed in Z-N systems in the near future. The donor influence has been considered by binding the donor to the  $\text{MgCl}_2$  surface, in close proximity to the titanium complex, a commonly accepted binding mode for the internal donor (see Figure 5b).

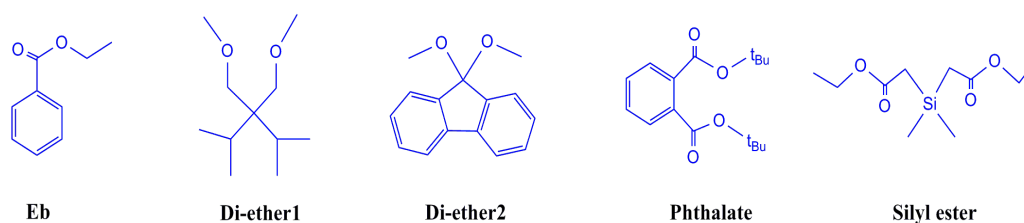


Figure 2. The five different donors have been considered in this study.

To represent the  $\text{MgCl}_2$  surface, the (110)  $\text{MgCl}_2$  lateral cut has been considered. This is because previous studies<sup>7,29,34,44,45</sup> have indicated this to be one of the most prominent  $\text{MgCl}_2$  surfaces present in Z-N systems, and one where the coordination of the titanium species is quite favorable (in contrast to the (104)  $\text{MgCl}_2$  surface, where the coordination of titanium was found to be weak). Specifically, the Corradini site has been considered, where the  $\text{TiCl}_4$  binds to the (110)  $\text{MgCl}_2$  surface through two bridging chlorine atoms (see Figure 3). We have checked the activation/donor structure relationship with two different  $\text{MgCl}_2$  model systems. The difference in the two model systems is based on the nature of  $\text{TiCl}_4$  complex coordination to the  $\text{MgCl}_2$  surface. In the first case, the  $\text{TiCl}_4$  complex is bound to the  $\text{MgCl}_2$  surface through two bridging chlorine atoms, where both the bridging chlorine atoms bind to the (110)  $\text{MgCl}_2$  surface (see Figure 3), and in the second case, one of the two bridging atoms binds to (110) surface and the other binds to the (104) surface. This latter model is called the “unified model” (see Figure 4), and has recently been developed by Cavallo and workers<sup>46</sup>. In this model, Cavallo and workers<sup>46</sup> had kept the  $\text{MgCl}_2$  layers fixed during the geometry optimization but in this current study, we have relaxed this

unified model system, in order to do an apples to apples proper comparison to the other  $\text{MgCl}_2$  model employed. It to be noted that after the relaxing of the  $\text{MgCl}_2$  layers in the unified model, the layers remain intact during the optimization (see Figure 4).

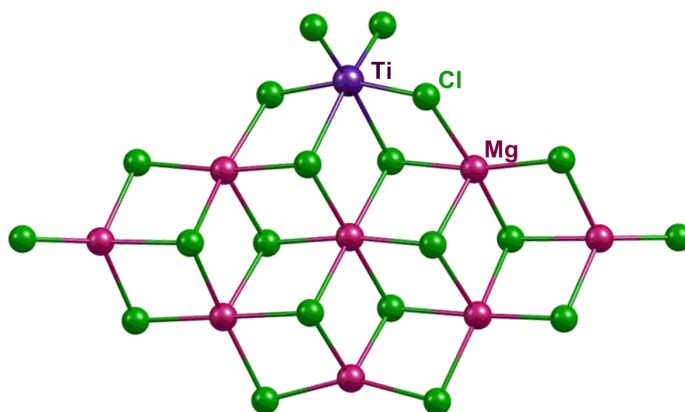


Figure 3. The  $\text{MgCl}_2$  model system, with  $\text{TiCl}_4$  absorbed on the (110)  $\text{MgCl}_2$  lateral cuts, that has been employed in this study.

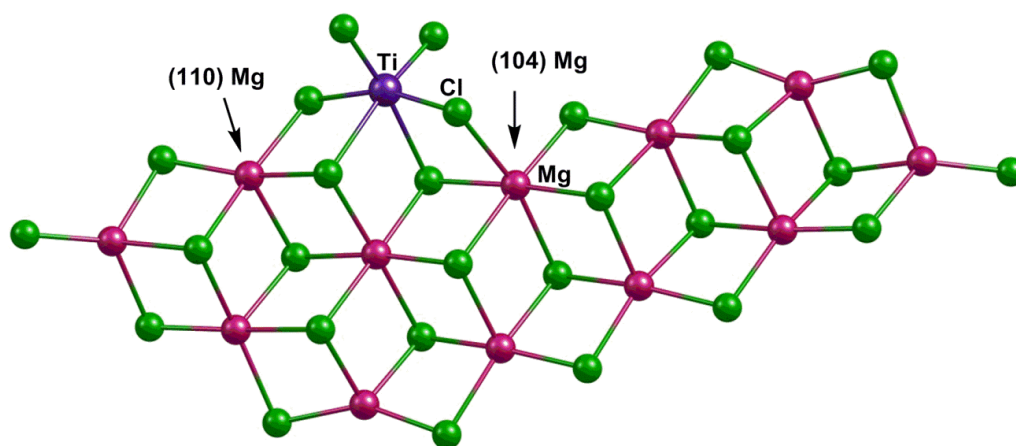


Figure 4. The optimized structures of the Cavallo unified model system, where  $\text{TiCl}_4$  binds to the (110) and (104)  $\text{MgCl}_2$  surfaces at the same time.

In addition to the primary objective of investigating the possible role of the donors in the activation process, we have also investigated the competing possibility of the donor detaching from the  $\text{MgCl}_2$  surface due to the interaction with the  $\text{AlEt}_3$  group, as has been observed in experimental studies, for the case of the *eb* donor<sup>47</sup>. This would diminish the donor influence on the activation process, and therefore has to be considered. It is also possible that the  $\text{AlEt}_3$  coordinated donor species can act as a

new “donor” for the system. Such possibilities have also been considered in the current work.

Furthermore, it is possible that the donor can decompose and lead to the formation of Ti-O bonds in the active catalyst species, as has been experimentally reported by Sautet and coworkers.<sup>33</sup> Therefore, the possibility of activation process with such species has also been investigated. Specifically,  $\text{TiCl}_3\text{-OC}_4\text{H}_8\text{Cl}$  has been considered as a representative example of such types of catalytic species. Figure 5 below encapsulates the calculations that have been considered in the current work. The results that we have obtained from these studies provide new insights into the nature of activation mechanism in Z-N catalysis.

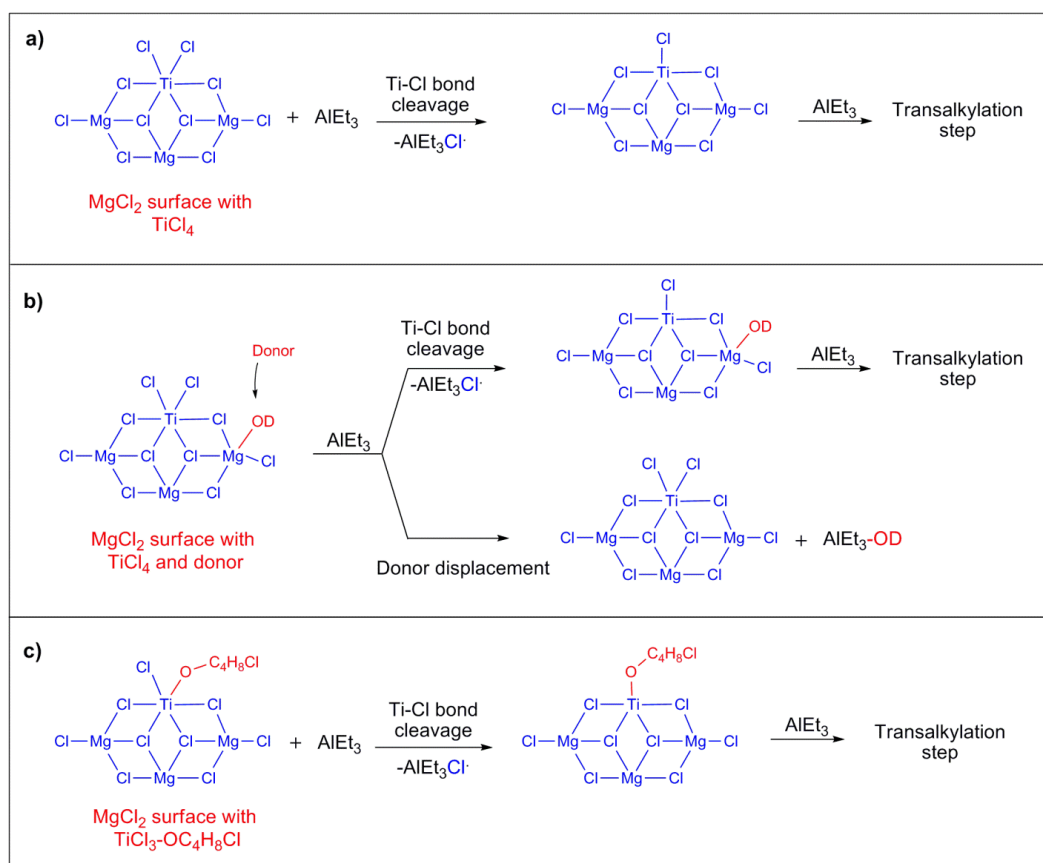


Figure 5. The general diagram of the three different types of model systems that have been considered in the study of the activation process: a)  $\text{MgCl}_2$  surface with  $\text{TiCl}_4$  complex, b)  $\text{MgCl}_2$  surface with  $\text{TiCl}_4$  and donor, and c)  $\text{MgCl}_2$  surface with the  $\text{TiCl}_3\text{-OC}_4\text{H}_8\text{Cl}$  complex; all the  $\text{MgCl}_2$  layers are not shown for the purpose of clarity.

## 5.2 Computational Details

Density functional theory (DFT) calculations have been done by employing the Turbomole 6.4 suite of programs.<sup>48</sup> Geometry optimizations for all the intermediate and transition state structures pertaining to this study have been carried out by using the Perdew, Burke, and Ernzerhof (PBE) functional,<sup>49,50</sup> followed by B3LYP<sup>51</sup> single-point calculations on all the PBE optimized structures. The electronic configurations of the atoms have been represented by a triple- $\xi$  basis set augmented by a polarization function (TURBOMOLE basis set TZVP).<sup>52</sup> The resolution of identity (RI)<sup>53</sup> along with the multipole accelerated resolution of identity (marij)<sup>54</sup> approximations have been employed for an accurate and efficient treatment of the electronic Coulomb term in the DFT calculations. The error bar value in the DFT calculations is expected to be in the range of  $\pm 1.0$  kcal/mol<sup>55</sup>.

The only exception to the TZVP/PBE/B3LYP approach employed throughout the manuscript is in the section where the validation of the MgCl<sub>2</sub> model with the “Cavallo Model” has been considered. For this validation section, the calculations were done at the BP86/TZVP/TZVPP level of theory. This was done in order to allow a comparison to the BP86/TZVPP level of theory that had been considered by Cavallo and workers<sup>29</sup>.

Along with this, for certain cases, we have also done further single point calculations with the PBE0 functional, on the geometries optimized with PBE. Specifically, this has been done for the activation process for the “*wd*(TiCl<sub>4</sub>)” (case where no donor is coordinated adjacent to the titanium center) and the *eb* donor cases. This has been done in order to check the difference in energy for the two hybrid functional cases (B3LYP and PBE0), i.e. to check whether the TZVP/PBE/B3LYP approach adopted in this study is robust. It was observed that there is not much difference in the  $\Delta G$  values obtained from both the TZVP/PBE/B3LYP and the TZVP/PBE/PBE0 approaches (see Table 1). Furthermore, the trend obtained for the energy profile for the reaction was also seen to be the same for both the cases.

Table 1. A comparative study of two different functionals (B3LYP and PBE0) for two different systems ( $wd(\text{TiCl}_4)$  and  $eb$ ). The fourth and the seventh columns (**in bold**) are the difference between  $eb$  and  $wd(\text{TiCl}_4)$  for the B3LYP and PBE0 cases respectively.

	$\Delta G$ in kcal/mol					
	<b>B3LYP</b>			<b>PBE0</b>		
	$wd(\text{TiCl}_4)$ <b>(1)</b>	$eb$ <b>(3)</b>	Diff. ( $eb - wd(\text{TiCl}_4)$ )	$wd(\text{TiCl}_4)$ <b>(1)</b>	$eb$ <b>(3)</b>	Diff. ( $eb - wd(\text{TiCl}_4)$ )
Xb	8.5	9.5	<b>1.0</b>	6.7	7.9	<b>1.2</b>
Xc	-4.2	-4.9	<b>-0.7</b>	-9.4	-9.9	<b>-0.5</b>
TS <sub>Xc,Xd</sub>	22.4	20.1	<b>-2.3</b>	16.4	13.9	<b>-2.5</b>
Xd	-23.2	-33.1	<b>-9.9</b>	-23.1	-32.0	<b>-8.9</b>
TS <sub>Xd,Xe</sub>	7.6	10.1	<b>2.5</b>	9.9	11.2	<b>1.3</b>
Xe	-9.6	-8.5	<b>1.1</b>	-8.3	-7.4	<b>0.9</b>
Xf	-8.5	-8.0	<b>0.5</b>	-3.4	-2.2	<b>1.2</b>

The  $\Delta G$  values, which are considered throughout this study, contain the zero-point energy, internal energy, and entropic contributions. For every transition state obtained, care has been taken to ensure that the obtained structure contained only one imaginary frequency related to the correct normal mode. For the determination of the transition state, the quasi-Newton-Josephson method has been employed. It is based on the restricted second-order method, which employs Hessian shift parameters. In the current study, the unrestricted formalism has been considered.

In 1998, Whitesides and coworkers<sup>56</sup> explained that the translational entropy is artificially increased when the reactants are considered separately in a reaction. To overcome this problem, all of the reaction pathways have been determined starting with the reactants (the  $\text{MgCl}_2$ -supported titanium species and the  $\text{AlEt}_3$  moiety) in the vicinity of each other, a procedure that has also been followed by other groups.<sup>57-65</sup>

Such an approach is particularly correct for the current systems, in which the substrate, the  $\text{AlEt}_3$  moiety, is a relatively small entity in comparison to the significantly larger  $\text{MgCl}_2$ -supported titanium active species.

## 5.3 Results and Discussion

### 5.3.1 Validation of the chosen $\text{MgCl}_2$ model system.

The  $\text{MgCl}_2$  model system used in this current study was originally proposed by Cavallo and co-workers<sup>29</sup> (see Figure 6). In this model,  $\text{MgCl}_2$  is in the  $\alpha$  crystalline phase and is characterized by an overall bond angle of  $120^\circ$  between the two five coordinated (104) lateral surfaces. The removal of one  $\text{MgCl}_2$  molecule from the layer leads to the exposure of a small four coordinated (110) lateral surface, which makes a  $150^\circ$  bond angle with the (104) layer (see Figure 6a). The  $\text{MgCl}_2$  (110) lateral cut was found to be more favorable for binding the pre-catalyst,  $\text{TiCl}_4$ , which validates the experimental and computational results in Z-N catalysis<sup>29,40,45,66,67</sup>. In our current studies, we have reduced the surface size from six layers (35  $\text{MgCl}_2$  molecules) to three (8  $\text{MgCl}_2$  molecules) (see Figure 6b). This has been done keeping the computational cost of the calculations in mind: the activation reaction has multiple steps (see Figure 1), and several possibilities also had to be considered with the different donor types. On the  $\text{MgCl}_2$  surface, those atoms that are close to the titanium center and donor have greater involvement in the activation reaction in comparison to the rest of the atoms in the lower layers, which indicates that the top layers of the  $\text{MgCl}_2$  surface require to be included and modeled properly, and that a reduction in layers should not adversely affect the  $\text{MgCl}_2$  model for the computational investigations. It should also be noted that during the optimization, for both the cases, all the  $\text{MgCl}_2$  layers were kept relaxed. The reason this was done was so that we could calculate the Gibbs free energy ( $\Delta G$ ) as well as the exact transition states for the activation process: both would be impossible if the lower layers of the  $\text{MgCl}_2$  surface were kept fixed. The fact that the structure of the  $\text{MgCl}_2$  layers remains compact even after the layers had been allowed to be completely relaxed during optimization provides proof of the robustness of the model employed.



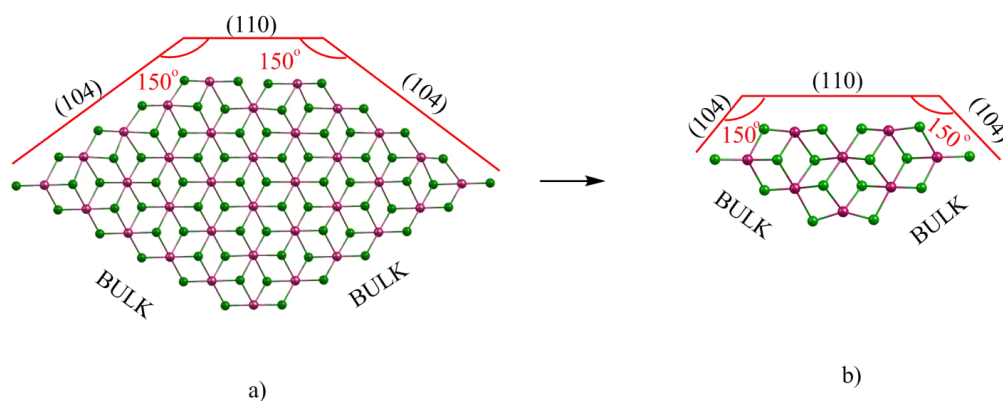


Figure 6. The MgCl<sub>2</sub> model systems: a) the six layer model proposed by Cavallo and coworkers<sup>29</sup> and b) the three layer model system employed in this study, which is a modification of the Cavallo model.

In order to further validate our modified MgCl<sub>2</sub> model system with the Cavallo model, we have performed calculations with our model for the purpose of comparison with calculations done by Cavallo and coworkers. The binding of different donors: diether, alkoxy silane and succinate, to the (104) lateral cut of MgCl<sub>2</sub> has been considered, with the same binding mode as Cavallo *et al.*<sup>29</sup> had considered. As mentioned in Table 2, the binding of the three donors were found to be exothermic by 30.5 kcal/mol, 30.1 kcal/mol and 40.4 kcal/mol respectively, comparing very well to the results obtained by Cavallo and coworkers: 29.8 kcal/mol, 30.5 kcal/mol and 42.2 kcal/mol respectively. Furthermore, as shown in Figure 7, we have also considered the binding of the diether donor on the six layered MgCl<sub>2</sub> Cavallo model system as well as our three layered modified model system. This was done to investigate whether any significant changes in geometry could be seen for the two cases, especially on the surface. As evidenced by the geometry values shown in Table 4, there was no significant distortion of the MgCl<sub>2</sub> surface in both the cases (our modified model and the Cavallo model); whatever little surface distortion was present, was present equally in both the cases.

Table 2. The  $\Delta E$  values (in kcal/mol) for three different donors binding to the (104) lateral cut of  $\text{MgCl}_2$  layer: comparison between the Cavallo Model and our modified  $\text{MgCl}_2$  model.

Donors	$\Delta E$ (in kcal/mol)	
	Cavallo Model	Our Model
1,3-diether	-29.8	-30.5
alkoxysilane	-30.5	-30.1
succinate	-42.2	-40.4

In addition to the validation done for the donor binding, discussed in the previous paragraph, a comparative study of the insertion barrier for the propylene monomer was considered for both the 1,2-*si* and 1,2-*re* faces. For this set of calculations, focused primarily at the titanium center, no donor was attached in the vicinity of the catalyst on the surface. The growing polymer chain, was represented by an isobutyl group, as also modeled by Cavallo *et al.*<sup>29</sup>. As shown in the Table 3, the difference between the barriers was found to be -0.1 kcal/mol with our modified model system. The corresponding value obtained by Cavallo and coworkers was -0.2 kcal/mol<sup>29</sup>. These validation calculations therefore prove the robustness of our adopted  $\text{MgCl}_2$  model, the calculations with which will be discussed henceforth in the subsequent sections.

Table 3. The  $\Delta\Delta E$  values (in kcal/mol) for the insertion barriers for propylene monomer insertion for the 1,2-*si* and 1,2-*re* face with no donor bound to the  $\text{MgCl}_2$  surface; comparison between the Cavallo model and our modified  $\text{MgCl}_2$  model.

Results	Insertion barriers (in kcal/mol)			
	Cavallo Model		Our Model	
Pathway	1,2- <i>re</i>	1,2- <i>si</i>	1,2- <i>re</i>	1,2- <i>si</i>
Without donor	0.0	-0.2	0.0	-0.1

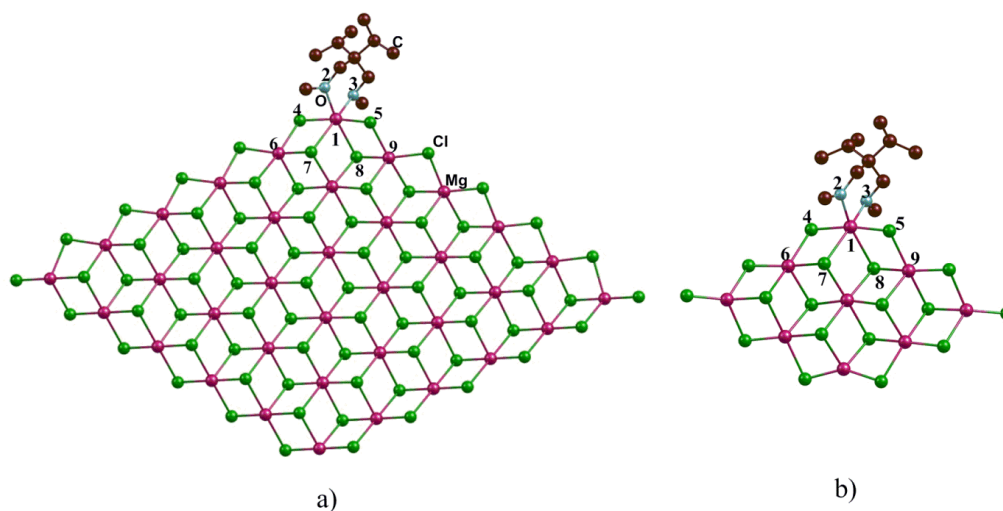


Figure 7. The optimized structures of two different model systems with the diether donor bound on the (110)  $\text{MgCl}_2$  lateral cut: a) the six layered Cavallo model system, and b) our modified three layered system.

Table 4. A comparative study of bond length and bond angle in the Cavallo and our modified model systems (shown in the Figure 7 above), where the diether donor being bound to the  $\text{MgCl}_2$  surface has been considered for both the cases.

Atom Number	Cavallo six layer model	Our three layer model
Bond length in $\text{Å}$		
1,2	2.115	2.101
1,3	2.110	2.088
1,7	2.694	2.676
1,8	2.656	2.714
4,6	2.411	2.410
5,9	2.404	2.419
Bond angle in degree ( $^\circ$ )		
2,1,3	83.42	85.68
1,4,6	101.97	104.77
1,5,9	100.29	103.89

### 5.3.2 Activation Study.

As mentioned in the Introduction, the donor influence has been considered by binding the donor to the (110)  $\text{MgCl}_2$  surface, in close proximity to the Ti (IV) center, leading to the formation of an octahedral complex. Such donor coordination is likely to be prevalent in the case of internal donors, since they are added to the ZN system during the catalyst preparation, before the introduction of  $\text{AlEt}_3$ . For the five donor cases considered, the *eb* donor would coordinate to the  $\text{MgCl}_2$  surface through a lone oxygen, while, in all the other donor cases, the binding of the donor has been considered through a chelate coordination of two oxygens to the  $\text{MgCl}_2$  surface. This is because there is only a lone ester group in *eb*, while there are two ester groups in the other donors, making the chelating mode of coordination likely for these donors. The optimized structures of the donor coordinated to the  $\text{MgCl}_2$  surface in proximity to the titanium center are shown in Figure 8. The favorability of this donor coordination to the  $\text{MgCl}_2$  surface adjacent to the titanium center is indicated in Table 5 below. The results indicate that the donor binding is favorable in all the cases. The least favorable case is that of *eb* binding, where the binding is still favorable by 9.8 kcal/mol ( $\Delta G$  value). This indicates that the presence of a bound donor in close proximity to the titanium center is quite a likely possibility in the Z-N systems.

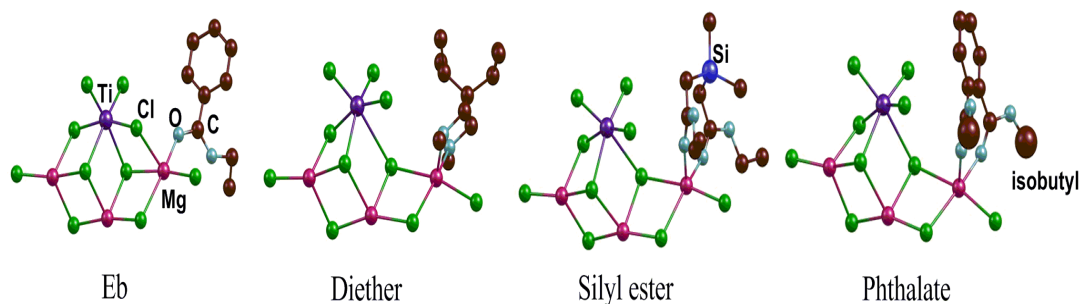


Figure 8. The different donor coordination modes to the (110)  $\text{MgCl}_2$  surface that have been considered in this study.

Table 5. The donor coordination to the  $\text{MgCl}_2$  (110) surface.

Donor	$\Delta G$ (in kcal/mol)
<i>eb</i>	-9.8
diether1	-18.9
diether2	-25.9
phthalate	-45.8
silyl ester	-37.6

The following sections discuss (i) the comparative study between the  $wd(\text{TiCl}_4)$  and the *eb* donor coordinated cases of the potential energy surface for the activation steps. Here,  $wd(\text{TiCl}_4)$  represents the case with no donor attached to the  $\text{MgCl}_2$ . (ii) The comparison of all the donor cases with the  $wd(\text{TiCl}_4)$  case, and (iii), the comparative study of the activation steps for the  $wd(\text{TiCl}_4)$  and the  $wd(\text{TiCl}_3\text{-OC}_4\text{H}_8\text{Cl})$  cases. The nomenclature employed in the energy profiles in the figures is **1**, **2**, **3**, **4**, **4'**, **5**, and **6** for the  $wd(\text{TiCl}_4)$ , the  $wd(\text{TiCl}_3\text{-OC}_4\text{H}_8\text{Cl})$ , *eb*, diether1, diether2, phthalate and silyl ester donor cases respectively.

**5.3.2.1 A Comparative Study of  $wd(\text{TiCl}_4)$  and the *eb* Donor Cases:** The free energy profile for a comparative study of the  $wd(\text{TiCl}_4)$  (**1**) and the *eb* (**3**) donor cases is shown in Figure 9 below. The titanium is assumed to be in an octahedral environment in both the cases, which is the commonly accepted<sup>6,43,44,68</sup> structure for Ti coordination to  $\text{MgCl}_2$ . As mentioned in the Introduction, the activation mechanism pathway follows the steps that have been elucidated earlier by Cavallo and co-workers<sup>43</sup>. The homolytic cleavage of the Ti-Cl bond occurs with the help of the  $\text{AlEt}_3$  moiety, and leads to the formation of two chemical species, an intermediate having a single vacancy on the titanium metal center and the  $\text{AlEt}_3\text{Cl}$  radical. The intermediates are **1b** and **3b** for the  $wd(\text{TiCl}_4)$  and the *eb* donor cases respectively, and are the starting point for the trans-alkylation step (see Figure 10). No transition state could be obtained for this conversion, despite a careful linear scan of the

potential energy surface. Therefore, for this step, only the thermodynamics of the reaction has been considered. There are several other groups<sup>43,69,70</sup> who have reported only the thermodynamics for reactions that show this type of conversion. This reaction is endergonic in nature by 8.5 kcal/mol and 9.5 kcal/mol (the difference in energy between the **3b** and **3a** structures in Figure 9) for the *wd*(TiCl<sub>4</sub>) and the *eb* donor cases respectively.

In the next, trans-alkylation step, the interaction between a second AlEt<sub>3</sub> moiety and the intermediates, **1b** and **3b**, is favorable by 4.3 kcal/mol and 4.9 kcal/mol respectively, and leads to the formation of the subsequent intermediates, **1c** and **3c**, for the *wd*(TiCl<sub>4</sub>) and the *eb* donor cases respectively. After this, **1c** and **3c** can further rearrange to form new intermediates, **1d** and **3d**, after the crossing of the four-membered transition states, **TS<sub>1c,1d</sub>** and **TS<sub>3c,3d</sub>**. This step is the rate limiting step for the activation process, having barriers of 22.4 kcal/mol and 20.1 kcal/mol respectively for the two cases. Along with ethyl migration in the trans-alkylation step, the hydride migration step has also been studied for this reaction and it was observed that this process is energetically less favourable by 3.6 kcal/mol and 3.1 kcal/mol for the *wd*(TiCl<sub>4</sub>) and the *eb* donor cases respectively. Henceforth, the ethyl migration pathway was considered for further activation study. Finally, the products, **1f** and **3f**, are formed *via* the respective transition states, **TS<sub>1d,1e</sub>** and **TS<sub>3d,3e</sub>**, and intermediates, **1e** and **3e** (see Figure 9). The AlEt<sub>2</sub>Cl species is also formed along with the final products along the reaction pathway. The overall process is exergonic by 7.0 kcal/mol and 24.6 kcal/mol for the *wd*(TiCl<sub>4</sub>) and the *eb* donor cases respectively (see Figure 9). The optimized structures of the transition states, **TS<sub>1c,1d</sub>** and **TS<sub>1d,1e</sub>**, for the *wd*(TiCl<sub>4</sub>) case have been shown in Figure 11. The final product of the trans-alkylation reaction contains one ethyl group on the titanium metal center, which is the actual active catalyst responsible for the chain growth in the Ziegler Natta olefin polymerization system. Hence, the reaction pathway constitutes the activation mechanism for the two cases considered.

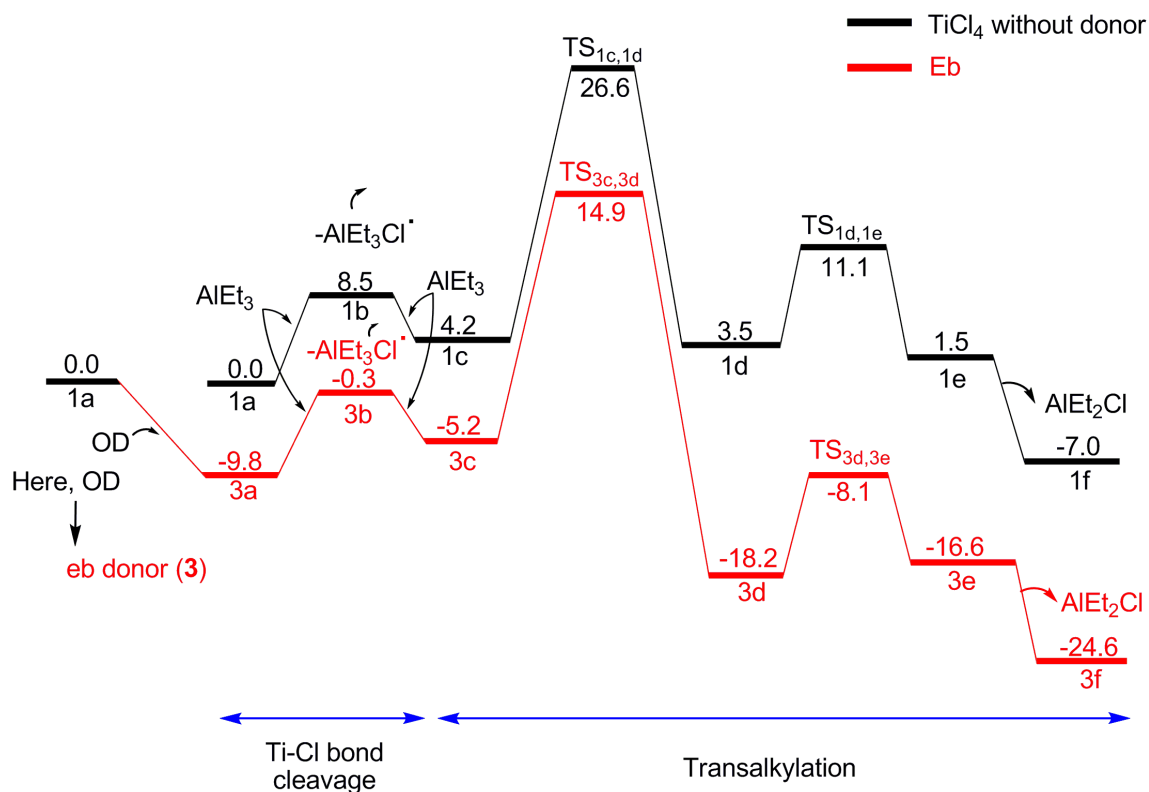


Figure 9. The free energy profile for a comparative study between the  $\text{TiCl}_4$  without donor case  $\{wd(\text{TiCl}_4)\}$  and the *eb* donor cases for two consecutive steps: a) Ti-Cl bond cleavage and b) trans-alkylation; the intermediate and transition state chemical structures are shown in Figure 10 below.

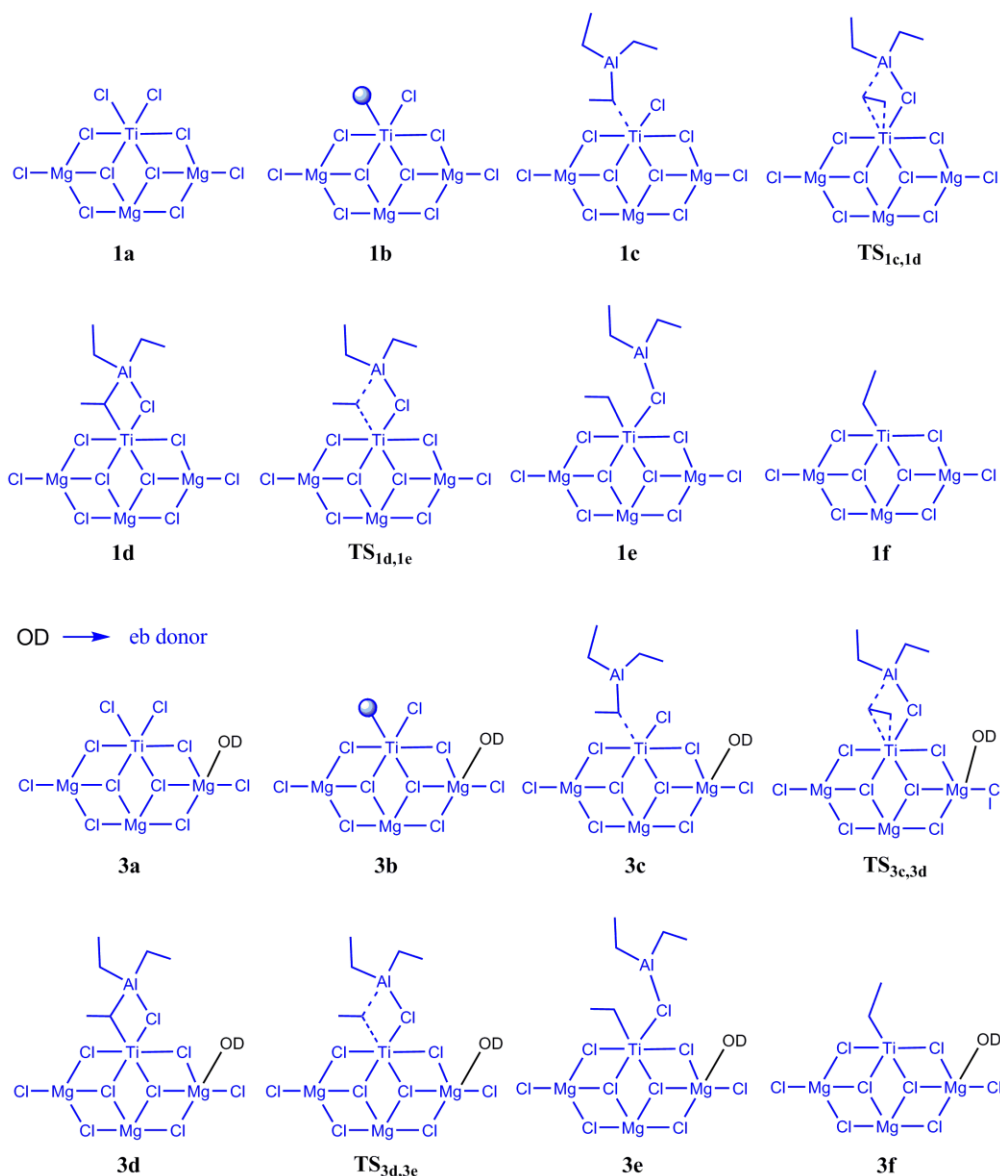


Figure 10. The chemical structures of the intermediate and transition state species indicated in Figure 9.

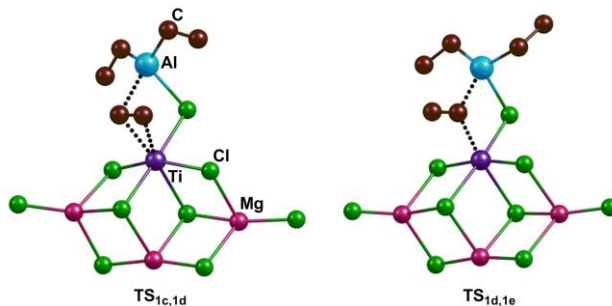


Figure 11. The optimized structures of the transition states, TS<sub>1c,1d</sub> and TS<sub>1d,1e</sub>, for the trans-alkylation reaction for the *wd*(TiCl<sub>4</sub>) case; all the MgCl<sub>2</sub> layers are not shown for the purpose of clarity.



Furthermore, we have also done some extra calculations with the six layered Cavallo model system in order to validate our three layered model. We have repeated the complete energy profile for the *wd*(TiCl<sub>4</sub>) and the *eb* donor cases to check the effect of the size of the model system. It was found that there is not much difference between the energy profiles (see the Figures 12 and 13). Hence, the size of the MgCl<sub>2</sub> model system does not affect the reaction pathways.

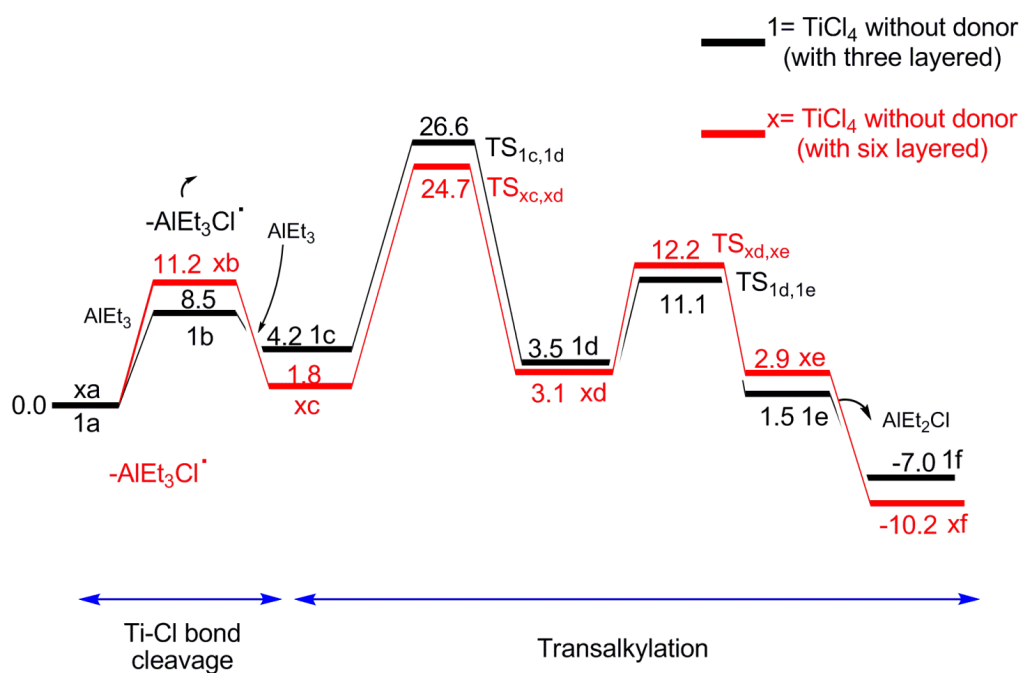


Figure 12. The energy profile for a comparative study of *wd*(TiCl<sub>4</sub>) with two different model systems a) six layered cavallo model system (in red), and b) our three layered modified model system (in black).

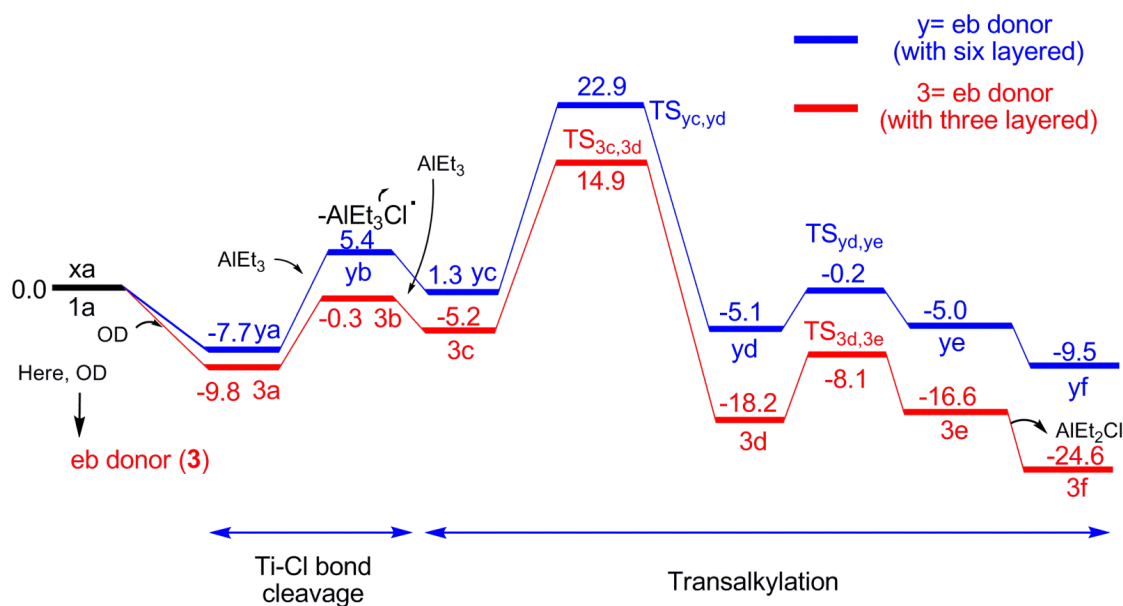


Figure 13. The energy profile for a comparative study of *eb donor* with two different model systems a) six layered cavallo model system (in red), and b) our three layered modified model system (in black).

In addition, as mentioned in the Introduction, we have considered the activation/donor structure relationship with two different  $MgCl_2$  model systems. In the first case, for the three  $MgCl_2$  layered model system based on the Cavallo model, the  $TiCl_4$  complex is bound to the  $MgCl_2$  surface through two bridging chlorine atoms, where both the bridging chlorine atoms bind to the (110)  $MgCl_2$  surface (see Figure 3). In the second case, for the “unified model” developed recently by Cavallo and coworkers<sup>46</sup>, among the two bridging chlorine atoms, one binds to the (110) surface and the other to the adjacent (104) surface (see Figure 4). The comparative study of both the  $MgCl_2$  model systems has been considered for the *wd*( $TiCl_4$ ) and the *eb* donor cases (see the Figures 14 and 15). The trend obtained for the energy profile was seen to be the same for the two  $MgCl_2$  model systems. This result indicates that the results obtained are consistent regardless of the nature of the  $MgCl_2$  surface model employed.

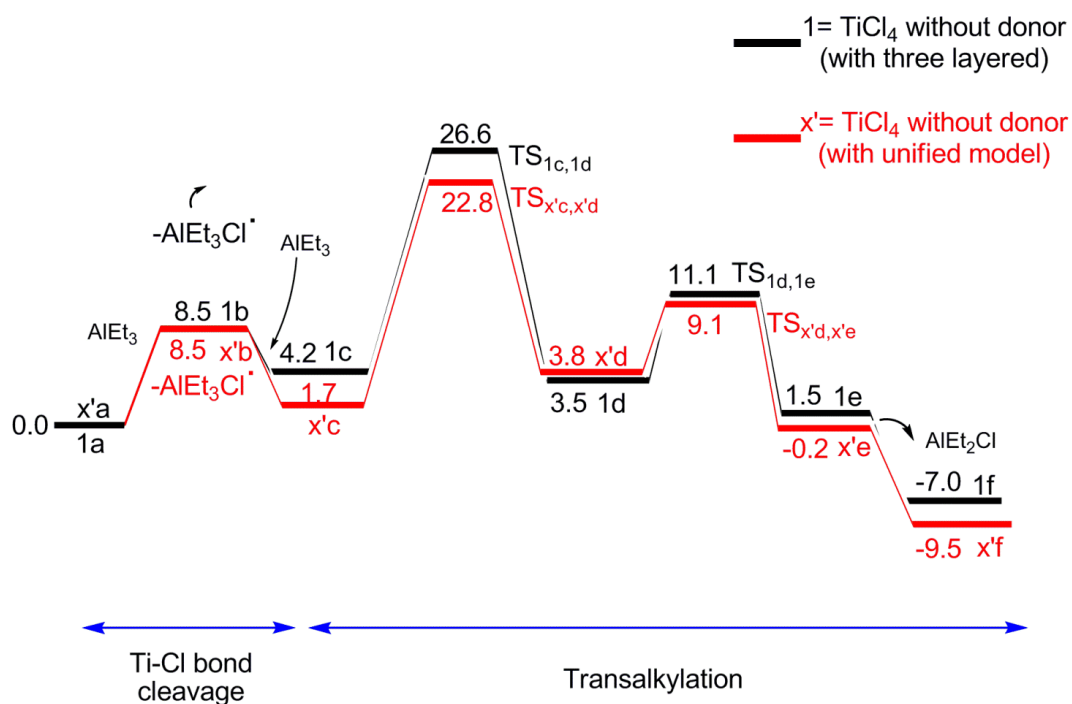


Figure 14. The energy profile for a comparative study of  $wd(\text{TiCl}_4)$  with two different model systems a) unified model system (in red), and b) our three layered modified model system (in black).

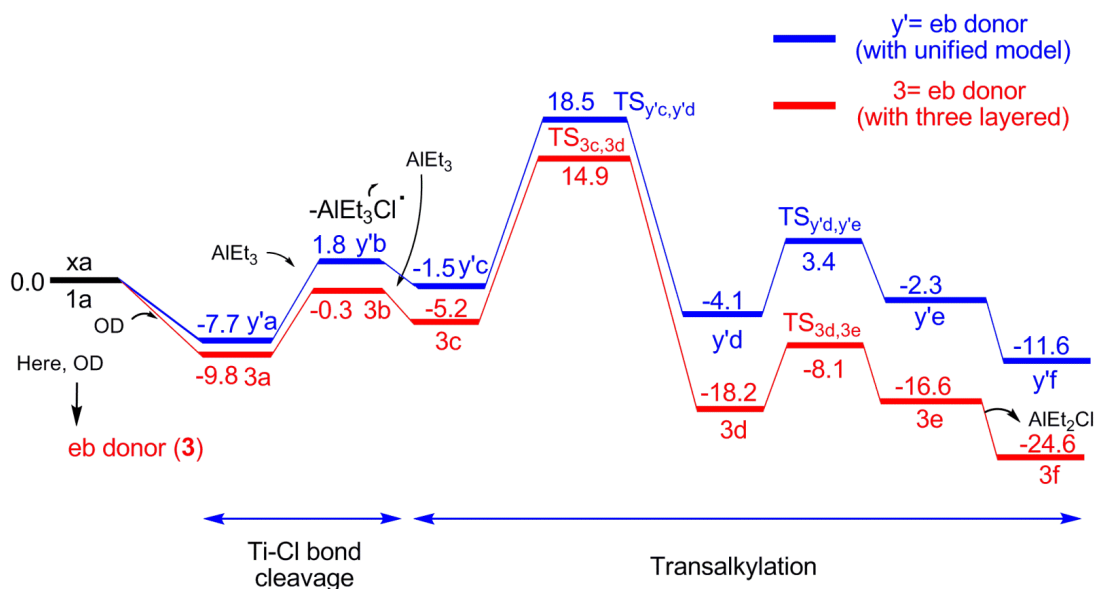


Figure 15. The energy profile for a comparative study of  $eb$  donor with two different model systems a) unified model system (in red), and b) our three layered modified model system (in black).

**5.3.2.2 The comparative study between  $wd(\text{TiCl}_4)$  and all the donors:** The previous section showed the results for the free energy profile comparing the activation steps for two cases: the  $wd(\text{TiCl}_4)$  case, and the  $eb$  donor case. In this section is discussed the comparative study between the  $wd(\text{TiCl}_4)$  case and all the five donor cases. The six free energy profiles are shown together in Figure 16, while the information with regard to the intermediates and transition states is collected together in Table 6 below. In all the cases, the rate limiting step is the trans-alkylation step involving the transfer of an ethyl group from aluminium to the titanium center, and a chloride from the titanium to the aluminium. The barrier for this step is shown explicitly in column 7 (labeled **Barrier**) of Table 6. Furthermore, a collection of bar graphs in 19 below shows how the rate limiting step for the different donor cases compares to  $wd(\text{TiCl}_4)$ .

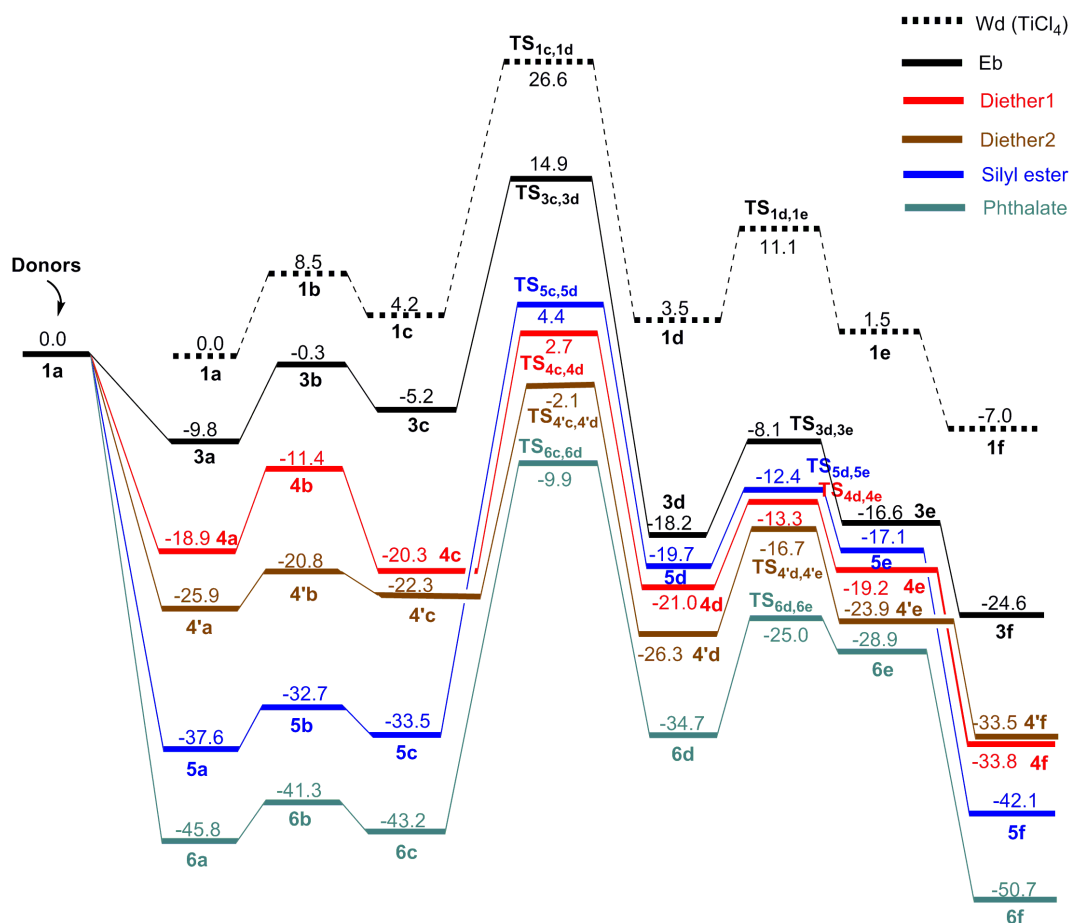


Figure 16. The energy profile for the comparative study between  $wd$  (no donor in the system, in black dotted lines) and different donors attached to the  $\text{MgCl}_2$  surface.

The values indicate that the *eb* and *diether2* donor cases have lower barriers for the rate limiting step in comparison to *wd*(TiCl<sub>4</sub>): the barriers for these donor cases are 20.1 kcal/mol and 20.2 kcal/mol respectively, while the corresponding value for *wd*(TiCl<sub>4</sub>) is 22.4 kcal/mol. This means that the inclusion of these donors as internal donors would make the activation step more favorable in the Z-N system. The other diether donor case considered: *diether1*, has a barrier of 23.0 kcal/mol for the rate limiting step (see Table 6 below), which means that the presence of this diether would not affect the activation process. However, the phthalate donor case has a barrier of 33.3 kcal/mol, which is 10.9 kcal/mol higher than *wd*(TiCl<sub>4</sub>). This significant increase indicates that the presence of the phthalate donor would lead to a considerable slowing down of the activation process in Z-N systems. This implies that Z-N systems employing the phthalate donor as an internal donor would experience an induction period before catalysis would begin, owing to the extra time it would take for the activation process to be completed. This, indeed, has been observed in Z-N systems employing a phthalate as the internal donor<sup>71</sup>. The results also indicate that employing a silyl ester donor (rate limiting step barrier of 37.9 kcal/mol) would lead to a significant induction period before catalysis would proceed. It should be noted that a significant induction period does not necessarily mean that the system would be ineffective/inefficient after the catalyst has been activated and is ready for polymerization. Nevertheless, having a catalyst system having a smaller/non-existent induction period would be preferable to having a catalyst system with a long induction period, if their subsequent activities are comparable, which is the case for most donor included ZN systems, as seen from previous calculations<sup>72</sup>. It is also to be noted that in the Z-N reaction, a barrier height of 37.9 kcal/mol is not formidable. This is because the temperature employed in Z-N catalysis systems is usually greater than 60°C<sup>73,74</sup>. Previous studies have shown that barrier heights of 40.0 kcal/mol are acceptable in systems where the temperature is above 50°C<sup>75-77</sup>.

The reason for the dissimilarity of energy barriers for all donor cases is because of the change in the stability of the reactant as well as the transition state structures corresponding to the rate limiting step of the reaction: the transfer of the ethyl group from the aluminum to the titanium metal center. This reactant, denoted as **1c** and **3c** in Figure 10, is the adduct formed by the interaction of AlEt<sub>3</sub> with the titanium center (see Figure 10). The current study shows that for the phthalate and

silyl ester cases, the adduct formed is not the  $\alpha$  carbon of the ethyl group of  $\text{AlEt}_3$  interacting with the titanium center (as in the other cases, and in **1c** and **3c** in Figure 10), but with the chloride attached with the titanium. The structure of the adducts for the phthalate and silyl ester cases is shown in Figure 17(**5c** and **6c**) respectively. The reason the **1c** and **3c** type adduct is less favorable for the phthalate cases is because of the larger steric influence of the phthalate donor: there is greater displacement of one of the  $\text{MgCl}_2$  layers from the  $\text{MgCl}_2$  surface, the  $\text{Mg}-\text{Cl}$  bond length in the distorted layer is  $3.655 \text{ \AA}$  (see Figure 17, **5c1** below) which is greater in comparison to without donor,  $wd(\text{TiCl}_4)$ , system  $\text{Mg}-\text{Cl}$  bond length of  $2.528 \text{ \AA}$  (see Figure 17, **1c** below). This displacement is less when the  $\text{AlEt}_3$  binds to the chloride attached to the titanium (see Figure 17, **5c** below). Similar  $\text{MgCl}_2$  layer dislocation has also been found in the corresponding transition state (see Figure 18, **TS<sub>5c,5d</sub>** below). Therefore, the reason for the higher barrier in case of the phthalate donor is the stability of the reactant structure: the binding of  $\text{AlEt}_3$  moiety to the chloride atom attached to the titanium (see Figure 17, **5c** below) and the less stable transition state in comparison to other donors (see Figure 18, **TS<sub>5c,5d</sub>** below). In case of the silyl ester donor, the reason for the stability of the adduct with  $\text{AlEt}_3$  binding to the chloride is the formation of an extra  $\text{Ti}-\text{O}$  bond between the donor and the titanium metal center (see Figure 17, **6c** below) – a bond that is not formed when  $\text{AlEt}_3$  binds to the titanium center, which is make the reactant structure more stable. Such an extra  $\text{Ti}-\text{O}$  bond formation is not possible in the other donor cases because of steric reasons: attempts to forcibly make such a bond in the other donor cases led to dissociation of the  $\text{Ti}-\text{O}$  bond. In addition, in the diether2 donor case, we did not get the **1c** and **3c** type of adduct – hence the binding of  $\text{AlEt}_3$  to the chloride attached to the titanium has been considered. The barrier height for this donor case is less in comparison to  $wd(\text{TiCl}_4)$  due to the stable transition state structure (see Figure 18, **TS<sub>4c,4d</sub>** below). This is also confirmed by the NBO<sup>78-80</sup> charge analysis where the charge on titanium in the reactant structure for the  $wd(\text{TiCl}_4)$  and diether2 cases is 1.296 and 1.423 respectively. In the diether2 case, the charge is slightly greater, which indicates that the transfer of the ethyl group from  $\text{AlEt}_3$  to the titanium is slightly more favorable in comparison to the  $wd(\text{TiCl}_4)$ .

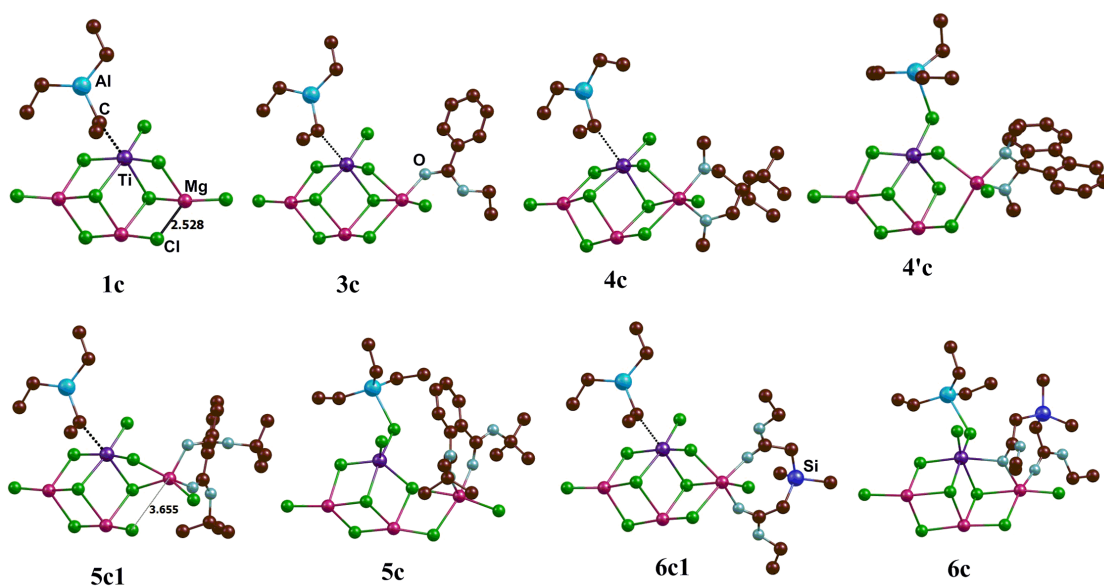


Figure 17. The optimized structure of the interaction of  $\text{AlEt}_3$  species with the titanium system, with different donors attached to the (110)  $\text{MgCl}_2$  surface as well as with no donor present in the system; only two  $\text{MgCl}_2$  layers and no hydrogen atoms are shown for the purpose of clarity.

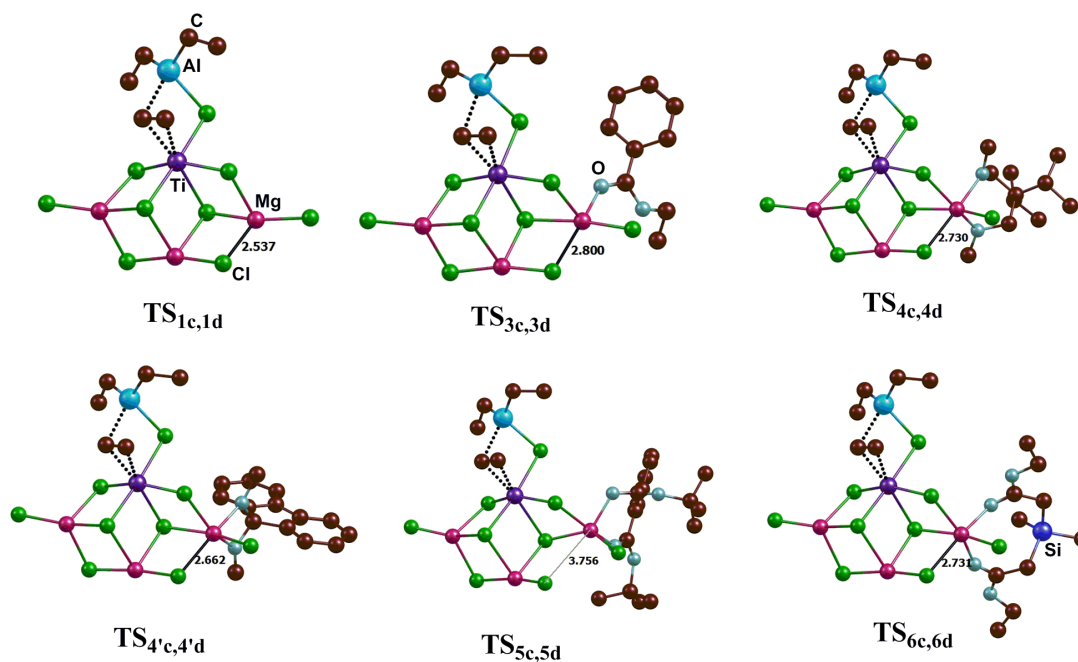


Figure 18. The optimized structure of the transition states, where the transfer of one ethyl group from the  $\text{AlEt}_3$  moiety to the titanium metal center has been considered for different donor cases and for the without donor case; only two  $\text{MgCl}_2$  layers and no hydrogen atoms are shown for the purpose of clarity.

Table 6. The relative free energies (in kcal/mol) for the comparative study between the without donor case { $wd(TiCl_4)$ } and all the donor included cases for Ti-Cl bond cleavage and the trans-alkylation reaction.

Activation Mechanism Step	Donor Coordination		Ti-Cl Bond Cleavage	Transalkylation							
	1a	Xa		Xb	Xc	TS <sub>Xc,X<sup>d</sup></sub>	Barrier (TS <sub>Xc,X<sup>d</sup></sub> )-Xc	Xd	TS <sub>Xd,X<sup>e</sup></sub>	Xe	Xf
Donor/ $wd$											
X= 1,3,4,4',5,6											
$wd(TiCl_4)$ (1)	0.0		8.5	4.2	26.6	<b>22.4</b>	3.5	11.1	1.5	-7.0	
$eb$ (3)	0.0	-9.8	-0.3	-5.2	14.9	<b>20.1</b>	-18.2	-8.1	-16.6	-24.6	
Diether1 (4)	0.0	-18.8	-11.4	-20.3	2.7	<b>23.0</b>	-21.0	13.3	-19.2	-33.8	
Diether2 (4')	0.0	-25.9	-20.8	-22.3	-2.1	<b>20.2</b>	-26.3	-16.7	-23.9	-33.5	
Phthalate (5)	0.0	-45.8	-41.3	-43.2	-9.9	<b>33.3</b>	-34.7	-25.0	-28.9	-50.7	
Silyl ester (6)	0.0	-37.6	-32.7	-33.5	4.4	<b>37.9</b>	-19.7	-12.4	-17.1	-42.1	

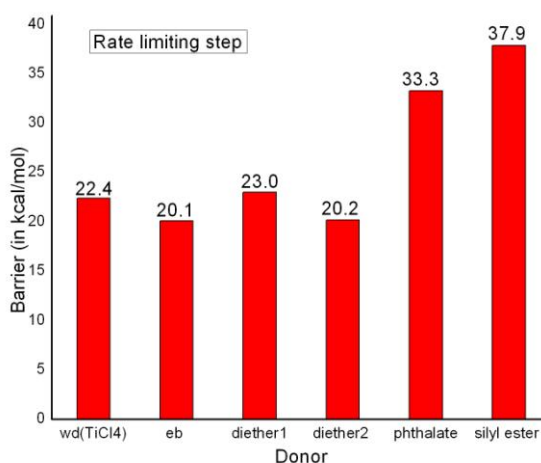


Figure 19. A bar graph showing a comparative study of the  $wd(TiCl_4)$  case with the donor included cases for the rate limiting step in the trans-alkylation reaction.



As mentioned in the Introduction, along with the Ti-Cl bond cleavage reaction, we have also investigated the competing possibility of the donor displacement from the  $\text{MgCl}_2$  surface with the aid of  $\text{AlEt}_3$  for all the donor included cases (the reaction is shown in Figure 5b). Figure 20 shows a collection of bar graphs comparing the thermodynamic value ( $\Delta G$ ) obtained for the donor displacement by  $\text{AlEt}_3$  with the corresponding  $\Delta G$  value for the Ti-Cl bond cleavage. The results indicate that the Ti-Cl bond cleavage – the first step in the activation process - is more favorable in comparison to the donor displacement reaction for the diether1, diether2, silyl ester and phthalate donor cases. The  $\Delta G$  values for these cases are in the range of 4.5 – 7.5 kcal/mol and of 23.5 – 33.9 kcal/mol for the Ti-Cl bond cleavage and donor displacement reactions respectively. This difference in the  $\Delta G$  values between the reactions is quite significant, and suggests that the donor displacement reaction is unlikely for the diether1, diether2, phthalate and silyl ester donor cases. However, for the *eb* donor case, the Ti-Cl bond cleavage and the donor displacement reactions are almost equally favourable - the  $\Delta G$  values for the two reactions are 9.5 kcal/mol and 9.1 kcal/mol respectively (see Figure 20). The reason for this is that the diether1, diether2, phthalate and silyl ester donors bind to the  $\text{MgCl}_2$  surface through two C=O groups in a chelating fashion (see Figure 8), while the *eb* donor binds to the  $\text{MgCl}_2$  surface through only its single available C=O group, and is therefore more prone to displacement with the aid of  $\text{AlEt}_3$ . It is to be noted that diether2 is seen to bind more strongly to the  $\text{MgCl}_2$  in comparison to diether1. The chief difference between the two is that diether2 has an aromatic backbone, and diether1 is aliphatic in nature (see Figure 2). This provides greater electron density to flow from the aromatic rings to the oxygen atoms coordinating to the magnesium, thereby stabilizing the  $\text{MgCl}_2$  coordinated diether2 complex.

Hence, the *eb* donor case is the one case where there exists the real possibility of the donor being displaced from the  $\text{MgCl}_2$  surface. This, indeed, shows agreement with experimental findings.<sup>47</sup> It should be noted, however, that the possibility exists of the donor displacement product,  $\text{AlEt}_3\text{-}eb$ , also being absorbed on the  $\text{MgCl}_2$  surface, in close proximity to the Ti (IV) center, i.e., of the  $\text{AlEt}_3\text{-}eb$  species acting as a donor. The free energy profile for the  $\text{AlEt}_3\text{-}eb$  donor is shown in Figure 21. **3'** is the nomenclature that has been employed to indicate the  $\text{AlEt}_3\text{-}eb$  donor case (**3** corresponds to the *eb* donor case). The free energy profile shown in Figure 21

indicates that the absorption of  $\text{AlEt}_3\text{-}eb$  donor on the  $\text{MgCl}_2$  surface makes the activation mechanism less effective in comparison to the  $eb$  donor, by increasing the barrier for the rate limiting step (22.9 kcal/mol in comparison to 20.1 kcal/mol for the  $eb$  donor case). The reason for this is that in case of  $eb$ , the donor binds to the  $\text{MgCl}_2$  surface through the oxygen bond (an Mg-O bonding), but in the case of  $\text{AlEt}_3\text{-}eb$ , it binds through the carbon of the ethyl group of the  $\text{AlEt}_3$  moiety (an Mg-C bonding), which is weaker in comparison to the Ti-O bond. However, since the barrier for the rate limiting step (22.9 kcal/mol) is still significantly less than the corresponding barriers for the phthalate and the silyl ester cases (10.4 kcal/mol and 15.0 kcal/mol respectively), the results indicate that the  $\text{AlEt}_3\text{-}eb$  species would also not serve to negatively influence the activation process in Z-N systems.

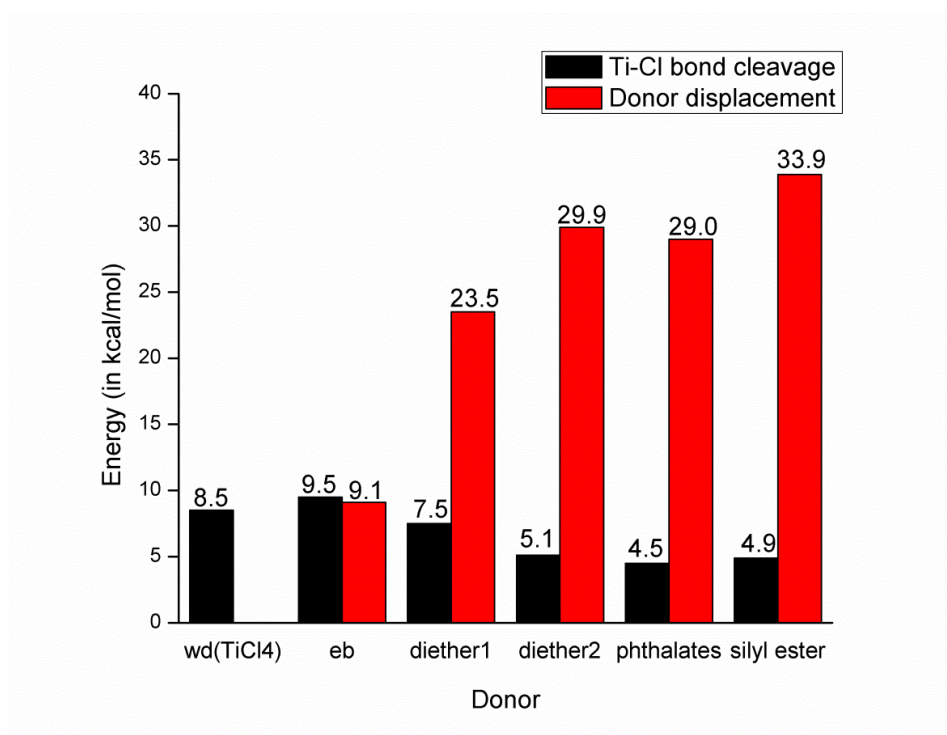


Figure 20. A bar graph for the comparative study of the Ti-Cl bond cleavage and the donor displacement reaction.

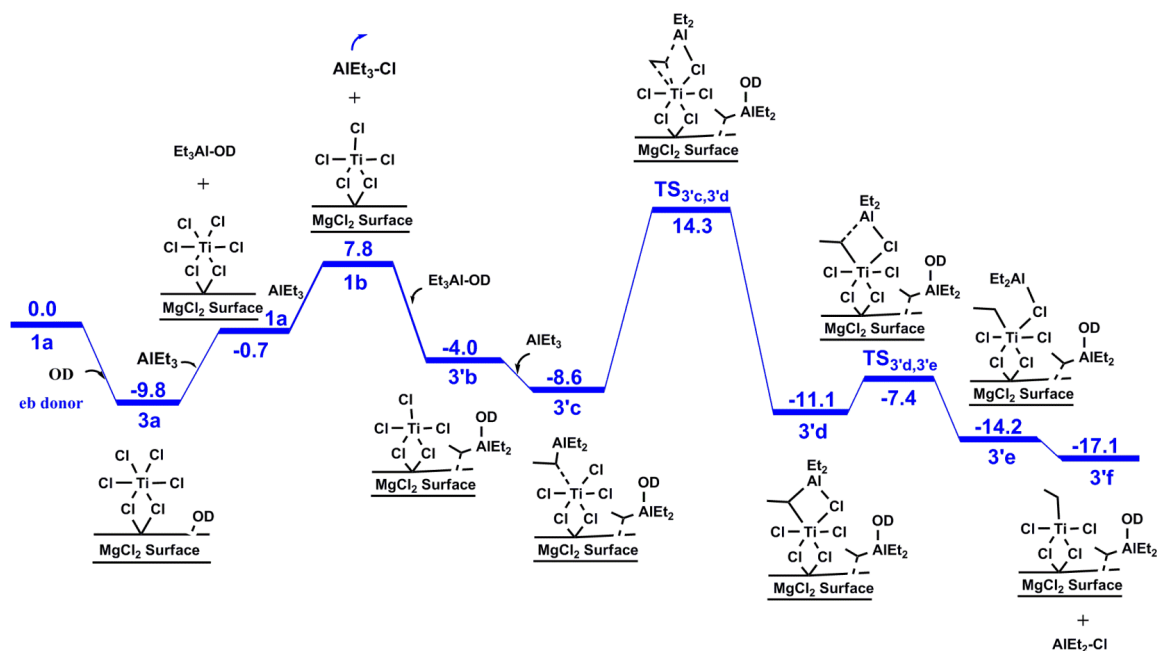


Figure 21. The energy profile for the  $\text{AlEt}_3$ - $\text{eb}$  species binding to the  $\text{MgCl}_2$  surface behaving as a donor.

### 5.3.2.3 The comparative study of the $\text{wd}(\text{TiCl}_4)$ and $\text{wd}(\text{TiCl}_3\text{-OC}_4\text{H}_8\text{Cl})$ complexes:

As mentioned in the Introduction, Sautet *et al.*<sup>33</sup> have reported that complexes such as  $\text{TiCl}_3\text{-OC}_4\text{H}_8\text{Cl}$  can be formed by the decomposition of donors such as tetrahydrofuran (THF) at the titanium center. Moreover, in a recent computational study, we have shown that the decomposition of donors such as esters at the titanium center can also lead to the formation of the  $\text{Ti-OR}$  species on the  $\text{MgCl}_2$  surface.<sup>35</sup> Therefore, in order to check whether such titanium species formed by donor decomposition favor or disfavor the activation process, a comparative study between  $\text{wd}(\text{TiCl}_4)$  and  $\text{wd}(\text{TiCl}_3\text{-OC}_4\text{H}_8\text{Cl})$  (as a representative example of a donor decomposed product) have been investigated. In the  $\text{wd}(\text{TiCl}_3\text{-OC}_4\text{H}_8\text{Cl})$  case, two possible conformations have been investigated. In the first conformation, the  $\text{-OC}_4\text{H}_8\text{Cl}$  group binds to the titanium metal center through the oxygen atom, and in the second, the  $\text{-OC}_4\text{H}_8\text{Cl}$  group binds to the titanium as well as to the magnesium of the  $\text{MgCl}_2$  layer. The binding in the second case is thermodynamically less favourable by 3.1 kcal/mol owing to the steric bulk of the  $\text{-OC}_4\text{H}_8\text{Cl}$  group. Hence, the binding mode corresponding to the first conformation has been considered for the further study of activation process. The  $\text{Ti-Cl}$  bond cleavage and the trans-alkylation

reactions have been considered as for the previous cases. In the first reaction, the homolytic cleavage of the Ti-Cl bond leads to the intermediate **2b**. The energy cost for this step is 15.9 kcal/mol. As shown in Figure 22, the interaction between the second AlEt<sub>3</sub> and **2b** is a favorable reaction by 4.5 kcal/mol, and leads to the formation of **2c**. The next reaction is the rate limiting step of the process for the ethyl group transfer from AlEt<sub>3</sub> to the titanium metal centre; the barrier for this step is 29.9 kcal/mol, and it leads to the formation of the **2d** intermediate. Till this point, the steps follow the activation process also seen for the TiCl<sub>4</sub> case (also shown, for the purpose of comparison, in the same figure). However, while the TiCl<sub>4</sub> case goes through a further, four-membered transition state, before yielding the final product (also discussed in the previous section), for **2d**, the transformation is seen to occur as the total dissociation of the AlEt<sub>2</sub>-OC<sub>4</sub>H<sub>8</sub>Cl species, leading to the formation of the final product **2f**. No transition state could be found for the conversion of **2d** to **2f**, and a linear transit scan led to a gradual increase in energy till **2f** was seen to form. This reaction was seen to be endergonic by 13.5 kcal/mol (see Figure 22). The reason for this is that the Ti-O bond is stronger in the TiCl<sub>3</sub>-OC<sub>4</sub>H<sub>8</sub>Cl case in comparison to the Ti-Cl bond in TiCl<sub>4</sub>, and so the breaking of the Ti-O bond is energetically more expensive in comparison to the Ti-Cl bond. Therefore, the formation of TiCl<sub>3</sub>-OC<sub>4</sub>H<sub>8</sub>Cl, or by extension, of Ti-O type species on the MgCl<sub>2</sub> surface, is not favorable for the activation process, in comparison to the TiCl<sub>4</sub> complex in Z-N systems, and a significant induction period can be expected if such a species is the site for olefin polymerization catalysis.

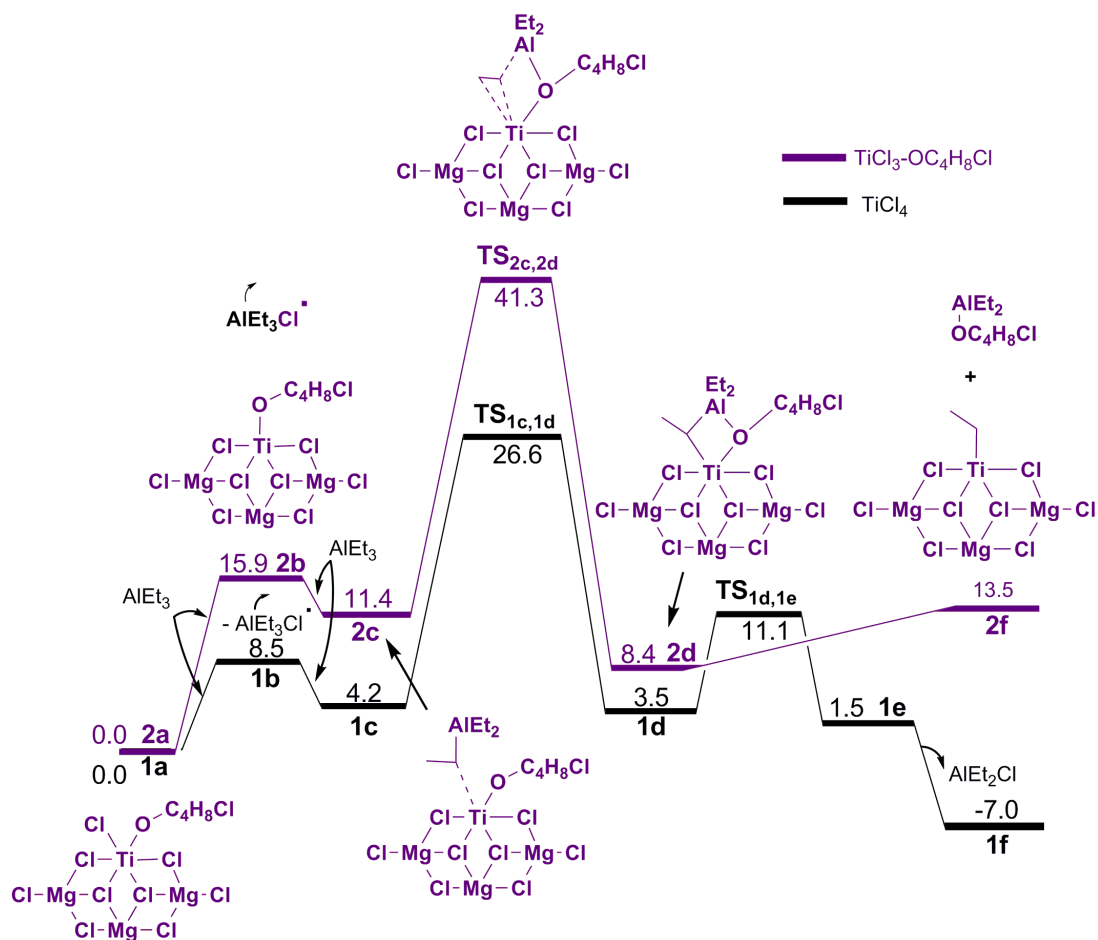


Figure 22. The energy profile for the comparative study of  $wd(\text{TiCl}_4)$  and  $wd(\text{TiCl}_3\text{-OC}_4\text{H}_8\text{Cl})$  for the Ti-Cl bond cleavage and the trans-alkylation steps; all the  $\text{MgCl}_2$  layers are not shown for the purpose of clarity.

## 5.4 Conclusions

Full quantum chemical studies, employing density functional theory (DFT), have been done in order to investigate the effect of different donors on the activation mechanism: the process of converting the  $\text{Ti(IV)Cl}_4$  catalyst precursor species to the  $\text{Ti(III)Cl}_2\text{Et}$  active catalyst species with the aid of  $\text{AlEt}_3$ . Two steps have been considered for the activation mechanism: (i) Ti-Cl bond cleavage and (ii) the trans-alkylation reaction where a  $\text{Cl}^-$  on the titanium is exchanged with an ethyl group on the  $\text{AlEt}_3$ . The influence of the donor has been considered by binding it adjacent to the titanium complex on the (110)  $\text{MgCl}_2$  surface during the computational investigation of the reactions (i) and (ii). In addition to these calculations, the possibility of

displacement of the donor from the  $\text{MgCl}_2$  surface has also been taken into account. Furthermore, the possibility of activation by the “bare”  $\text{TiCl}_4$  system (without donor coordinated adjacently), and by systems such as  $\text{TiCl}_3\text{-OC}_4\text{H}_8\text{Cl}$ , which can be formed by donor decomposition at the titanium center<sup>33</sup>, have also been considered.

From this study, the following interesting results have been obtained:

1. The binding of the donor to the  $\text{MgCl}_2$  surface was seen to be a favorable reaction for all the donor cases considered. The displacement of the donor by  $\text{AlEt}_3$ , leading to the formation of a  $\text{AlEt}_3$ -donor species, is not a favorable reaction for four of the five donors considered (the two diethers, the phthalate and the silyl ester), and is seen to be competitive with the first Ti-Cl cleavage step only for the *eb* donor case. This agrees with experimental findings showing donor displacement from the  $\text{MgCl}_2$  surface for the *eb* donor case.
2. The rate limiting step of the activation process is the trans-alkylation step. The calculations indicate that this step is facile for the bare  $\text{TiCl}_4$  case, and for the cases where the *eb* donor, and the diethers are coordinated beside the titanium complex. However, for the phthalate and the silyl ester cases, the barrier for this step is seen to be significantly higher. This suggests that systems employing them as internal donors will experience an induction period prior to the commencement of the catalysis process. Indeed, an experimental report exists indicating a significant induction period<sup>71</sup> in a Ziegler-Natta (Z-N) system where a phthalate was employed as the internal donor. Silyl esters have not yet been employed as donors in Z-N systems, but the current studies indicate that they, too, would lead to induction periods before catalysis could begin.
3. As mentioned in point (1) above, *eb* can be displaced from the  $\text{MgCl}_2$  surface by  $\text{AlEt}_3$ . However, the  $\text{AlEt}_3$ -*eb* species formed from this reaction can also potentially act as a donor, and the calculations indicate that its impact on the activation mechanism would be similar to that of the *eb* donor.
4. Species such as  $\text{TiCl}_3\text{-OC}_4\text{H}_8\text{Cl}$  would lead to higher barriers for the activation mechanism. Hence, the decomposition of the donor at the titanium center and the formation of species with Ti-O bonds would lead to greater induction periods in Z-N systems.

The current investigations have therefore provided greater insight into the important activation step in Z-N catalysis, especially pertaining to the influence of the donors on

the same, and should guide experimentalists in designing Z-N system where the induction period before catalysis can be reduced, thereby favorably impacting the activity.

## 5.5 References:

- (1) Cavallo, L.; Del Piero, S.; Ducere, J.-M.; Fedele, R.; Melchior, A.; Morini, G.; Piemontesi, F.; Tolazzi, M. *J. Phys. Chem. C* **2007**, *111*, 4412-4419.
- (2) Yaluma, A. K.; Tait, P. J. T.; Chadwick, J. C. *J. Polym. Sci., Part A: Polym. Chem.* **2006**, *44*, 1635-1647.
- (3) Chadwick, J. C.; Morini, G.; Balbontin, G.; Camurati, I.; Heere, J. J. R.; Mingozzi, I.; Testoni, F. *Macromol. Chem. Phys.* **2001**, *202*, 1995-2002.
- (4) Andoni, A.; Chadwick, J. C.; Niemantsverdriet, H. J. W.; Thuene, P. *C. J. Catal.* **2008**, *257*, 81-86.
- (5) Wondimagegn, T.; Ziegler, T. *J. Phys. Chem. C* **2012**, *116*, 1027-1033.
- (6) Busico, V.; Cipullo, R.; Polzone, C.; Talarico, G.; Chadwick, J. C. *Macromolecules* **2003**, *36*, 2616-2622.
- (7) Shen, X.-r.; Fu, Z.-s.; Hu, J.; Wang, Q.; Fan, Z.-q. *J. Phys. Chem. C* **2013**, *117*, 15174-15182.
- (8) Sacchi, M. C.; Forlini, F.; Tritto, I.; Locatelli, P.; Morini, G.; Noristi, L.; Albizzati, E. *Macromolecules* **1996**, *29*, 3341-3345.
- (9) Sacchi, M. C.; Shan, C.; Locatelli, P.; Tritto, I. *Macromolecules* **1990**, *23*, 383-386.
- (10) Lu, L.; Niu, H.; Dong, J.-Y. *J. Appl. Polym. Sci.* **2012**, *124*, 1265-1270.
- (11) Sacchi, M. C.; Tritto, I.; Shan, C.; Mendichi, R.; Noristi, L. *Macromolecules* **1991**, *24*, 6823-6826.
- (12) Busico, V.; Corradini, P.; De Martino, L.; Proto, A.; Savino, V.; Albizzati, E. *Die Makromolekulare Chemie* **1985**, *186*, 1279-1288.
- (13) Busico, V.; Cipullo, R.; Monaco, G.; Talarico, G.; Vacatello, M.; Chadwick, J. C.; Segre, A. L.; Sudmeijer, O. *Macromolecules* **1999**, *32*, 4173-4182.
- (14) Barino, L.; Scordamaglia, R. *Macromol. Theory Simul.* **1998**, *7*, 407-419.
- (15) Brambilla, L.; Zerbi, G.; Piemontesi, F.; Nascetti, S.; Morini, G. *J. Phys. Chem. C* **2010**, *114*, 11475-11484.

- (16) Thushara, K. S.; Gnanakumar, E. S.; Mathew, R.; Jha, R. K.; Ajithkumar, T. G.; Rajamohanam, P. R.; Sarma, K.; Padmanabhan, S.; Bhaduri, S.; Gopinath, C. S. *J. Phys. Chem. C* **2011**, *115*, 1952-1960.
- (17) Vestberg, T.; Denifl, P.; Parkinson, M.; WilÉN, C.-E. *J. Polym. Sci., Part A: Polym. Chem.* **2010**, *48*, 351-358.
- (18) Singh, G.; Kaur, S.; Makwana, U.; Patankar, R. B.; Gupta, V. K. *Macromol. Chem. Phys.* **2009**, *210*, 69-76.
- (19) Bukatov, G. D.; Zakharov, V. A. *Macromol. Chem. Phys.* **2001**, *202*, 2003-2009.
- (20) Morini, G.; Albizzati, E.; Balbontin, G.; Mingozi, I.; Sacchi, M. C.; Forlini, F.; Tritto, I. *Macromolecules* **1996**, *29*, 5770-5776.
- (21) Taniike, T.; Terano, M. *J. Catal.* **2012**, *293*, 39-50.
- (22) Boero, M.; Parrinello, M.; Weiss, H.; Hueffer, S. *J. Phys. Chem. A* **2001**, *105*, 5096-5105.
- (23) Weiss, H.; Boero, M.; Parrinello, M. *Macromolecular Symposia* **2001**, *173*, 137-148.
- (24) Soga, K.; Shiono, T.; Doi, Y. *Polym. Bull.* **1983**, *10*, 168-174.
- (25) Soga, K.; Shiono, T.; Doi, Y. *Die Makromolekulare Chemie* **1988**, *189*, 1531-1541.
- (26) Taniike, T.; Terano, M. *Macromol. Rapid Commun.* **2007**, *28*, 1918-1922.
- (27) Stukalov, D. V.; Zakharov, V. A.; Zilberberg, I. L. *J. Phys. Chem. C* **2010**, *114*, 429-435.
- (28) Stukalov, D. V.; Zakharov, V. A.; Potapov, A. G.; Bukatov, G. D. *J. Catal.* **2009**, *266*, 39-49.
- (29) Correa, A.; Credendino, R.; Pater, J. T. M.; Morini, G.; Cavallo, L. *Macromolecules* **2012**, *45*, 3695-3701.
- (30) Cui, N.; Ke, Y.; Li, H.; Zhang, Z.; Guo, C.; Lv, Z.; Hu, Y. *J. Appl. Polym. Sci.* **2006**, *99*, 1399-1404.
- (31) Potapov, A. G.; Bukatov, G. D.; Zakharov, V. A. *J. Mol. Catal. A: Chem.* **2010**, *316*, 95-99.
- (32) Vanka, K.; Singh, G.; Iyer, D.; Gupta, V. K. *J. Phys. Chem. C* **2010**, *114*, 15771-15781.



- (33) Grau, E.; Lesage, A.; Norsic, S. b.; Coperet, C.; Monteil, V.; Sautet, P. *ACS Catal.* **2012**, *3*, 52-56.
- (34) Correa, A.; Piemontesi, F.; Morini, G.; Cavallo, L. *Macromolecules (Washington, DC, U. S.)* **2007**, *40*, 9181-9189.
- (35) Kumawat, J.; Gupta, V. K.; Vanka, K. *Organometallics* **2014**, *33*, 4357-4367.
- (36) Stukalov, D. V.; Zakharov, V. A. *J. Phys. Chem. C* **2009**, *113*, 21376-21382.
- (37) Xie, K.; Zhu, B.; Xu, R.; Xu, J.; Liu, P. *RSC Advances* **2016**, *6*, 13137-13144.
- (38) Trubitsyn, D. A.; Zakharov, V. A.; Zakharov, I. I. *J. Mol. Catal. A Chem.* **2007**, *270*, 164-170.
- (39) Zheng, S.; Pfaendtner, J. *Molecular Simulation* **2015**, *41*, 55-72.
- (40) Boero, M.; Parrinello, M.; Terakura, K. *J. Am. Chem. Soc.* **1998**, *120*, 2746-2752.
- (41) Barducci, A.; Bonomi, M.; Parrinello, M. *Wiley Interdisciplinary Reviews: Computational Molecular Science* **2011**, *1*, 826-843.
- (42) textbook *Parallel Computing: Accelerating Computational Science and Engineering (CSE)* IOS Press **2014** ISBN 978-1-61499-380-3
- (43) Bahri-Laleh, N.; Correa, A.; Mehdipour-Ataei, S.; Arabi, H.; Haghighi, M. N.; Zohuri, G.; Cavallo, L. *Macromolecules* **2011**, *44*, 778-783.
- (44) Boero, M.; Parrinello, M.; Terakura, K. *J. Am. Chem. Soc.* **1998**, *120*, 2746-2752.
- (45) Monaco, G.; Toto, M.; Guerra, G.; Corradini, P.; Cavallo, L. *Macromolecules* **2000**, *33*, 8953-8962.
- (46) Credendino, R.; Liguori, D.; Fan, Z.; Morini, G.; Cavallo, L. *ACS Catal.* **2015**, *5*, 5431-5435.
- (47) Potapov, A. G.; Bukatov, G. D.; Zakharov, V. A. *J. Mol. Catal. A: Chem.* **2009**, *301*, 18-23.
- (48) Ahlrichs, R.; Bar, M.; Haser, M.; Horn, H.; Kolmel, C. *Chem. Phys. Lett.* **1989**, *162*, 165-169.
- (49) Perdew, J. P.; Burke, K.; Ernzerhof, M. *Phys. Rev. Lett.* **1996**, *77*, 3865-3868.
- (50) Perdew, J. P.; Wang, Y. *Phys. Rev. B* **1992**, *45*, 13244-13249.

- (51) Becke, A. D. *J. Chem. Phys.* **1993**, *98*, 5648-5652.
- (52) Schaefer, A.; Horn, H.; Ahlrichs, R. *J. Chem. Phys.* **1992**, *97*, 2571-7.
- (53) Eichkorn, K.; Treutler, O.; Oehm, H.; Haeser, M.; Ahlrichs, R. *Chem. Phys. Lett.* **1995**, *240*, 283-90.
- (54) Sierka, M.; Hogeckamp, A.; Ahlrichs, R. *J. Chem. Phys.* **2003**, *118*, 9136-9148.
- (55) Houk, K. N.; Cheong, P. H.-Y. *Nature* **2008**, *455*, 309-313.
- (56) Mammen, M.; Shakhnovich, E. I.; Whitesides, G. M. *J. Org. Chem.* **1998**, *63*, 3168-3175.
- (57) Kelly, E.; Seth, M.; Ziegler, T. *J. Phys. Chem. A* **2004**, *108*, 2167-2180.
- (58) Yin, H.; Wang, D.; Valiev, M. *J. Phys. Chem. A* **2011**, *115*, 12047-12052.
- (59) Williams, V. M.; Kong, J. R.; Ko, B. J.; Mantri, Y.; Brodbelt, J. S.; Baik, M.-H.; Krische, M. J. *J. Am. Chem. Soc.* **2009**, *131*, 16054-16062.
- (60) Janse van Rensburg, W.; Grove, C.; Steynberg, J. P.; Stark, K. B.; Huyser, J. J.; Steynberg, P. J. *Organometallics* **2004**, *23*, 1207-1222.
- (61) Qi, Y.; Dong, Q.; Zhong, L.; Liu, Z.; Qiu, P.; Cheng, R.; He, X.; Vanderbilt, J.; Liu, B. *Organometallics* **2010**, *29*, 1588-1602.
- (62) Bagno, A.; Kantlehner, W.; Kress, R.; Saielli, G.; Stoyanov, E. *J. Org. Chem.* **2006**, *71*, 9331-9340.
- (63) Li, J.-N.; Pu, M.; Ma, C.-C.; Tian, Y.; He, J.; Evans, D. G. *J. Mol. Catal. A: Chem.* **2012**, *359*, 14-20.
- (64) Nikiforidis, I.; Görling, A.; Hieringer, W. *J. Mol. Catal. A: Chem.* **2011**, *341*, 63-70.
- (65) Cao, X.; Cheng, R.; Liu, Z.; Wang, L.; Dong, Q.; He, X.; Liu, B. *J. Mol. Catal. A: Chem.* **2010**, *321*, 50-60.
- (66) Seth, M.; Ziegler, T. *Macromolecules* **2003**, *36*, 6613-6623.
- (67) Seth, M.; Margl, P. M.; Ziegler, T. *Macromolecules* **2002**, *35*, 7815-7829.
- (68) Monaco, G.; Toto, M.; Guerra, G.; Corradini, P.; Cavallo, L. *Macromolecules* **2000**, *33*, 8953-8962.
- (69) Dahy, A. A.; Koga, N.; Nakazawa, H. *Organometallics* **2013**, *32*, 2725-2735.

- (70) Kinuta, H.; Takahashi, H.; Tobisu, M.; Mori, S.; Chatani, N. *Bull. Chem. Soc. Jpn.* **2014**, *87*, 655-669.
- (71) Ohnishi, R.; Konakazawa, T. *Macromol. Chem. Phys.* **2004**, *205*, 1938-1947.
- (72) Kumawat, J.; Kumar Gupta, V.; Vanka, K. *Eur. J. Inorg. Chem.* **2014**, *2014*, 5063-5076.
- (73) Zohuri, G. H.; Kasaeian, A. B.; Torabi Angagi, M.; Jamjah, R.; Mousavian, M. A.; Emami, M.; Ahmadjo, S. *Polym. Int.* **2005**, *54*, 882-885.
- (74) Wen, X.; Ji, M.; Yi, Q.; Niu, H.; Dong, J.-Y. *J. Appl. Polym. Sci.* **2010**, *118*, 1853-1858.
- (75) Zimmerman, P. M.; Paul, A.; Zhang, Z.; Musgrave, C. B. *Inorg. Chem.* **2009**, *48*, 1069-1081.
- (76) Ghatak, K.; Vanka, K. *Comput. Theor. Chem.* **2012**, *992*, 18-29.
- (77) Nguyen, M. T.; Nguyen, V. S.; Matus, M. H.; Gopakumar, G.; Dixon, D. A. *J. Phys. Chem. A* **2007**, *111*, 679-690.
- (78) Foster, J. P.; Weinhold, F. *J. Am. Chem. Soc.* **1980**, *102*, 7211-7218.
- (79) Reed, A. E.; Weinhold, F. *J. Chem. Phys.* **1983**, *78*, 4066-4073.
- (80) Reed, A. E.; Weinstock, R. B.; Weinhold, F. *J. Chem. Phys.* **1985**, *83*, 735-746.

## Chapter 6

### Abstract

Density functional theory (DFT) has been used for the study of ethylene polymerization in the Ziegler-Natta (ZN) olefin polymerization system for five different titanium based catalysts (**Cat-A-E**),  $\text{Ti(III)Et(OR)(OR')}$  (where  $\text{R} = -\text{CH}_3, -\text{Et}, -\text{t-butyl}$ ,  $\text{R}' = -\text{CH}_3, -\text{Et}, -\text{t-butyl}$ ). What is of significance is that the catalysts studied were all considered to be tethered to the (104)  $\text{MgCl}_2$  surface, which has traditionally been considered a “dormant” surface in ZN catalysis systems, in contrast to the “more active” (110)  $\text{MgCl}_2$  surface. Our calculations indicate that the binding of all the five catalysts to the (104) surface was favourable, even after taking entropic effects into account. For purposes of comparison, ethylene polymerization was investigated, for the **Cat-C** ( $\text{TiEt(OEt)}_2$ ) and the **Cat-F** ( $\text{TiEt(Cl)(OC}_4\text{H}_8\text{Cl)}$ ) cases, for both the (i) (110) and the (ii) (104)  $\text{MgCl}_2$  surfaces. It was seen that for both (i) and (ii), the energy gap between insertion and the termination barriers was nearly the same for both the **Cat-C** and **Cat-F** cases, which shows that ethylene polymerization on the (104)  $\text{MgCl}_2$  surface is likely to be a prominent occurrence in Z-N catalysis, when ethoxy groups are bound to the titanium center. Given that a major portion of the  $\text{MgCl}_2$  support is made up of (104) lateral cuts, the current findings are of considerable relevance.

## 6.1 Introduction

Heterogeneous Ziegler-Natta (ZN) olefin polymerization catalysis is one of the most important processes in the polymer industry today. While it was discovered in the 1950s, a major breakthrough was obtained in the early 1970s when the  $\text{MgCl}_2$  support was substituted in place of  $\alpha\text{TiCl}_3$  in the ZN systems. This is now the standard support employed and has become one of the key components of ZN systems today. The other main components are as follows:  $\text{TiCl}_4$ , the catalyst precursor and  $\text{AlR}_3$  (R = alkyl group), the catalyst activator. In the 1980s, organic Lewis bases called “donors” began to be added, and have now become the important fourth component in ZN systems. It is believed that the role of the donor is to sit beside the titanium catalyst on the  $\text{MgCl}_2$  surface and thereby significantly improve the isotacticity and molecular weight distribution of the polyolefin products. The most common donors in the ZN system are as follows: (i) donors added during the catalysts preparation, called the internal donors, e.g. ethyl benzoate (*eb*)<sup>1,2</sup>, phthalates<sup>2,3</sup>, and diethers<sup>2-8</sup>, succinate<sup>2,4</sup> and (ii) the donors added during the polymerization, called the external donors, e.g. *p*-ethoxyethylbenzoate (*peeb*)<sup>2</sup> and silyl ethers.<sup>2</sup>

Several experimental<sup>2,7-35</sup> and computational<sup>1,3,4,36-55</sup> studies have been done in order to understand and improve ZN catalysis. However, owing to its multi-component nature, the actual role of each component in ZN systems is not yet clear. Experimental studies<sup>56</sup> indicate that the majority of the  $\text{MgCl}_2$  surface is composed of the five coordinated (104) lateral cuts, with the four coordinated (110)  $\text{MgCl}_2$  lateral cuts found to be make up a minor portion of the available  $\text{MgCl}_2$  surface. However, the binding of the  $\text{TiCl}_4$  complex is energetically more favourable on the more acidic (110)  $\text{MgCl}_2$  surface in comparison to the (104), which has led researchers to believe that it is this minor portion of the surface that is the location of all the ZN catalysis. There are several reports<sup>4,43,50</sup> in the literature stating that the olefin polymerization reaction takes place on the (110)  $\text{MgCl}_2$  surface, and this is the accepted picture of ZN catalysis today. However, it is worth noting that the acidity of the titanium center would be enhanced if oxygen containing groups were to be coordinated as ligands at the titanium center. Such an enhancement could lead to the favorable coordination of the titanium to the (104) surface, and thus, to the (104) surface also contributing to the polymerization process. That this idea is worth exploring becomes clear when one

observes that ethoxy ligand containing titanium centers can be produced by the decomposition of the oxygen containing donors on the titanium center, as has been experimentally observed by Sautet and co-workers<sup>9</sup>. Furthermore, since the majority of the  $\text{MgCl}_2$  lateral cuts available for coordination are (104), one can see that the role of donors could well be that of creating new active titanium catalysts containing ethoxy groups, and thus allowing the complete exploitation of the available (104) surface.

To date, there has been no study of ethylene polymerization on the (104)  $\text{MgCl}_2$  surface, and this is the focus of the current work. We have investigated insertion and termination steps for the ethylene monomer on the (104)  $\text{MgCl}_2$  surface for six different catalyst systems (**Cat-A-F**), each of which contain two ethoxy groups. Such ethoxy group containing titanium systems have been explored before in the literature<sup>57</sup>, though no system coordinating to the (104) lateral cut has ever been considered. The structures of the catalyst systems are shown in Figure 1 below. These  $\text{Ti(III)Et(OR)(OR')}$  catalysts differ in the nature of the R and R' groups. For the sake of comparison, for two catalyst systems: **Cat-C** and **Cat-F**, the ethylene polymerization study has been investigated on the (104) as well as on the (110)  $\text{MgCl}_2$  surface.

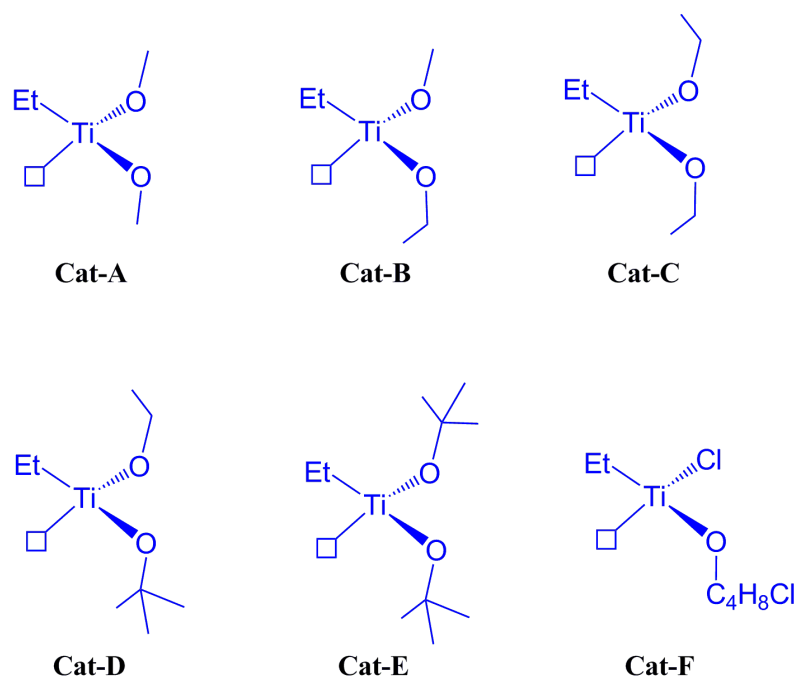


Figure 1. The different catalyst structures (**Cat-A-F**) that have been used in this study.

As will be shown in the Results and Discussion Section, these full quantum chemical calculations provide important new insights in ZN catalysis, and the role of the donors in the same, showing that the presence of ethoxy groups at the titanium center leads to active titanium catalysts that are able to exploit the (104) MgCl<sub>2</sub> surface, in addition to the much more sparse (110) surface.

## 6.2 Computational Details

The Turbomole 7.0 suite of programs<sup>58</sup> has been employed for the geometry optimizations for all the intermediate and transition state structures with the help of density functional theory (DFT). The calculations have been carried out by using the Becke and Perdew (BP86) functional,<sup>59-61</sup> followed by single-point calculations with B3LYP<sup>62</sup> on all the BP86 optimized structures. The electronic configurations of the atoms have been represented by a triple- $\xi$  basis set augmented by a polarization function (TURBOMOLE basis set TZVP).<sup>63</sup> The resolution of identity (RI)<sup>64</sup> along with the multipole accelerated resolution of identity (marij)<sup>65</sup> approximations have been employed for an accurate and efficient treatment of the electronic Coulomb term in the DFT calculations. The error bar value in the DFT calculations is expected to be in the range of  $\pm 1.0$  kcal/mol<sup>66</sup>. The dispersion correction has also been included to capture the minor interactions in the system which has been developed by Grimme *et al.*<sup>67</sup>

The Gibbs free energy ( $\Delta G$ ) values contain the zero-point energy, internal energy, and entropic contributions. For every transition state obtained, care has been taken to ensure that the obtained structure contained only one imaginary frequency related to the correct normal mode. For the determination of the transition state, the quasi-Newton-Josephson method has been employed. It is based on the restricted second-order method, which employs Hessian shift parameters. In the current study, the unrestricted formalism has been considered.

## 6.3 Results and Discussions

### 6.3.1 Validation of MgCl<sub>2</sub> Model

The MgCl<sub>2</sub> model system that has been used in this study is a modification of the surface that had been originally proposed by Cavallo and coworkers<sup>4</sup>. Our MgCl<sub>2</sub> surface model has been validated with the Cavallo six layered model in a previous study<sup>43</sup>. The optimized structure of the our MgCl<sub>2</sub> model system with two lateral cuts, (110) and (104), is shown below in Figure 2.

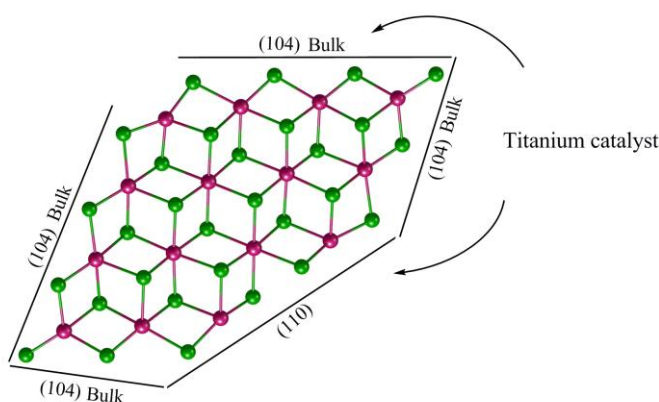


Figure 2. The MgCl<sub>2</sub> model system employed in the current work, with two different lateral cuts, (110) and (104).

Furthermore, this MgCl<sub>2</sub> model has also been validated with the “Unified Model” that has been recently proposed by Cavallo and coworkers<sup>40</sup>. In order to validate our MgCl<sub>2</sub> model, as shown in Table 1, a comparative study of the ethylene polymerization reaction on the (104) MgCl<sub>2</sub> surface has been investigated for both the MgCl<sub>2</sub> model systems (Unified and our model). The optimized structure of both the MgCl<sub>2</sub> models are shown in Figure 3, where the TiEt(OEt)<sub>2</sub> catalyst (**Cat-C**) binding on the (104) MgCl<sub>2</sub> lateral cuts has been considered. In the first step, the formation of the ethylene  $\pi$ -complex on the titanium center has been studied. The energy values for the  $\pi$ -complexes are 4.3 kcal/mol and 4.0 kcal/mol for our model and the Unified systems respectively. As shown in Table 1, the barriers for the ethylene monomer insertion into the Ti–C bond are 20.4 kcal/mol and 19.5 kcal/mol respectively. These



barriers lead to the final product  $\text{Ti-C}_4\text{H}_9$ , which is exergonic in nature by 29.4 kcal/mol and 28.5 kcal/mol respectively. In short, there is considerable similarity in the free energy surfaces obtained for the two cases. In addition to this, we have also studied the termination step (chain transfer to monomer) in order to compare with the insertion step in the two models. The barriers for the termination step are 25.3 kcal/mol and 25.5 kcal/mol for our model and the Unified model respectively (see Table 1). Hence, our  $\text{MgCl}_2$  model system is seen to provide results that compare very well with previously reported  $\text{MgCl}_2$  models.

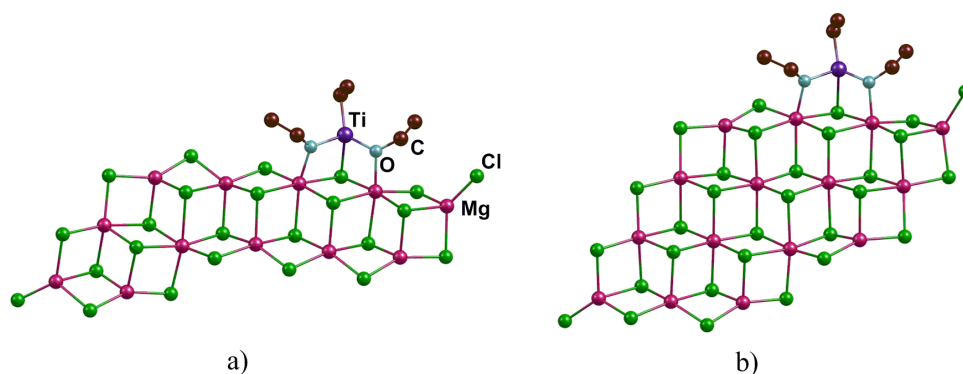


Figure 3. The optimized structures of the  $\text{TiEt(OEt)}_2$  catalyst (**Cat-C**) bound to the (104)  $\text{MgCl}_2$  model systems, a) the Unified model system recently proposed by Cavallo and coworkers<sup>40</sup> and b) our model system: all the hydrogens are not shown for the purpose of clarity.

Table 1. The free energy ( $\Delta G$ ) values for the comparative study for the case of the  $\text{TiEt(OEt)}_2$  catalyst (**Cat-C**) binding to the Cavallo Unified Model and our model.

$\Delta G$ values (in kcal/mol)						
Cavallo Unified Model						
$\pi$ -Complex	Insertion (in blue)			Termination (in red)		
	barrier	Total barrier	product	barrier	Total barrier	Product
4.0	15.5	19.5	-28.5	21.5	25.5	-14.2
Our Model						
4.3	16.1	20.4	-29.4	21.0	25.3	-25.2

### 6.3.2 The binding of different $\text{Ti}(\text{Cl})_{4-n}(\text{OEt})_n$ ( $n= 1-4$ ) catalysts to the (110) and (104) $\text{MgCl}_2$ surfaces

As shown in Table 2, the binding of different  $\text{Ti}(\text{Cl})_{4-n}(\text{OEt})_n$  ( $n= 1-4$ ) catalyst conformers to the (110) and (104)  $\text{MgCl}_2$  surfaces have been studied. For the  $n=1$  case, the binding of  $\text{TiCl}_3(\text{OEt})$  catalyst to the (110)  $\text{MgCl}_2$  surface is more favorable by 6.1 kcal/mol in comparison to the (104)  $\text{MgCl}_2$  surface. When we increase the number of  $n$ , (for  $n=2-4$ ), the catalyst binding shifts from the (110) surface to the (104) surface (see Table 2).

Table 2. The free energy ( $\Delta G$ ) for the binding of different  $\text{Ti}(\text{Cl})_{4-n}(\text{OEt})_n$  ( $n= 1-4$ ) catalysts to the (110) and (104)  $\text{MgCl}_2$  surfaces.

$\text{Ti}(\text{Cl})_{4-n}(\text{OEt})_n$ ( $n= 1-4$ )	$\Delta G$ in kcal/mol		
	(110) $\text{MgCl}_2$ Surface	(104) $\text{MgCl}_2$ Surface	Diff. between (110) – (104) surface
$\text{Ti}(\text{Cl})_3(\text{OEt})$ ( $n= 1$ )	-14.3	-8.2	6.1
	-14.2	-7.4	6.8
$\text{Ti}(\text{Cl})_2(\text{OEt})_2$ ( $n= 2$ )	-31.0	-29.9	1.1
	-33.1	-34.4	-1.3
$\text{Ti}(\text{Cl})_1(\text{OEt})_3$ ( $n= 3$ )	-33.7	-34.4	-0.7
$\text{Ti}(\text{OEt})_4$ ( $n= 4$ )	-44.6	-46.3	-1.7

For the ethylene polymerization study, the  $\text{TiEt}(\text{OEt})_2$  catalyst has been considered for the (110) and the (104)  $\text{MgCl}_2$  surfaces. As shown in Figure 4, in the first step, the ethylene monomer forms the  $\pi$ -complex with the titanium center, a reaction that is endergonic by 6.4 kcal/mol and 4.3 kcal/mol for the (110) and (104)  $\text{MgCl}_2$  surface cases respectively. Then, this ethylene monomer inserts in the Ti-C bond through chain migratory insertion and leads to the four carbon containing titanium product (see Figure 4). The overall barrier for this insertion step is 22.2 kcal/mol and 20.4

kcal/mol for the (110) and (104)  $\text{MgCl}_2$  surface cases (see Table 3). Along with the insertion step, we have also studied the chain transfer to the monomer, i.e., the termination step (see Figure 4). The barriers for this step are 25.2 kcal/mol and 25.3 kcal/mol respectively for the (110) and (104)  $\text{MgCl}_2$  surface cases. As shown in Figure 4 and Table 3, the gap between the insertion and the termination barriers, ( $\Delta X$ ), is 3.0 kcal/mol and 3.9 kcal/mol, which indicates that the length of the polymer chain would be likely to be higher for ethylene polymerization on the (104)  $\text{MgCl}_2$  surface.

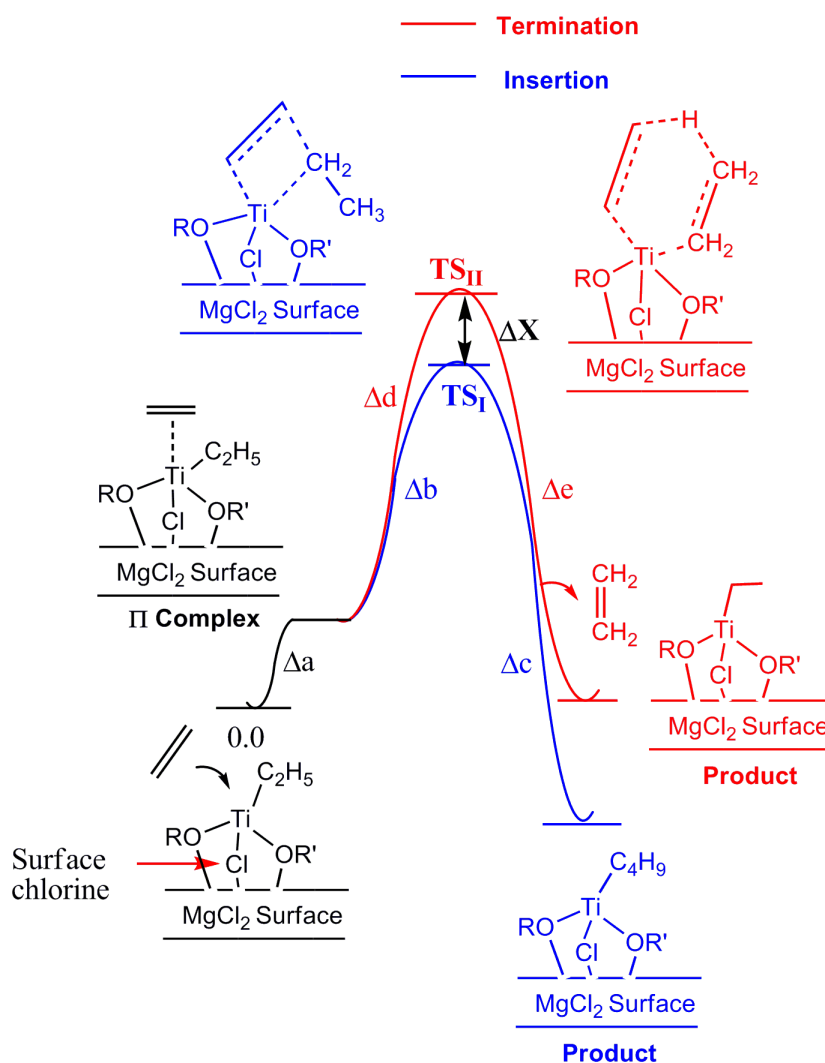


Figure 4. The energy profile for the comparative study of the insertion and the termination (chain transfer to monomer) steps on the (104)  $\text{MgCl}_2$  surface.

Table 3. The free energy ( $\Delta G$ ) values for the comparative study of the ethylene polymerization on the (110) and (104)  $\text{MgCl}_2$  surfaces for the  $\text{TiEt}(\text{OEt})_2$  catalyst.

$\Delta G$ values (in kcal/mol)							
(110) $\text{MgCl}_2$ Surface							Diff. between Insertion – Termination barriers ( $\Delta X$ )
$\pi$ -Complex	Insertion (in blue)			Termination (in red)			
$\Delta a$	$\Delta b$	barrier	$\Delta e$	$\Delta c$	barrier	$\Delta d$	
6.4	15.8	22.2	-30.5	18.8	25.2	-25.3	<b>3.0</b>
(104) $\text{MgCl}_2$ Surface							
4.3	16.1	20.4	-29.4	21.0	25.3	-25.2	<b>3.9</b>

### 6.3.3 The Comparative Study of All the Titanium Catalysts (Cat-A-E):

As mentioned in the Introduction (see Figure 1), a modification of the  $\text{TiEt}(\text{OEt})(\text{OEt})$  catalyst has been studied by changing the different alkyl groups, R and R', on the titanium center. This study has only been considered on the (104) lateral cuts of the  $\text{MgCl}_2$  surface. As shown in Table 4, the  $\pi$ -complexation is endergonic for all the catalysts. When we increase the steric bulk on the titanium (R and R' from  $\text{CH}_3$  to *tert*-butyl),  $\pi$ -complexation on the titanium center becomes less favorable. The reason for this is the space at the titanium center, which decreases with increase in the sterics; leading to less space for the ethylene monomer to approach the titanium to form the  $\pi$ -complex. In the next step, the monomer inserts in the Ti–C bond through chain migratory insertion and leads to the four carbon containing polymer chain on the titanium. The barrier for this step is in the range of 18.4 – 38.1 kcal/mol (see Table 4). The barriers obtained were in the range 18.4 kcal/mol (for **Cat-B**) to 38.1 kcal/mol (for **Cat-E**). For the insertion step, the energy barriers were also seen to increase with increase in the bulkiness at the titanium center and the same trend was also seen for the chain transfer to monomer step, i.e., termination. In case of termination, the barriers increased even more in comparison to the insertion step because a more sterically constrained transition state was formed in comparison to the insertion transition state, (see Figure 5). The difference in the barriers between insertion and

termination ( $\Delta X$ ) for the different titanium catalysts (**Cat-A-E**) are shown in Figure 6. The results suggest that increase in the bulkiness in the R and R' groups of the TiEt(OR)(OR') catalyst first leads to  $\Delta X$  increasing from **Cat-A** to **Cat-B**, where the R and R' groups change from  $-\text{CH}_3$  and  $-\text{CH}_3$  to  $-\text{CH}_3$  and  $-\text{Et}$ , then gradually decreasing with increase in the bulkiness of the R and R' groups at the titanium center (see Figure 6).

Table 4. The free energy ( $\Delta G$ ) values for the comparative study of all the TiEt(OR)(OR') catalyst, (**Cat-A-E**), of ethylene polymerization on the (104)  $\text{MgCl}_2$  surface.

S. N.	Ti(OR)(OR')Et  R an R' =  CH <sub>3</sub> , Et, <i>t</i> -butyl	$\Delta G$ values (in kcal/mol)							
		(104) $\text{MgCl}_2$ Surface							Diff. between  Insertion – Termination barriers  ( $\Delta X$ )
		$\pi$ - complex  $\Delta a$	Insertion (in blue)			Termination (in red)			
			$\Delta b$	barrier	$\Delta c$	$\Delta d$	barrier	$\Delta e$	
<b>Cat-A</b>	R and R' = $-\text{CH}_3$	4.2	15.3	19.5	-28.4	18.2	22.4	-22.4	<b>2.9</b>
<b>Cat-B</b>	R = $-\text{CH}_3$ , R' = $-\text{Et}$	4.2	14.2	18.4	-27.2	19.3	23.5	-23.5	<b>5.1</b>
<b>Cat-C</b>	R and R' = $-\text{Et}$	6.4	15.8	22.2	-30.5	18.8	25.2	-25.2	<b>3.9</b>
<b>Cat-D</b>	R = $-\text{Et}$ , R' = <i>t</i> -butyl	9.0	17.9	26.9	-37.7	19.8	28.8	-28.8	<b>1.9</b>
<b>Cat-E</b>	R and R' = <i>t</i> -butyl	14.9	23.2	38.1	-47.7	24.0	38.9	-38.9	<b>0.8</b>

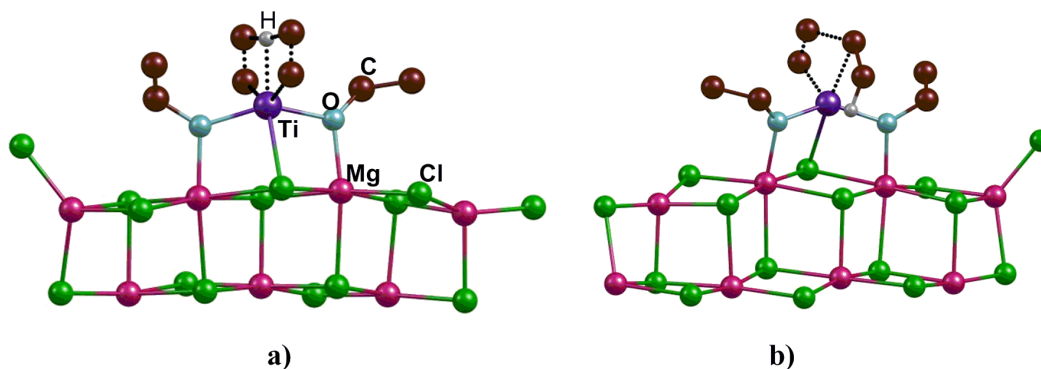


Figure 5. The optimized structure of the transition states: a) chain migratory insertion, b) chain transfer to monomer (termination) for the  $\text{TiEt(OEt)}_2$  catalyst; only a lone hydrogen atom has been shown for the purpose of the clarity.

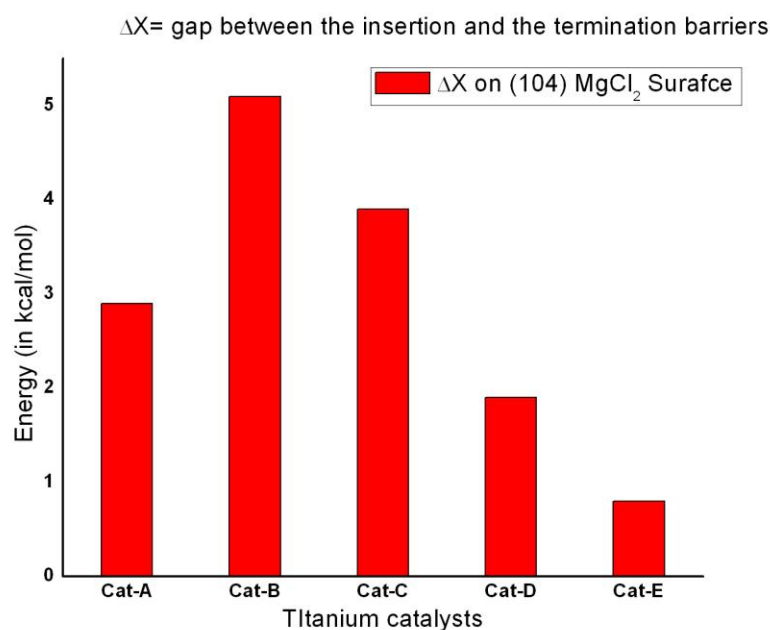


Figure 6. A bar graph for the comparative study of the titanium based catalysts (**Cat-A-E**), with respect to the gap between the insertion and termination barriers. All calculations consider the catalyst tethered to the (104)  $\text{MgCl}_2$  surface.

Since a substantial gap in insertion and termination barriers is a necessary requirement for an effective polymerization process, the results discussed here suggest that, for

ethoxy containing titanium systems, a balance between sterics and electronics at the titanium center is necessary in order to produce high molecular weight polymers in ZN catalyst systems. It is also to be noted that the similarity in the gap for the (110) and (104)  $\text{MgCl}_2$  surface indicate that the (104)  $\text{MgCl}_2$  surface would be just as important as (110) for ethylene polymerization, for the ethoxy containing titanium systems that have been considered here.

#### 6.3.4 $\text{TiCl}_3(\text{OC}_4\text{H}_8\text{Cl})$ catalyst

The  $\text{TiCl}_3(\text{OC}_4\text{H}_8\text{Cl})$  (**Cat-F**) catalyst model has been considered next in our exploration of the interaction and subsequent catalysis on the (104)  $\text{MgCl}_2$  surface. The reason for the choice of this particular system is the fact that this species has been experimentally obtained by Philippe Sautet's group, from the decomposition of the tetrahydrofuran (THF) donor at the titanium center<sup>9</sup>. Hence,  $\text{TiCl}_3(\text{OC}_4\text{H}_8\text{Cl})$  represents an example of a typical system that might formed and exist in ZN systems having oxygen containing donors.

The binding of **Cat-F** to the (110) and (104)  $\text{MgCl}_2$  surfaces was determined, and was seen to be favorable by 13.7 kcal/mol and 14.3 kcal/mol respectively. The reason that the binding is more favorable for the (104) case is due to the fact that the chloride at the end of the ethoxy chain can bind to the (104) surface, thereby providing additional stability. Such a chloride-surface interaction was not seen for the (110) case, due to the greater sterics involved in the interaction. The insertion and termination pathways have been studied for **Cat-F**. A perusal of the values in Figure 7 and Table 5 show that the gap between insertion and chain transfer to monomer termination steps are 7.7 kcal/mol and 12.0 kcal/mol respectively for the (110) and (104)  $\text{MgCl}_2$  surfaces. The energy gap between both the  $\text{MgCl}_2$  surfaces is quite large-about 4.3 kcal/mol-which indicates that ethylene polymerization is actually more favourable on the (104)  $\text{MgCl}_2$  surface in comparison to the (110). This interesting result showcases the fact that donor decomposition at the titanium center could indeed be one of the principal means of creating effective new catalyst species that can not only begin to exploit all the available  $\text{MgCl}_2$  surface, but do so more effectively than when only limited to the (110) surface.

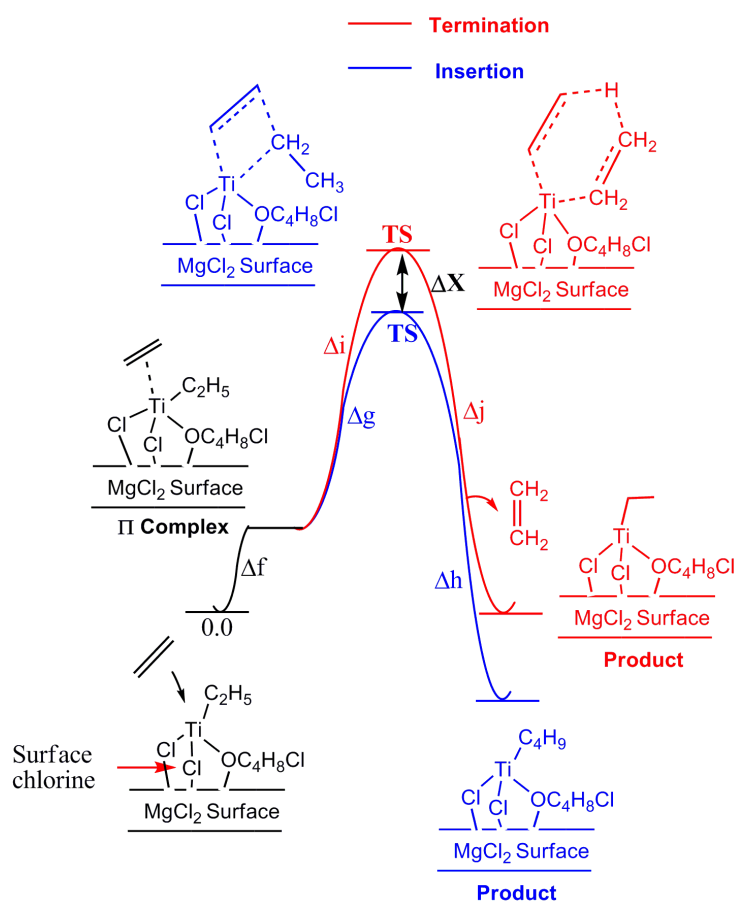


Figure 7. The energy profile for the comparative study of insertion and termination (chain transfer to monomer) steps for the **Cat-F**.

Table 5. The free energy ( $\Delta G$ ) values for the comparative study of the ethylene polymerization on the (110) and (104)  $MgCl_2$  surfaces for **Cat-F**.

$\Delta G$ values (in kcal/mol)							
(110) $MgCl_2$ Surface							Diff. between Insertion – Termination barriers ( $\Delta X$ )
$\pi$ -Complex	Insertion (in blue)			Termination (in red)			
$\Delta f$	$\Delta g$	barrier	$\Delta h$	$\Delta i$	barrier	$\Delta j$	
-2.7	9.1	9.1	-15.9	16.8	16.8	-14.2	<b>7.7</b>
(104) $MgCl_2$ Surface							
2.7	12.7	15.4	-24.9	24.7	27.4	-25.2	<b>12.0</b>



## 6.4 Conclusions

Density functional theory (DFT) has been employed to investigate the ethylene polymerization process on the (104)  $\text{MgCl}_2$  surface in Ziegler-Natta (ZN) systems. Six different ethoxy ligand containing titanium catalysts (**Cat-A-F**) have been considered, with the difference between them stemming from a modification of alkyl R and R' groups on the ethoxy ligands, i.e., by considering  $\text{TiEt}(\text{OR})(\text{OR}')$  systems. It was observed that increase in the bulkiness of the R and R' groups on the titanium center decreases the energy gap between the insertion and the termination barriers ( $\Delta X$ ). For termination, chain transfer to monomer has been considered. For the sake of comparison, for two titanium catalysts, **Cat-C** ( $\text{TiEt}(\text{OEt})(\text{OEt})$ ) and **Cat-F** ( $\text{TiEt}(\text{Cl})(\text{OC}_4\text{H}_8\text{Cl}')$ ), ethylene polymerization has been investigated on the (110) surface as well, which is the surface that is widely considered to be the one where olefin polymerization takes place in ZN systems. The favorability of binding of the titanium catalysts to (104) is quite comparable to the bonding to the (110) surface, when two ethoxy groups on the titanium are considered, indicating that the binding of such titanium catalysts at the (104) surface is as likely as its binding to (110). Furthermore, our results indicate that  $\Delta X$  is quite similar for both the (110) and the (104) cases. This suggests that, if ethoxy containing titanium catalysts are present in ZN systems, they will be able to exploit not only the (110) surface, but also the much more available (104) surface for successfully catalyzing the ethylene polymerization reaction. Indeed, recent studies<sup>1,9</sup> indicate that ethoxy containing titanium catalysts can be produced *in situ* during olefin polymerization by donor decomposition at the titanium center, which suggests that an unsuspected role of donors in ZN systems could be the creation of new active catalysts that are more versatile and able to exploit all the available support for enabling the polymerization reaction. This hypothesis is further proved by calculations in the current work that show that the experimentally observed species,  $\text{TiCl}_3(\text{OC}_4\text{H}_8\text{Cl})$ , formed by decomposition of the tetrahydrofuran (THF) donor at the titanium center, would not only bind more strongly to the (104)  $\text{MgCl}_2$  surface, but would also produce higher molecular weight polyethylene in comparison to the (110) surface. As such, the current computational work sheds new light on the nature of the interaction of titanium catalysts with the support in ZN systems, and also shows how the role of the internal and external donors in ZN catalysis can be significantly broader than had been suspected earlier.

## 6.5 References:

- (1) Kumawat, J.; Gupta, V. K.; Vanka, K. *Organometallics* **2014**, *33*, 4357-4367.
- (2) Chadwick, J. C.; Van der Burgt, F. P. T. J.; Rastogi, S.; Busico, V.; Cipullo, R.; Talarico, G.; Heere, J. J. R. *Macromolecules* **2004**, *37*, 9722-9727.
- (3) Credendino, R.; Liguori, D.; Morini, G.; Cavallo, L. *The Journal of Physical Chemistry C* **2014**, *118*, 8050-8058.
- (4) Correa, A.; Credendino, R.; Pater, J. T. M.; Morini, G.; Cavallo, L. *Macromolecules* **2012**, *45*, 3695-3701.
- (5) Cui, N.; Ke, Y.; Li, H.; Zhang, Z.; Guo, C.; Lv, Z.; Hu, Y. *Journal of Applied Polymer Science* **2006**, *99*, 1399-1404.
- (6) Chadwick, J. C. *Macromol. Symp.* **2001**, *173*, 21-35.
- (7) Morini, G.; Albizzati, E.; Balbontin, G.; Mingozi, I.; Sacchi, M. C.; Forlini, F.; Tritto, I. *Macromolecules* **1996**, *29*, 5770-5776.
- (8) Sacchi, M. C.; Forlini, F.; Tritto, I.; Locatelli, P.; Morini, G.; Noristi, L.; Albizzati, E. *Macromolecules* **1996**, *29*, 3341-3345.
- (9) Grau, E.; Lesage, A.; Norsic, S. b.; Coperet, C.; Monteil, V.; Sautet, P. *ACS Catalysis* **2012**, *3*, 52-56.
- (10) Potapov, A. G.; Bukatov, G. D.; Zakharov, V. A. *Journal of Molecular Catalysis A: Chemical* **2010**, *316*, 95-99.
- (11) Wen, X.; Ji, M.; Yi, Q.; Niu, H.; Dong, J.-Y. *Journal of Applied Polymer Science* **2010**, *118*, 1853-1858.
- (12) Andoni, A.; Chadwick, J. C.; Niemantsverdriet, H. J. W.; Thuene, P. C. *J. Catal.* **2008**, *257*, 81-86.
- (13) Zhong, C.; Gao, M.; Mao, B. *Macromolecular Chemistry and Physics* **2005**, *206*, 404-409.
- (14) Shen, X.-r.; Fu, Z.-s.; Hu, J.; Wang, Q.; Fan, Z.-q. *The Journal of Physical Chemistry C* **2013**, *117*, 15174-15182.
- (15) Thushara, K. S.; Gnanakumar, E. S.; Mathew, R.; Jha, R. K.; Ajithkumar, T. G.; Rajamohanam, P. R.; Sarma, K.; Padmanabhan, S.; Bhaduri, S.; Gopinath, C. S. *The Journal of Physical Chemistry C* **2011**, *115*, 1952-1960.
- (16) Gnanakumar, E. S.; Thushara, K. S.; Bhanghe, D. S.; Mathew, R.; Ajithkumar, T. G.; Rajamohanam, P. R.; Bhaduri, S.; Gopinath, C. S. *Dalton Transactions* **2011**, *40*, 10936-10944.
- (17) Arlman, E. J. *J. Catal.* **1964**, *3*, 89-98.
- (18) Cossee, P. *J. Catal.* **1964**, *3*, 80-8.

- (19) Coutinho, F. B.; Costa, M. S.; Santa Maria, L. *Polymer Bulletin* **1992**, *28*, 55-59.
- (20) Baba, Y. *Bulletin of the Chemical Society of Japan* **1968**, *41*, 1022-1023.
- (21) Baba, Y. *Bulletin of the Chemical Society of Japan* **1968**, *41*, 1020-1021.
- (22) Xu, D.; Liu, Z.; Zhao, J.; Han, S.; Hu, Y. *Macromolecular Rapid Communications* **2000**, *21*, 1046-1049.
- (23) Kissin, Y. V.; Rishina, L. A. *J. Polym. Sci., Part A: Polym. Chem.* **2002**, *40*, 1353-1365.
- (24) Kissin, Y. V.; Rishina, L. A.; Vizen, E. I. *J. Polym. Sci., Part A: Polym. Chem.* **2002**, *40*, 1899-1911.
- (25) Kissin, Y. V.; Mink, R. I.; Nowlin, T. E.; Brandolini, A. J. *J. Polym. Sci., Part A: Polym. Chem.* **1999**, *37*, 4281-4294.
- (26) Kissin, Y. V.; Mink, R. I.; Nowlin, T. E.; Brandolini, A. J. *Top. Catal.* **1999**, *7*, 69-88.
- (27) Panchenko, V. N.; Goryachev, A. N.; Vorontsova, L. V.; Paukshtis, E. A.; Zakharov, V. A. *The Journal of Physical Chemistry C* **2014**, *118*, 28572-28579.
- (28) Chirinos, J.; Fernandez, J.; Perez, D.; Rajmankina, T.; Parada, A. *Journal of Molecular Catalysis A: Chemical* **2005**, *231*, 123-127.
- (29) Chadwick, J. C.; Morini, G.; Balbontin, G.; Camurati, I.; Heere, J. J. R.; Mingozzi, I.; Testoni, F. *Macromolecular Chemistry and Physics* **2001**, *202*, 1995-2002.
- (30) Vähäsarja, E.; Pakkanen, T. T.; Pakkanen, T. A.; Iiskola, E.; Sormunen, P. *Journal of Polymer Science Part A: Polymer Chemistry* **1987**, *25*, 3241-3253.
- (31) Koo, K.; Marks, T. J. *Journal of the American Chemical Society* **1999**, *121*, 8791-8802.
- (32) Chien, J. C. W.; Wu, J.-C. *Journal of Polymer Science: Polymer Chemistry Edition* **1982**, *20*, 2445-2460.
- (33) Chien, J. C. W.; Wu, J.-C. *Journal of Polymer Science: Polymer Chemistry Edition* **1982**, *20*, 2461-2476.
- (34) Sergeev, S. A.; Bukatov, G. D.; Zakharov, V. A. *Die Makromolekulare Chemie* **1984**, *185*, 2377-2385.
- (35) Huang, Y.; Qin, Y.; Zhou, Y.; Niu, H.; Yu, Z.-Z.; Dong, J.-Y. *Chemistry of Materials* **2010**, *22*, 4096-4102.
- (36) Bahri-Laleh, N.; Correa, A.; Mehdipour-Ataei, S.; Arabi, H.; Haghighi, M. N.; Zohuri, G.; Cavallo, L. *Macromolecules* **2011**, *44*, 778-783.
- (37) Cavallo, L.; Del Piero, S.; Ducere, J.-M.; Fedele, R.; Melchior, A.; Morini, G.; Piemontesi, F.; Tolazzi, M. *The Journal of Physical Chemistry C* **2007**, *111*, 4412-4419.

- (38) Cavallo, L.; Guerra, G.; Corradini, P. *J. Am. Chem. Soc.* **1998**, *120*, 2428-2436.
- (39) Correa, A.; Piemontesi, F.; Morini, G.; Cavallo, L. *Macromolecules (Washington, DC, U. S.)* **2007**, *40*, 9181-9189.
- (40) Credendino, R.; Liguori, D.; Fan, Z.; Morini, G.; Cavallo, L. *ACS Catalysis* **2015**, *5*, 5431-5435.
- (41) Credendino, R.; Pater, J. T. M.; Liguori, D.; Morini, G.; Cavallo, L. *The Journal of Physical Chemistry C* **2012**, *116*, 22980-22986.
- (42) Monaco, G.; Toto, M.; Guerra, G.; Corradini, P.; Cavallo, L. *Macromolecules* **2000**, *33*, 8953-8962.
- (43) Kumawat, J.; Kumar Gupta, V.; Vanka, K. *European Journal of Inorganic Chemistry* **2014**, *2014*, 5063-5076.
- (44) Stukalov, D. V.; Zakharov, V. A.; Zilberberg, I. L. *The Journal of Physical Chemistry C* **2010**, *114*, 429-435.
- (45) Ghorbani, N.; Mahdizadeh Ghohe, N.; Torabi, S.; Yates, B. F.; Ariaifard, A. *Organometallics* **2013**, *32*, 1687-1693.
- (46) Flisak, Z.; Spaleniak, G. P.; Bremmek, M. *Organometallics* **2013**, *32*, 3870-3876.
- (47) Boero, M.; Parrinello, M.; Weiss, H.; Hueffer, S. *J. Phys. Chem. A* **2001**, *105*, 5096-5105.
- (48) Correa, A.; Bahri-Laleh, N.; Cavallo, L. *Macromolecular Chemistry and Physics* **2013**, *214*, 1980-1989.
- (49) Wondimagegn, T.; Ziegler, T. *The Journal of Physical Chemistry C* **2012**, *116*, 1027-1033.
- (50) Seth, M.; Margl, P. M.; Ziegler, T. *Macromolecules* **2002**, *35*, 7815-7829.
- (51) Seth, M.; Ziegler, T. *Macromolecules* **2004**, *37*, 9191-9200.
- (52) Seth, M.; Ziegler, T. *Macromolecules* **2003**, *36*, 6613-6623.
- (53) Flisak, Z. *Macromolecules (Washington, DC, U. S.)* **2008**, *41*, 6920-6924.
- (54) Trubitsyn, D. A.; Zakharov, V. A.; Zakharov, I. I. *J. Mol. Catal. A Chem.* **2007**, *270*, 164-170.
- (55) Mukhopadhyay, S.; Kulkarni, S. A.; Bhaduri, S. *Journal of Organometallic Chemistry* **2005**, *690*, 1356-1365.
- (56) Busico, V.; Causa, M.; Cipullo, R.; Credendino, R.; Cutillo, F.; Friederichs, N.; Lamanna, R.; Segre, A.; Van Axel Castelli, V. *The Journal of Physical Chemistry C* **2008**, *112*, 1081-1089.
- (57) Zhao, M. X., *Yi Shiyou Huagong* **1987**, *16*, 206-212.

- (58) Ahlrichs, R.; Bar, M.; Haeser, M.; Horn, H.; Kolmel, C. *Chemical Physics Letters* **1989**, *162*, 165-169.
- (59) Becke, A. D. *Physical Review A* **1988**, *38*, 3098-3100.
- (60) Perdew, J. P. *Physical Review B* **1986**, *33*, 8822-8824.
- (61) Perdew, J. P. *Physical Review B* **1986**, *34*, 7406-7406.
- (62) Becke, A. D. *The Journal of Chemical Physics* **1993**, *98*, 5648-5652.
- (63) Schaefer, A.; Horn, H.; Ahlrichs, R. *J. Chem. Phys.* **1992**, *97*, 2571-7.
- (64) Eichkorn, K.; Treutler, O.; Oehm, H.; Haeser, M.; Ahlrichs, R. *Chem. Phys. Lett.* **1995**, *240*, 283-90.
- (65) Sierka, M.; Hoge Kamp, A.; Ahlrichs, R. *J. Chem. Phys.* **2003**, *118*, 9136-9148.
- (66) Houk, K. N.; Cheong, P. H.-Y. *Nature* **2008**, *455*, 309-313.
- (67) Grimme, S.; Antony, J.; Ehrlich, S.; Krieg, H. *The Journal of Chemical Physics* **2010**, *132*, 154104.

# **Chapter 7**

## **Summary of the Thesis**

The aim of this thesis work is to get a clear picture of the role of donors (internal and external) in the ZN system. As mentioned in Chapter 1, oxygen containing Lewis Bases “donors” have become one of the most important components in ZN systems. Except for some limited understanding based on experimental and computational studies, it is still a mystery as to what the donor exactly does in the ZN system. Therefore, in the current thesis, we have attempted to understand the role of donors on the different ZN reactions such as activation, insertion and the termination steps.

In conventional ZN catalysis, it has been mentioned that the donor binds to the  $\text{MgCl}_2$  surface beside the titanium center and thereby influences the ZN catalysis. However, one of our objectives in Chapter 3 was to verify the effect of the donors on the insertion and termination steps in olefin polymerization, where the donor directly binds to the titanium center instead of the  $\text{MgCl}_2$  surface. This study has been done with a different range of oxygen containing donors in order to compare the catalyst activity. It was observed that the donor influences the insertion and the termination barriers. The difference between the insertion and the terminations barriers ( $\Delta X$ ) decides the molecular weight of the polymer and it was observed that donors increase the  $\Delta X$ . Furthermore, we have also modified the titanium catalysts, where we substituted one of the chlorine (-Cl) atoms of the titanium with an ethoxy (-OEt) group in order to verify the effect of these groups on the  $\Delta X$ . It was seen that the  $\Delta X$  significantly increases in the ethoxy group coordinated case. This same study has also been done for the propylene monomer case and the same trend was found as for the ethylene monomer case.

The decomposition of donor has been studied as an unwanted side reaction in Chapter 4. The donor decomposition mechanism has been investigated in the presence of different Lewis acidic species ( $\text{Al}_2\text{Et}_6$  and  $\text{TiCl}_2\text{Et}$  complex on  $\text{MgCl}_2$  surface). Two different pathways, (i) the ketone pathway – in this pathway, the transfer of ethide from triethylaluminum to the carbonyl carbon of the ester donor has been considered and (ii) the aldehyde pathway, where the transfer of hydride from the ethyl group of triethylaluminum to the carbonyl carbon of the ester donor has been considered (if the Lewis acidic species is  $\text{Al}_2\text{Et}_6$ ). In order to make the donor more robust and to diminish the possibilities for donor decomposition, a modification in the silyl ester donor has been done where the alkyl group (-R) was replaced by the more

bulky alkyl groups. It was observed that for certain sterically bulky ligands, the decomposition barrier is higher, but that there is decrease with increasing steric bulk on the donor. Hence, we have concluded that to decrease donor decomposition, there should be balance between the sterics and the electronics on the alkyl group of the donor.

In ZN catalysis, the role of the co-catalyst, triethylaluminium (*teal*), is to convert the inactive titanium ( $\text{Ti}^{\text{IV}}\text{Cl}_4$ ) into the active titanium ( $\text{Ti}^{\text{III}}\text{Cl}_2\text{Et}$ ) catalyst. This phenomenon is known as activation. In the fifth chapter, we have studied the effect of five different donors on the activation mechanism. This mechanism has been investigated as consisting of two consecutive steps (i) Ti-Cl bond cleavage, (ii) the transalkylation – where transfer of ethyl group from triethylaluminium to titanium center was considered. Furthermore, along with the first step, the Ti-Cl bond cleavage, donor displacement study has also been investigated, which leads to the donor displacement product,  $\text{AlEt}_3\text{-donor}$ . This  $\text{AlEt}_3\text{-donor}$  complex has also been studied for the activation mechanism as a separate donor. It was observed that the presence of the donor in the activation mechanism significantly influences the activation mechanism.

It has been accepted in the  $\text{MgCl}_2$  supported ZN catalysis that the majority of the lateral cuts on the  $\text{MgCl}_2$  surface are the five coordinated (104) with the four coordinated (110)  $\text{MgCl}_2$  lateral cuts in the minority. In the sixth chapter, we have studied the ethylene polymerization on the (104) lateral cuts of the  $\text{MgCl}_2$  surface with five different titanium catalysts. These catalysts differ in the nature of the ethoxy (OEt) groups attached to the titanium center. The titanium based catalysts are  $\text{Ti}(\text{III})\text{Et}(\text{OR})(\text{OR}')$  (where  $\text{R} = -\text{CH}_3, -\text{Et}, -t\text{-butyl}$ ,  $\text{R}' = -\text{CH}_3, -\text{Et}, -t\text{-butyl}$ ). Furthermore, for the sake of comparison, the olefin polymerization study has been done on the (104) as well as the (110)  $\text{MgCl}_2$  surfaces. It was observed that the (104) was equally important for the olefin polymerization, when ethoxy ligand containing catalysts were employed.